Molecular and cellular studies on the 2-oxoglutarate-dependent oxygenase MINA53

Eline Hendrix

A thesis submitted to the University of Birmingham for the degree of **DOCTOR OF PHILOSOPHY**



UNIVERSITY OF BIRMINGHAM

Institute of Cancer and Genomic Sciences
College of Medical and Dental Sciences
University of Birmingham

March 2021

UNIVERSITY OF
BIRMINGHAM

University of Birmingham Research Archive

e-theses repository

This unpublished thesis/dissertation is copyright of the author and/or third parties. The intellectual property rights of the author or third parties in respect of this work are as defined by The Copyright Designs and Patents Act 1988 or as modified by any successor legislation.

Any use made of information contained in this thesis/dissertation must be in accordance with that legislation and must be properly acknowledged. Further distribution or reproduction in any format is prohibited without the permission of the copyright holder.

Abstract

Human 2-oxoglutarate (2OG) and iron-dependent oxygenases catalyse an emerging post-translational modification, hydroxylation, on a range of substrates including DNA, RNA and protein. Despite the well-recognised roles of 2OG oxygenases in oxygen sensing and epigenetic regulation of transcription, much work remains to be done to elucidate the roles of the less well-characterised family members in physiology and disease. Myc-induced nuclear antigen (MINA) is a 2OG oxygenase that catalyses histidyl hydroxylation of the large ribosomal subunit protein RPL27A. The paradoxical role of MINA in cancer, however, suggests the potential existence of additional substrates or functions. Here, we identify and explore a novel role of MINA in epithelial morphogenesis. We begin by characterising the physiological and pathological cues that contribute to the nucleolar retention and release of MINA. We then identify and characterise a novel activity-dependent and extra-nucleolar interaction between MINA and a membrane-associated guanylate kinase, membrane palmitoylated protein 6 (MPP6). Subsequent studies explored the role of MINA localisation, activity and MPP6 in epithelial morphogenesis. Overall, our findings suggest that extra-nucleolar MINA functions as a tumour suppressor, possibly through its interaction with MPP6. Moreover, the work presented in this thesis suggests a novel mechanism by which the tumour suppressor function of MINA may be broadly inactivated in cancer.

Acknowledgements

First and foremost, I would like to thank Mat for your endless support and encouragement over the years, and for letting me photoshop your face onto basically everything imaginable; from astronauts and Super Mario to Aristotle statues and feathered dinosaurs.

Thank you to all past and present members of the Coleman lab, and by extension everyone on our side of the 2nd floor IBR West, for the help with all things related to science, but also the great times in and especially outside the lab. Thanks to Char for organising the best shindigs, and to Sally and Charlotte for introducing me to the TOG Harriers. Thanks also to Christian for only changing the radio to Radio 4 when nobody else was around. Thank you Uncaar for your willingness to help with literally everything.

Special thanks go to Regina, for getting us a coffee machine and the subsequent many, many conversations over coffee and, when required, something stronger. I am beyond grateful for your support and friendship. You're my lobster.

I would also like to say thank you to my family, for your continuous support and confidence in me. To my dad, without whom I never would have made it here. Thank you to all my friends here in England, across the Channel and across the Pond, for the occasional –much needed– reminder that there is life outside the lab. Thank you to everyone who's visited me in Brum over the years. I am also very grateful to Greg and Lisa Thiele for making my industrial placement the best experience I could ever have wished for, and for treating me like family. Thanks also Ashley and Dean for the countless hours-long FaceTime chats that got me through lockdown. And to my friend Wim, for always lending an ear whenever I needed to vent.

Finally, I would like to express my gratitude to the Midlands Integrative Biosciences Training Partnership and the Biotechnology and Biological Sciences Research Council for providing me with the opportunity and resources to complete my research.

Declaration

I declare that this thesis is entirely my own work, with the exception of the following:

Proteomic screens presented in Tables 3.4 and 3.5 were performed by Dr Mathew Coleman.

Experimental data shown in Figure 3.6 was generated in close collaboration with Dr Regina Andrijes.

Data for 3 of 4 replicates presented in Figure 5.2E were provided by Dr Regina Andrijes.

Generation of MINA, NO66, MPP6 and LIN7C cDNAs and their cloning into pFLAG, pEF6, pIPZ, pTIPZ or pTIBZ vectors was carried out by others, including Dr Mathew Coleman, Dr Adam Zayer, Dr Helen Smith, Dr James Bundred and Mr Uncaar Boora.

Primer design and site-directed mutagenesis to generate MINA H179A and NoLS mutants was carried out by Mr Uncaar Boora and Dr Helen Smith. Cloning of $MPP6^{1\text{-}306Fs}$ was performed by Dr James Bundred.

Primer design to generate $MPP6^{110\text{-}541}$, $MPP6^{210\text{-}541}$, $MPP6^{1\text{-}212}$, MINA D333A and MINA M405A was carried out by Mr Uncaar Boora.

Contents

Abstract i
Acknowledgements ii
Declaration iii
Contents iv
List of Figures vii
List of Tables xi
List of Abbreviations xii
Chapter 1: Introduction 1
1.1 Hydroxylation, a post-translational modification catalysed by 2-oxoglutarate oxygenases . . . 1
1.1.1 Structural features and catalytic mechanism . . . 1
1.1.2 Overview of the functionally diverse roles of 2OG oxygenases . . . 5
1.1.2.1 Hydroxylation of extracellular and membrane proteins 5
1.1.2.2 Epigenetic regulation of gene expression . . . 8
1.1.2.3 Regulators of cellular stress responses . . . 10
1.1.2.4 Regulation of translation by 2OG oxygenases . . . 12
1.1.2.5 Fatty acid metabolism . . . 14
1.1.2.6 Hydroxylases of the JmjC-only family . . . 16
1.2 Ribosomal hydroxylation . . . 21
1.2.1 Overview of the ribosome and translation . . . 21
1.2.2 Ribosomal hydroxylases . . . 22
1.2.2.1 OGFOD1 . . . 22
1.2.2.2 NO66, MINA and YcfD . . . 23
1.3 Additional targets for NO66 and MINA? . . . 26
1.3.1 NO66 . . . 26
1.3.2 MINA . . . 28
1.3.2.1 Roles for MINA in immunology . . . 28
1.3.2.2 Roles for MINA in cancer . . . 30
1.4 Aim of this study . . . 31

Chapter 2: Physiological and pathological regulation of MINA localisation **32**
2.1 Introduction . . . 32
2.2 Results . . . 33
2.2.1 Localisation of MINA in common cancer cell lines . . . 33
2.2.2 Generation and characterisation of stable doxycycline-inducible 3xFLAG-MINA Caco-2 cell lines . . . 34
2.2.3 MINA localisation depends on cell confluence . . . 38
2.2.4 MINA re-locates to the nucleolus following disruption of the monolayer . . . 39
2.2.5 MINA localisation correlates with ribosome biogenesis . . . 41
2.2.6 Nucleolar MINA localisation is not dependent on high oxygen availability . . . 45
2.2.7 Identification of a nucleolar localisation signal in MINA . . . 47
2.3 Discussion . . . 53
Chapter 3: Identification and characterisation of a novel protein complex interacting with extra-nucleolar MINA **57**
3.1 Introduction . . . 57
3.2 Results . . . 58
3.2.1 Identification of a novel, extra-nucleolar, candidate substrate complex . . . 58
3.2.2 Subcellular localisation of the MINA:MPP6 complex . . . 70
3.2.3 Biochemical characterisation of the MINA:MPP6 complex . . . 75
3.2.3.1 MPP6 interacts with MINA in a specific and substrate-like manner . . . 75
3.2.3.2 Mapping the domains in MPP6 that are necessary and sufficient for activity-dependent MINA binding . . . 80
3.2.3.3 Mass spectrometry analyses of MPP6 oxidation . . . 86
3.3 Discussion . . . 93
Chapter 4: Role of MINA in epithelial morphogenesis **99**
4.1 Introduction . . . 99
4.2 Results . . . 104
4.2.1 Caco-2 as a model to study epithelial morphogenesis/cell polarity 104
4.2.2 Loss of MINA interferes with Caco-2 spheroid growth and lumen formation without affecting apico-basal polarity . . . 106
4.2.3 Stable re-expression of MINA in inducible knockdown cell lines . 112
4.3 Discussion . . . 118

Chapter 5: Role of MPP6 and the MPP6:MINA complex in epithelial morphogenesis **126**
5.1 Introduction . . . 126
5.2 Results . . . 127
5.2.1 Effect of MPP6 depletion on Caco-2 spheroid development . . . 127
5.2.2 Effect of MINA on MPP6 expression and localisation . . . 129
5.3 Discussion . . . 132
Chapter 6: Final discussion **141**
6.1 MPP6 as a candidate MINA substrate . . . 141
6.2 Could defective MINA activity contribute to altered epithelial morphogenesis in response to changes in nutrient availability or metabolism? . . . 143
6.3 Nucleolar sequestration as a mechanism of hydroxylase signalling and tumour suppression . . . 145
6.4 The relationship between MINA and MPP6 in cancer . . . 148
6.5 Conclusion . . . 151
Chapter 7: Materials and methods **152**
7.1 Molecular biology techniques . . . 152
7.1.1 Plasmid constructs and cloning procedures . . . 152
7.2 Cell biology techniques . . . 156
7.2.1 Cell culture . . . 156
7.2.2 Transient transfection . . . 156
7.2.3 Generation of stable cell lines . . . 157
7.2.4 Cell treatments . . . 157
7.2.5 Cell viability assays . . . 157
7.2.6 Metabolic labelling of newly synthesised proteins . . . 159
7.2.7 Proximity ligation assay . . . 159
7.2.8 Immunofluorescence staining and image acquisition . . . 159
7.3 Biochemical techniques . . . 161
7.3.1 Whole cell extracts . . . 161
7.3.2 Immunoprecipitation . . . 161
7.3.3 SDS-PAGE and Western blot analysis . . . 162
7.3.4 Mass Spectrometry . . . 162
7.3.5 *In vitro* hydroxylation assays . . . 165
7.3.6 Subcellular fractionation . . . 165
7.4 Illustration plotting, statistical analysis and reproducibility . . . 166
Appendix A **167**
Appendix B **168**
Appendix C **171**
Bibliography **182**

List of Figures

Chapter 1: Introduction

1.1 Structural features and catalytic mechanisms of 2OG oxygenases 3
1.2 Molecular consequences of hydroxylation by 2OG oxygenases 4
1.3 Overview of the functional diversity of 2OG oxygenases in cell biology . 6
1.4 Histone lysine demethylases 9
1.5 Nucleotide demethylation catalysed by the TET, ALKBH5 and FTO enzymes 11
1.6 Lipid hydroxylation and regulation of fatty acid metabolism by 2OG oxygenases 15
1.7 MINA and NO66 target conserved histidine residues in ribosomal proteins located close to functionally important sites 24
1.8 NO66 in skeletal development 27
1.9 MINA is involved in T-cell differentiation and cell proliferation 29

Chapter 2: Physiological and pathological regulation of MINA localisation

2.1 Differential localisation of MINA in cancer cell lines 35
2.2 Characterisation of stable Caco-2 cell lines expressing doxycycline-inducible 3xFLAG-MINA 37
2.3 3xFLAG-MINA enriches in the nucleoli of some, but not all of the cells 38
2.4 MINA localisation in Caco-2 depends on cell confluence and catalytic activity 40
2.5 MINA relocates to the nucleolus upon disruption of the monolayer . . . 41
2.6 MINA localisation correlates with the rate of translation 43
2.7 Active ribosome biogenesis retains MINA in the nucleolus in Caco-2 . . 44
2.8 Active ribosome biogenesis retains MINA in the nucleolus in SW620 . . 46
2.9 Moderate hypoxia does not trigger MINA translocation 47
2.10 Prediction of a nucleolar localisation signal (NoLS) in MINA 49
2.11 Conservation of candidate NoLS residues 50
2.12 Localisation of R125/K126 and effect of mutation on subcellular localisation 52

2.13 Mutation of R125G/K126G does not affect the intrinsic enzymatic activity of MINA 53

Chapter 3: Identification and characterisation of a novel protein complex interacting with extra-nucleolar MINA

3.1 Stable expression of doxycycline-inducible 3xFLAG-MINA and mutants in Caco-2 59
3.2 Network and functional enrichment analysis of MINA interactors 62
3.3 Wild-type and extra-nucleolar MINA interact with MPP6 and LIN7 in an activity-dependent manner 66
3.4 Wild-type and extra-nucleolar MINA interact with MPP6 and LIN7 in an activity-dependent manner in SW620 cells 68
3.5 Wild-type and exta-nucleolar MINA interact with MPP6 in an activity-dependent manner in U2OS cells 69
3.6 The interaction between MINA and MPP6 is independent of LIN7A/C 71
3.7 MPP6 binding to MINA increases upon extra-nucleolar localisation . . 72
3.8 Nuclear localisation of MPP6 in proliferating cells 74
3.9 MINA and MPP6 co-localise in the nucleoplasm 76
3.10 MINA and MPP6 preferentially interact in subconfluent cells 77
3.11 MPP6 binds MINA in a substrate-like manner 79
3.12 Interaction between MINA and MPP6 is not conserved between ribosomal oxygenases or MPP family members 81
3.13 Domain organisation of MAGUK proteins 82
3.14 MPP6 amino acids 285-338 are required for activity-dependent MINA binding 83
3.15 MPP6 amino acids 285-338 are sufficient for activity-dependent MINA binding 84
3.16 MINA binds to the N-terminal end of the MPP6 SH3-GUK interdomain 85
3.17 MPP6 P296 and F297 are not sufficient for MINA binding 86
3.18 Preliminary MS analysis of MPP6 oxidations in the minimal binding domain 88
3.19 Preliminary MS analysis of MINA-dependent oxidations in the minimal binding domain 89
3.20 MPP6 oxidation in response to MINA overexpression, proteasome inhibition and confluence 91
3.21 MPP6 G295, P296 and F297, C298 and G299 are required for binding to MINA 92

3.22 Genetic alterations of MPP6 and LIN7 in cancer 98

Chapter 4: Role of MINA in epithelial morphogenesis

4.1 Overview of the main cell junctions and core polarity complexes 102
4.2 Caco-2 cells spontaneously polarise in two-dimensional cell culture . . . 105
4.3 Caco-2 cells spontaneously polarise in three-dimensional cell culture . . 107
4.4 MINA expression in stable Caco-2 cell lines expressing inducible shRNA against MINA 109
4.5 MINA depletion affects 3D spheroid growth and lumen formation . . . 110
4.6 Loss of MINA expression inhibits Caco-2 cell proliferation in 3D 111
4.7 MINA depletion affects dome formation in Caco-2 monolayers 113
4.8 MINA is dispensable for the establishment of apico-basal polarity in Caco-2 cells 114
4.9 Characterisation of Caco-2 cells stably expressing cumate-inducible untagged MINA 116
4.10 Transient re-expression of 3xFLAG-tagged MINA in doxycycline-inducible shRNA cell lines: 2D dome assays 119
4.11 Transient re-expression of 3xFLAG-tagged MINA in doxycycline-inducible shRNA cells lines: 3D spheroid assays 120
4.12 Effect of hygromycin B on Caco-2 dome formation 120
4.13 Re-expression of 3xFLAG-tagged MINA in doxycycline-inducible shRNA cells lines: dome and lumen formation assays following hygromycin selection. 121

Chapter 5: Role of MPP6 and the MPP6:MINA complex in epithelial morphogenesis

5.1 Characterisation of stable Caco-2 cell lines expressing doxycycline-inducible MPP6-targeting shRNA sequences 128
5.2 Effect of MPP6 depletion on Caco-2 spheroid growth and lumen formation 130
5.3 Expression and localisation of cell junction proteins in MPP6-depleted Caco-2 cells 131
5.4 Effect of mutation or MINA depletion on MPP6 expression 133
5.5 Localisation of MPP6-HA in Caco-2 monolayers and spheroids 134
5.6 Localisation of MPP6-HA C298A in Caco-2 monolayers and spheroids . 135
5.7 OncoPrint analysis of MPP6, CADM1 and MINA mutations across cancer types 139

Chapter 6: Final discussion

6.1 Current working hypothesis 150
6.2 Distribution of mutations in MPP6 151

Appendices

Appendix A: Schematics of the lentiviral vectors used in this thesis 167

Appendix B: Sequence alignment of human MPPs 168

Appendix C: Uncropped western blot images 171

List of Tables

Chapter 3: Identification and characterisation of a novel protein complex interacting with extra-nucleolar MINA

3.1 List of 28 proteins interacting with wild-type MINA in Caco-2. 61
3.2 List of nucleolar/nucleoplasmic-dependent MINA interactors 63
3.3 List of activity-dependent MINA interactors 64
3.4 List of MINA interactors first identified in Caco-2 and validated in U2OS 64
3.5 List of MINA interactors first identified in Caco-2 and validated in K-Ras G12V MEFs 65
3.6 List of activity-dependent MINA interactors first identified in Caco-2 and validated in K-Ras G12V MEFs 66

Chapter 7: Materials and methods

7.3 Primers used for site-directed mutagenesis 155
7.4 List of chemicals 158
7.5 List of unconjugated primary antibodies 163
7.6 List of horseradish peroxidase (HRP)-conjugated primary antibodies . . 164
7.7 List of secondary antibodies 164

List of Abbreviations

2OG	2-oxoglutarate
AA	Amino acid
AHA	L-azidohomoalanine
ALKBH	alkB homologue
AMD	actinomycin D
AspH	Aspartate/asparagine-β-hydroxylase
BBOX	β-butyrobetaine hydroxylase
BSA	Bovine serum albumine
CADM1	Cell adhesion molecule 1
CARMA	Caspase recruitment domain-containing MAGUK
CASK	Calcium/calmodulin-dependent serine protein kinase
CHX	Cycloheximide
CRB	Crumbs
CTRL	Control
DAPI	4',6-diamidino-2-phenylindole
DFO	Desferrioxamine
DLG	Discs large
DMOG	Dimethyl-N-oxalylglycine
DNMT	DNA methyltransferase
Dox	Doxycycline
DRG	Developmentally regulated GTPase
DSBH	double-stranded β-helix
ECM	Extracellular matrix
EGFD	Epidermal growth factor-like domain
emPAI	Exponentially modified protein abundance index
EMT	Epithelial-mesenchymal transition
ER	Endoplasmic reticulum

eRF	Eukaryotic release factor
EV	Empty vector
FAO	Fatty acid oxidation
FIH	Factor-inhibiting HIF
FTO	Fat mass and obesity-associated protein
GFP	Green fluorescent protein
GUK	Guanylate kinase
HA	Hemagglutinin
HDAC	Histone deacetylase
HEK293T	Human embryonic kidney 293 T-antigen
HIF	Hypoxia-inducible factor
HSPBAP1	Heat shock protein beta-1 associated protein 1
HUVEC	Human umbilical vein endothelial cell
IF	Immunofluorescence
IP	Immunoprecipitation
JAM	Junctional adhesion molecule
JmjC	Jumonji-C
JMJD	Jumonji domain-containing protein
KDM	Histone lysine demethylase
LC-MS/MS	Liquid chromatography and tandem mass spectrometry
LGL	Lethal giant larvae
LSD	Lysine-specific demethylase
MAGUK	Membrane-associated guanylate kinase
MEF	Mouse embryonic fibroblast
MET	Mesenchymal-epithelial transition
MINA	Myc-Induced Nuclear Antigen
MPP	Membrane palmitoylated protein
NCL	Nucleolin
NO52	Nucleolar protein 52 kDa
NO66	Nucleolar protein 66 kDa
NOG	N-oxalylglycine
NoLS	Nucleolar localisation signal
NPM	Nucleophosmin
OGFOD1	2-oxoglutarate and Fe(II)-dependent oxygenase domain-containing protein 1

Osx	Osterix
P3H	Prolyl 3-hydroxylase
P4HA	Prolyl 4-hydroxylase α-subunit
PAR	Partitioning-defective
PBS	Phosphate-buffered saline
PDB	Protein data bank
PFA	Paraformaldehyde
PHD	Prolyl hydroxylase-domain containing protein
PHYH	phytanoyl-CoA hydroxylase
PLOD	Procollagen-lysine-2-oxoglutarate-5-dioxygenase
PTC	Peptidyl transferase centre
PTM	Post-translational modification
pVHL	Von Hippel-Lindau
RIOX	Ribosomal oxygenase
RP	Ribosomal protein
RPL	Ribosomal protein large subunit
RPS	Ribosomal protein small subunit
RT	Room temperature
SH3	Src homology 3
shRNA	Short hairpin RNA
TCGA	The Cancer Genome Atlas
TET	Ten-eleven translocation
TMLH	N^{ϵ}-trimethyl lysine hydroxylase
TS	Tumour suppressor
TYW5	RNA-yW synthesising enzyme 5
WH	Winged helix domain
WT	Wild-type
ZO	Zona occludens

Chapter 1: Introduction

1.1 Hydroxylation, a post-translational modification catalysed by 2-oxoglutarate oxygenases

1.1.1 Structural features and catalytic mechanism

The enzymatic incorporation of an alcohol or hydroxyl group (-OH) into an organic molecule, *hydroxylation*, is a ubiquitous post-translational modification that occurs in plants, prokaryotes and higher organisms including humans (Islam et al., 2018).

2-oxoglutarate (2OG) oxygenases, named as such due to their dependence on Krebs' cycle intermediate 2-oxoglutarate (α-ketoglutarate), are a large family of proteins that catalyse hydroxylation reactions. Whereas 2OG oxygenases in prokaryotes catalyse a range of oxidative modifications, including desaturation, epoxidation, halogenation, ring formation as well as hydroxylation (Islam et al., 2018), eukaryotic 2OG oxygenases have, so far, only been found to catalyse hydroxylation or demethylation (which occurs *via* a hydroxylation reaction).

Catalytic mechanism

In addition to 2-oxoglutarate, 2OG oxygenases require ferrous iron (Fe^{2+}) and molecular oxygen (O_2) for catalytic activity. To assemble these cofactors, 2OG oxygenases contain a conserved catalytic pocket that consists of eight anti-parallel β-sheets which form a barrel-like structure known as a 'double-stranded β-helix' (DSBH, also often

referred to as 'jelly-roll' or cupin fold, Figure 1.1A). An overview of the conserved catalytic mechanism in presented in Figure 1.1B. Fe(II) binding is mediated by a conserved 2-His/1-Carboxylate ($HX(D/E)X_nH$) motif, often referred to as a 'facial triad' (Clifton et al., 2006; Loenarz and Schofield, 2011). Water (H_2O) molecules occupy the remaining three iron-coordination sites. The catalytic cycle is initiated by binding of 2OG, followed by the substrate and, finally, O_2. 2OG binds through hydrogen bonding and electrostatic interactions with semi-conserved amino acids (K/R) and replaces water on two of the three remaining Fe(II) coordination sites. Oxygen binding displaces the final water molecule and initiates oxidative decarboxylation of 2OG into succinate and carbon dioxide (CO_2), thereby generating a highly reactive Fe(IV)=O (ferryl-oxo) intermediate, which then oxidises the substrate (Loenarz and Schofield, 2011). The catalytic cycle is completed by the dissociation of the hydroxylated substrate product and succinate. Some hydroxylation reactions require the presence of an additional cofactor, ascorbate (Vitamin C), as a reducing agent.

Chemical and molecular consequences of hydroxylation

2OG oxygenase-catalysed hydroxylation occurs at a carbon-hydrogen bond and is a small and chemically neutral modification. However, the presence of a hydroxyl group increases polarity and may act as a hydrogen bond donor or acceptor, and can change the conformational preferences of the substrate (Loenarz and Schofield, 2011). Accordingly, albeit a chemically small modification, the molecular consequences of hydroxylation can be diverse (Figure 1.2). Hydroxylation can generate a stable product, for instance modulating an interaction with binding partners (Lando et al., 2002; Yang et al., 2011b) or influencing the substrate's stability (Myllyharju, 2003; Yang et al., 2011b). Alternatively, the hydroxylated product may be recognised and further modified by other enzymes (Ivan et al., 2001; Jaakkola et al., 2001). Moreover, hydroxylation of methyl groups gives rise to an unstable intermediate that causes spontaneous release of the hydroxymethyl group as formaldehyde (Klose et al., 2006). This reaction is referred to as demethylation *via* hydroxylation. Although theoretically possible, to date no enzymes have been identified that can reverse stable hydroxylation.

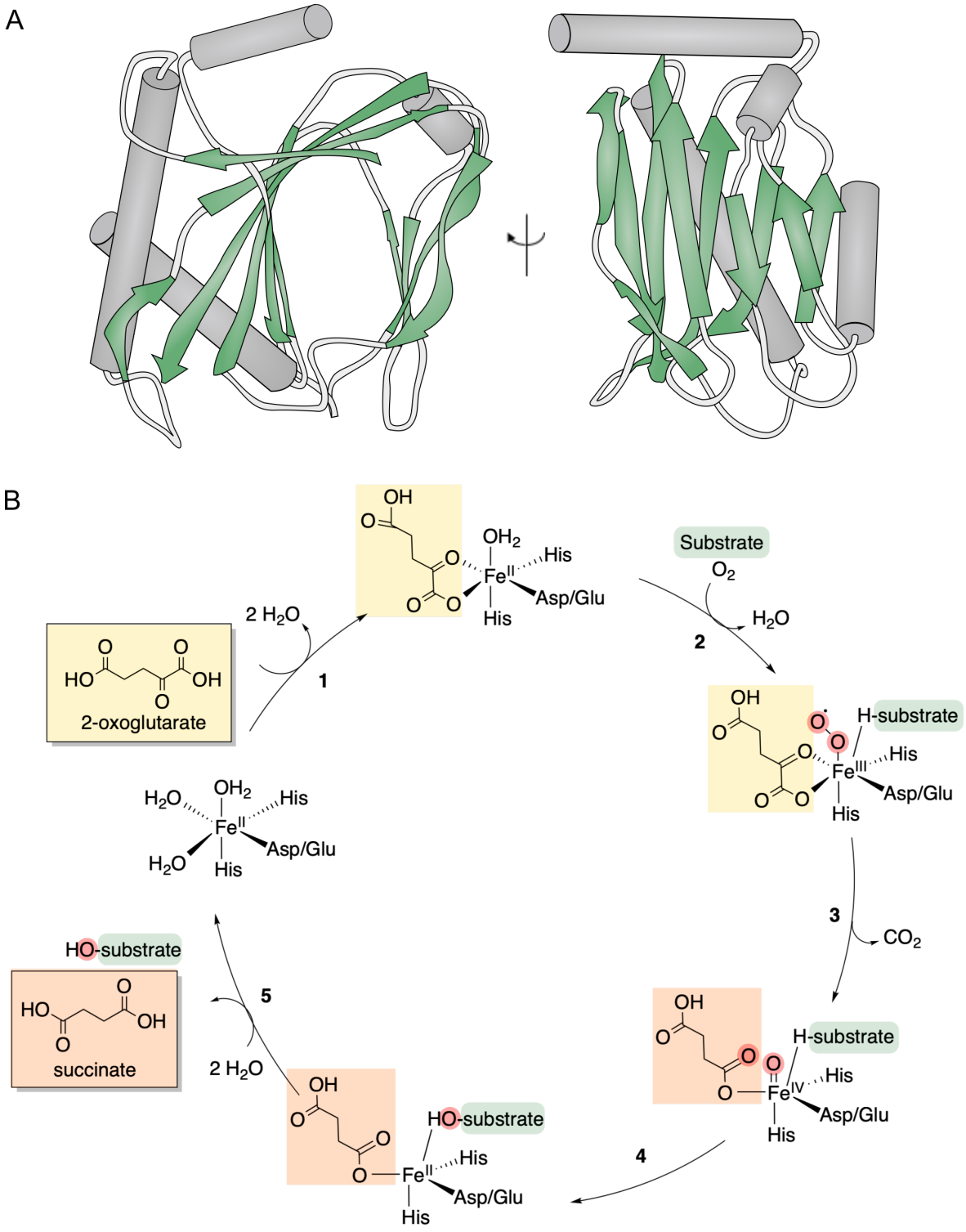


Figure 1.1: Structural features and catalytic mechanisms of 2OG oxygenases. (**A**) 2OG oxygenases are characterised by a conserved catalytic pocket that consists of eight anti-parallel β-sheets. Figure was adapted from Ploumakis and Coleman (2015). (**B**) Iron-binding is mediated by 2-His/1-carboxylate (Asp/Glu) motif. The catalytic cycle is initiated by 2-oxoglutarate binding, thereby releasing two water (H_2O) molecules (1). Subsequent substrate and oxygen (O_2) binding displaces the final water molecule resulting in generation of a reactive oxygen-species (2). Oxidative decarboxylation of 2OG results in generation of succinate and substrate oxidation, with release of CO_2 (3,4). Finally, succinate and the hydroxylated substrate are released (5).

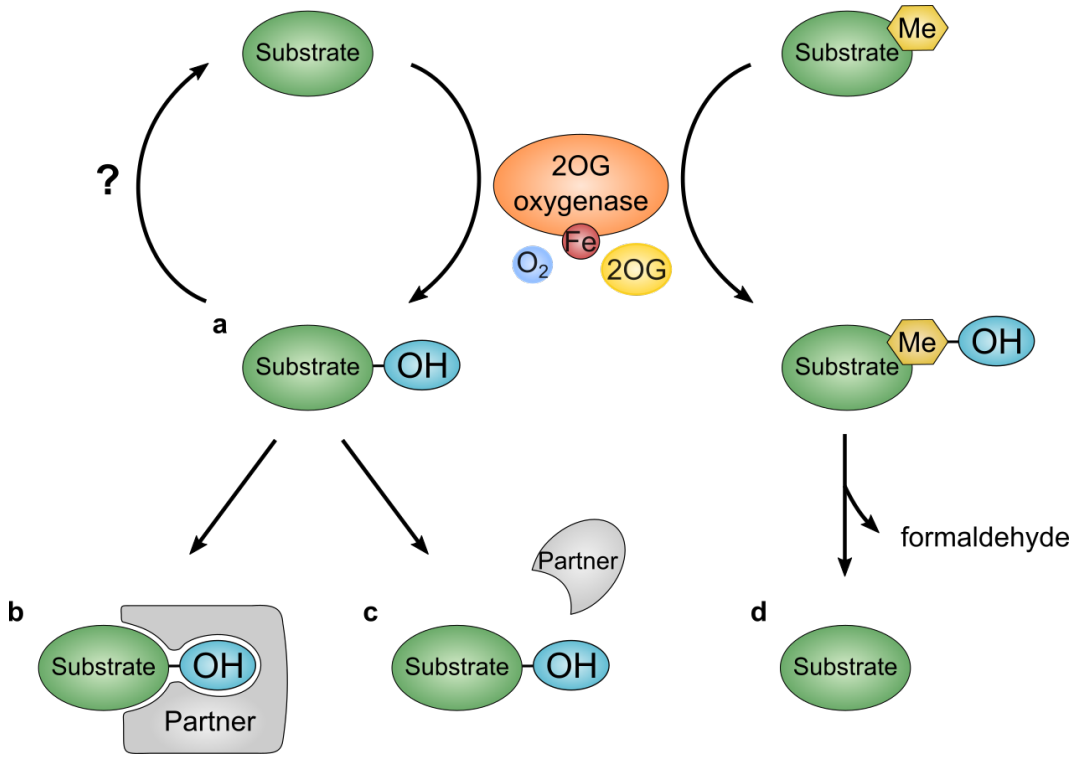


Figure 1.2: Molecular consequences of hydroxylation by 2OG oxygenases. Stable hydroxylation (**a**) can alter the chemical properties of the substrate such as stability, or mediate interactions between the substrate and its binding partners (**b**), including recognition by other enzymes that catalyse subsequent modification of the hydroxylated substrate. Hydroxylation can prevent binding of a partner (**c**). Hydroxylation of methyl groups triggers spontaneous release of the hydroxymethyl group as formaldehyde, resulting in a demethylated product (**d**).

1.1.2 Overview of the functionally diverse roles of 2OG oxygenases

Once considered rare, it is now appreciated that 2OG oxygenase-catalysed hydroxylation is a more common modification, with over 60 2OG oxygenases identified in mammals. Besides the conserved catalytic core, 2OG oxygenases are structurally diverse. The presence of additional functional domains allows 2OG oxygenases to target a range of biomolecules including proteins, nucleotides (DNA/RNA) and lipids (Islam et al., 2018). So far, the 2OG oxygenases that modify proteins have been reported to catalyse prolyl, lysyl, asparaginyl, arginyl, aspartyl, and histidyl hydroxylation (Singleton et al., 2014; Feng et al., 2014; Markolovic et al., 2018; Lando et al., 2002; Wilkins et al., 2018; Stenflo et al., 1989; Ge et al., 2012).

Consistent with wide-ranging substrate specificities, 2OG oxygenases are functionally diverse, with a variety of reported roles including gene expression regulation, translation, extracellular matrix modelling and fatty acid metabolism (Figure 1.3). Moreover, a significant proportion of 2OG oxygenases remains largely understudied and their functions have yet to be fully understood. Nonetheless, it is clear that 2OG oxygenases regulate fundamentally important processes as most have been linked with at least one, and in many cases, multiple disorders. These include developmental, neurological, cardiovascular and immunological disorders, as well as cancer (reviewed in Johansson et al., 2014; Ploumakis and Coleman, 2015).

1.1.2.1 Hydroxylation of extracellular and membrane proteins

Historically, hydroxylation was first identified in humans as a post-translational modification in fibrillar collagen (Kivirikko and Prockop, 1967). Collagens account for 90% of the extracellular matrix (ECM) and are not only essential for the structural integrity of the extracellular space, but also perform signalling functions (Cox, 2021).

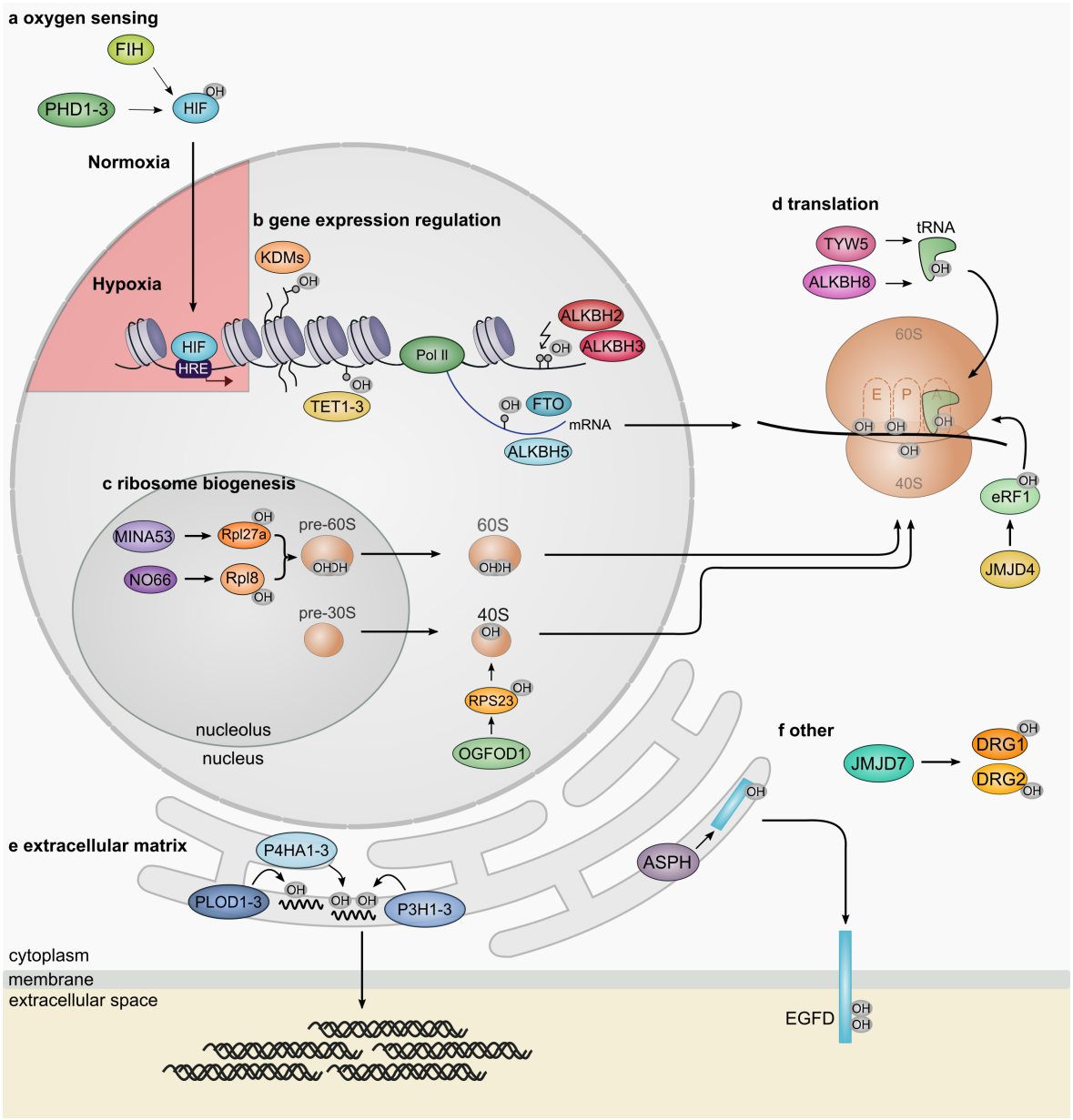


Figure 1.3: Overview of the functional diversity of 2OG oxygenases in cell biology. (**a**) Prolyl hydroxylases (PHD1-3) and Factor-inhibiting HIF (FIH) regulate the hypoxia response through hydroxylation of the hypoxia-induced factor (HIF). (**b**) Histone lysine demethylases (KDMs) and ten-eleven-translocation (TET1-3) proteins regulate gene expression through demethylation of histone tails and DNA, respectively. Alkylated DNA repair protein alkB homologue 5 (ALKBH5) and fat mass and obesity-associated protein (FTO) regulate mRNA by catalysing demethylation of N^6-methyladenosine. Genomic integrity is guarded by ALKBH2/3. (**c**) Ribosomal oxygenases myc-induced nuclear antigen 53 (MINA53) and nucleolar protein 66 kDa (NO66) hydroxylate large ribosomal subunit proteins RPL27A and RPL8, respectively. OGFOD1 targets the small ribosomal subunit protein RPS23. (**d**) ALKBH8 and tRNA-yW synthesising enzyme 5 (TYW5) hydroxylate tRNA to ensure accurate translation. Hydroxylation of eRF1 by JMJD4 is required for efficient translation termination. (**e**) Procollagens are hydroxylated on prolyl and lysyl residues by P3/4HA1-3 and PLOD1-3, respectively, during collagen biogenesis in the endoplasmic reticulum. (**f**) The functional consequence of hydroxylation of DRG1/2 and EGFD-containing proteins by JMJD7 and ASPH, respectively, remains to be fully elucidated. Figure was created using Inkscape.

Collagen fibrils consist of helices composed of three collagen chains. During the biogenesis process, collagens are extensively modified by a variety of modifications, including hydroxylation. Three subfamilies of 2OG oxygenases catalyse hydroxylation of proline and lysine residues (reviewed in Gjaltema and Bank, 2017): three **prolyl 4-hydroxylase α-subunit (P4HA1-3)** enzymes mediate hydroxylation of various proline to 4-hydroxyproline in procollagen which is important for thermal stability of the triple helix. An additional three **prolyl 3-hydroxylases (P3H1-3)** hydroxylate specific residues (Pro987, Pro944 and Pro707, respectively), which destabilises the collagen fold to allow for other modifications. Conversion of lysine to hydroxylysine is catalysed by three **procollagen-lysine-2-oxoglutarate-5-dioxygenases (PLOD1-3)** and is subsequently further modified by glycosylation.

Aberrant hydroxylation of procollagen results in degradation with a consequent reduction in collagen deposition in the extracellular space, which is, perhaps unsurprisingly, associated with both genetic and acquired connective tissue disorders such as osteogenesis imperfecta or osteoporosis (reviewed in Gjaltema and Bank, 2017). Abnormalities in the ECM also support cancer progression, including through regulation of cell proliferation, differentiation, cell survival, invasion and migration (reviewed in Cox, 2021).

Aspartate/asparagine-β-hydroxylase (AspH, BAH) is a 2OG oxygenase that is anchored to the membrane of the endoplasmic reticulum (ER) and catalyses asparaginyl and aspartyl hydroxylation in epidermal growth factor-like domains (EGFDs; Stenflo et al., 1989). EGFDs are typically present in extracellular domains of transmembrane proteins, including Notch (Campbell and Bork, 1993). Although the function of EGFD hydroxylation remains unclear, aberrant AspH expression (both overexpression and loss of expression) evokes tumour promoting properties such as increased cell proliferation, invasion and migration (Dinchuk et al., 2002; de la Monte et al., 2006; Dong et al., 2015). Interestingly, recent insights into the crystal structure revealed that AspH binds EGFDs in an unusual manner, which led the authors to speculate that AspH could act as a chaperone recognising misfolded (EGFDs; Pfeffer et al., 2019).

1.1.2.2 Epigenetic regulation of gene expression

During normal development, as cells transition from a stem cell-like phenotype to differentiated cells, they switch specific sets of genes on and off. Regulation of gene expression at this level is achieved through proteins that covalently modify either the DNA directly, or the histone proteins around which the chromatin is organised (Gibney and Nolan, 2010). Over the last decade, it has become increasingly clear that 'epigenetic' gene expression regulation plays a pivotal role in the progression of diseases such as cancer (Sharma et al., 2010).

Histone proteins are octamers (comprising two copies of H2A, H2B, H3 and H4) that contain N-terminal tails which are subject to a variety of reversible post-translational modifications including phosphorylation, acetylation, methylation, sumoylation and ubiquitination (reviewed by Bannister and Kouzarides, 2011). Histone tail modifications affect chromatin structure and gene transcription and represent a major level of epigenetic gene expression regulation (Bannister and Kouzarides, 2011). Histone tail methylation is catalysed by histone methyltransferases that transfer methyl groups onto the ε-amino groups of lysine (K) and arginine (R) residues in histones H3 and H4. Lysines can be mono-, di- or trimethylated, whereas arginines can be mono- and dimethylated. Depending on the residue, methylation can either activate or repress transcription (Bannister and Kouzarides, 2011; Gibney and Nolan, 2010).

Two distinct protein families are known to catalyse the reverse reaction, demethylation. First identified were the flavin-dependent lysine-specific demethylases (LSDs/ KDM1) that can demethylate mono- and di-methylation (Shi et al., 2004). The second family of histone demethylases is a subfamily of 2OG oxygenases characterised by the presence of a 'jumonji-C' (JmjC) catalytic domain. This domain was first identified in the protein product of the *jumonji* (*jmj*) gene. Jumonji means 'cruciform' in Japanese and the gene was named after the abnormal development of the neural groove of *jmj* mutant mice (Takeuchi et al., 1995). It was later appreciated that JmjC domain-containing proteins belong to the larger family of 2OG oxygenases.

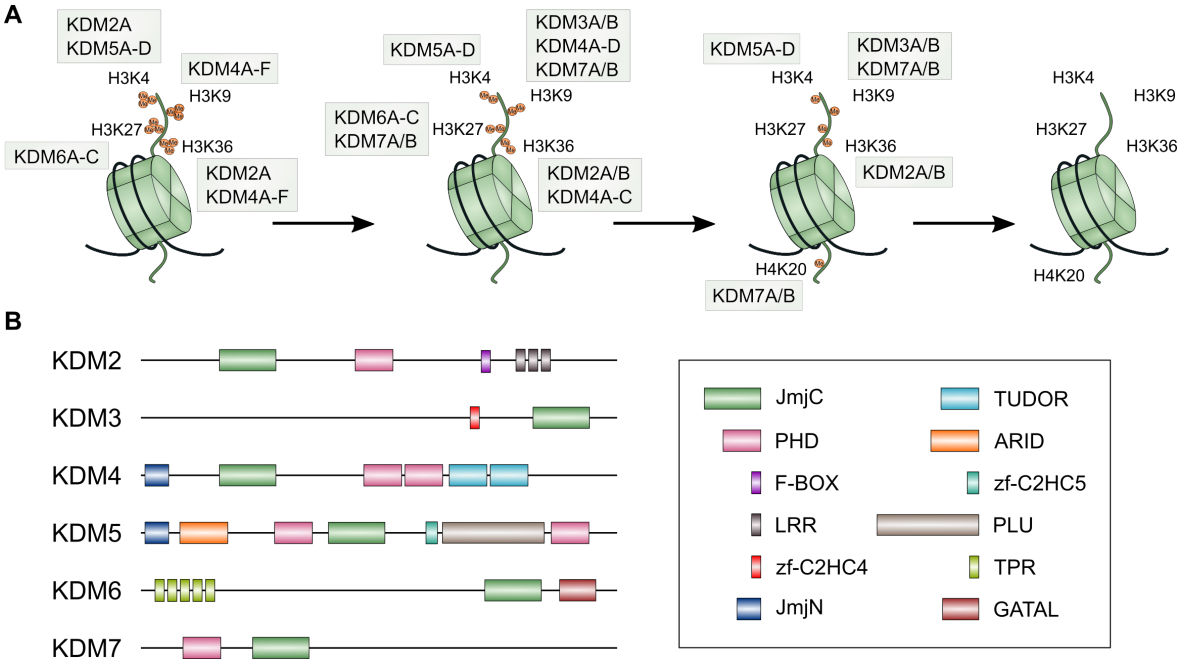


Figure 1.4: Histone lysine demethylases. (**A**) Overview of substrate specificities. KDMs target mono-, di- and trimethylated lysine residues on lysine 4 (H3K4), 9 (H3K9), 27 (H3K27) and 36 (H3K36) on the tail of histone 3 and lysine 20 on histone 4 (H4K20). (**B**) Summary of the domain organisation of the KDM subfamilies. Note: not all members of a subfamily contain all domains outlined in this figure. Abbreviations: JmjC/JmjN = Jumonji-C/Jumonji-N, PHD = plant homeobox, LRR = leucine-rich repeat, zf = zinc finger, ARID = AT-rich interaction domain, TPR = tetratricopeptide repeat, GATAL = GATA-like. (**A-B**) Figure was created with Inkscape.

Approximately 20 human JmjC domain-containing histone lysine demethylases (KDMs) catalyse demethylation *via* a hydroxylation reaction. Hydroxylation of the ε-methyl group produces an unstable intermediate that triggers spontaneous release of the methyl group as formaldehyde. Unlike the flavin-dependent demethylases (LSDs), KDMs can remove all three mono-, di- and trimethylated methyl groups (Johansson et al., 2014). They represent the largest subfamily of 2OG oxygenases and can be subdivided into 7 groups (KDM2-7) based on sequence homology, domain organisation and substrate specificity (reviewed in Johansson et al., 2014 and summarised in Figure 1.4). Along with a JmjC catalytic domain, KDMs generally contain additional functional domains (e.g. ARID, plant homeobox (PHD) domains or Zinc fingers) to mediate nucleotide interaction (Figure 1.4B). Mutations in KDMs are frequently associated with developmental disorders and cancer (Johansson et al., 2014).

In addition to histone tail modifications, gene expression can be regulated through direct methylation of the DNA. DNA methyltransferases (DNMTs) catalyse methylation of the fifth carbon of cytosines (5-methylcytosine, 5mC), mostly in CpG dinucleotides. DNA methylation in somatic cells generally induces transcriptional repression (Greenberg and Bourc'his, 2019). Active reversal of DNA methylation is catalysed by the **Ten-Eleven Translocation (TET)** subfamily of 2OG oxygenases. TET1-3 consecutively catalyse conversion of 5-methylcytosine (5mc) to 5-hydroxymethylcytosine (5hmC), 5-formylcytosine and 5-carboxylcytosine, all of which promote demethylation (Figure 1.5; Tahiliani et al., 2009; Ito et al., 2011). Like DNA, RNA can be modified to regulate gene expression. One of the most prevalent mRNA modifications that is thought to regulate stability, splicing and translation, is N^6-methyladenosine (m^6A; Meyer and Jaffrey, 2014). The reverse reaction is catalysed by two 2OG oxygenases, **alkylated DNA repair protein alkB homologue** (**ALKBH5**; Zheng et al., 2013) and **fat mass and obesity-associated protein** (**FTO**; Jia et al., 2011). An overview of the m^6A demethylation reaction is shown in Figure 1.5.

1.1.2.3 Regulators of cellular stress responses

2OG oxygenases are dependent on the availability of cofactors for catalytic activity and are therefore susceptible to changes in metabolism/cellular environment. Consequently, all 2OG oxygenases may act as stress responders (reviewed by Fletcher and Coleman, 2020). For instance, gene expression regulation by histone lysine demethylases KDM3A/B is regulated by ascorbate availability (Ebata et al., 2017). Moreover, 2OG oxygenases have been implicated in DNA repair and are vital in regulating the hypoxic stress response.

Oxygen sensing by the prolyl hydroxylases and factor-inhibiting HIF

Probably the most famous members of the wider 2OG oxygenase family are the hydroxylases that function as oxygen sensors through modification of the transcription factor Hypoxia-Inducible Factor (HIF). HIF is a heterodimer consisting of an alpha

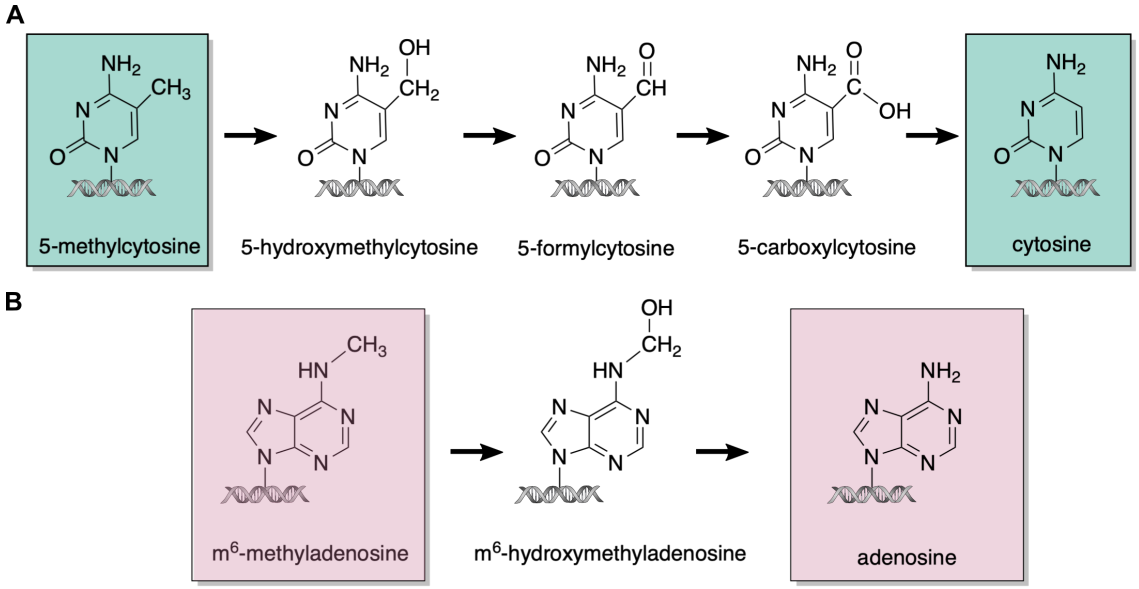


Figure 1.5: Nucleotide demethylation catalysed by the TET, ALKBH5 and FTO enzymes. (**A**) Ten-Eleven Translocation (TET) 1-3 catalyse the conversion of 5-methylcytosine to 5-hydroxymethylcytosine, 5-formylcytosine and 5-carboxylcytosine. (**B**) Alkylated DNA repair protein alkB homologue (ALKBH5) and fat mass and obesity-associated protein (FTO) catalyse demethylation of N^6-methyladenosine to adenosine via hydroxylation. (**A,B**) Figure was created using ChemDraw 19.1 and Inkscape.

(HIFα) and beta (HIFβ) subunit. HIF is only activated in response to low oxygen, when it initiates transcription of a wide range of target genes that regulate various cellular processes such as differentiation, angiogenesis, cell survival, metabolism, etc. (Schofield and Ratcliffe, 2004).

While HIFβ is constitutively expressed, activity and stability of HIFα is carefully regulated. In the presence of oxygen, three **prolyl hydroxylase-domain containing proteins** (**PHD1-3**, also called EglN2, EglN1 and EglN3, respectively) hydroxylate HIFα on two conserved prolyl residues, P402 and P564 (Ivan et al., 2001; Masson et al., 2001; Epstein et al., 2001; Bruick and McKnight, 2001). Hydroxylated HIFα is subsequently recognised by the E3 ligase von Hippel-Lindau (pVHL), ubiquitinated and degraded by the proteasome (Maxwell et al., 1999; Ohh et al., 2000; Ivan et al., 2001; Jaakkola et al., 2001). In addition to the prolyl hydroxylases, a fourth hydroxylase was identified to interact with and inhibit HIF transcriptional activity (Mahon et al., 2001). **Factor-inhibiting HIF** (**FIH**) catalyses hydroxylation of asparagine 803 in

a transactivation domain of HIFα, a modification which interferes with binding of the transcriptional co-activators p300/CREB-binding protein (CBP; Lando et al., 2002; Hewitson et al., 2002).

In hypoxic conditions, the PHDs and FIH are rendered inactive, thereby stabilising HIFα and allowing association with the constitutively expressed HIFβ subunit and transcriptional co-activators p300/CBP. In the nucleus, HIF binds to over a hundred HIF responsive elements (HREs) and initiates transcription of HIF target genes (Schofield and Ratcliffe, 2004; Figure 1.3a).

Reversal of DNA methylation damage by ALKBH2/3

In addition to enzymatic methylation by means of gene regulation, as discussed in section 1.1.2.2, 'random' DNA methylation can occur as a result of exposure to alkylating agents. This type of damage threatens genome integrity and therefore requires repair. In eukaryotes, two members of the alkylated DNA repair protein alkB homologue (ALKBH) subfamily, **ALKBH2** and **ALKBH3**, are responsible for demethylation of 1-methyladenine and 3-methylcytosine (Duncan et al., 2002).

ALKBH2 and ALKBH3 are homologues of the *Escherichia coli* protein alkB that also functions as a DNA demethylase (Falnes et al., 2002). Six other human homologues exist (ALKBH1,4-8), one of which (ALKBH5) demethylates mRNA and has been mentioned above. The functions and biochemical activities of the other five are less clear but include hydroxylation/demethylation of protein, RNA and/or DNA (Ploumakis and Coleman, 2015).

1.1.2.4 Regulation of translation by 2OG oxygenases

Translation is a central theme in 2OG oxygenase biology (reviewed in Zhuang et al., 2015) that starts at the earliest step: production of the translation machinery. Ribosomes are the molecular machines that translate the mRNA messages to functional proteins. Therefore, the rate of translation is directly correlated with the number of ribosomes present in the cell. Ribosome biogenesis starts with the transcription of ri-

bosomal RNA (rRNA) in the nucleolus (Pelletier et al., 2017). A subset of the histone demethylases, KDM2 family members KDM2A and KDM2B, and KDM7 family member PHF8 localise to the nucleolus and regulate rRNA transcription (Frescas et al., 2007; Tanaka et al., 2010; Feng et al., 2010). Moreover, abovementioned 2OG oxygenase ALKBH2 has been implicated in repair of ribosomal DNA (rDNA) methylation damage (Li et al., 2013).

Transcribed rRNAs are subsequently assembled into ribosomal subunits together with ribosomal proteins (RPs) that were translated in the cytoplasm and subsequently imported in the nucleolus (Pelletier et al., 2017). RPs are subject to a range of post-translational modifications, including hydroxylation. Two related hydroxylases, **myc-induced nuclear antigen 53 kDa** (**MINA53**; herein referred to as MINA) and **nucleolar protein 66 kDa (NO66)**, catalyse histidyl hydroxylation of, respectively, large ribosomal subunit proteins RPL27A and RPL8 (uL15 and uL2 according to the new naming system (Ban et al., 2014)) on pre-60S subunits (Ge et al., 2012). Moreover, a third hydroxylase that is distantly related to the HIF prolyl hydroxylases, **2-oxoglutarate and Fe(II)-dependent oxygenase domain-containing protein 1 (OGFOD1)**, targets the small ribosomal subunit protein RPS23 (uS12 according to the new naming system (Ban et al., 2014)) on proline-62 (Singleton et al., 2014). The function of ribosomal hydroxylation remains elusive, but structural analyses have indicated that the hydroxylated proteins occupy functionally important sites within the ribosome (Yanshina et al., 2015; Singleton et al., 2014; Chandramouli et al., 2008; Yanshina et al., 2020). Ribosomal hydroxylation will be further discussed in section 1.2.

Following assembly, the ribosomal subunits are transported to the cytoplasm where the mature ribosome is assembled and translation can be initiated (Pelletier et al., 2017). Accurate translation requires post-transcriptional modifications at the level of tRNA (an overview of tRNA modifications, their functions and associated diseases is presented in Duechler et al., 2016). Some tRNAs, for instance, contain hypermodified bases that are acquired through biosynthetic pathways. Arginine and glycine tR-

NAs, for example, contain a hypermodified 5-methoxycarbonyl-hydroxymethyluridine ($mchm^5U$) within the anticodon loop, and synthesis of this hypermodified base requires the 2OG oxygenase **ALKBH8** (Fu et al., 2010; van den Born et al., 2011). Likewise, hydroxywybutosine is a hypermodified guanosine at position 37 found in mammalian phenylalanine-tRNA. Modification of wybutosine to hydroxywybutosine occurs in the penultimate step of its biosynthetic pathway and is catalysed by the 2OG oxygenase **tRNA-yW synthesising enzyme 5** (**TYW5**; Noma et al., 2010).

Finally, hydroxylation of eukaryotic release factor 1 (eRF1) by **jumonji domain-containing protein 4 (JMJD4)** is required for efficient translational termination (Feng et al., 2014). In eukaryotes, translation termination is triggered by hydrolysis of peptidyl-tRNA in the peptidyl transferase centre, which is mediated by a heterodimeric complex consisting of release factors eRF1 and eRF3. eRF1 is responsible for initial recognition of a stop codon in the mRNA sequence, after which eRF3 hydrolyses GTP. Following GTP hydrolysis, eRF1 initiates hydrolysis of the peptidyl tRNA and release of the polypeptide (Alkalaeva et al., 2006). JMJD4 catalyses C4 lysyl hydroxylation of K63 in a highly conserved NIKS motif within the stop codon recognition domain of eRF1 and promotes release of the protein product from the ribosome. Inhibition of K63 hydroxylation results in stop codon readthrough *in vivo* (Feng et al., 2014). Hydroxylation of K63 in eRF1 is nearly complete (>90%), consistent with a positive role for JMJD4 in translation termination (Feng et al., 2014).

1.1.2.5 Fatty acid metabolism

β-oxidation of fatty acids in the mitochondria produces acetyl-CoA which can be used in the Krebs' cycle to produce ATP (Figure 1.6). For β-oxidation to occur, fatty acids must be transported into the mitochondria, a process which requires carnitine as a carrier. Carnitine can either be ingested *via* the diet or it can be synthesised by the cell from proteins that contain trimethylated lysines (i.e. histones, see above). N^{ε}-trimethyl lysine is generated by lysosomal hydrolysis, after which carnitine is synthesised in the cytosol in four steps, the first and last of which are catalysed by the 2OG oxygenases

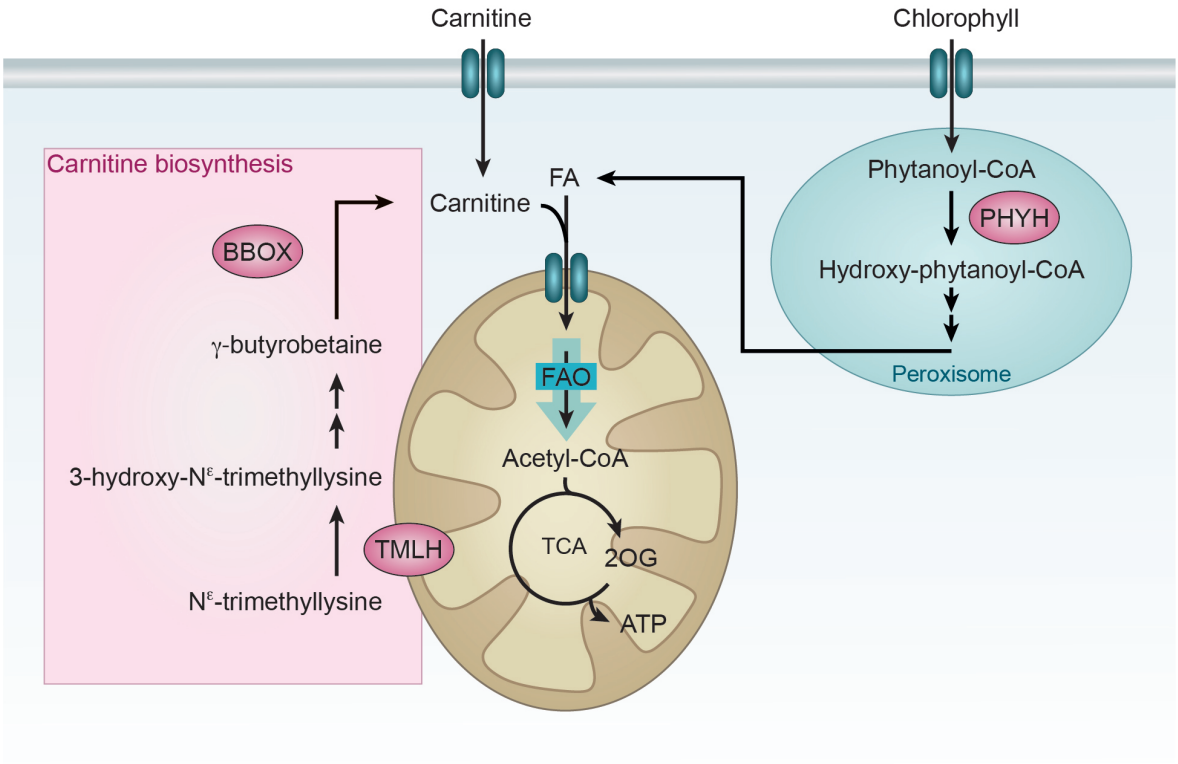


Figure 1.6: Lipid hydroxylation and regulation of fatty acid metabolism by 2OG oxygenases. Following lysosomal proteolysis, N^{ε}-trimethyllysine is hydroxylated by the mitochondrion-associated 2OG oxygenase N^{ε}-trimethyl lysine hydroxylase (TMLH). Following subsequent modifications of 3-hydroxy-N^{ε}-trimethyllysine, the resulting γ-butyrobetaine is hydroxylated by γ-butyrobetaine (BBOX) hydroxylase to form carnitine. In addition to biosynthesis, carnitine can also be transported into the cell following dietary food intake. Dietary chlorophyll is converted into phytanoyl-CoA, which is subsequently subjected to a series of peroxisomal modifications, including hydroxylation by phytanoyl-CoA hydroxylase (PHYH), that allow metabolisation of the fatty acid through mitochondrial β-oxidation (fatty acid oxidation, FAO). Abbreviations: FA = fatty acid. TCA = tricarboxylic acid. 2OG = 2-oxoglutarate. Figure was created using Adobe Illustrator.

N^{ε}-trimethyl lysine hydroxylase (TMLH) and **β-butyrobetaine hydroxylase (BBOX)**, respectively (Vaz and Wanders, 2002; Loenarz and Schofield, 2011).

Some dietary fatty acids require modification before they can be metabolised. One example of this is phytanic acid (phytanoyl-CoA), which is converted to hydroxy-phytanoyl-CoA by the 2OG oxygenase **phytanoyl-CoA hydroxylase (PHYH)**. Mutations in PHYH cause Refsum's disease, which is characterised biochemically by the accumulation of phytanic acid and can have detrimental neurological effects if untreated (McDonough et al., 2005).

1.1.2.6 Hydroxylases of the JmjC-only family

The aforementioned hydroxylases FIH, MINA, NO66, TYW5 and JMJD4 belong to a subfamily of 2OG oxygenases called the 'JmjC-only' family. As the name suggests, these proteins are characterised by the presence of a JmjC catalytic domain, but lack other immediately recognisable functional domains. The JmjC-only subfamily comprises 10 members - MINA, NO66, FIH, JMJD4-8, TYW5 and HSPBAP1. With the exception of TYW5, all JmjC-only proteins are confirmed or predicted protein hydroxylases. Whereas substrate specificity of the JmjC-only hydroxylases has historically been disputed (discussed below), their functional importance is clear, as evidenced by their association with a variety of diseases including cancer (Ploumakis and Coleman, 2015).

JMJD5 is proposed to regulate a range of biological processes, including cell cycle regulation and mitosis (Hsia et al., 2010; Ishimura et al., 2012; Huang et al., 2013; Wu et al., 2016a; He et al., 2016), p53 signalling (Huang et al., 2015; Ishimura et al., 2016), metabolism (Wang et al., 2014b, 2019a), DNA repair (Suzuki et al., 2006; Amendola et al., 2017), differentiation (Youn et al., 2012; Zhu et al., 2014; Munehira et al., 2017; Fuhrmann et al., 2018) and circadian rhythm (Jones et al., 2010). However, it remains unclear how these observations are linked to its biochemical activity. An *in vitro* peptide screening recently identified JMJD5 as capable of catalysing arginyl hydroxylation of peptides from regulator of chromosome condensation domain-containing protein 1 (RCCD1) and ribosomal protein S6 (RPS6; Wilkins et al., 2018). It is not yet confirmed, however, whether these proteins act as JMJD5 substrates *in vivo*. Nonetheless, *jmjd5* is a fundamentally important gene as demonstrated by its embryonic lethality (Oh and Janknecht, 2012; Ishimura et al., 2012) and links with cancer (Zhang et al., 2015; Zhao et al., 2015; Wang et al., 2018).

The gene encoding **JMJD6** was originally identified in a screen aimed at identifying receptors for phosphatidylserine, a phospholipid that is displayed on apoptotic cells and targets them for clearance (Fadok et al., 2000). However, later studies found

that JMJD6 contains a JmjC domain and localises to the nucleus, rather than being a membrane receptor (Cikala et al., 2004; Cui et al., 2004). Following the identification of the JmjC domain, a domain then considered to be characteristic of histone demethylases, JMJD6 was reported to catalyse histone arginine demethylation (Chang et al., 2007). Later, JMJD6 was also reported to hydroxylate methylated arginine residues of non-histone substrates, including the oestrogen receptor α (Poulard et al., 2014), RNA helicase A (Lawrence et al., 2014), heat shock protein 70 (HSP70; Gao et al., 2015), TNF receptor-associated factor 6 (Tikhanovich et al., 2015) and stress granule-nucleating protein G3BP1 (Tsai et al., 2017). In addition to arginine, JMJD6 was also proposed to function as a histone lysine hydroxylase (Unoki et al., 2013). Biochemical and crystallographic studies have however indicated that the catalytic activity of JMJD6 is likely to be restricted to lysyl hydroxylation of non-histone proteins (Mantri et al., 2010; Islam et al., 2019). Reported lysine hydroxylation substrates include the arginine-serine-rich (RS) domain of splicing factor U2 small nuclear ribonucleoprotein auxiliary factor 65-kilodalton subunit (U2AF65; Webby et al., 2009; Mantri et al., 2011) and p53 (Wang et al., 2015b). In support of a role in RNA biology, proteomic analyses identified interactions between JMJD6 and other splice factors, and JMJD6 also binds single-stranded RNA (Heim et al., 2014; Hong et al., 2010). Treatment of cells with DNase I or RNase A confirmed that JMJD6 is more likely to associate with RNA (Hahn et al., 2010). Perhaps consistent with a broad range of reported substrates, JMJD6 is reported to regulate a variety of cellular processes, including cell cycle regulation, angiogenesis and apoptosis (Boeckel et al., 2011; Wan et al., 2019). Furthermore, JMJD6 also has reported functions that are independent of its catalytic activity, including adipocyte differentiation (Reyes-Gutierrez et al., 2019). Altered JMJD6 expression in humans has been associated with chronic hepatitis B pathogenesis (Chen et al., 2014), Huntington's disease (Ratovitski et al., 2015), pre-eclampsia (Alahari et al., 2015, 2018), diabetes (Yanagihara et al., 2017) and Waardenburg syndome, a genetic condition characterised by facial abnormalities, hypopigmentation and hearling loss (Wu et al., 2015). Furthermore, overexpression of JMJD6 has been noted

in various cancers such as breast cancer (Lee et al., 2012; Poulard et al., 2015; Aprelikova et al., 2016), lung cancer (Zhang et al., 2013), colorectal cancer (Wang et al., 2014a), oral squamous cell carcinoma (Lee et al., 2016), melanoma (Liu et al., 2017), hepatocellular carcinoma (Wan et al., 2019) and glioblastoma (Miller et al., 2017). Although some of the molecular mechanisms have been attributed to now challenged catalytical activities, *jmjd6* is undisputedly an essential gene, as knockout mice die shortly after birth and show significant developmental defects of multiple organs, including the intestine, liver, kidneys, lungs, eyes and heart (Böse et al., 2004; Schneider et al., 2004).

JMJD7 was recently found to target Developmentally Regulated GTPase 1 and 2 (DRG1/2), two closely related members of a highly conserved family of TRAnslation FACtor (TRAFAC) GTPases, for hydroxylation (Markolovic et al., 2018). The functional consequences of hydroxylation of lysine 22 and 21 in DRG1 and DRG2, respectively, are yet to be fully elucidated. Previous studies identified DRGs as RNA interactors (Ishikawa et al., 2003). Consistent with this, Markolovic and colleagues found that mutation of K21 or knockdown of JMJD7 affects the RNA binding affinity of DRG2 *in vitro* (Markolovic et al., 2018). Although further work is required to confirm this hypothesis in a cellular context, this observation potentially further expands the emerging roles for 2OG oxygenases in gene expression/translation.

The catalytic potential of **JMJD8** has been questioned as it contains an aspartic acid-to-histidine substitution at one of the conserved iron-coordinating residues (Yeo et al., 2017). Studies on FIH have however indicated that two histidines may be sufficient for iron binding and catalytic activity (Hewitson et al., 2008), raising the possibility that JMJD8 substrates may exist and are yet to be identified. JMJD8 localises to the cytoplasm and is enriched in the endoplasmic reticulum due to the presence of a signal peptide. Removal of the signal peptide, however, allows translocation to the nucleus (Yeo et al., 2017; Khoueiry et al., 2017). Nuclear JMJD8 has been proposed to function as a transcriptional co-repressor of the DNA hydroxylase TET1 (Khoueiry

et al., 2017). JMJD8 also has reported roles in cellular metabolism (Boeckel et al., 2016; Yeo et al., 2017), NFκB-signalling (Yeo et al., 2016; Su and Wang, 2019; Wang et al., 2019b) and abberrant expression has been associated with cancer (Ding et al., 2013; Wang et al., 2019b).

In addition to the aforementioned protein HIF, **FIH** targets arginine residues in proteins that contain ankyrin repeat domains (ARDs) for hydroxylation. ARDs are protein-protein interaction modules found in over 300 functionally diverse proteins. Among those shown to be targeted by FIH are NFκB precursor p105 and the NFκB inhibitor IκBα (Cockman et al., 2006), the intracellular domain of Notch1 (Coleman et al., 2007), suppressor of cytokine signalling box protein 4 (ASB4; Ferguson et al., 2007), myosin phosphatase target subunit 1 (MYPT1; Webb et al., 2009), cytoskeletal ankyrin family member AnkyrinR (Yang et al., 2011a) and HECT domain and ankyrin repeat-containing E3 ubiquitin protein ligase 1 (HACE1; Kim et al., 2019). However, proteomic screens have indicated that these may just be the tip of the iceberg, and that asparaginyl hydroxylation may be a ubiquitous modification of ARD-containing proteins (Cockman et al., 2009). The functional consequences of FIH-catalysed ARD hydroxylation may include modulation of protein-protein interactions, as has been proposed for AnkyrinR and the recently identified E3 ubiquitin ligase HACE1 (Yang et al., 2011a; Kim et al., 2019).

Heat shock protein beta-1 (HSPB1/Hsp27) associated protein 1 (HSPBAP1) was originally identified as interacting with heat shock protein 27 (Liu et al., 2000; Jiang et al., 2001) and has mainly been studied in relation to neurological conditions, including epilepsy (Xi et al., 2007, 2009; Kumar and Reddy, 2018; Srivastava et al., 2012). Nonetheless, HSPBAP1 is expressed in other tissues (Jiang et al., 2001) and has been linked with cancer (Saeed et al., 2015; Yang et al., 2015). Thus far, a substrate has not been identified.

The JmjC-only family: hydroxylases or histone demethylases?

Given the presence of the JmjC catalytic domain, several of the JmjC-only family members have been proposed to catalyse histone demethylation. Indeed, KDMs and JmjC-only hydroxylases have likely evolved from a common prokaryotic ancestor (Chowdhury et al., 2014). However, extensive biochemical and crystallographic studies have indicated that KDMs and JmjC-only hydroxylases represent two subfamilies with distinct structural features and substrate specificities, and that most JmjC-only oxygenases function as hydroxylases rather than demethylases (Chowdhury et al., 2014; Williams et al., 2014; Markolovic et al., 2016; Islam et al., 2019).

Key differences between KDMs and JmjC-only hydroxylases can be observed in their overall domain architecture. KDMs generally contain multiple additional non-catalytic domains required for nucleotide and/or histone binding (Markolovic et al., 2016). JmjC-only hydroxylases lack these characteristic domains and are much shorter. Instead, a common feature of JmjC-only hydroxylases, but not histone demethylases, is the presence of a dimerisation domain that may mediate non-histone substrate binding (Lancaster et al., 2004; Mantri et al., 2010; Kato et al., 2011; Del Rizzo et al., 2012; Chowdhury et al., 2014; Markolovic et al., 2018).

Structural differences are also observed within the catalytic pocket itself. Hydroxylases that target carbons in the middle of the amino acid side chain, like the JmjC-only hydroxylases, generally contain an open active site conformation. In contrast, methylation of lysine occurs at the terminus of the side chain, and therefore the catalytic site of lysine demethylases tend to be narrower and the hydroxylation reaction occurs deeper within the catalytic domain (Markolovic et al., 2016). Furthermore, as discussed by Markolovic and colleagues, the type of interactions between enzyme and substrate differ between KDM and JmjC-only hydroxylases. Whereas KDMs form hydrophobic interactions, JmjC-only hydroxylases appear to use hydrogen bonds. Available enzyme-substrate crystal structures also suggest that JmjC-only hydroxylases bind their substrates with opposite N-to-C directionality, compared to KDMs (Chowdhury et al., 2014; Markolovic et al., 2016).

Despite the seemingly subfamily-specific structural variations, the question remains whether flexibility within the catalytic pocket would make it possible for members of the JmjC-only family to accommodate histone substrates. *In vitro* studies, however, do not support this possibility. Neither MINA (Ge et al., 2012), NO66 (Ge et al., 2012), JMJD5 (Wilkins et al., 2018), JMJD6 (Islam et al., 2019) or JMJD7 (Markolovic et al., 2018) are successful in catalysing demethylation of their reported histone substrates under conditions in which other histone demethylases are active. Importantly, under the same conditions all these enzymes were capable of catalysing stable hydroxylation of peptide substrates.

1.2 Ribosomal hydroxylation

Thus far, four 2OG oxygenases have been identified that catalyse ribosomal protein hydroxylation, one in prokaryotes, and three in eukaryotes. Before reviewing ribosomal hydroxylase biology and function, an introduction to protein synthesis is provided.

1.2.1 Overview of the ribosome and translation

The mature human 80S ribosome consists of a large (60S) and small (40S) subunit. The two subunits, each containing a set of ribosomal proteins (RPs) as well as ribosomal RNAs (rRNAs), cooperate in order to translate messenger RNAs into polypeptides (Lodish et al., 2007). The 40S subunit is responsible for binding and scanning of the mRNAs. Upon recognition of a start codon, tRNAs are recruited to the 60S subunit, which generates the peptide bonds. The 60S subunit contains three tRNA binding sites. The amino acid-carrying tRNA is initially recruited to the acceptor (A) site, where the mRNA codon is base-paired with the tRNA anticodon. Subsequently, the tRNA moves to the polypeptide (P) site. Here, the amino acid is transferred from the tRNA to the polypeptide chain. Peptide bond formation is catalysed in the peptide transferase centre (PTC) of the large subunit. Finally, the tRNA is translocated to the exit (E) site, from where it is released for recycling in the cytoplasm (Lodish et al., 2007).

rRNAs and RPs are subject to a variety of modifications (Venezia et al., 2019). Post-translational modifications of RPs include methylation, acetylation, phosphorylation and ubiquitination (Odintsova et al., 2003; Yu et al., 2005). Many of these PTMs occur during biogenesis and are vital for the structural integrity and function of the ribosome (Ren et al., 2010; Jack et al., 2011). However, emerging evidence suggests that PTMs of rRNAs and RPs could also regulate translation of specific mRNAs by giving rise to a heterogenetic pool of 'specialised' ribosomes (Xue and Barna, 2012). For example, a recent study indicated that phosphorylation of RPL12 regulates translation of specific mRNAs subsets during mitosis (Imami et al., 2018).

1.2.2 Ribosomal hydroxylases

Consistent with a continuously growing body of evidence supporting a widespread role for 2OG oxygenases in the regulation of gene expression/translation, ribosomal proteins have recently been identified as hydroxylation targets. Moreover, hydroxylation of ribosomal proteins is an evolutionary conserved modification. To date, three 2OG oxygenases have been reported to target ribosomal proteins in humans, MINA, NO66 and OGFOD1 (Ge et al., 2012; Singleton et al., 2014).

1.2.2.1 OGFOD1

2-Oxoglutarate and Fe(II)-dependent oxygenase domain-containing protein 1 (OGFOD1) is a prolyl hydroxylase that is distantly related to the HIF prolyl hydroxylases (Horita et al., 2015). OGFOD1 localises to the nucleus, where it targets the 40S ribosomal sprotein S23 (RPS23) on proline 62 (Singleton et al., 2014). Within the mature ribosome, RPS23 Pro-62 is situated in a conserved loop in the decoding centre (Singleton et al., 2014; Chandramouli et al., 2008). This is a functionally important area responsible for guaranteeing translational accuracy. Indeed, reduced OGFOD1 expression induces a translational stress phenotype, as evidenced by the formation of stress granules (Singleton et al., 2014). Similar phenotypes were observed in primary

fibroblasts carrying a mutation in RPS23 (Arg67Lys) that interferes with hydroxylation (Paolini et al., 2017). Moreover, Paolini and colleagues noted an increase in stopcodon readthrough, an indication of impaired translational fidelity. The patient that carried the mutation presented with intellectual disability, autism spectrum disorder, hearing loss and a range of dysmorphic features (Paolini et al., 2017). Although the function of hydroxylation is not yet fully understood, hydroxylation at Pro-62 is essentially complete, suggesting a positive role safeguarding the structural integrity of the ribosome.

The functional importance of RPS23 hydroxylation is further exemplified by its evolutionary conservation. RPS23 Pro-62 hydroxylation is present in *Drosophila* as well as yeast (Loenarz et al., 2014; Katz et al., 2014). In yeast, loss of OGFOD1 homologue Tpa1p is associated with reduced translational accuracy (Loenarz et al., 2014). In addition to a translational stress phenotype, loss of OGFOD1 is associated with reduced growth and translation both in *Drosophila* and mammals (Loenarz et al., 2014; Katz et al., 2014; Singleton et al., 2014). Consistent with a positive role in translation, high expression of OGFOD1 has been noted in breast cancer (Kim et al., 2015) and laryngeal papilloma (Yin et al., 2020). Moreover, in both reports, OGFOD1 was found to support cell proliferation.

1.2.2.2 NO66, MINA and YcfD

A first hint at a possible function for NO66 and MINA (also called nucleolar protein 52 kDa, NO52) in ribosome biogenesis came from two studies that identified each protein as expressed in nucleoli isolated from *Xenopus laevis* oocytes (Eilbracht et al., 2004, 2005). Moreover, subsequent immunolocalisation studies revealed that both MINA and NO66 localise to the granular component, a nucleolar compartment associated with later stages of ribosome biogenesis, particularly the processing of the preribosomal particles. Succeeding these early studies, combined proteomic and biochemical analyses identified NO66 and MINA as histidyl hydroxylases of 60S ribosomal proteins RPL8 His-216 and RPL27A His-39, respectively. Nuclear magnetic resonance (NMR) analyses

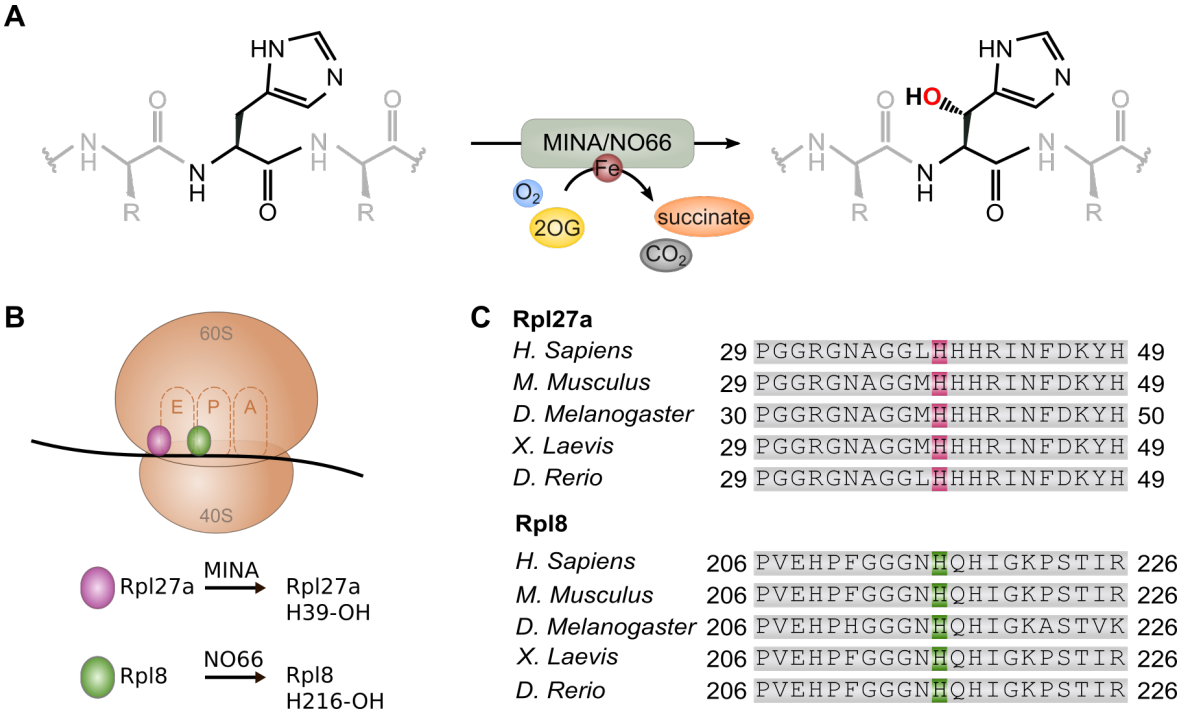


Figure 1.7: MINA and NO66 target conserved histidine residues in ribosomal proteins located close to functionally important sites. (**A**) MINA and NO66 catalyse β-carbon histidyl hydroxylation. (**B**) MINA catalyses hydroxylation of RPL27a His-39, which localised near the tRNA exit site (E-site). NO66 target His-216 of RPL8, located near the peptidyl transferase centre where the peptide bonds formed. (**C**) His-39 and His-216 are evolutionary conserved residues within RPLa and RPL8, respectively. Figure adapted from Bundred, Hendrix, and Coleman (2018).

indicate that hydroxylation occurs on the β-carbon (Ge et al., 2012; Figure 1.7A). Despite the similarities between MINA and NO66, hydroxylation of RPL27A and RPL8 occurs in a non-redundant fashion (Ge et al., 2012).

The consequences of RPL27A and RPL8 hydroxylations are, like RPS23, yet to be fully elucidated, though hydroxylation of both sites was found to be essentially complete (>90%) in several human cancer cell lines and tumour samples as well as in normal human placenta, again supportive of a structural role (Ge et al., 2012). Consistent with this, recent structural studies aimed at predicting the function of RPL8 and RPL27A within the mature ribosome indicated that hydroxylation of both proteins is likely required for proper conformation and stability (Yanshina et al., 2015, 2020). RPL8 is located close to the peptidyl transferase centre (PTC) within the 60S subunit where peptide bond formation is catalysed. Moreover, His-216 is located near the site where P-site tRNA contacts 28S rRNA. The data presented by Yanshina and

colleagues suggest that the hydroxyl group at His-216 introduces a structural rearrangement of the 23S rRNA that ensures proper conformation of the PTC in the mature ribosome (Yanshina et al., 2015). RPL27A is located in the vicinity of the tRNA exit (E) site. Based on recent structural models of the ribosome, Yanshina and colleagues suggested that hydroxylation-mediated hydrogen bonding may stabilise the ribosome and ensure translational activity (Yanshina et al., 2020). Indeed, transfection of exogenous RPL27A mutated at His-39 reduced translational activity of Human Embryonic Kidney 293 T-antigen (HEK293T) cells (Yanshina et al., 2020).

Recent structural and biochemical studies have indicated that ribosomal hydroxylation is evolutionary conserved in prokaryotes. MINA and NO66 share a common ancestor in *Escherichia coli*, YcfD, that catalyses arginyl hydroxylation of the large ribosomal subunit protein L16 at position 81 (Ge et al., 2012). RPL16 Arg-81 is located in proximity to the P-site tRNA. Although the function of Arg-81 is still unclear, RPL16 is reportedly essential for peptidyl transferase activity, association of the subunits and stabilisation of A-site tRNA (Moore et al., 1975; Kazemie, 1975; Voorhees et al., 2009).

Consistent with a function in translation, the ribosomal oxygenases have links with cell proliferation. An increased growth potential was noted upon overexpression of NO66 in NIH3T3 cells, whereas the inverse was true upon NO66 depletion by RNA interference in the lung cancer cell lines LC219 and A549 (Suzuki et al., 2007). Likewise, MINA depletion with small-interfering RNA (siRNA) suppressed the proliferation of human cervical (HeLa), lung (A549) and colon (SW620) carcinoma cells (Tsuneoka et al., 2002; Yu et al., 2014; Teye et al., 2004). However, both NO66 and MINA have reported roles in addition to cell growth, that are unlikely to be explained via their respective roles in bulk ribosome biogenesis, raising the possibility that additional substrates may exist (further discussed in the next section). For instance, in addition to a positive role in proliferation, increased NO66 expression has been associated with an increased invasion and migration potential in colorectal cancer (Nishizawa et al., 2017).

1.3 Additional targets for NO66 and MINA?

Despite the similarities between NO66 and MINA, a growing number of studies would suggest that NO66 and MINA have additional, separate, functions that are likely independent of their roles in ribosome biogenesis.

1.3.1 NO66

A proteomic screen identified NO66 as an interactor and repressor of Osterix (Osx), an osteoblast-specific transcription factor that regulates osteoblast differentiation (Sinha et al., 2010). Short hairpin RNA (shRNA)-mediated suppression of NO66 increased the expression Osx target genes and accelerated osteoblast differentiation in proteoblast cells (Sinha et al., 2010). Although the mechanism for NO66-mediated transcriptional repression remains unclear, a variety of possible mechanisms have been suggested (Figure 1.8). These include recruitment of epigenetic modifiers such as the polycomb repressive complex 2 (PRC2; Brien et al., 2012) or histone deacetylase 1A (HDAC1A; Sinha et al., 2014; reviewed in Bundred et al., 2018). Moreover, like other JmjC-only oxygenases, NO66 has been reported to directly regulate gene expression via histone demethylation (Sinha et al., 2010, 2014). Although unbiased biochemical and structural analyses have indicated that it is unlikely that NO66 has histone demethylase activity (Ge et al., 2012; Chowdhury et al., 2014; Wang et al., 2015a), repression of Osterix target genes is evidently dependent on the catalytic activity of NO66 (Sinha et al., 2010). Taken together, these experiments suggest that NO66 may have additional hydroxylation targets. Consistent with this idea, in addition to nucleolar localisation, NO66 is enriched in nucleoplasmic 'dots' in a variety of cell lines (Eilbracht et al., 2004). The function of NO66 in these dots is unknown, but could perhaps involve a novel substrate related to a cellular process independent of ribosome biogenesis.

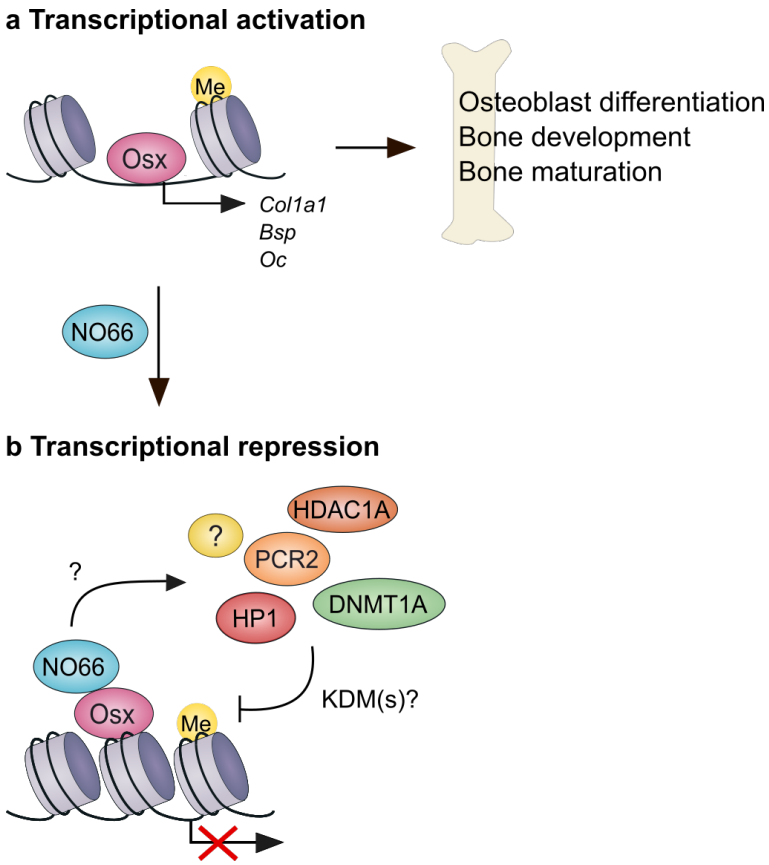


Figure 1.8: NO66 in skeletal development. (**a**) The transcription factor Osterix (Osx) promotes osteoblast differentiation and bone development/maturation via regulation of osteoblast-specific target genes. (**b**) NO66 interacts with the transactivation domain of Osx, ultimately leading to transcriptional repression of Osx target genes. The underlying molecular mechanism remains unclear, but may involve recruitment of epigenetic modifiers. Figure adapted from Bundred, Hendrix, and Coleman (2018).

1.3.2 MINA

Like NO66, MINA has reported cellular activities of which the underlying molecular mechanisms have yet to be confirmed, but that are potentially difficult to explain via a role in protein translation. These include a role in regulation of T-cell differentiation and paradoxical roles in tumourigenesis.

1.3.2.1 Roles for MINA in immunology

Expression studies in mouse tissues identified MINA as a ubiquitously expressed protein, with increased expression in a few organs including testis, colon, spleen and thymus (Tsuneoka et al., 2006). Consistent with high expression in organs with well-known function within the immune system, MINA has been reported to regulate T-cell differentiation: genetic and transcriptional profiling studies in mice identified MINA as a determinant of T helper type 2 (T_H2) bias (Okamoto et al., 2009). T_H2 bias is the tendency of naïve T cells to differentiate into interleukin-4 (IL-4) secreting T_H2 effector cells. Okamoto et al. found that MINA specifically binds, and thereby represses, the IL4 promoter (Figure 1.9). In addition to T_H2 bias, MINA has been reported to promote T_H17 differentiation (Yosef et al., 2013). In this study, MINA expression was found to be strongly induced during T_H17 differentiation, and signature T_H17 cytokines and transcription factors such as Rorc, Batf and Irf4 were repressed following nanowire-mediated knockdown of MINA by siRNA. Furthermore, knockdown of MINA upregulated the expression of Foxp3, the master regulator of Treg differentiation (Figure 1.9).

Imbalances between T-cell subsets have been linked with autoimmune and inflammatory diseases (Raphael et al., 2016). Consistent with a role for MINA in regulation of multiple T-cell subsets, ablation of MINA expression in mice has been associated with reduced T_H2 and T_H17-related pathological immune responses following treatment with methacholine or silica, respectively (Mori et al., 2013; Thakur et al., 2015).

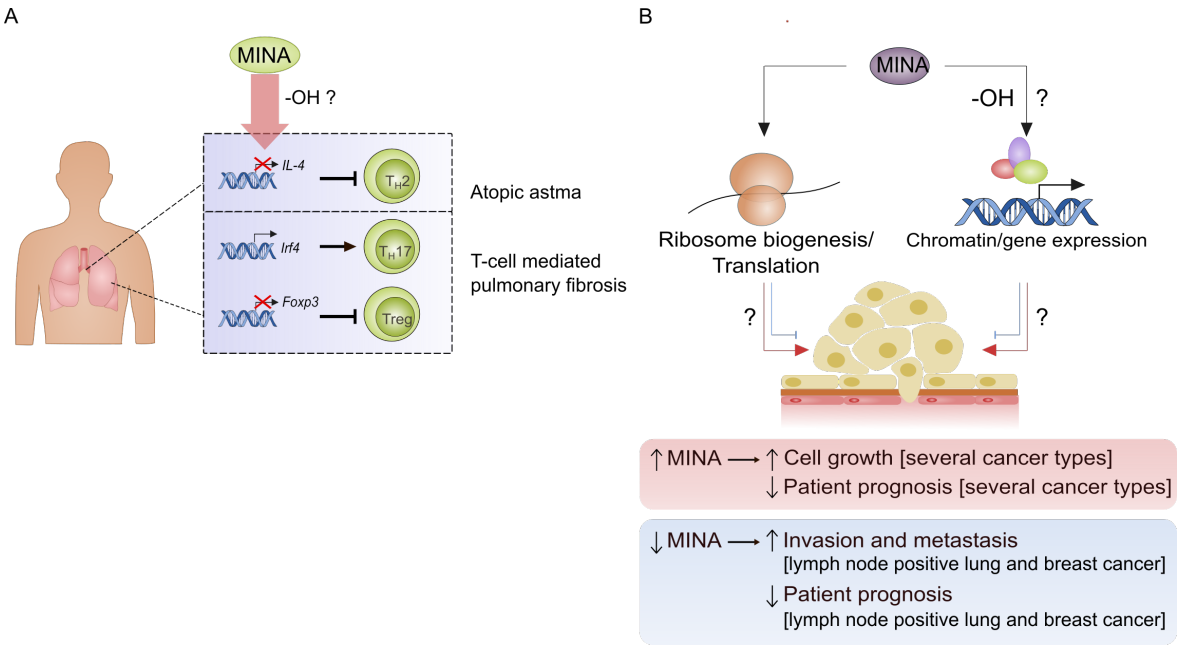


Figure 1.9: MINA is involved in T-cell differentiation and cell proliferation. (**A**) MINA promotes T_H2 differentiation through repression of interleukin (IL-4) expression (top). T_H17 differentiation is promoted through activation of transcription factors such as Irf4, whilst repressing expression of the signature Treg-specific transcription factor Foxp3 (bottom). (**B**) Paradoxical roles of MINA in tumourigenesis. MINA is overexpressed in several human cancer types (red box), potentially through regulation of ribosome biogenesis/translation and chromatin/gene expression. However, MINA may also function as a tumour suppressor in some contexts (blue box), possibly through regulation of invasion/metastasis. Figure adapted from Bundred, Hendrix, and Coleman (2018).

Moreover, MINA has been implicated in the onset of atopic asthma in humans. A study in the Chinese Han population identified a single nucleotide polymorphism (SNP) of the *mina* gene that was associated with an increased risk of atopic asthma (Chen et al., 2011).

Overall, the molecular mechanisms underlying the roles of MINA in immunology are poorly understood. Whether or not they require MINA hydroxylase activity has not yet been studied. However, the links to transcriptional regulation and chromatin association might be consistent with an extra-nucleolar function that is distinct from ribosome biogenesis.

1.3.2.2 Roles for MINA in cancer

Elevated MINA expression levels have been observed in several cancer types, including colon (Teye et al., 2004), oesophageal (Tsuneoka et al., 2004), lung (Zhang et al., 2005; Komiya et al., 2010), gingival squamous cell carcinoma (Kuratomi et al., 2006), renal (Ishizaki et al., 2007), lymphoma (Teye et al., 2007), neuroblastoma (Fukahori et al., 2007), liver (Ogasawara et al., 2010; Huo et al., 2017), gastric (Xing et al., 2014; Aziz et al., 2020), pancreatic (Tan et al., 2014; Kumar et al., 2017), breast cancer (Thakur et al., 2014) and multiple myeloma (Wu et al., 2016b). Moreover, MINA overexpression was associated with poor prognosis in several of these studies (Tsuneoka et al., 2004; Thakur et al., 2015; Fukahori et al., 2007; Xing et al., 2014; Wu et al., 2016b).

Interestingly, evidence has emerged supporting a more complex role for MINA in cancer. Komiya et al. discovered that low MINA expression levels in early stage lung cancer were associated with poor prognosis (Komiya et al., 2010). Overexpression of MINA inhibited cell proliferation in the human lung adenocarcinoma cell line A549, but not in the squamous lung cancer cell line H226B. Instead, manipulation of MINA levels by shRNA increased the number of invading H226B cells (Komiya et al., 2010). Consistent with this observation, MINA knockdown was recently reported to affect the expression of important cell differentiation markers in A549 cells (Geng et al., 2017). Additionally, a study in breast cancer patients underlined the potential context-dependent role of MINA. In this study, MINA expression was found to predict a poor outcome in lymph node negative patients, however the opposite effect was observed in lymph node positive breast cancer patients (Thakur et al., 2014). Furthermore, a study investigating MINA expression levels in oesophageal squamous cell carcinoma highlighted that high MINA expression does not always correlate with high levels of proliferation, as assessed by Ki-67 staining (Tsuneoka et al., 2004).

Although the links between MINA expression in tumours and patient survival are clear, little attention has yet been paid to its relative subcellular distribution in normal versus tumour samples. As such it is not yet clear whether tumour-associated functions

of MINA are restricted to ribosome biogenesis and the nucleolus, or could be related to alternative functions in other subcellular compartments. Furthermore, there has been a general paucity of studies investigating the role of MINA hydroxylase activity in cell biology and disease, including cancer. As such, there is an urgent need to explore alternative functions of MINA and to relate these to its nucleolar versus extra-nucleolar localisation.

1.4 Aim of this study

In this thesis, we aim to increase our understanding of the functions and regulation of 2OG oxygenases, with a specific focus on MINA. It is clear from MINA's complex and evidently context-dependent role in cancer, as outlined in the previous section, that the biology of MINA likely exceeds its role in ribosome biogenesis. However, it is not currently clear which mechanisms might explain some of the observed disease-associated phenotypes, and how MINA's activity is regulated to exert these different roles.

The specific aims of this study were to 1) examine the subcellular localisation of MINA and investigate the factors contributing to the regulation of its localisation; 2) identify and characterise potential novel candidate substrates; 3) examine the extra-nucleolar cellular functions of MINA and investigate to which extent these are dependent on its catalytic activity.

Chapter 2: Physiological and pathological regulation of MINA localisation

2.1 Introduction

MINA expression has been extensively studied in the context of cancer. Studies performed in a range of cancer cell lines have linked high MINA expression levels with a pro-proliferative role (Tsuneoka et al., 2002; Teye et al., 2004; Yu et al., 2014). However, as mentioned in Chapter 1, MINA expression does not always correlate with high levels of proliferation (Tsuneoka et al., 2004; Teye et al., 2004; Tsuneoka et al., 2006). Furthermore, evidence has emerged suggesting that low expression levels could contribute to increased invasion and migration and could therefore promote tumourigenesis (Komiya et al., 2010; Geng et al., 2017). As discussed by Bundred, Hendrix, and Coleman (2018), the molecular mechanisms behind MINA's role in physiology, as well as disease, have yet to be established.

Several studies have characterised the expression and subcellular localisation of MINA. Nucleolar enrichment of MINA is reported in many cancer cell lines, including HeLa cervical adenocarcinoma, SW620 colorectal adenocarcinoma, TE-11 oesophageal squamous cell carcinoma and A549 lung adenocarcinoma cells (Tsuneoka et al., 2002;

Teye et al., 2004; Tsuneoka et al., 2004; Yu et al., 2014). In addition, most of these studies also acknowledged nucleoplasmic localisation of MINA (Tsuneoka et al., 2002, 2004). One study even noted differences in nucleolar/nuclear distribution when comparing cell lines: Eilbracht and colleagues reported that, whereas MINA was highly enriched in the nucleoli of SV80 human lung fibroblasts, MINA was mostly nuclear in human umbilical vein endothelial cells (HUVECs, Eilbracht et al., 2005). However, despite the fact that variations in MINA localisation have been described across cell lines, little consideration has been given to the possibility that MINA might have distinct roles depending on where it is localised in the cell. Although different functional assignments might be consistent with this, including a proposed histone lysine demethylase (KDM) activity, such activities are currently disputed. This raises the possibility that compartment-specific functions of MINA are yet to be fully understood.

Based on MINA's apparent context-dependent oncogenic versus tumour suppressor role (see Chapter 1), as well as its differential localisation, we hypothesise that MINA's subcellular localisation might be regulated, and that MINA's extra-nucleolar functions might contribute to its tumour suppressor activity. The work presented in this chapter describes our efforts to characterise the determinants of MINA's subcellular localisation. The initial observation that MINA staining is heterogeneous in the human colorectal adenocarcinoma cell line Caco-2 prompted us to further explore MINA's response to a variety of factors, including cell density, the presence of ribosomal RNA and oxygen availability.

2.2 Results

2.2.1 Localisation of MINA in common cancer cell lines

Most of the work aimed at characterising MINA has been performed in rapidly proliferating cancer cell lines or tumour samples (Tsuneoka et al., 2002; Teye et al., 2004; Yu et al., 2014). Consistent with a role in protein translation, it is perhaps unsurprising that MINA has been found highly expressed and enriched in the nucleoli of tumour

cells (Tsuneoka et al., 2002; Teye et al., 2004; Tsuneoka et al., 2004; Yu et al., 2014). As a first effort to explore MINA localisation in more detail, we set out to confirm the subcellular localisation of endogenous MINA in a small set of readily available common cancer cell lines. The proto-oncogene *KRAS* is a common driver of cell proliferation in cancer cells, and is often associated with a highly transformed phenotype. Hence, we selected two *KRAS* wild-type cell lines (the colorectal cancer cell line Caco-2 and osteosarcoma cell line U2OS) and two cell lines in which KRAS is constitutively active (the lung adenocarcinoma cell line A549 (KRAS G12S) and colorectal cancer cell line SW620 (KRAS G12V)). Caco-2 and U2OS cells have a more epithelial and flattened morphology, whereas A549 and SW620 cells are mesenchymal and 'transformed' in appearance. As presented in Figure 2.1, indirect immunofluorescence (IF) analysis showed that MINA is enriched in the nucleoli in Caco-2 and U2OS, but also present in a diffuse manner in the nucleoplasm of these cell lines. Interestingly, in Caco-2, we noted a heterogeneous staining pattern: whereas nucleolar enrichment was evident in some cells, in others MINA was found evenly distributed in the nucleoli and nucleoplasm. In contrast to Caco-2 and U2OS, MINA was observed almost exclusively in the nucleoli of A549 and SW620 cells (Figure 2.1).

2.2.2 Generation and characterisation of stable doxycycline-inducible 3xFLAG-MINA Caco-2 cell lines

Caco-2 is an intestinal epithelial cell line derived from a human colorectal adenocarcinoma and is a relatively well-differentiated cell line that undergoes spontaneous enterocytic differentiation in culture and is widely used as a model to study cell polarity/differentiation (Sambuy et al., 2005). As depicted in Figure 2.1, a heterogeneous staining pattern of endogenous MINA was noted in these cells, suggesting that perhaps some level of physiological regulation of MINA localisation might be retained in these cells. For these reasons, we decided that this cell line would be a suitable model to study the localisation of MINA in a semi-physiological context.

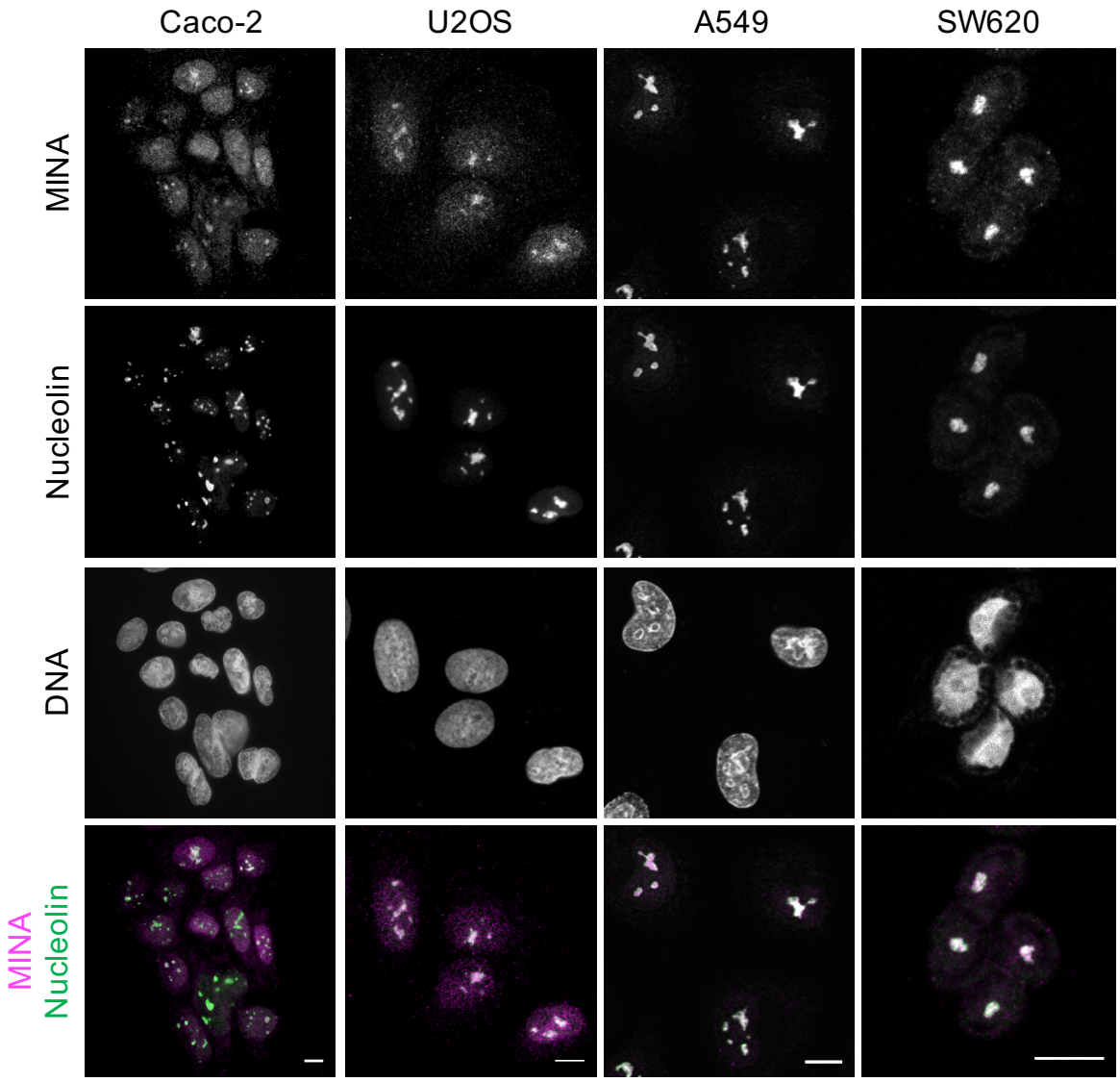


Figure 2.1: Differential localisation of MINA in cancer cell lines. Representative immunofluorescence images showing nucleolar and/or nucleoplasmic MINA staining. Cells were fixed with methanol and stained for endogenous MINA (Invitrogen, cat. no. 39-7300; shown in magenta) and the nucleolar marker nucleolin (green). Nuclei were visualised with DAPI. Scale bars represent 10 µm. Images were acquired using a Zeiss LSM 880 confocal microscope equipped with a 40x (Caco-2, U2OS and A549) or 60x (SW620) C-Apochromat 1.2 W Korr M27 objective and ZEN black software.

In order to study further the determinants controlling MINA localisation, we generated stable cell lines expressing doxycycline (Dox)-inducible 3xFLAG-tagged MINA. Expression of exogenous, tagged MINA does not only allow for easier detection, it also allows us to study MINA variants. cDNA sequences encoding wild-type or catalytically inactive 3xFLAG-tagged MINA were cloned into the pTIPZ lentiviral vector. The sequence encoding catalytically inactive MINA contains an alanine substitution at iron-coordinating residue His-179 (H179A). The pTIPZ vector is a derivative of the commercially available pTRIPZ™ vector (Open Biosystems) that lacks the Turbo red fluorescent protein (TurboRFP) reporter gene. pTIPZ is a Tet-On vector that contains a tetracycline-inducible promoter which, upon addition of doxycycline, drives expression of the gene of interest. Constitutive expression of a puromycin resistance gene allows for selection of successfully transduced cells. A schematic of the pTIPZ vector is shown in Appendix A.

Following antibiotic selection and elimination of any untransduced cells, a doxycycline dose titration was performed to compare overexpression levels between wild-type and catalytically inactive MINA, as well as to compare endogenous and exogenous MINA protein levels, with the ultimate aim of identifying a doxycyline concentration sufficient for physiological expression of exogenous MINA (Figure 2.2). Similar protein levels of 3xFLAG-MINA^{WT} and 3xFLAG-MINA^{H179A} were obtained with each dose of doxycycline (Figure 2.2A). Furthermore, a low dose of doxycycline of 0.1 µg/mL was sufficient for overexpression of 3xFLAG-MINA (Figure 2.2B).

Next, to test whether exogenous, tagged MINA behaved similarly to endogenous MINA, the subcellular localisation was assessed following induction with doxycycline at a concentration of 0.1 µg/mL. Unless otherwise indicated, exogenous 3xFLAG-MINA was detected with an antibody raised against endogenous MINA that was a gift from Dr Schmidt-Zachmann. Empty vector controls were used in each experiment to confirm that the detected signal was of exogenously expressed MINA (an example is shown in Figure 2.4A). Interestingly, and analogous to our previous observation in Caco-2, wild-type 3xFLAG-MINA was enriched in the nucleoli in some, but not all of the cells

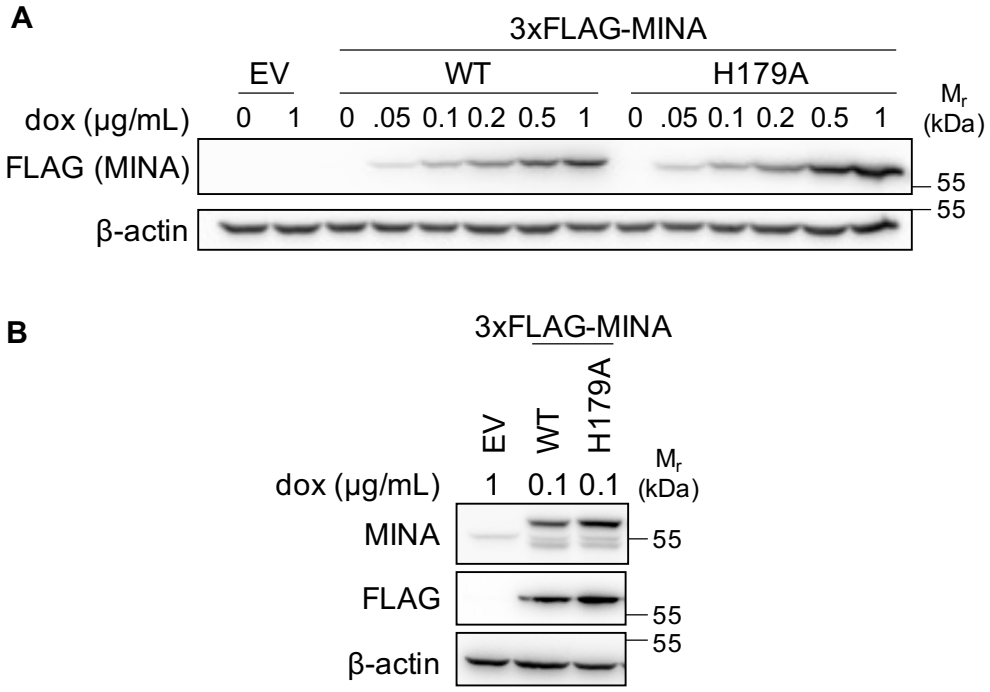


Figure 2.2: Characterisation of stable Caco-2 cell lines expressing doxycycline-inducible 3xFLAG-MINA. (**A,B**) Cell extracts from stable Caco-2 cells expressing either pTIPZ empty vector (EV), wild-type (WT) or catalytically inactive (H179A) 3xFLAG-MINA were immunoblotted for FLAG (A,B) and MINA (B). β-actin (42 kDa) was used as loading control. Cells were treated with doxycycline (dox) at the indicated concentrations for 48 hours to allow for expression of 3xFLAG-MINA. Uncropped images of all Western blots presented in this thesis can be found in Appendix C.

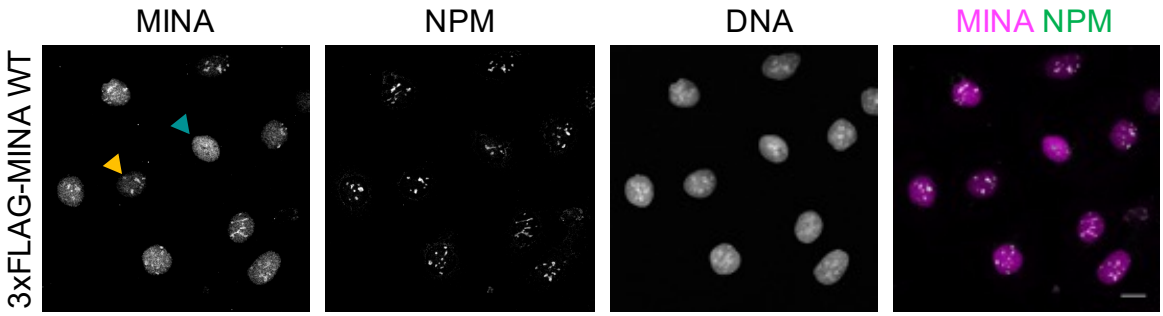


Figure 2.3: 3xFLAG-MINA enriches in the nucleoli of some, but not all of the cells. Representative immunofluorescence images of stable Caco-2 cells expressing wild-type (WT) 3xFLAG-MINA. Expression of exogenous 3xFLAG-MINA (magenta) was induced with 0.1 µg/mL doxycycline for 48 hours before the cells were fixed with 4% (w/v) paraformaldehyde (PFA) and 3xFLAG-MINA was detected using an antibody raised against endogenous MINA. To confirm that the detected signal was of overexpressed, exogenous 3xFLAG-MINA, an empty vector control was used (not shown). Cells were counterstained for the nucleolar marker nucleophosmin-1 (NPM, green). Nuclei were visualised with DAPI. Scale bar represents 20 µm. Images were acquired using a Zeiss LSM 880 confocal microscope equipped with a 40x C-Apochromat 1.2 W Korr M27 objective and ZEN black software.

(yellow arrow, Figure 2.3). Indeed, in a significant proportion of the cells MINA was localised in the nucleoplasm (cyan arrow).

2.2.3 MINA localisation depends on cell confluence

As previously mentioned, most studies in which MINA was found highly enriched in the nucleoli were performed in rapidly proliferating mesenchymal-like cancer cells such as HeLa (Tsuneoka et al., 2002). Caco-2 cells are different in this respect as they are capable of forming a functional monolayer by establishing cell:cell contacts such as tight junctions (Sambuy et al., 2005). Moreover, Caco-2 differentiation in culture is associated with a withdrawal from the cell cycle (Mariadason et al., 2002). Interestingly, diffuse staining of MINA in the nucleoplasm has been reported in the breast adenocarcinoma cell line MCF-7 (Eilbracht et al., 2005). Like Caco-2, MCF-7 cells retain certain characteristics of a differentiated epithelium (Comşa et al., 2015). Based on these reports, together with our own observations, we hypothesised that MINA translocation could be part of the transition from individually proliferating cells

to a polarised epithelium. To test this, cells were either seeded at a low density and fixed before they reached confluency, or they were seeded at a higher density and allowed to grow to a confluent monolayer. Subsequently, MINA localisation was analysed by indirect immunofluorescence. As shown in Figure 2.4, wild-type 3xFLAG-MINA was enriched in the nucleoli of most cells (63%) in subconfluent cultures. However, in the cells grown to confluence, it was evident that all MINA had translocated to the nucleoplasm. Moreover, we found that MINA localisation might be partially dependent on its catalytic activity, as 3xFLAG-MINA H179A was enriched in the nucleoli of only 37% of the cells in subconfluent cultures, compared to 63% of cells expressing wild-type 3xFLAG-MINA (Figure 2.4B).

2.2.4 MINA re-locates to the nucleolus following disruption of the monolayer

The transition from proliferating cells to a differentiated epithelium, mesenchymal-epithelial transition (MET), is a reversible process of which the reverse, epithelial-mesenchymal transition (EMT), is often utilised by cancer cells to escape growth restrictions. Given our observation that MINA translocates from the nucleolus to the nucleoplasm in cells that have formed a monolayer, we hypothesised that, when these cell:cell contacts are disrupted, MINA would re-enter the nucleolus. To test this, in a confluent monolayer, a scratch was made to disrupt the monolayer. Subsequently, the cells were given 24 hours to recover, after which they were fixed and MINA localisation was analysed. First, it was confirmed that, in confluent cells at a distance from the disrupted monolayer, MINA was localised in the nucleoplasm (Figure 2.5, panel 1). However, at the site of the scratch (indicated by the dotted line), the cells were less confluent and MINA had translocated back into the nucleolus, as evidenced by colocalisation of MINA with the nucleolar marker nucleophosmin (NPM; Figure 2.5, panel 2), thus confirming our hypothesis.

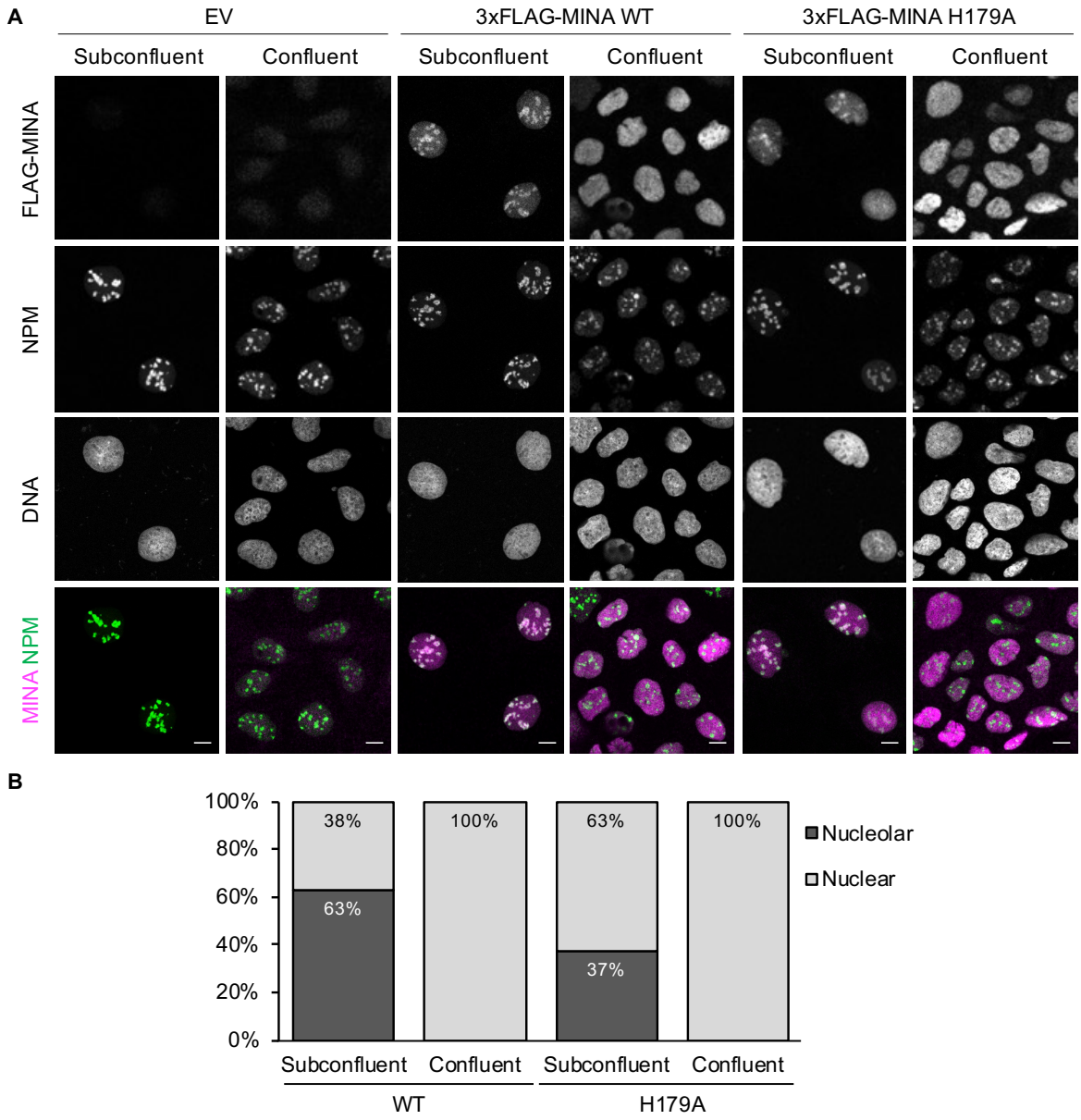


Figure 2.4: MINA localisation in Caco-2 depends on cell confluence and catalytic activity. (**A**) Representative immunofluorescence images showing the localisation of wild-type (WT) and catalytically inactive (H179A) 3xFLAG-MINA in subconfluent and confluent conditions. Cells were incubated with 0.1 µg/mL doxycycline for 48 hours to induce expression of 3xFLAG-MINA. Cells were fixed with PFA and stained for MINA (magenta) and the nucleolar marker nucleophosmin (NPM, green). Nuclei were visualised with DAPI. Scale bars represent 20 µm. Images were acquired using a Zeiss LSM 880 confocal microscope equipped with a 40x C-Apochromat 1.2 W Korr M27 objective and ZEN black software. (**B**) Quantification of (A). Samples were blinded and cells were quantified based on whether or not nucleolar enrichment could be observed. Bar graph represents an average of two independent experiments. A total of two hundred cells were counted for each condition in each experiment.

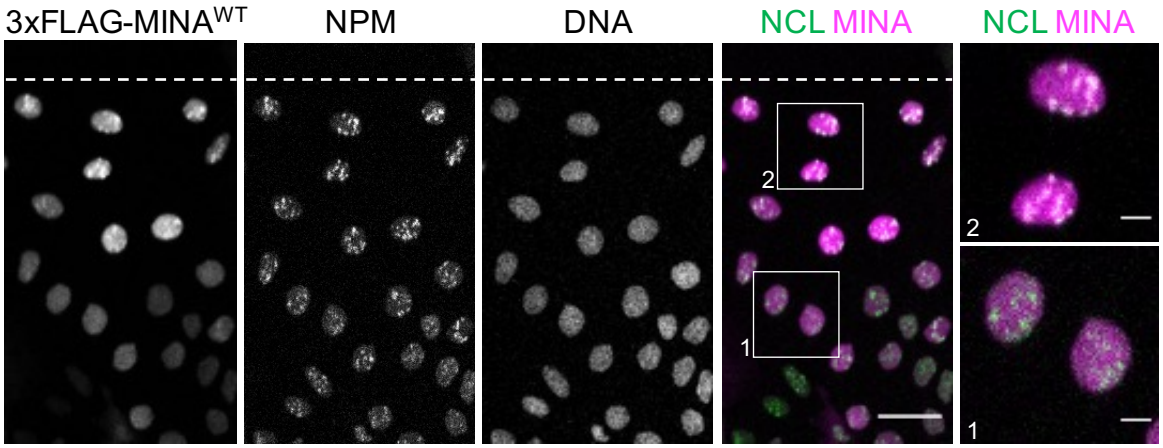


Figure 2.5: MINA relocates to the nucleolus upon disruption of the monolayer. A scratch was introduced to disrupt a confluent monolayer of Caco-2 cells expressing wild-type (WT) 3xFLAG-MINA. Cells were fixed 24 hours after the scratch was made. Re-localisation of 3xFLAG-MINA to the nucleolus was observed at the site of the scratch (top, indicated by the dashed white line). In contrast, at a distance of the scratch, 3xFLAG-MINA remained in the nucleus (bottom). Cells were stained for MINA (magenta) and nucleolin (NCL, green). Nuclei were visualised with DAPI. Scale bars represent 50 or 10 (enlargements) µm. Images were acquired using a Zeiss LSM 880 confocal microscope equipped with a 40x C-Apochromat 1.2 W Korr M27 objective and ZEN black software. Expression of 3xFLAG-MINA was induced with 0.1 µg/mL for 24 hours before the scratch was made.

2.2.5 MINA localisation correlates with ribosome biogenesis

MINA has been reported to hydroxylate the large ribosomal subunit protein RPL27A (Ge et al., 2012). Hence, we hypothesised that MINA might be localised in the nucleoli when cells are actively proliferating (i.e. at low density) because of the greater demand for ribosomes and protein translation. To begin to explore this, we first compared protein synthesis rates in confluent and subconfluent cells where we had observed differential MINA localisation. Nascent protein synthesis was monitored using a Click-iT Assay Kit (Invitrogen). This approach involves the incorporation of an azide-containing methionine analogue, L-azidohomoalanine (AHA), into newly synthesised proteins. Subsequently, after cell fixation, the click reaction is performed using a fluorescently labelled alkyne. In the presence of copper sulphate ($CuSO_4$), the azide and alkyne form a triazole conjugate (Figure 2.6A), allowing specific detection of AHA-containing proteins. This assay was first validated by confirming that pro-

tein translation was inhibited (and thus no signal was generated) following treatment with the protein synthesis inhibitor cycloheximide (CHX, Figure 2.6B). Thereafter, we compared AHA incorporation in cells where MINA is predominantly nucleolar with cells showing nucleoplasmic MINA staining. As shown in Figure 2.6C, the overall level of AHA signal (nuclear, nucleolar and cytoplasmic) was lower in confluent cells with nuclear MINA staining, consistent with the hypothesis that the overall translation rate is decreased in these cells. Furthermore, in cells cultured in subconfluent conditions, the most intense AHA signal was detected in the nucleoli (Figure 2.6C). We speculate that this is due to highly abundant newly synthesised nucleolar proteins. Interestingly, 3xFLAG-MINA co-localised with these, consistent with a role for nucleolar MINA in the early stages of ribosome biogenesis (Figure 2.6C).

Next, since ribosome biogenesis is dependent on the coordinated transcription of ribosomal RNA (rRNA) by RNA polymerase I and synthesis of ribosomal proteins, we considered whether rRNA transcription might regulate MINA localisation. It was previously reported that actinomycin D (AMD), a dose-dependent RNA polymerase I/II inhibitor, affects MINA localisation in the breast adenocarcinoma cell line MCF-7 (Eilbracht et al., 2005). Consistent with this, short treatment of Caco-2 cells with a low (RNA polymerase I specific) dose of AMD (40 ng/mL) was sufficient to induce translocation of MINA from the nucleolus to the nucleoplasm (Figure 2.7). To confirm that inhibition of RNA polymerase I is responsible for this change in localisation, we tested two other drugs, CX-5461 and ML-60218, which have been reported to specifically inhibit RNA polymerase I and III, respectively (Drygin et al., 2011; Wu et al., 2003). Whereas RNA polymerase I localises to the nucleolus and only transcribes ribosomal RNAs, RNA polymerase III functions in the nucleoplasm and is responsible for the transcription of tRNAs, some stable RNAs as well as 5S rRNA (Paule and White, 2000). As depicted in Figure 2.7, whereas CX-5461 interfered with nucleolar localisation of MINA, ML-60218 did not, demonstrating that MINA translocation results specifically from RNA polymerase I inhibition, consistent with an important role for active rRNA transcription and/or ribosome biogenesis in the nucleolus.

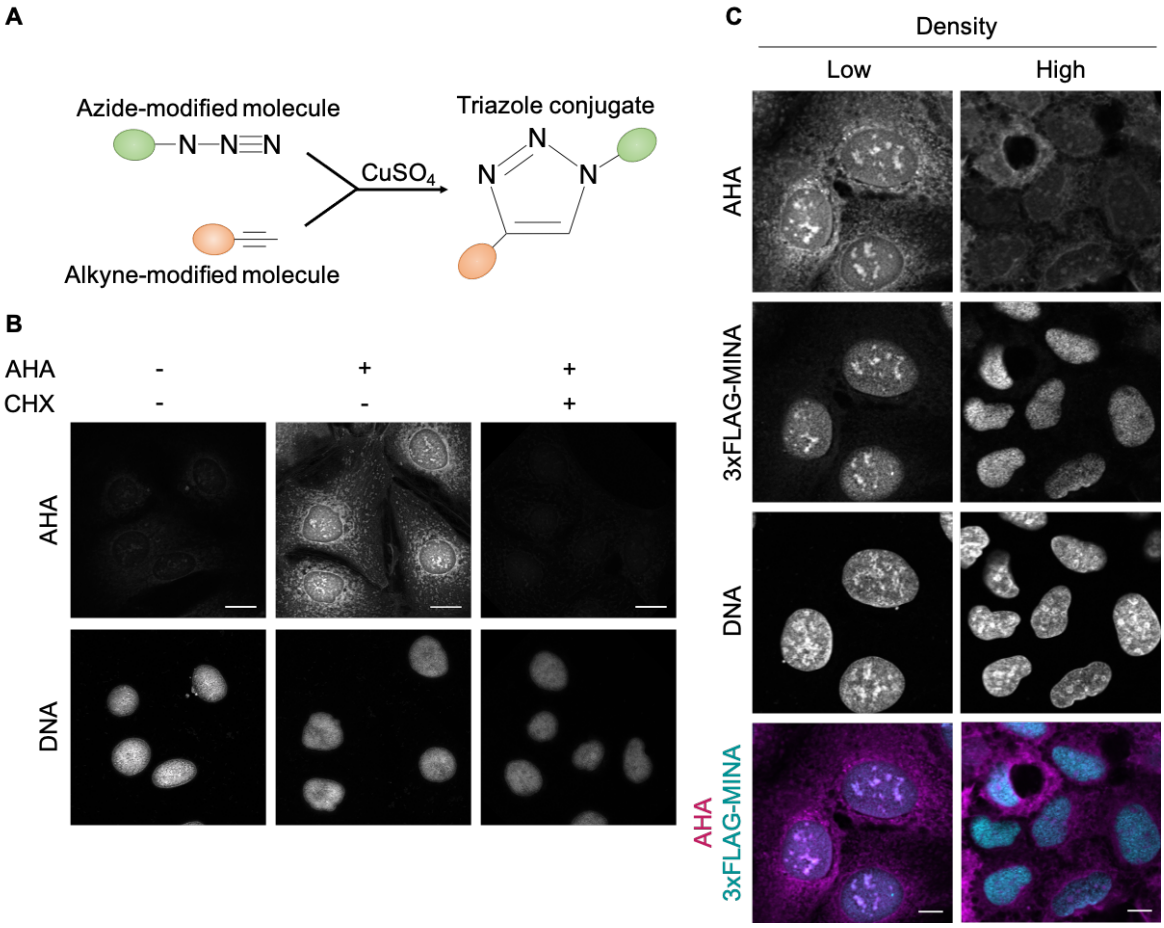


Figure 2.6: MINA localisation correlates with the rate of translation. (**A**) Schematic of the azide-alkyne click reaction. (**B**) Incubation with L-azidohomoalanine (AHA) to monitor protein synthesis. Caco-2 cells were either untreated, treated with AHA or AHA and cycloheximide (CHX) for 1 hour before the cells were fixed and the click reaction was performed. (**C**) 3xFLAG-MINA is enriched in the nucleoli of cells with high levels or protein synthesis. Stable Caco-2 cells expressing wild-type 3xFLAG-MINA and seeded at a high or low density were treated with AHA (magenta) for 1 hour before the cells were fixed and the click reaction was performed. Expression of 3xFLAG-MINA was induced for 48 h with 0.1 µg/mL doxycycline. 3xFLAG-MINA was detected by immunostaining with an antibody raised against MINA (cyan). (**B,C**) Nuclei were visualised with DAPI. Scale bars represent 20 (B) or 10 (C) µm. Images were acquired using a Zeiss LSM 780 confocal system equipped with a 40x C-Apochromat 1.2 W Korr M27 objective and ZEN black software.

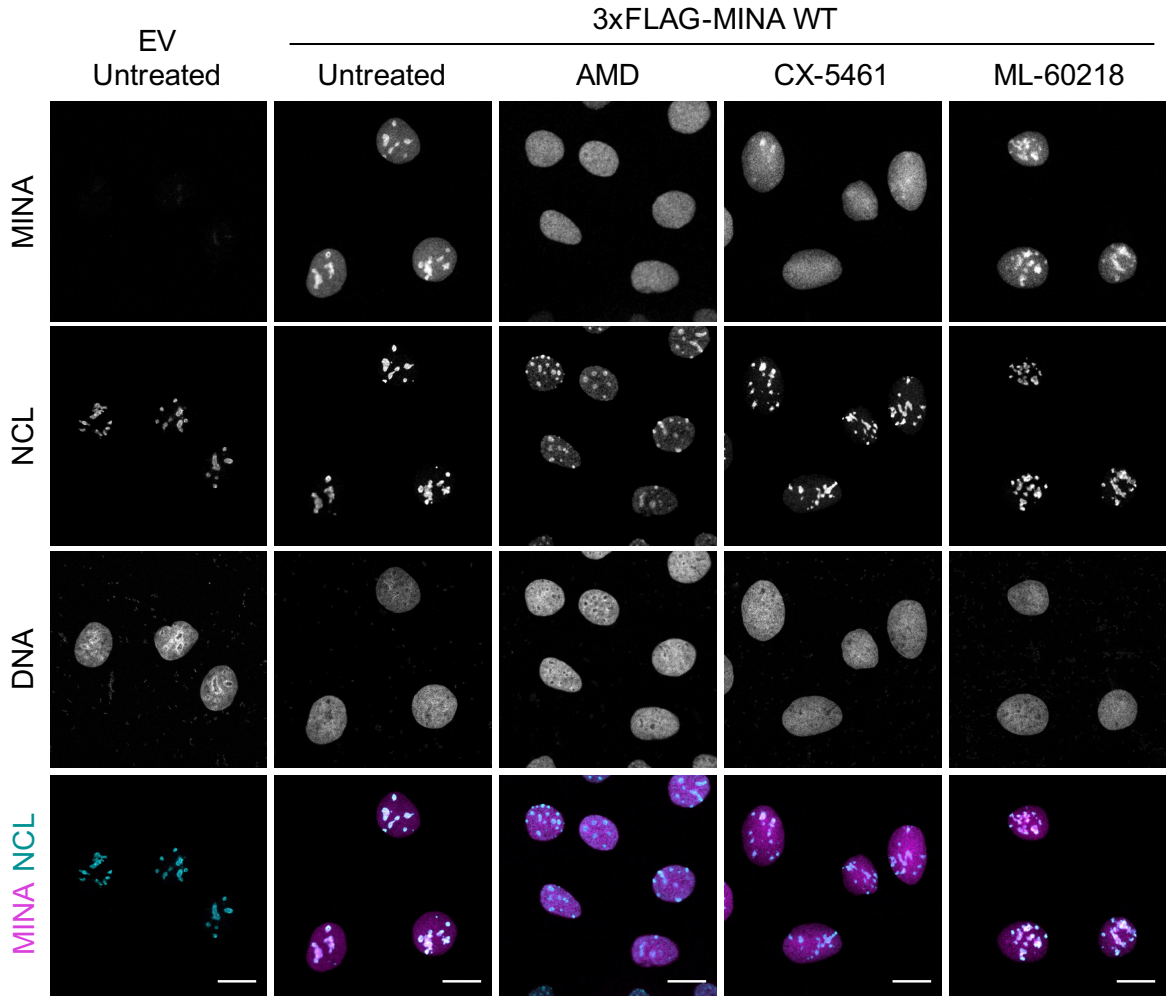


Figure 2.7: Active ribosome biogenesis retains MINA in the nucleolus in Caco-2. Caco-2 cells expressing an empty vector (EV) or wild-type (WT) 3xFLAG-MINA were either untreated or treated with 40 ng/mL actinomycin D (AMD), RNA polymerase I inhibitor CX-5461 or RNA polymerase III inhibitor ML-60218 . Prior to treatment, expression of 3xFLAG-MINA was induced for 48 h using 0.1 µg/mL doxycycline. Cells were stained for MINA (magenta) and nucleolin (NCL, cyan). Nuclei were visualised with DAPI. Scale bars represent 20 µm. Images were acquired using a Zeiss LSM 880 confocal microscope equipped with a 40x C-Apochromat 1.2 W Korr M27 objective and ZEN black software.

We next wanted to explore whether ribosome biogenesis was as critical a determinant of MINA localisation in cells in which we had observed a more homogenous and predominantly nucleolar localisation than Caco-2. As shown in Figure 2.1, MINA is mostly nucleolar in the colorectal cancer cell line SW620. Therefore, we reasoned that this cell line would be a suitable model to study interventions that trigger nucleolar release, such as drug treatment. Analogous to section 2.2.2, stable cell lines were generated by transduction with a pTIPZ empty vector (EV) or a vector containing doxycycline-inducible 3xFLAG-MINA. Initial characterisation of 3xFLAG-MINA expression showed that a concentration of 50 ng/mL doxycycline is sufficient to induce overexpession of 3xFLAG-MINA (Figure 2.8A). Next, it was confirmed that also in this cell line, translocation of MINA from the nucleolus to the nucleoplasm is induced by the inhibition of RNA polymerase I (AMD and CX-5461), but not III (ML-60218; Figure 2.8B).

2.2.6 Nucleolar MINA localisation is not dependent on high oxygen availability

Protein synthesis in an energy-consuming process that is highly sensitive to cellular stress. One type of stress that is particularly relevant to 2OG oxygenases is hypoxia, as these enzymes depend on the availability of cofactors, including oxygen, for catalytic activity. During hypoxia, global protein synthesis is reduced in order to conserve ATP (Liu and Simon, 2004). As we have observed that MINA is preferentially localised in the nucleoplasm in cells with reduced ribosomal protein synthesis, we sought to characterise the effect of low oxygen levels on MINA localisation. Caco-2 cells expressing 3xFLAG-MINA seeded at low density (where we anticipate nucleolar localisation) were placed in a hypoxia chamber containing 1% oxygen for 16 hours. Subsequently, the cells were fixed and stained for MINA and the nucleolar marker nucleolin (NCL). However, no significant differences in the localisation of MINA or the morphology of the nucleoli were observed, at least not at this level of oxygen (Figure 2.9).

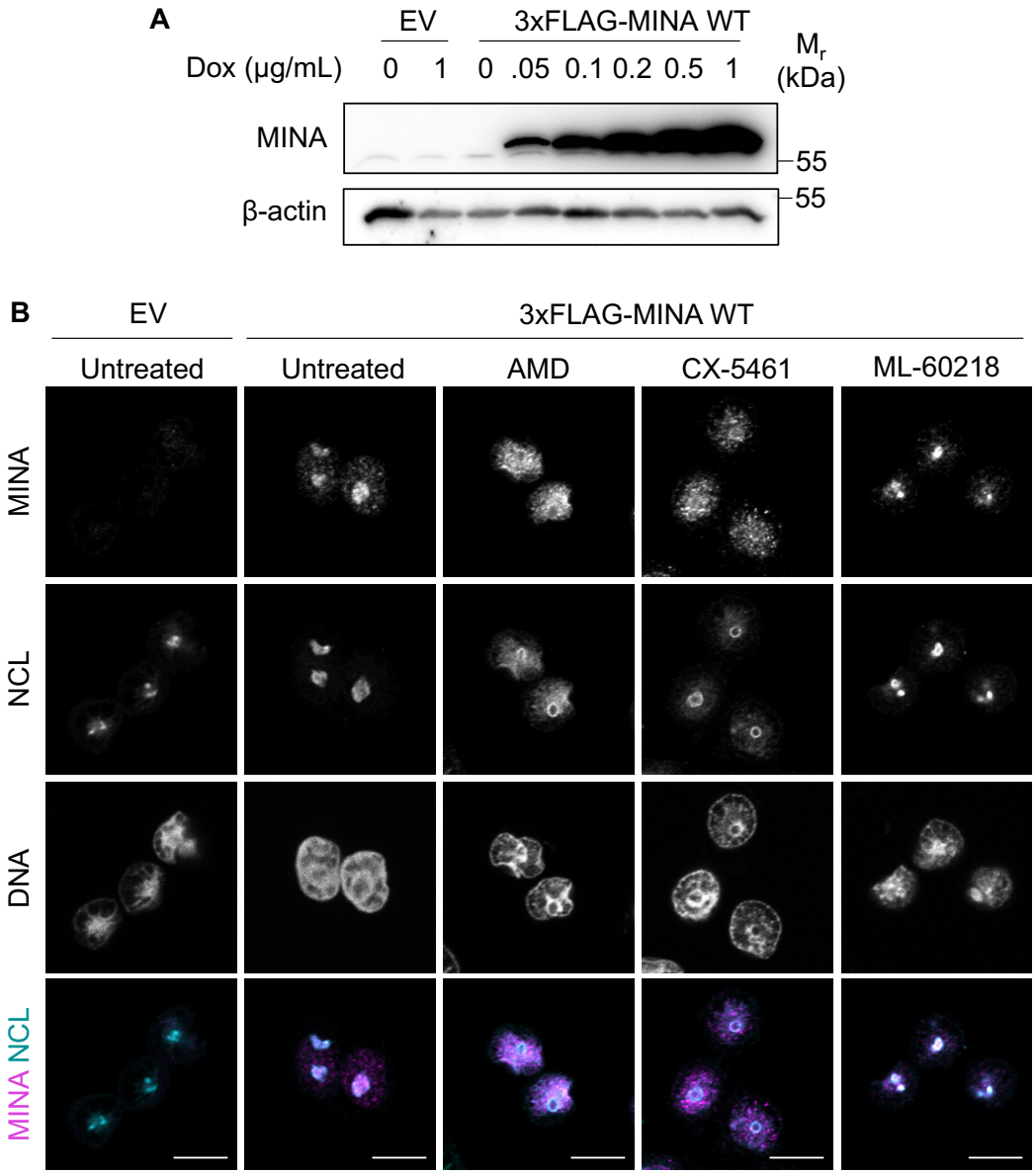


Figure 2.8: Active ribosome biogenesis retains MINA in the nucleolus in SW620. (**A**) Characterisation of stable SW620 cell lines transduced with lentivirus encoding a pTIPZ empty vector (EV) or doxycycline-inducible wild-type (WT) 3xFLAG-MINA. Expression of 3xFLAG-MINA was induced for 48 h with the indicated concentrations of doxycycline (dox). Cell extracts were immunoblotted for MINA (53 kDa). β-actin (42 kDa) was used as loading control. (**B**) SW620 cells expressing an empty vector (EV) or 3xFLAG-MINA were either untreated or treated with 40 ng/mL actinomycin D (AMD), RNA polymerase I inhibitor CX-5461 or RNA polymerase III inhibitor ML-60218. Prior to treatment, expression of 3xFLAG-MINA was induced for 48 h using 0.1 µg/mL dox. Cells were stained for MINA (magenta) and nucleolin (NCL, cyan). Nuclei were visualised with DAPI. Scale bars represent 10 µm. Images were acquired using a Zeiss LSM 880 confocal microscope equipped with a 60x C-Apochromat 1.2 W Korr M27 objective and ZEN black software.

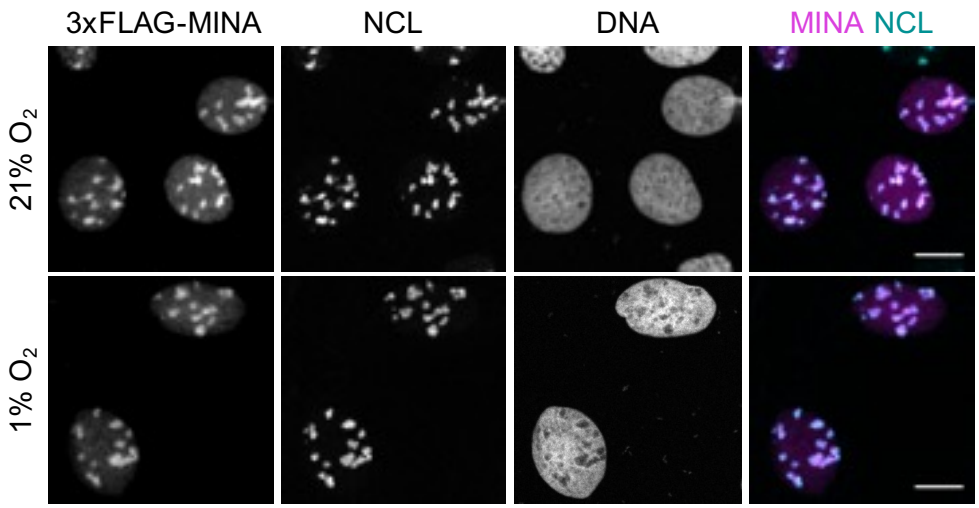


Figure 2.9: Moderate hypoxia does not trigger MINA translocation. Representative images of Caco-2 cells expressing wild-type 3xFLAG-MINA. Expression of 3xFLAG-MINA was induced with 0.1 µg/mL doxycycline for 48 h before the cells were incubated at 21% (normoxia) or 1% (moderate hypoxia) oxygen for 16 hours. Following fixation with PFA, the cells were stained for MINA (magenta), nucleolin (NCL, cyan). Nuclei were visualised with DAPI. Scale bars represent 15 µm. Images were acquired using a Zeiss LSM 780 confocal microscope equipped with a 40x C-Apochromat 1.2 W Korr M27 objective and ZEN black software.

2.2.7 Identification of a nucleolar localisation signal in MINA

Having observed that MINA localisation may be regulated by the cell, it was of interest to investigate whether nucleolar localisation is achieved by a nucleolar localisation signal: if MINA contains such a signal, it could be experimentally mutated in order to specifically explore the extra-nucleolar functions of MINA. Whereas it is widely appreciated that nuclear proteins contain sequences for nuclear entry and export, it is less well known if such sequences exist for nucleolar localisation. Nonetheless, nucleolar localisation sequences have been described for a number of proteins. Recently, a systematic analysis of 46 reported nucleolar localisation sequences (NoLSs) was conducted by Scott et al. to investigate whether there is any consensus among these reported motifs (Scott et al., 2010). Whereas no specific consensus motif was derived from their analysis, the authors concluded that, in general, nucleolar localisation signals are characterised by the presence of basic residues (48% of the residues within reported NoLSs were found to be basic) that are solvent-accessible and almost exclusively located in

α-helices (42%) or coils (57%). Subsequently, Scott et al. used the sequence and secondary structure (predicted using the JPred server) of the 46 reported NoLSs to train an artificial neural network (ANN) to computationally predict NoLSs and designed a publicly available web tool (NoD; Scott et al., 2010, 2011). Here, the entered amino acid sequence is divided into consecutive windows of 13 residues and each window is scored based on residue prevalence, secondary structure elements and position within the full-length protein. If the average score of 8 consecutive windows >0.8, a region spanning 20 residues is predicted as a NoLS. The threshold score of 0.8 was selected based on the ratio of true versus false positives.

Based on MINA's primary amino acid sequence and JPred-predicted secondary structure, the NoD algorithm did not predict a high scoring NoLS. However, two regions nearly reached the threshold score, one at the N-terminal end (Figure 2.10A, red box), and one around amino acids (AAs) 100-125 (Figure 2.10A, blue box). The latter was of particular interest as AAs 109-126 (KKK(X_{13})RK) were previously proposed, but not experimentally confirmed, to form a bipartite nuclear localisation signal (Eilbracht et al., 2004).

We next sought to evaluate whether any of the basic residues within the identified regions are evolutionary conserved. Phylogenetic analyses of the ribosomal oxygenases NO66 (RIOX1) and MINA (RIOX2) indicated that both proteins have likely evolved from a common ancestor (Chowdhury et al., 2014; Bräuer et al., 2018). Moreover, in contrast to NO66 which is found throughout the animal kingdom, MINA is absent in most invertebrates as well as certain lower eukaryotes such as *Drosophila melanogaster* and *Caenorhabditis elegans*, indicating that MINA has likely more recently evolved from NO66. Therefore, sequence comparisons were performed in higher eukaryotes. As depicted in Figure 2.11, high levels of sequence conservation are evident across all organisms assessed, including the residues within the regions of interest.

We then mapped the basic residues within the identified regions on the crystal structure. As the N-terminus of MINA is not included in the reported structure, we first focussed on amino acids 100-125. Within this region, amino acids R125/K126 are

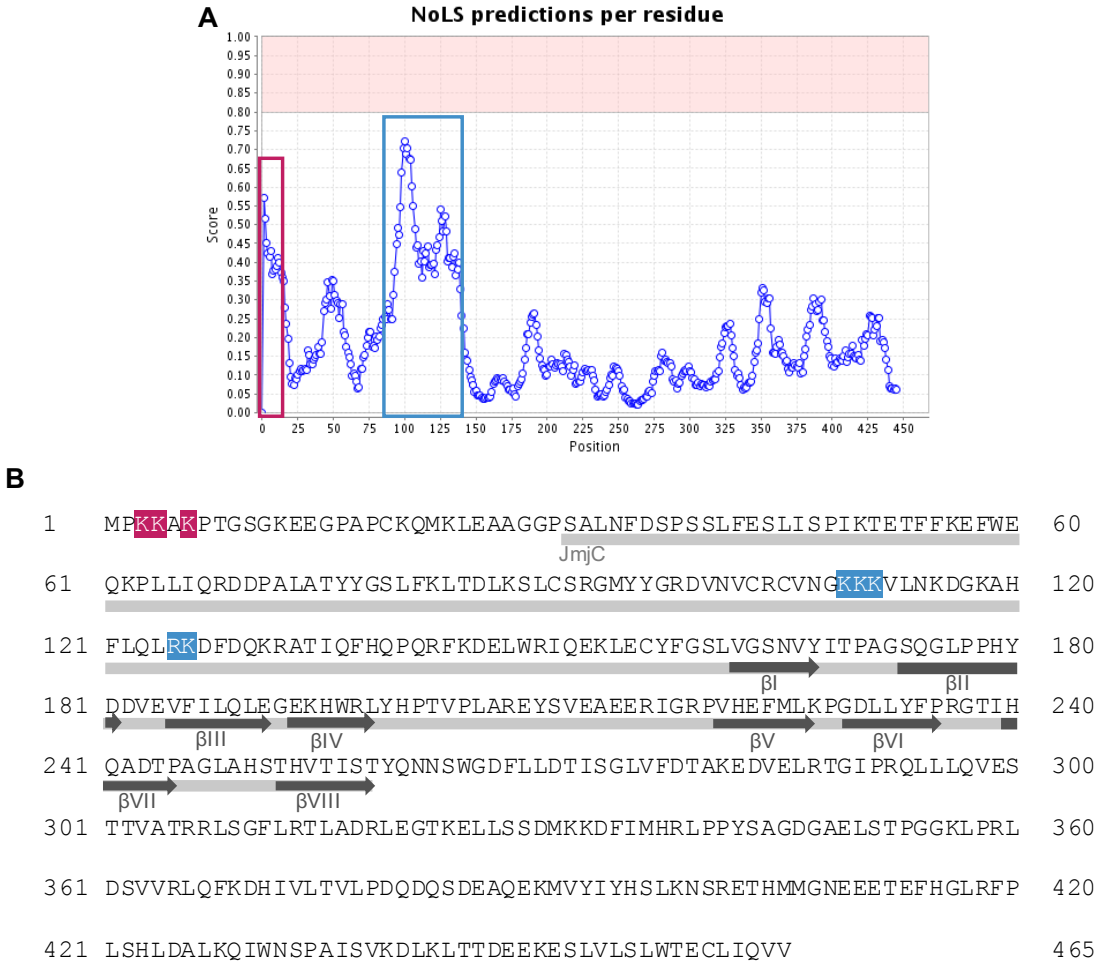


Figure 2.10: Prediction of a nucleolar localisation signal (NoLS) in MINA. (**A**) NoLS prediction by NoD (http://www.compbio.dundee.ac.uk/nod) identifies two candidate regions in MINA. (**B**) Protein sequence of human MINA. Basic residues potentially required for nucleolar localisation are indicated in pink and blue. JmjC catalytic domain is indicated in light grey. Dark grey arrows represent the eight β-sheets (βI - βVIII) that make up the catalytic core. UniProt ID = Q8IUF8.

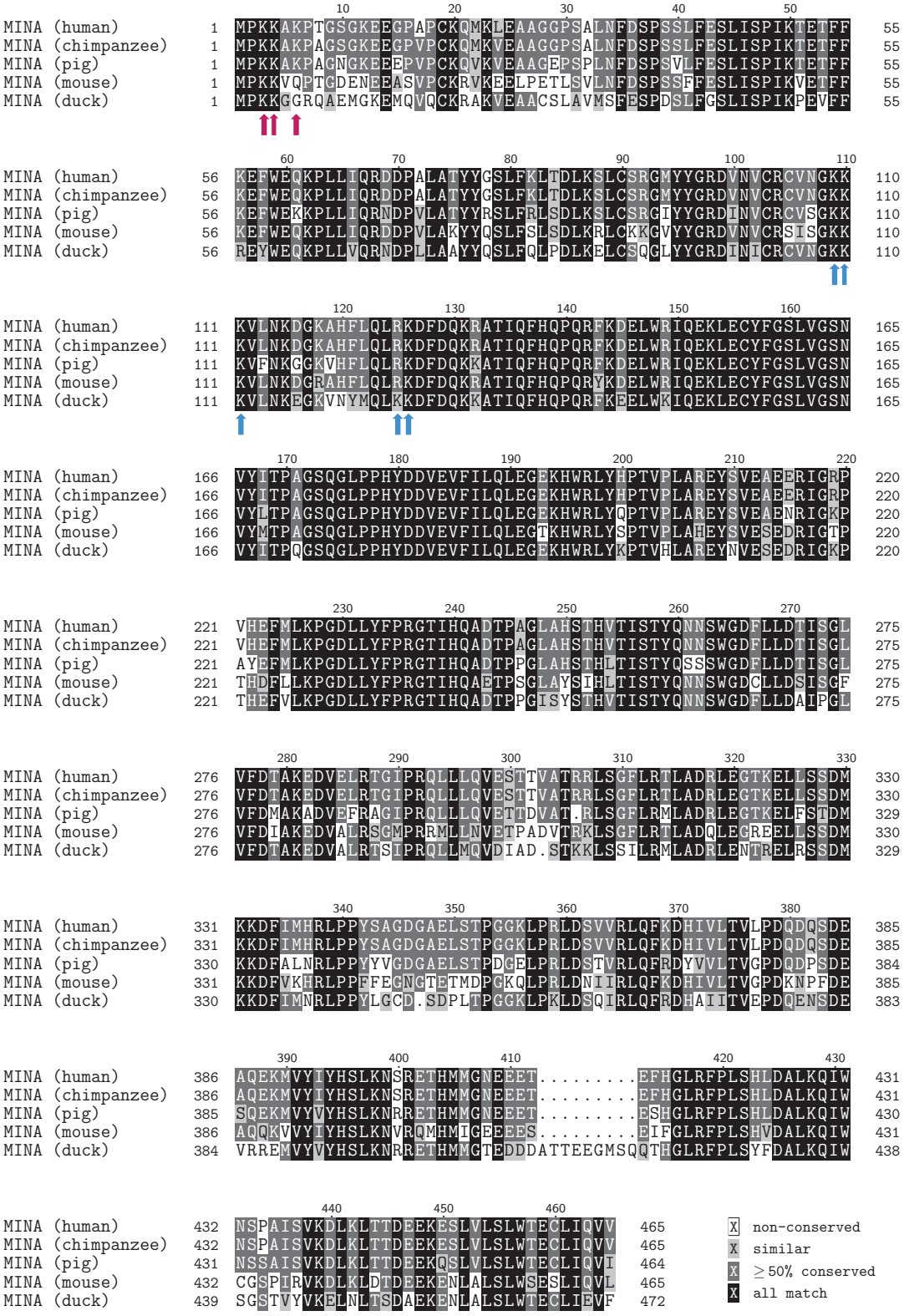


Figure 2.11: Conservation of candidate NoLS residues. Sequence alignment of human (*Homo sapiens*, UniProt ID = Q8IUF8), chimpanzee (*Pan troglodytes*, Uniprot ID = H2QMZ6), pig (*Sus scrofa*, UniProt ID = M3V811), mouse (*Mus musculus*, Q8CD15) and duck (*Anas platyrhynchos platyrhynchos*, Uniprot ID = U3IAG8) MINA protein sequence. Arrows indicate residues of interest within in the regions identified as candidate NoLSs. Sequence alignment was generated using Clustal Omega.

within an α-helix and their side chains are solvent-exposed (Figure 2.12). In contrast, K109-111 are within a β-sheet (not shown), which was found to be particularly unusual for NoLSs (Scott et al., 2010). Moreover, the C-terminal part of a bipartite NLS within certain nucleolar proteins has previously been shown to be involved in targeting the protein to the nucleolus (Scott et al., 2010). Therefore, we considered R125/K126 as residues of interest to experimentally test their contribution to MINA nucleolar localisation. To investigate whether R125/K126 are indeed involved in nucleolar localisation, these residues were mutated to glycine and the effect on subcellular localisation was analysed by indirect immunofluorescence. As shown in Figure 2.12B, mutation of R125G/K126G (NoLS) is sufficient for exclusion from the nucleolus. Interestingly, and perhaps importantly, nuclear localisation remains unaffected.

Having identified a nucleolar localisation mutant with potential utility for future functional studies, we next wanted to investigate whether MINA retains its hydroxylase activity upon mutation of R125/K126. It was important to test whether or not the nucleolar mutant is catalytically active for two reasons. Firstly, in order to interpret the effects of the mutations on localisation, as we have previously observed that nucleolar enrichment is partially dependent on MINA's catalytic activity (Figure 2.4B). Secondly, to support the correct interpretation of results arising from future functional experiments. To this end, vectors encoding hemagglutinin (HA)-tagged MINA that was either wild-type, catalytically dead (H179A) and/or unable to localise to the nucleolus (R125G/K126G, NoLS) were transfected into HEK293T cells, immunoprecipitated and subjected to an *in vitro* hydroxylation assay. HA-MINA was used rather than FLAG-MINA due to the existence of an established protocol for measuring HA-MINA purified from HEK293T cells. It was previously published that MINA efficiently catalyses hydroxylation of an RPL27A peptide *in vitro* (Ge et al., 2012). Consequently, HA-tagged MINA was incubated at 37°C with or without RPL27A peptide in buffer containing Fe(II), 2OG and ascorbate. Hydroxylase activity was detected indirectly using a Succinate-Glo™ JmjC Demethylase/Hydroxylase Assay kit purchased from Promega. Here, succinate, produced as a by-product of the hydroxylation reaction (Figure 1.1B),

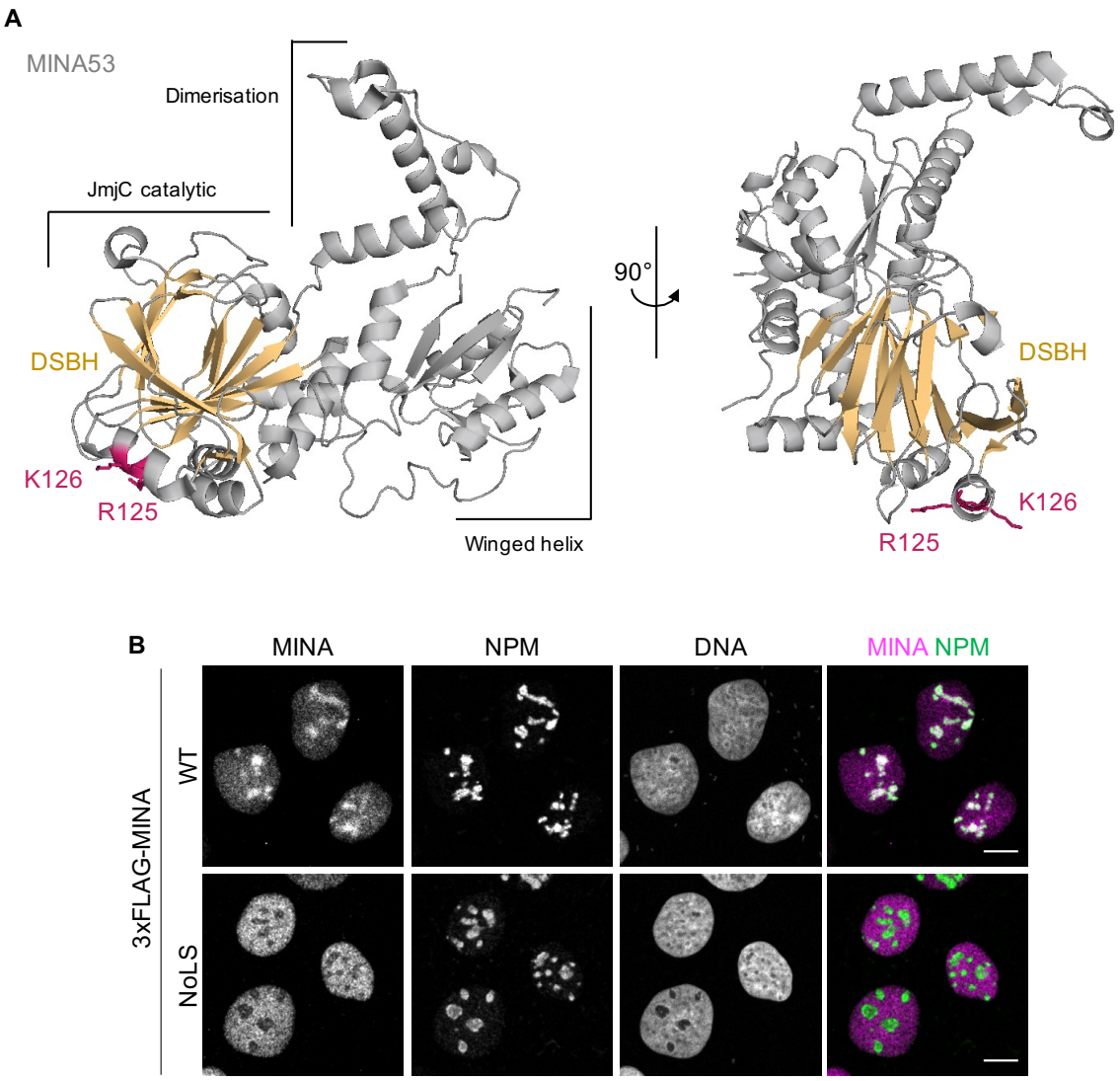


Figure 2.12: Localisation of R125/K126 and effect of mutation on subcellular localisation. (**A**) Ribbon representation of a MINA monomer showing residues that contribute to MINA nucleolar localisation (R125/K126) in pink and the catalytic domain in yellow. Protein Data Bank (PDB) ID = 4BXF. Structures were visualised using PyMOL. DSBH = double-stranded beta helix. (**B**) Effect of R125G/K126 mutations on subcellular localisation. Caco-2 cells expressing either wild-type or 3xFLAG-MINA R125G/K126G (NoLS) were fixed and stained for MINA (magenta) and nucleolar protein nucleophosmin (NPM, green). Expression of 3xFLAG-MINA was induced by treatment with 0.1 µg/mL doxycycline for 48 hours. Nuclei were visualised with DAPI. Scale bars represent 10 µm. Images were acquired using a Zeiss LSM 880 confocal microscope equipped with a 40x C-Apochromat 1.2 W Korr M27 objective and ZEN black software.

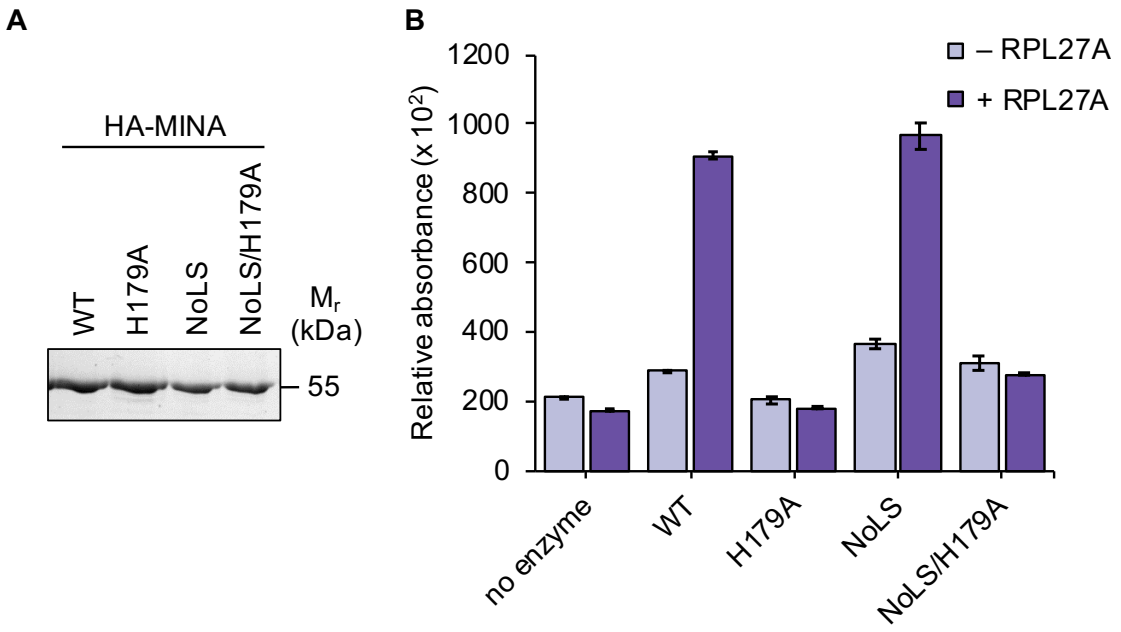


Figure 2.13: Mutation of R125G/K126G does not affect the intrinsic enzymatic activity of MINA. *In vitro* hydroxylation assay of RPL27A peptide using HA-MINA immunopurified from transiently transfected HEK293T cells. (**A**) Coomassie blue staining showing the amount of enzyme used in (B). (**B**) The indicated HA-MINA variants were incubated with 2OG, ascorbate, Fe(II) and with or without RPL27A peptide for 5 min at 37°C before hydroxylation was measured indirectly using a Succinate-Glo assay. Representative result from 1 biological repeat is shown. The experiment was repeated twice. Values represent the average + SD of three technical repeats. Absorbance was adjusted to correct for differences in MINA loading (see A). This experiment was performed in collaboration with Dr Regina Andrijes.

is converted into ATP, which is subsequently converted into light in a luciferase reaction. As shown in Figure 2.13, MINA retains its catalytic activity following mutation of the nucleolar localisation signal (NoLS). Furthermore, as expected, MINA is catalytically inactivated upon mutation of iron-coordinating site His179 (H179A, Figure 2.13).

2.3 Discussion

Combined sequence and structural analysis of MINA allowed us to identify two residues (R125/K126) that contribute to the nucleolar localisation of MINA. Although we have not confirmed if both residues are required, and whether other residues also contribute, mutation of these residues was sufficient for exclusion of MINA from the nucleolus

(Figure 2.12). Instead, MINA$^{R125G/K126G}$ localises to the nucleoplasm. R125/K126 were previously suggested to be part of a bipartite nuclear localisation signal (NLS), together with K100/K101/K102 (Eilbracht et al., 2005). It is not unprecedented that the C-terminal part of a proposed bipartite NLS in a nucleolar protein is in fact responsible for nucleolar localisation (Huang et al., 2005).

Several mechanisms have been described to control subcellular protein localisation. Transport to membrane-bound structures, such as the nucleus or mitochondria, is mainly controlled by short targeting sequences that are well characterised. However, unlike many other subcellular compartments, the nucleolus is not contained by a membrane. For this reason, it is widely believed that nucleolar localisation is achieved through binding and retention by core nucleolar proteins. Nonetheless, evidence is emerging supporting the existence of nucleolar localisation sequences (Scott et al., 2010). Although R125/K126 fit the definition of (part of) a NoLS, as proposed by Scott et al., it is possible that other factors contribute to nucleolar entry and/or retention. Proteomic screens performed by ourselves and others have identified nucleophosmin (NPM), a prominent nucleolar protein, as interacting with MINA in a variety of cell lines including Caco-2 (Wang et al., 2015a and Coleman Lab, unpublished). The MINA residues contributing to this interaction are currently unknown, but could potentially include R125/K126.

The work described in this chapter suggests that multiple factors may be involved in the nucleolar retention of MINA, including active rRNA transcription and nucleolar protein synthesis. We would predict that the latter is related to the abundance of ribosomal proteins, including the MINA substrate RPL27A. Consistent with this, an experimental mutation in MINA (H179A) that interferes with substrate binding and RPL27A hydroxylation, partially interferes with nucleolar retention. It is interesting to speculate whether expression of an RPL27A hydroxylation site mutant (H39A) might also interfere with nucleolar localisation MINA. It is currently unclear if mutation of His-39 in RPL27A interferes with MINA binding, but this would be expected based on the interaction profile of related JmjC oxygenases, including FIH and JMJD7, with

their substrates (Cockman et al., 2006; Markolovic et al., 2018).

Other factors contributing to nucleolar retention could include direct or indirect binding to rRNA. Indeed, inhibition of rRNA transcription by inhibitors actinomycin D and CX-5461 interfered with the nucleolar localisation of MINA (Figure 2.7, 2.8B and Eilbracht et al., 2005). Similarly, it was previously reported that treatment of cells with RNase, but not DNase, triggers nucleolar release of MINA (Eilbracht et al., 2005). How rRNA could directly contribute to MINA nucleolar localisation is unclear. Ribosomal oxygenases MINA and NO66 possess a C-terminal winged helix (WH) domain of unknown function. In other proteins, winged helix domains have been reported to mediate nucleic acid binding (Teichmann et al., 2012). However, sequence analysis of the WH domain in MINA has revealed an overall negative charge, making direct binding to nucleic acids unlikely (Chowdhury et al., 2014).

Ribosome biogenesis is one of the most energy-consuming cellular processes. As a result, nucleoli are highly dynamic structures that respond to cellular growth and metabolic requirements, but also to (metabolic) stress (Boulon et al., 2010). Consistent with the latter, Eilbracht and colleagues have previously reported nuclear translocation of MINA in response to serum starvation (Eilbracht et al., 2005). Another type of stress relevant to both ribosome biogenesis and 2OG oxygenases is hypoxic stress. In the conditions tested (16 h incubation at 1% O_2), we did not observe major effects of hypoxia on MINA localisation (Figure 2.8). However, neither did we note alterations in the number or morphology of the nucleoli, as evaluated by nucleolin (NCL; Figure 2.8). We could speculate that perhaps Caco-2 cells are relatively resistant to reduced oxygen levels: non-invasive studies have shown that epithelial cells in the colonic regions of the intestine can be exposed to physiological oxygen ('physioxia') levels as low as 2 - 0.04% (He et al., 1999). Moreover, MINA reportedly has a high affinity for oxygen and is therefore relatively insensitive to hypoxia, maintaining approximately 50% activity even in severe hypoxia (0.1% O_2; Dr Mathew Coleman, personal communication). In light of this, it would be of interest to perform further studies looking at the effect of severe and prolonged hypoxia on MINA localisation and function.

Consistent with high levels of rRNA transcription and protein synthesis, our data predict that cells that are actively proliferating have MINA sequestered in the nucleolus. We observed relocation from the nucleoplasm to the nucleolus following disruption of a monolayer in a wound healing assay (Figure 2.5). Moreover, our preliminary data suggest MINA is enriched in the nucleolus of cells with a less differentiated and more mesenchymal phenotype (Figure 2.1), consistent perhaps with the frequent nucleolar localisation of MINA in tumour samples and rapidly proliferating normal tissues such as the testes (Teye et al., 2004; Tsuneoka et al., 2006). Several studies, so far, have compared fast-proliferating and differentiated cell types in both normal and tumour tissues (Teye et al., 2004; Tsuneoka et al., 2004; Teye et al., 2007). However, these studies have only focussed on relative staining intensity and overall expression levels, with little consideration for how the subcellular localisation of MINA correlates with proliferation or clinical parameters. It would therefore be of interest to study MINA localisation during mesenchymal-epithelial transition in non-transformed tissues, or to examine how the subcellular localisation of MINA in tumour samples correlates with the genomic profile and markers of proliferation such as Ki67. Interestingly, although not discussed in detail by the authors, clear differences in the staining intensity of nuclear MINA (diffusely nuclear versus predominantly nucleolar) can be observed between sections of (moderately) well-differentiated versus poorly differentiated colon cancer tissues (Teye et al., 2004).

Overall, our observations indicate that the subcellular localisation of MINA may be regulated and support the notion of separate functions for MINA, including yet to be determined extra-nucleolar functions. In the next chapter, using the nucleolar localisation mutant identified in this chapter, we begin to explore what these functions might be.

Chapter 3: Identification and characterisation of a novel protein complex interacting with extra-nucleolar MINA

3.1 Introduction

In the previous chapter, we characterised the factors contributing to the retention of MINA in the nucleolus and investigated which signals trigger translocation to the nucleoplasm. Subsequently, we successfully identified the residues required for nucleolar localisation of MINA. This work raises questions about what other functions of MINA might exist, and which of these might take place in the nucleoplasm, as opposed to the nucleolus.

MINA has been implicated in a variety of cellular processes in addition to RPL27A hydroxylation, ribosome biogenesis and translation. One of these is a role in T-cell differentiation (Okamoto et al., 2009; Yosef et al., 2013), which was discussed in Chapter 1 of this thesis. Additionally, MINA has also been proposed to regulate the expression of proteins involved in cell cycle progression (Ma et al., 2015; Zhang et al., 2005; Aziz et al., 2020) and a proteomic screen linked MINA with proteins involved in DNA

double-strand break repair (Wang et al., 2015b). MINA was also reported to suppress epithelial-mesenchymal transition (EMT) through regulation of the GSK-3β/β-catenin signalling pathway (Geng et al., 2017). Recently, reduced expression of genes regulating stemness and stem cell proliferation was reported following CRISPR-Cas9 mediated MINA knockout (Zhang et al., 2020). Most of these roles were linked with a previously reported histone demethylase activity of MINA, which was likely assigned incorrectly based on more recent structural and biochemical analyses (as discussed in more detail in Chapter 1). Although it is possible that MINA has a direct or indirect role in at least some of the above mentioned pathways, more extensive research is required, particularly with respect to its catalytic activity and the importance of its subcellular localisation.

In this chapter, an unbiased proteomic approach was employed to identify extra-nucleolar interactors of MINA in order to try and help improve our understanding of its alternative functions. Having identified a novel candidate substrate, the interaction was extensively validated and characterised both biochemically and in a variety of cellular contexts.

3.2 Results

3.2.1 Identification of a novel, extra-nucleolar, candidate substrate complex

In 2OG oxygenases, iron coordination is essential for catalytic activity (Lando et al., 2002; Coleman et al., 2007; Ge et al., 2012; Singleton et al., 2014; Feng et al., 2014; Markolovic et al., 2018). Mutation of one or more of the Fe(II) binding residues can prevent substrate binding: this method has previously led to the successful discovery of eRF1 and DRG1/2 as substrates of JMJD4 and JMJD7, respectively (Feng et al., 2014; Markolovic et al., 2018). Indeed, binding of RPL27A to MINA is reduced upon alanine substitution of iron-coordinating site His-179 (H179A; see Figures 3.4C and 3.11C

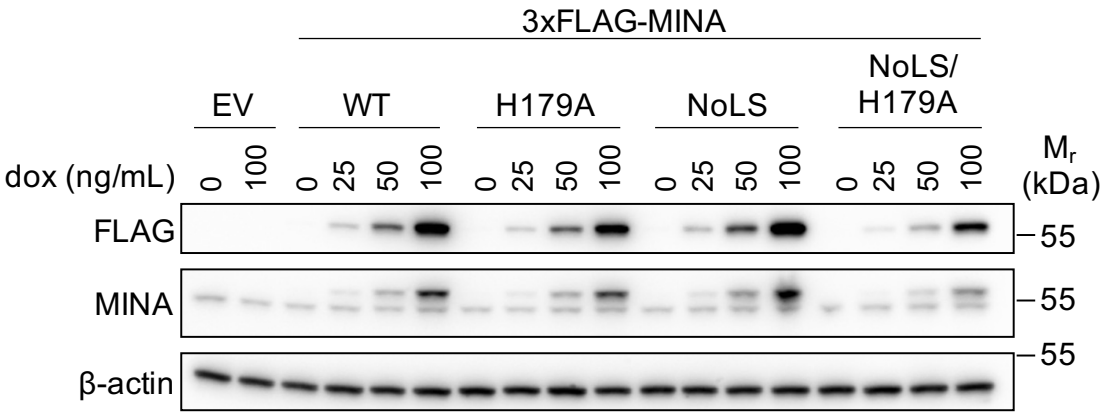


Figure 3.1: Stable expression of doxycycline-inducible 3xFLAG-MINA and mutants in Caco-2. Caco-2 cells were transduced with a pTIPZ empty vector (EV) or vectors encoding the indicated 3xFLAG-tagged MINA mutants, selected with puromycin and expression was induced for 48 hours using the indicated concentrations of doxycycline (dox). Cell extracts were immunoblotted for MINA (53 kDa) and FLAG. β-actin (42 kDa) was used as loading control.

for examples). In order to search for novel MINA candidate substrates resident in different subcellular compartments, vectors encoding doxycycline-inducible 3xFLAG-MINA NoLS and NoLS/H179A mutants were generated (as described in section 2.2.2). Following transduction and puromycin selection of caco-2 cells, inducibility by doxycycline was assessed by a dose titration, shown in Figure 3.1. Subsequently, FLAG-tagged MINA was immunopurified and interactors were identified by liquid chromatography and tandem mass spectrometry (LC-MS/MS). Sample preparation, LC-MS/MS and subsequent analysis were performed by the Advanced Mass Spectrometry Facility at the University of Oxford. Following LC-MS/MS analysis, the spectra were cross-referenced with the human Universal Protein Resource (UPR) database using the Mascot software (Matrix Science). Over a thousand proteins were identified in each sample. The top 250 identified interactors in the 3xFLAG-MINA WT sample were filtered against an empty vector control to remove contaminants, after which 36 hits remained. Subsequently, the score threshold was set to 100 or more, and the emPAI threshold was set to 1 or more. Finally, 28 interactions were assigned as specific to wild-type MINA.

Table 3.1 lists the 28 identified MINA interactors according to the Exponentially Modified Protein Abundance Index (emPAI). The emPAI is calculated based on the

protein coverage by peptide matches and provides a relative quantitative value (see Ishihama et al., 2005 for reference). Importantly, this list includes two known MINA interactors, ribosomal protein 27A (RPL27A) and nucleophosmin (NPM1), which thus validates the screen. Perhaps consistent with the biochemical and structural evidence that MINA is a hydroxylase rather than a histone demethylase (Ge et al., 2012; Chowdhury et al., 2014), no histone proteins co-purified with MINA. Moreover, we did not detect any RPL8, confirming that there is no overlap in substrate specificity between MINA and NO66. The 28 identified interactors were subsequently subjected to STRING analysis (Szklarczyk et al., 2019). An overview of the identified networks is presented in Figure 3.2A. Interestingly, functional enrichment analysis according to biological process indicated enrichment of several processes related to membrane biology (Figure 3.2B) which were attributed to the protein network highlighted in orange in Figure 3.2A. We next filtered the 28 identified interactors for those that showed altered binding between wild-type and extra-nucleolar (NoLS) MINA (Table 3.2) and those that interact with MINA in an activity-dependent manner (Table 3.3). We identified one protein that showed increased interaction with extra-nucleolar MINA and that was dependent on the activity of MINA, membrane palmitoylated protein 6 (MPP6).

Next, we queried the results of additional MINA proteomic screens that had been performed by the Coleman group in other contexts. A preliminary screen in the epithelial bone osteosarcoma cell line U2OS focussed on only wild-type MINA, and identified the interactors shown in Table 3.4. Interestingly, 19 of the 28 candidates identified in Caco-2 were also identified in U2OS (11 when applying the same filtering criteria as Caco-2).

Finally, the results of the Caco-2 screen were cross-referenced with results from a previous screen performed in K-Ras G12V transformed mouse embryonic fibroblasts (MEFs). A list of the interactors also identified in this screen is shown in Table 3.5. It should be noted that, due to low abundance of the bait (approximately 10 times lower than in Caco-2), the filtering thresholds were amended to a score of >40 and an

Protein Name	Accession no.	WT emPAI	H179A emPAI	NoLS emPAI	N/H emPAI
MINA	Q8IUF8	4253	1120	3312	1224
PRDX1	Q06830	11.4	7.2	11.7	14.3
DLG3	Q92796	10.6	5.0	6.0	9.4
MPP7	Q5T2T1	9.8	25.0	7.1	7.1
NPM1	P06748	8.2	3.2	0.4	0.9
WDR55	Q9H6Y2	6.4	2.0	0.7	0.4
LIN7C	Q9NUP9	5.8	5.8	2.6	1.9
RPL27A	E9PLL6	5.67	0.57	2.12	0
KLHL36	Q8N4N3	4.3	3.3	3.3	3.6
CRIPT	Q9P021	3.9	3.9	6.3	3.9
VIM	P08670	3.9	4.3	0	0.6
RCC2	Q9P258	3.8	6.3	7.7	8.4
GNL1	P36915	3.8	4.9	2.0	2.7
LIN7A	O14910	3.2	3.2	1.9	0
NME1	P15531	3.1	1.6	0	0
LLGL1	Q15334	3.0	3.3	6.9	5.7
ARMCX3	Q9UH62	2.7	10.2	20.7	23.2
ALKBH5	Q6P6C2	2.5	2.2	3.9	4.4
MAPK1	P28482	2.1	3.9	3.9	2.9
PRDX2	P32119	1.9	1.9	3.9	2.9
FAU	J3KN89	1.7	1.7	1.7	1.7
PPFIBP2	Q8ND30	1.6	3.4	1.9	3.0
DLG1	Q12959	1.6	1.6	1.0	2.7
PPP2CB	P62714	1.5	0.0	1.5	0.9
MPP6	Q9NZW5	1.3	0.0	5.2	0.0
STRAP	Q9Y3F4	1.3	1.9	1.9	1.0
NACA	Q13765	1.3	0.2	0.5	0.2
BTF3	P20290	1.2	0.3	0.3	1.2
MARCKS	P29966	1.1	0.3	0.8	0.8

Table 3.1: List of 28 proteins interacting with wild-type MINA in Caco-2. Shown are names, accession numbers and emPAI values of proteins identified as interacting with wild-type MINA in descending order of abundance. The bait is highlighted in grey. Last three columns represent the abundance of the indicated proteins as identified in H179A, NoLS and NoLS/H179A mutant samples. Expression of 3xFLAG-MINA was induced for 48 hours using 1 µg/mL doxycycline. Abbreviations: WT = wild-type; H179A = catalytically inactive MINA mutant; NoLS = nucleolar localisation mutant; N/H = NoLS/H179A; EEF1A1 = elongation factor 1α1; PRDX1 = peroxiredoxin-1; DLG3 = disks large homolog 3; MPP7 = membrane palmitoylated protein 7; NPM1 = nucleophosmin 1; WDR55 = WD repeat-containing protein 55; LIN7C = Lin-7 homolog C; RPL27A = 60S ribosomal protein L27A; KLHL36 = Kelch-like protein 36; CRIPT = cysteine-rich PDZ-binding protein; VIM = vimentin; RCC2 = required for completion of mitosis and cytokinesis 2; GNL1 = guanine nucleotide-binding protein-like 1; LIN7A = Lin-7 homolog A; NME1 = nucleoside-binding protein like 1; LLGL1 = lethal giant larvae protein homolog 1; ARMCX3 = armadillo repeat-containing X-linked protein 3; ALKBH5 = alkB homologue 5; MAPK1 = mitogen-activated protein kinase 1; PRDX2 = peroxiredoxin-2; PPFIBP2 = liprin-beta-2; DLG1 = discs large homolog 1; PPP2CB = protein phosphatase 2A catalytic subunit beta isoform; MPP6 = membrane palmitoylated protein 6; STRAP = serine-threonine kinase receptor-associated protein; NACA = nascent polypeptide-associated complex subunit alpha; BTF3 = basic transcription factor 3; MARCKS = myristoylated alanine-rich C-kinase substrate.

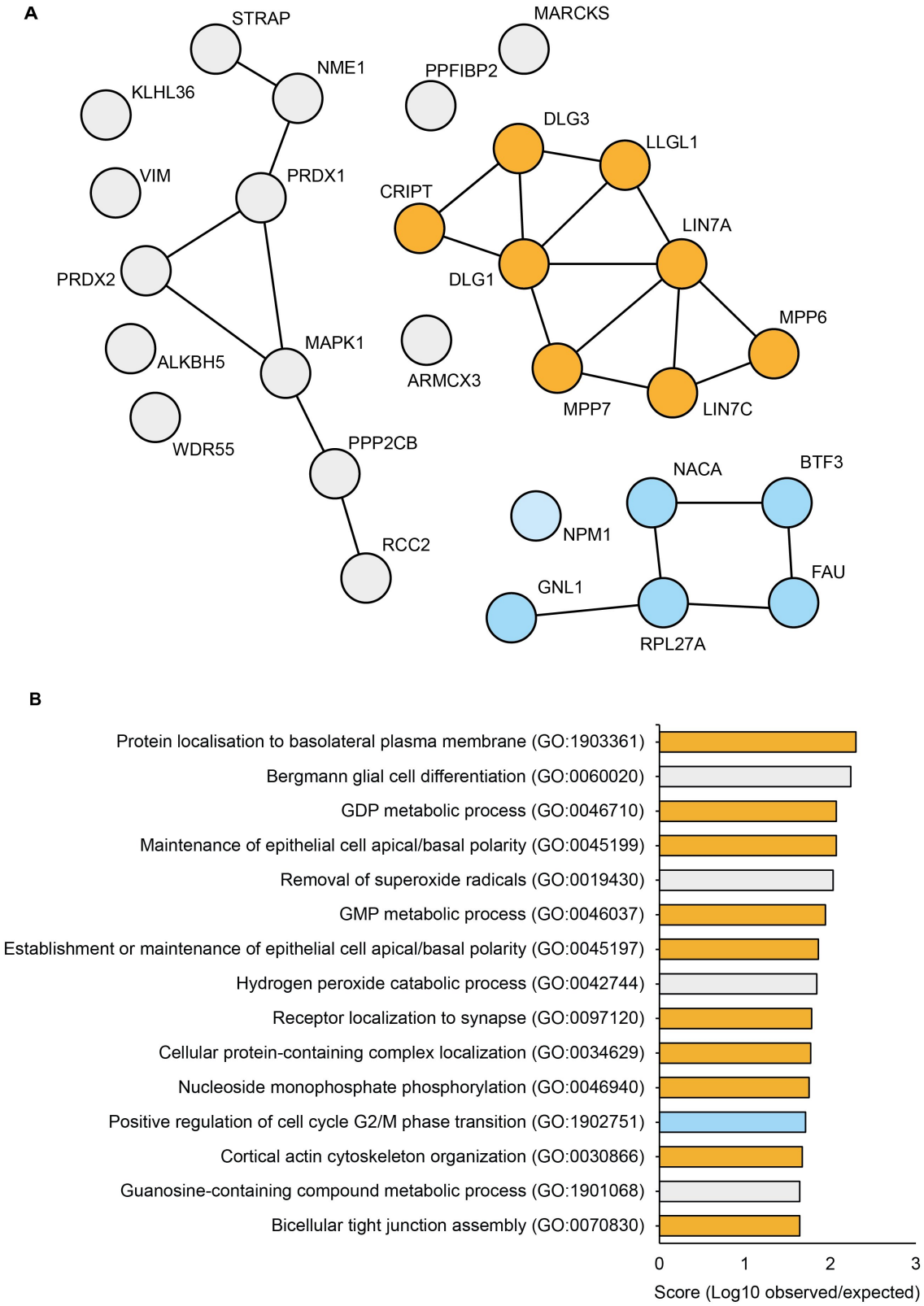


Figure 3.2: Network and functional enrichment analysis of MINA interactors. (**A**) STRING network analysis (https://string-db.org). Network involving known substrate RPL27A and nucleolar components are shown in blue. Newly identified network including peripheral membrane proteins is shown in orange. (**B**) Top 15 categories of Gene Ontology (GO) biological processes as identified by STRING enrichment analysis (https://string-db.org). Score represents the log10 of observed proteins in the sample / expected number of proteins in a random sample of the same size.

Protein name	WT	NoLS
MINA	4253	3312
ARMCX3	2.7	20.7
RCC2	3.8	7.7
LLGL1	3.0	6.9
MPP6	1.3	5.2
NPM1	8.2	0.4
WDR55	6.4	0.7
LIN7C	5.8	2.6
RPL27A	5.7	2.1
VIM	3.9	0.0
NME1	3.1	0.0
NACA	1.3	0.5
BTF3	1.2	0.3

Table 3.2: List of nucleolar/nucleoplasmic-dependent MINA interactors. Table shows emPAI values of proteins that showed either increased (red) or decreased (blue) interaction (fold change >2) with extra-nucleolar (NoLS) MINA compared to wild-type MINA. emPAI values for the bait are shown in grey.

emPAI >0.5. Despite these limitations, this screen successfully identified RPL27A and nucleophosmin (NPM1; Table 3.5). Moreover, MPP6 and LIN7C were also identified as interacting with MINA in an activity-dependent manner (Table 3.6).

Overall, the results of the proteomic screens point towards a possibly novel function for MINA in membrane biology, with MPP6 and LIN7 as extra-nucleolar, activity-dependent interactors that warrant further investigation. Both proteins are suggested or confirmed scaffold proteins that mediate protein complex formation at the plasma membrane (Chytła et al., 2020; Straight et al., 2006). MPP6 belongs to the wider family of membrane-associated guanylate kinases (MAGUKs) that play important roles in epithelial and neuronal membrane biology (Funke et al., 2005; Ye et al., 2018). This family also includes the above identified proteins MPP7, DLG1 and DLG3. A more detailed introduction on epithelial cell polarity and the functions of MPP6, LIN7 and other MAGUKs will be provided in the next Chapter. For the remainder of this Chapter, we focus on validating and characterising the interaction between MINA, MPP6 and LIN7C biochemically and in cellular a context.

Protein	WT	H179A	NoLS	NoLS/H179A
MINA	4253	1120	3312	1224
RPL27A	5.7	0.6	2.1	0
MPP6	1.3	0	5.2	0
NACA	1.3	0.2	0.5	0.2

Table 3.3: List of activity-dependent MINA interactors. Results of the proteomic screen were filtered (fold change >2) for proteins that were identified as interacting with catalytically active (wild-type (WT) or extra-nucleolar (NoLS)) MINA but not with catalytically dead iron-binding mutants (H179A and NoLS/H179A). Shown are emPAI values. Bait values are highlighted in grey.

Protein name	Accession no.	Score	emPAI	No. of sequences
MINA	Q8IUF8	18908	1025	55
NPM1	P06748	1723	26.2	17
MPP6	Q9NZW5	1445	20.7	39
WDR55	Q9H6Y2	1067	10.4	22
PRDX1	Q06830	659	27.7	16
VIM	P08670	603	3.1	16
GNL1	P36915	526	1.6	14
LIN7C	Q9NUP9	522	11.9	11
RCC2	Q9P258	397	1.9	13
RPL27A	E9PLL6	391	15.4	10
LIN7A	O14910	323	4	8
CRIPT	Q9P021	123	2.3	3
DLG1	Q12959	335	0.5	9
KLHL36	Q8N4N	249	0.68	7
NACA	H0YHX	163	0.8	3
ALKBH5	Q6P6C2	136	0.4	3
BTF3	P20290	56	1.6	2
MPP7	Q5T2T1	56	0.1	1
NME1	P15531	39	0.6	1
STRAP	Q9Y3F4	32	0.1	1

Table 3.4: List of MINA interactors first identified in Caco-2 and validated in U2OS. Highlighted in grey are proteins that meet the criteria set for Caco-2 filtering (score >100, emPAI >1). The bait (MINA) is highlighted in blue. This screen was performed by Dr Mathew Coleman.

Protein name	Accession no.	Score	emPAI	No. of sequences
MINA	Q8CD15	4714	134	44
NPM1	Q61937	1068	22.5	16
RPL27A	P14115	213	4.3	6
MPP6	Q9JLB0	138	0.6	6
MAPK1	P63085	68	0.6	4
LIN7C	O88952	48	0.5	2
WDR55	Q9CX97	34	0.1	1
STRAP	Q9Z1Z2	31	0.1	1
PRDX1	ns	ns	ns	ns
VIM	ns	ns	ns	ns
RCC2	ns	ns	ns	ns
GNL1	ns	ns	ns	ns

Table 3.5: List of MINA interactors first identified in Caco-2 and validated in K-Ras G12V MEFs. Highlighted in grey are proteins that meet the criteria of a score >40 and emPAI >0.5. Criteria were revised due to lower abundance of the bait (approx. 10 times lower than Caco-2; highlighted in blue). ns = non-specific (also detected in empty vector control). This screen was performed by Dr Mathew Coleman.

The results of the proteomic screen were first validated by immunoblot against MPP6 and LIN7C following immunoprecipitation (IP) of HA- or FLAG-tagged MINA from extracts of HEK293T or Caco-2 cells, respectively (Figure 3.3). Antibody validation by siRNA revealed that the LIN7C antibody recognises both LIN7C (22 kDa, lower band) and LIN7A (26 kDa, upper band) (Dr James Bundred, data not shown). Furthermore, consistent with the results of the proteomic screen (Tables 3.1 and 3.2), both proteins were also detected as interacting with the nucleolar localisation mutant (NoLS), suggesting they are possible extra-nucleolar substrates (Figure 3.3). Interestingly, although preliminary at this point, we noted that binding of MPP6 to the NoLS mutant was stronger than to wild-type MINA (Figure 3.3A and B). The interaction between endogenous MINA and MPP6 was also confirmed by immunoprecipitation of endogenous MPP6 from HEK293T cells (Figure 3.3C).

Next, we sought to test the activity-dependent and extra-nucleolar interaction between MINA and MPP6/LIN7 in other cell lines. For this reason, a pTIPZ empty vector (EV) or vectors containing the doxycycline-inducible 3xFLAG-MINA WT, H179A, NoLS or NoLS/H179A series were first transduced into SW620. A doxycycline titra-

Protein name	WT	H179A
MINA	134	112
RPL27A	4.3	0.7
MPP6	0.6	0
LIN7C	0.5	0

Table 3.6: List of activity-dependent MINA interactors first identified in Caco-2 and validated in K-Ras G12V MEFs. Values represent emPAI. The bait is highlighted in blue. This screen was performed by Dr Mathew Coleman.

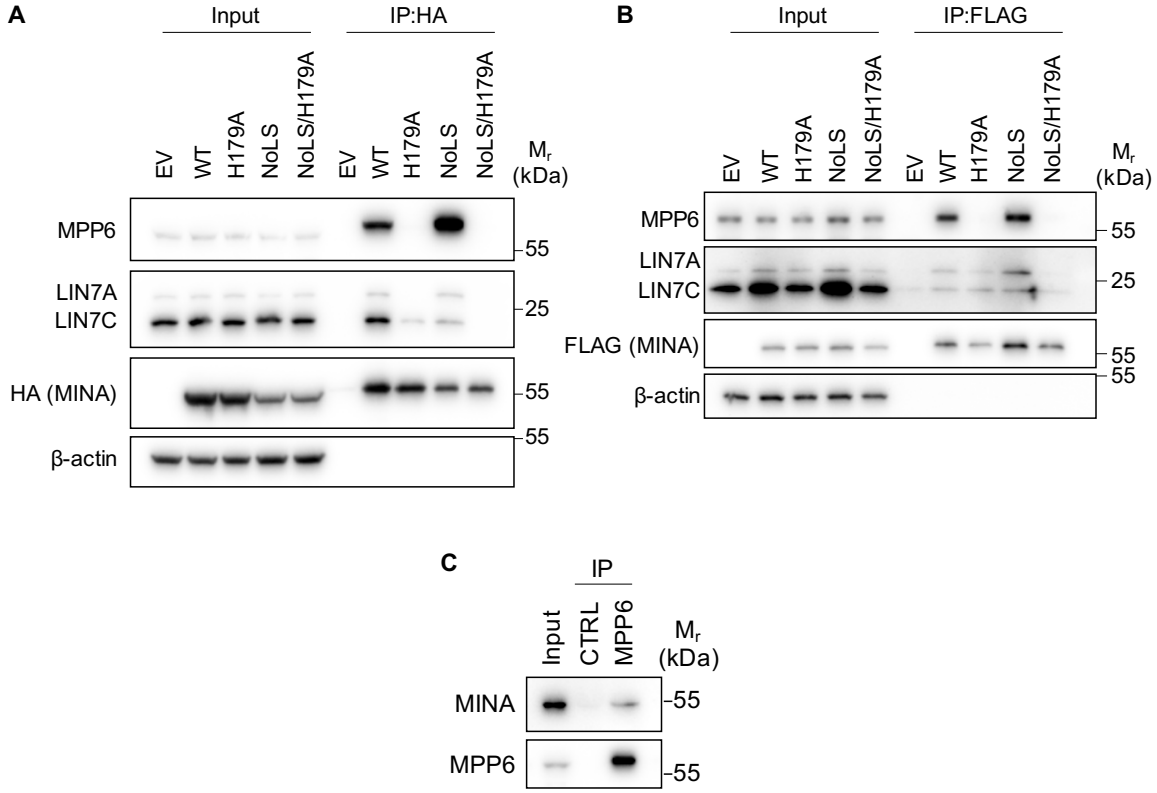


Figure 3.3: Wild-type and extra-nucleolar MINA interact with MPP6 and LIN7 in an activity-dependent manner. (**A**) Anti-HA immunoprecipitates from extracts of HEK293T cells transiently transfected with the indicated HA-MINA constructs were immunoblotted for MPP6 (61 kDa), LIN7A/C (26/22 kDa), HA (MINA, 53 kDa) and β-actin (42 kDa). Input = cell extract prior to immunoprecipitation (IP). The amount of input sample loaded, relative to the amount of material of the IP, is 5% (MPP6, LIN7C), 100% (HA, β-actin). (**B**) Anti-FLAG immunoprecipitates from lysates of stable Caco-2 cells expressing the indicated doxycycline-inducible 3xFLAG-MINA constructs were immunoblotted as indicated. Expression of exogenous 3xFLAG-MINA was induced for 48 h using 1 µg/mL doxycycline. Input = 0.6% (MPP6, LIN7A/C), 31% (FLAG, β-actin). (**C**) Co-immunoprecipitation of endogenous MINA with MPP6. Endogenous MPP6 was purified from extracts of HEK293T cells and immunoblotted for MINA (53 kDa) and MPP6 (61 kDa, GeneTex antibody). MINA coprecipitates with anti-MPP6 but not with the control (CTRL; species-matched control IgG) IP. Input = 0.14% (MINA), 11% (MPP6).

tion is shown in Figure 3.4A. We confirmed that, when overexpressed in this cell line, wild-type 3xFLAG-MINA and H179A localise to the nucleoli, whereas the nucleolar mutants (NoLS and NoLS/H179A) were excluded from this subnuclear compartment (Figure 3.4B). Subsequently, anti-FLAG immunoprecipitation experiments showed that LIN7C and/or MPP6 coprecipitate with 3xFLAG-MINA WT and NoLS in an activity-dependent manner (Figures 3.4C). Consistent with the results shown in Figure 3.3, it appears as though more MPP6 may coprecipitate with the NoLS mutant than with WT MINA (Figure 3.4C). Importantly, RPL27A was confirmed to coprecipitate with wild-type MINA, but not with the nucleolar localisation mutant (Figure 3.4C).

U2OS cells were also transduced with the 3xFLAG-MINA-containing vector series (Figure 3.5). A doxycycline titration is shown in Figure 3.5A. Although expression levels of exogenous MINA were similar to endogenous MINA when using a doxycycline concentration of 10 ng/mL, indirect immunofluorescence analysis showed significant heterogeneity in expression levels of 3xFLAG-MINA, with no detectable expression in many cells (data not shown). Therefore, to validate the results of the proteomic screen by immunoprecipitation experiments, we used a concentration of 1 µg/mL of doxycycline. As presented in Figure 3.5B, the activity-dependent association between 3xFLAG-MINA and endogenous MPP6 was confirmed also in this cell line. Moreover, MPP6 also precipitated with the nucleolar mutant (NoLS), but not with the double mutant (NoLS/H179A). It should be noted however, that at this concentration, similar to Caco-2, exogenous MINA is expressed in the nucleoli as well as nucleoplasm (Figure 3.5). This may explain why similar amounts of MPP6 precipitated with WT and NoLS-mutated MINA. In summary, the experiments presented in Figures 3.3, 3.4 and 3.5 suggest that MPP6 and LIN7A/C are extra-nucleolar interactors of MINA and that this interaction is prevalent in a range of cell lines.

Next, it was of interest to investigate how the MINA-MPP6-LIN7 complex is formed. The interaction between MPP6 and LIN7 was previously reported (Kamberov et al., 2000; Tseng et al., 2001) and is mediated *via* the highly conserved N-terminal L27 domain of MPP6 (Tseng et al., 2001). Having identified both proteins as MINA

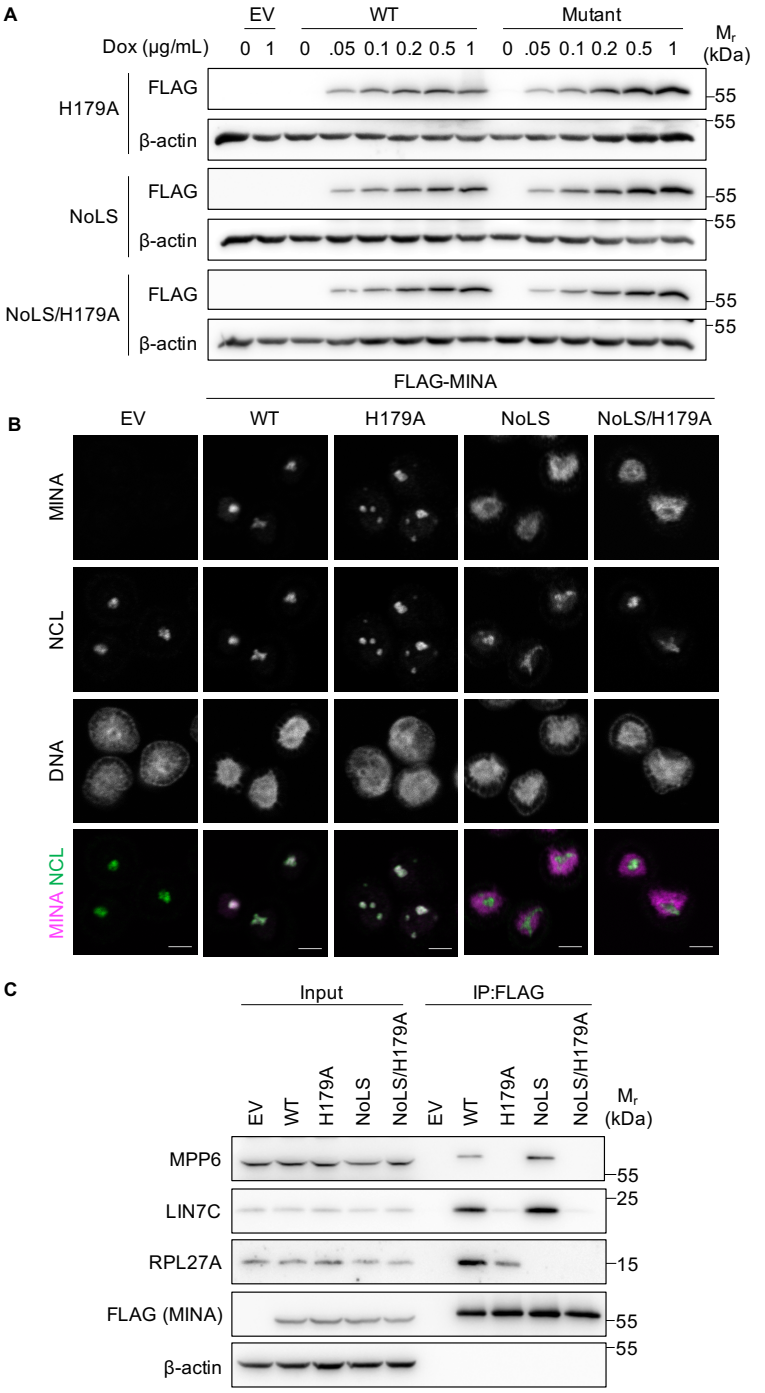


Figure 3.4: Wild-type and extra-nucleolar MINA interact with MPP6 and LIN7 in an activity-dependent manner in SW620 cells. (**A**) Doxycycline (Dox) dose titration of exogenous 3xFLAG-MINA in stable SW620 cells. Extracts from cells expressing the indicated constructs, treated with the indicated doses of doxycycline for 48 hours were immunoblotted for FLAG. (**B**) Localisation of 3xFLAG-MINA mutants in SW620. Stable SW620 cells expressing the indicated 3xFLAG-MINA constructs were fixed and stained for MINA (magenta) and nucleolin (NCL, green). Nuclei were visualised with DAPI. Scale bars represent 5 µm. Images were acquired using a Zeiss LSM 880 confocal microscope equipped with a 60x C-Apochromat 1.2 W Korr M27 objective and ZEN black software. (**C**) Anti-FLAG immunoprecipitates from cell extracts of SW620 cells stably expressing the indicated 3xFLAG-MINA mutants were immunoblotted for MPP6 (61 kDa, GeneTex antibody), LIN7C (22 kDa), RPL27A (16 kDa) and FLAG (MINA, 53 kDa). Input = 2.5% (MPP6), 0.125% (LIN7C/RPL27A), 37% (FLAG/β-actin) (**A,C**) β-actin was used as loading control. (**B,C**) Cells were treated with 0.2 µg/mL doxycycline for 48 hours to induce expression of 3xFLAG-MINA.

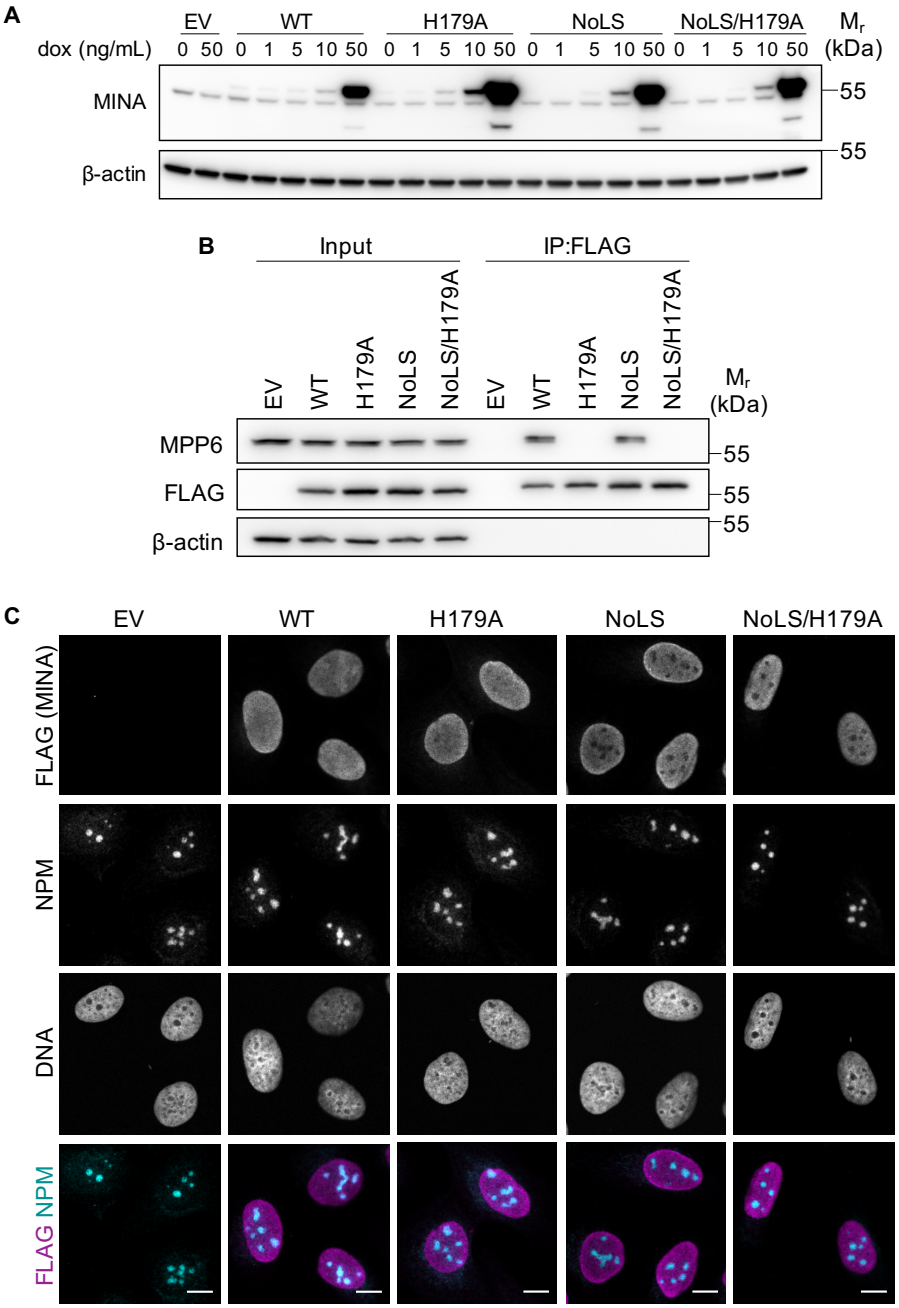


Figure 3.5: Wild-type and exta-nucleolar MINA interact with MPP6 in an activity-dependent manner in U2OS cells. (**A**) Doxycycline (Dox) dose titration of exogenous 3xFLAG-MINA in stable U2OS cells. Extracts from cells expressing the indicated constructs, treated with the indicated doses of doxycycline for 48 hours were immunoblotted for FLAG. (**B**) Anti-FLAG immunoprecipitates from lysates of U2OS cells, treated with 1 µg/mL doxycycline for 48 h to induce expression of the indicated 3xFLAG-MINA constructs were immunoblotted for MPP6 (61 kDa, Atlas Antibodies) and FLAG (MINA, 53 kDa). Input = 1.7% (MPP6), 16.7% (FLAG, β-actin). (**A,B**) β-actin (42 kDa) was used as loading control. (**C**) Localisation of 3xFLAG-MINA in U2OS. Stable U2OS cells were treated with doxycycline as in (B) to express expression of the indicated 3xFLAG-MINA constructs were fixed with PFA and stained for FLAG (magenta) and nucleolin (NCL, cyan). Nuclei were visualised with DAPI. Scale bars represent 10 µm. Images were acquired using a Zeiss LSM 880 confocal microscope equipped with a 40x C-Apochromat 1.2 W Korr M27 objective and ZEN black software.

interactors, we therefore sought to clarify whether MPP6 independently interacts with MINA or whether LIN7 mediates complex formation. To this end, HA- and FLAG-tagged MPP6 and MINA constructs were generated, respectively. We first confirmed that, when co-overexpressed in HEK293T cells, the interaction between MPP6 and MINA remains activity-dependent (Figure 3.6A). We noted that MINA overexpression did not affect the interaction between MPP6-HA and endogenous LIN7A/C (Figure 3.3A). Next, FLAG-MINA was co-overexpressed with MPP6-HA that was either full-length (FL) or that lacked the L27 domains responsible for LIN7 binding ($MPP6^{110\text{-}541}$, a schematic is shown in Figure 3.6B). As shown in Figure 3.6C, whereas LIN7 only coprecipitated with full-length MPP6, FLAG-MINA was bound to both $MPP6^{FL}$ and $MPP6^{110\text{-}541}$. Therefore, we conclude that the interaction between MPP6 and MINA is largely independent of LIN7 binding (Figure 3.6C), and we next focussed on characterising the interaction between MPP6 and MINA in more detail.

3.2.2 Subcellular localisation of the MINA:MPP6 complex

To extend the validation of the proteomic screen, which suggests that MPP6 is an extra-nucleolar MINA-interacting protein, we characterised the interaction in conditions where MINA is either enriched in the nucleolus or in the nucleoplasm. As shown in Chapter 2, MINA is predominantly nucleolar in SW620 colorectal cancer cells (Figure 2.1), and translocation to the nucleoplasm is successfully triggered by treatment with 40 ng/mL actinomycin D (AMD, Figure 2.8). Further to this, we found that an increased amount of MPP6 co-precipitated with wild-type MINA (Figure 3.7) following AMD treatment. Importantly, as noticed before, the interaction of MPP6 with FLAG-MINA NoLS was greater than wild-type MINA, and this was not further elevated by AMD treatment (Figure 3.7), consistent with the possibility that MINA and MPP6 interact outside of the nucleolus. These data therefore suggest that nucleolar localisation is not required for, and might even interfere with, MPP6 binding.

The data presented in Chapter 2 suggest that MINA can be localised in either in the nucleolus or in the nucleoplasm. However, mammalian MPP6, as well as its *Drosophila*

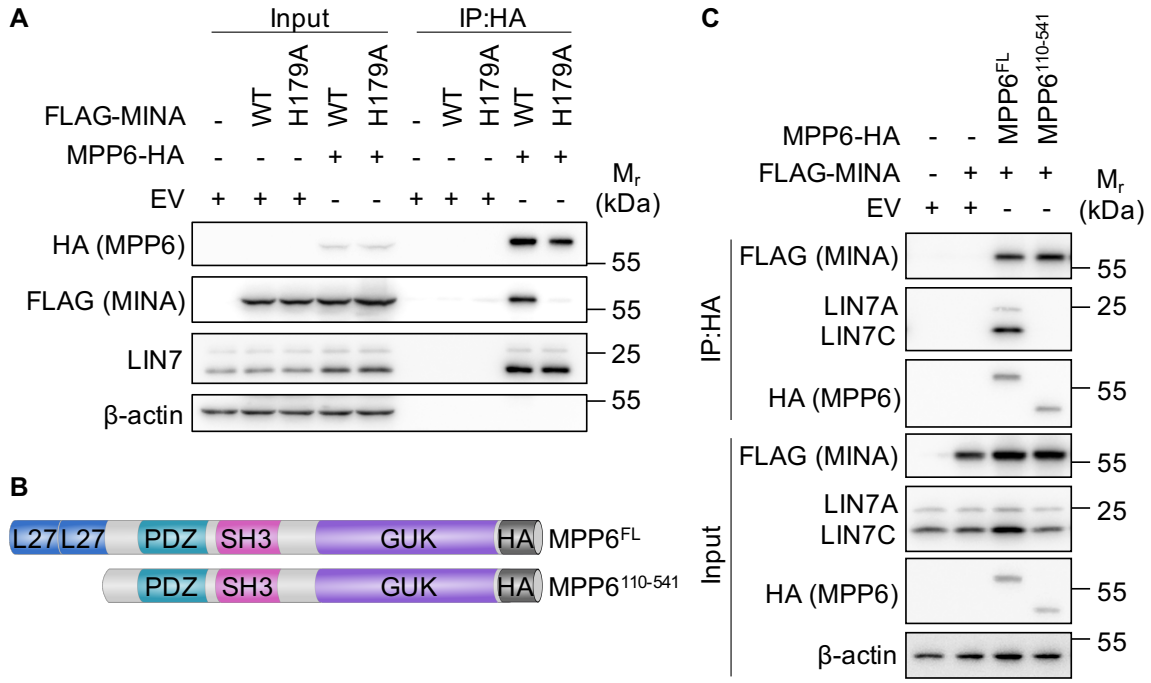


Figure 3.6: The interaction between MINA and MPP6 is independent of LIN7A/C. (**A**) Activity-dependent interaction between overexpressed MPP6-HA and FLAG-MINA. Anti-HA immunoprecipitates from cell extracts of HEK293T cells expressing the indicated constructs were immunoblotted for FLAG (MINA, 53 kDa), HA (MPP6, 61 kDa) and LIN7A/C (26/22 kDa). (**B**) Domain structures of MPP6 mutants used in (C). (**C**) FLAG-MINA coprecipitates with MPP6-HA that is defective in LIN7 binding ($MPP6^{110\text{-}541}$). Anti-HA immunoprecipitates from cell extracts of HEK293T cells expressing the indicated constructs were immunoblotted as indicated. (**A,C**) EV = empty vector. β-actin (42 kDa) was used as loading control. Input = 20%. (**B,C**) FL = full-length.

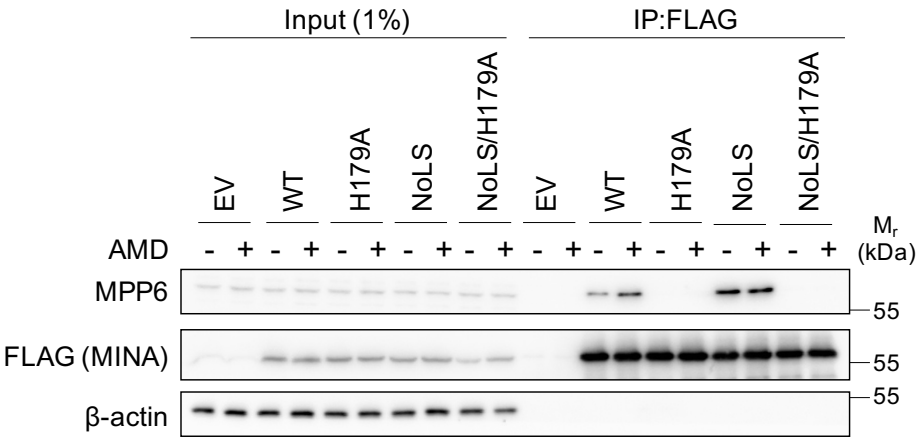


Figure 3.7: MPP6 binding to MINA increases upon extra-nucleolar localisation. Anti-FLAG immunoprecipitates from extracts of stable SW620 cells expressing an empty vector (EV) or the indicated 3xFLAG-MINA constructs were immunoblotted for MPP6 (61 kDa, GeneTex antibody) and FLAG (MINA, 53 kDa). β-actin (42 kDa) was used as loading control. Expression of 3xFLAG-MINA was induced with 0.2 µg/mL doxycycline for 24 hours before the cells were treated with 40 ng/mL actinomycin D (AMD) for 4 hours. Abbreviations: WT = wild type; NoLS = nucleolar localisation mutant; H179A = catalytically inactive mutant.

melanogaster orthologue, are reported to be peripheral membrane proteins (Shingai et al., 2003; Wu et al., 2007; Moyer and Jacobs, 2008; Kamijo et al., 2016), raising questions about how and when MINA and MPP6 co-localise. It was therefore of interest to investigate the subcellular localisation of MPP6 and, specifically, to assess whether at least in some conditions, MPP6 might localise to the nucleus. Due to initial suspicions about the specificity of the available reagents for the detection of endogenous MPP6 by immunofluorescence, stable cell lines constitutively expressing C-terminally HA-tagged MPP6 were generated. First, MPP6-HA localisation in low *versus* high density cultures was assessed, given the observation that MINA translocates depending on cell density. As expected based on published reports, MPP6 was localised in close proximity to the membrane in a confluent monolayer (Figure 3.8A). Interestingly however, in low density cell culture conditions, we also noted nuclear MPP6 in a proportion of the cells. In addition to indirect immunofluorescence, nuclear and cytoplasmic localisation of MPP6-HA was confirmed by subcellular fractionation (Figure 3.8B). Furthermore, in the highly transformed and rapidly proliferating cervical adenocarcinoma cell line HeLa, MPP6, either transiently expressed (MPP6-HA) or endogenous, was consistently

absent from the membrane, but was instead present in the nucleus and cytoplasm (Figure 3.8C and D).

Having independently observed both MINA and MPP6 in the nucleoplasm, we next sought to investigate whether they in fact co-localise. First, we assessed the localisation of FLAG-MINA and MPP6-HA by indirect immunofluorescence in Caco-2 cell lines stably expressing FLAG-MINA and transiently transfected with MPP6-HA and confirmed that both proteins are partly co-localised in the nucleoplasm (Figure 3.9A). Although co-localisation by immunofluorescence is consistent with a potential interaction, it is not sufficient in isolation to conclude that two proteins physically interact in a specific compartment. Therefore, additional orthogonal assays are beneficial. One example of such an experiment is a proximity ligation assay (PLA). Here, the secondary antibodies are conjugated with oligonucleotide probes that circularise only when two proteins are in very close proximity (<40 nm) to each other, consistent with them interacting (Jarvius et al., 2007). Moreover, this technique allows detection of interactions at the single protein level. Further details about the multi-step PLA protocol are presented in the Materials and Methods chapter in this thesis. As shown in Figure 3.9B, PLA foci were concentrated in the nucleoplasm of cells co-overexpressing FLAG-MINA and MPP6-HA, consistent with the immunofluorescence data shown in Figure 3.9A. Moreover, PLA foci were also observed following co-expression of MPP6-HA with the nucleolar localisation mutant (FLAG-MINA$^{\mathrm{NoLS}}$), consistent with our coprecipitation data. Furthermore, PLA foci were only present in cells that were fixed whilst at low density, before a confluent monolayer had been formed (Figure 3.9C), consistent with the redistribution of MPP6 to the membrane in confluent cells (shown in Figure 3.8). Taken together, our immunofluorescence and proximity ligation studies suggest that MINA and MPP6 colocalise in the nucleoplasm of low density cells.

In order to further investigate the effect of confluence on the MINA:MPP6 interaction we performed an immunoprecipitation experiment. Specifically, FLAG-MINA was immunoprecipitated from Caco-2 cells expressing an empty vector (EV), FLAG-MINA WT or a nucleolar localisation mutant (NoLS) that were either seeded at a low or high

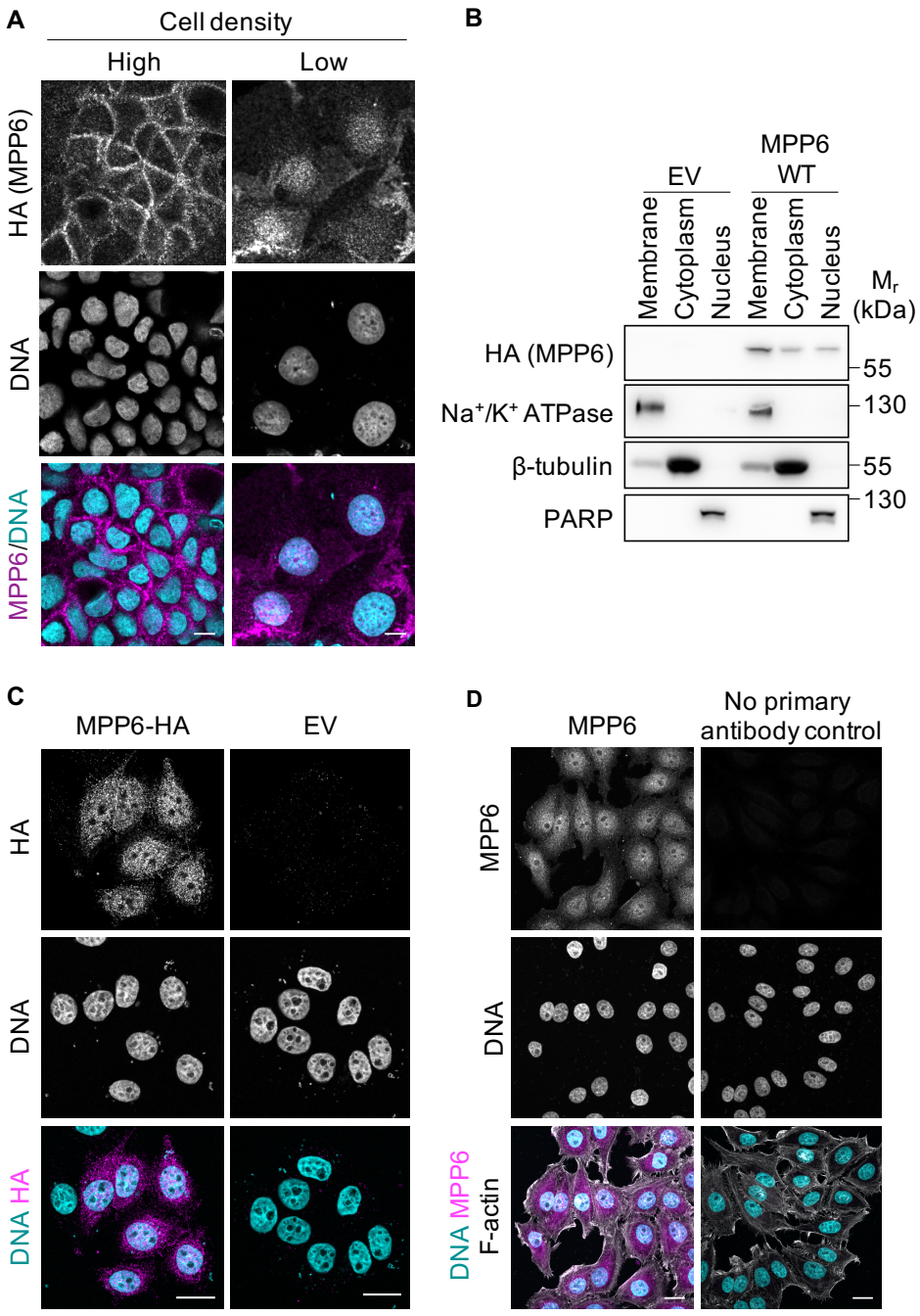


Figure 3.8: Nuclear localisation of MPP6 in proliferating cells. (**A**) Localisation of MPP6-HA in high and low density Caco-2 cultures. Stable Caco-2 cells constitutively expressing C-terminally HA-tagged MPP6 were fixed with PFA and stained for HA (magenta). Scale bar represents 10 µm. (**B**) Biochemical fractionation of a confluent monolayer of stable Caco-2 cells constitutively expressing an empty vector (EV) or MPP6-HA. Cell extracts were immunoblotted for HA (MPP6, 61 kDa), Na^+/K^+ ATPase subunit α-1 (113 kDa), β-tubulin (50 kDa) and Poly (ADP-ribose) polymerase (PARP, 113 kDa). (**C,D**) Nuclear/cytoplasmic localisation of MPP6 in HeLa. Scale bars represent 20 µm. (**C**) HeLa cells transiently transfected with an empty vector (EV) or MPP6-HA were fixed with PFA and stained for HA (MPP6, magenta). (**D**) HeLa cells were fixed with PFA and stained for endogenous MPP6 (Atlas Antibodies, shown in magenta) and F-actin (grey). (**A,C-D**) Nuclei were visualised with DAPI (cyan). Images were acquired using a Zeiss LSM 880 confocal microscope equipped with a 40x C-Apochromat 1.2 W Korr M27 objective and ZEN black software.

density, and coprecipitation of endogenous MPP6 was assessed. Consistent with the data presented in Figure 3.9, more MPP6 co-precipitated with wild-type FLAG-MINA extracted from subconfluent cells than from confluent cells (Figure 3.10A). We also noted increased coprecipitation of MPP6 with the NoLS mutant in subconfluent cells, even though the localisation of the NoLS mutant in subconfluent and confluent cells appears to be identical (Figure 3.10B), indicating that nuclear enrichment of MPP6 may be an important factor for the interaction. Overall, the data presented in this section suggest that a (narrow) window may exist where MINA and MPP6 are both present in the nucleoplasm at the same time. Although further analyses are required, we could speculate that this window may be cell cycle-specific or exist in response to certain growth-associated signalling cues.

3.2.3 Biochemical characterisation of the MINA:MPP6 complex

In addition to characterising where and when the interaction between MINA and MPP6 occurs in cells, it was of interest to characterise the molecular determinants of the MINA:MPP6 interaction. We considered that understanding this in more detail might support subsequent studies investigating the function of the interaction.

3.2.3.1 MPP6 interacts with MINA in a specific and substrate-like manner

The observation that MINA interacts with MPP6 in a manner that is dependent on its catalytic activity (i.e. MINA H179A does not bind MPP6) would suggest that MPP6 is possibly a substrate. Following on from this observation, we sought to further explore MPP6's candidacy as a novel MINA substrate.

The crystal structure of MINA in complex with an RPL27A peptide revealed that, in addition to residues that are located within the catalytic domain, residues within the dimerisation (Asp333) and winged helix (Met405) domains also form interactions with RPL27A that are essential for efficient hydroxylation of H39 *in vitro* (Chowdhury

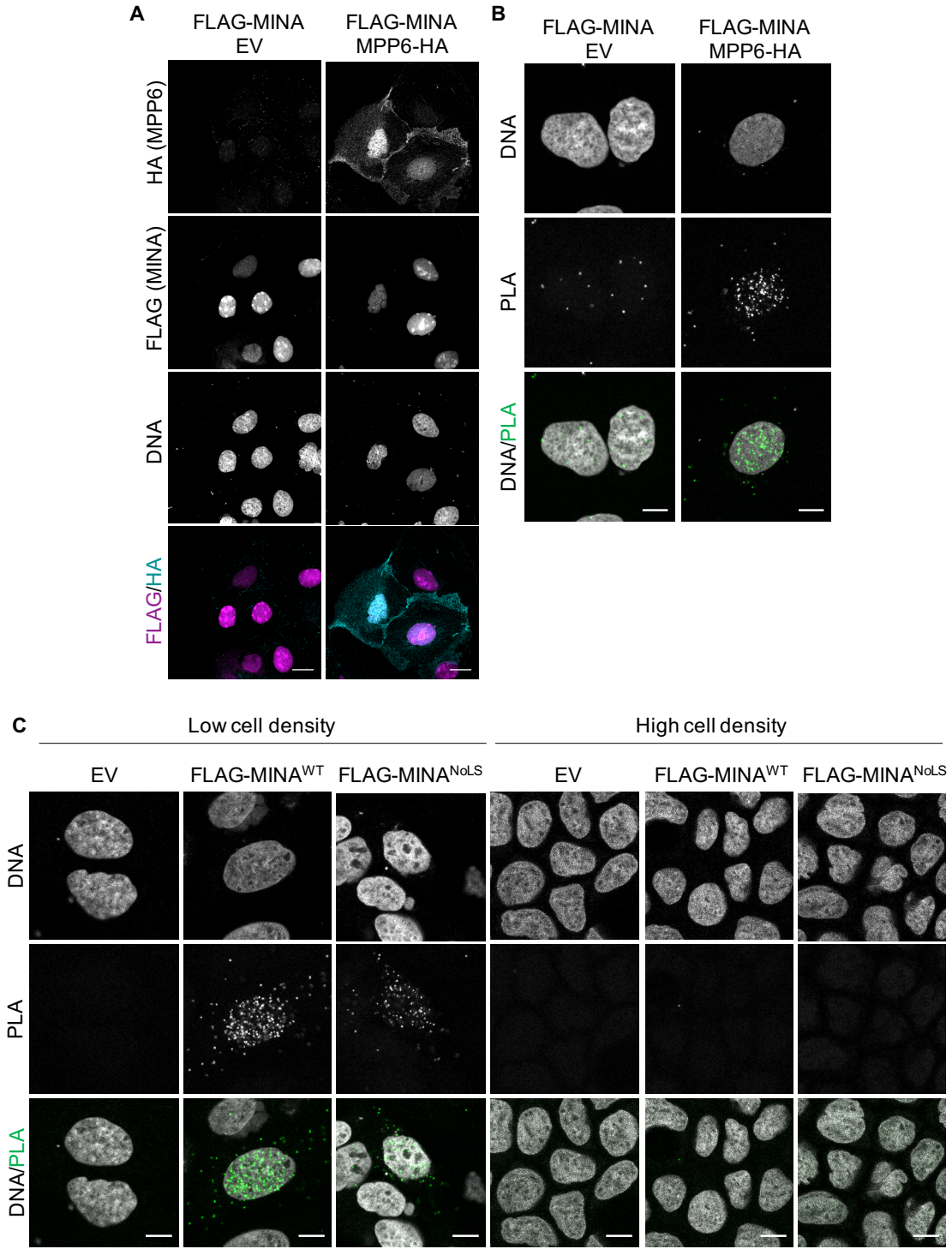


Figure 3.9: MINA and MPP6 co-localise in the nucleoplasm. (**A,B**) Co-localisation of 3xFLAG-MINA and MPP6-HA in stable Caco-2 cells expressing doxycycline-inducible 3xFLAG-MINA and transiently transfected with MPP6-HA was assessed by indirect immunofluorescence using antibodies against the FLAG (MINA, magenta) and HA (MPP6, cyan) tags (A) and a proximity ligation assay (PLA, green foci, B). Scale bars represent 20 µm (A) and 10 µm (B). (**C**) Co-localisation of 3xFLAG-MINA WT/NoLS and endogenous MPP6 was revealed by PLA (green foci) in subconfluent, but not in confluent Caco-2 cells. Scale bars represent 10 µm. (**A-C**) Expression of 3xFLAG-MINA was induced for 48 h using 0.1 µg/mL doxycycline. Cells were fixed with PFA. Nuclei were visualised with DAPI (grey). Images were acquired using a Zeiss LSM 880 confocal system equipped with a 40x C-Apochromat 1.2 W Korr M27 objective and ZEN black software.

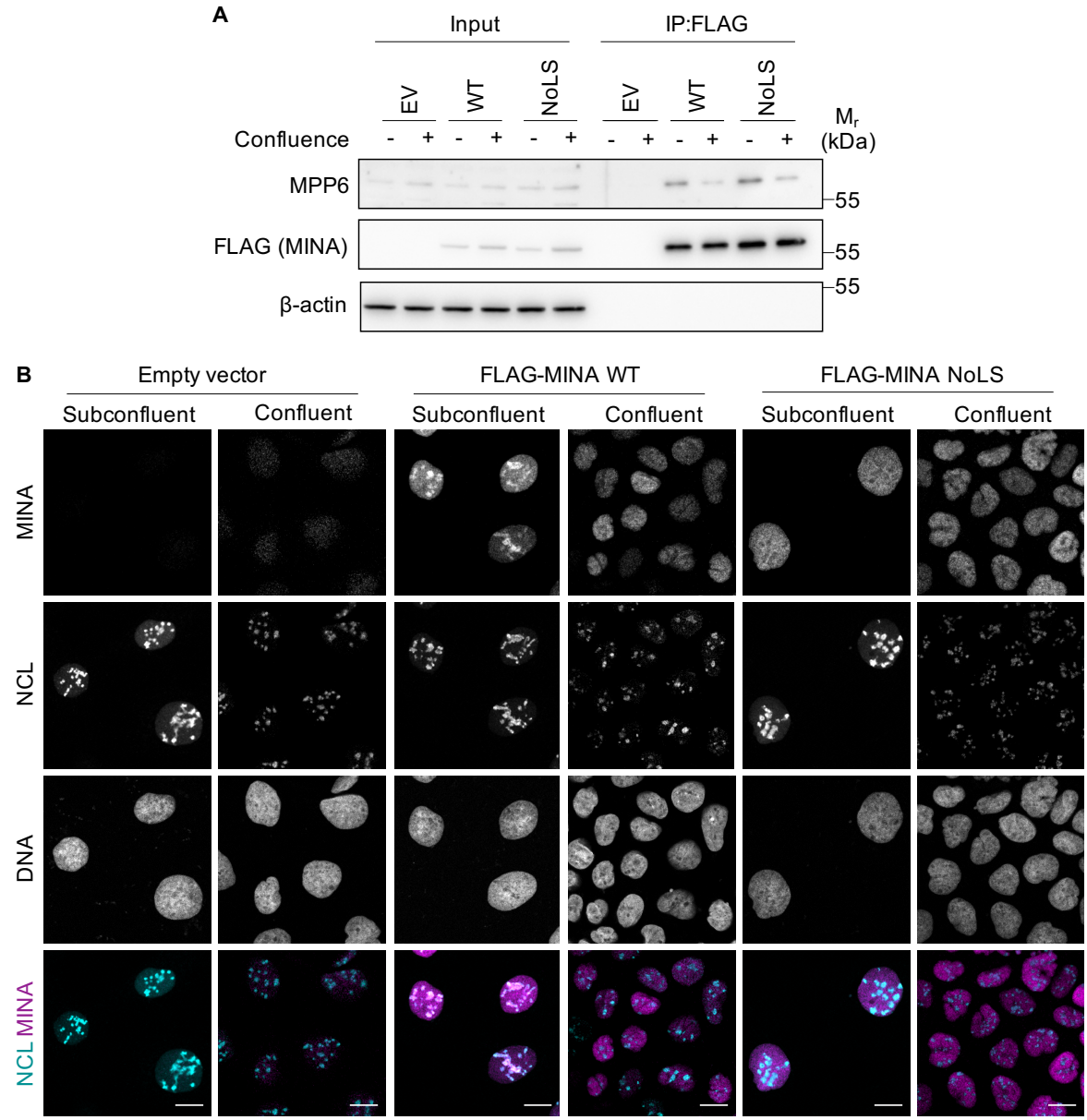


Figure 3.10: MINA and MPP6 preferentially interact in subconfluent cells. (**A**) Anti-FLAG immunoprecipitates from extracts of stable Caco-2 cells expressing the indicated constructs were immunoblotted for MPP6 (61 kDa, GeneTex antibody) and FLAG (MINA, 53 kDa). Expression of 3xFLAG-MINA was induced for 48 hours using 1 µg/mL doxycycline. β-actin (42 kDa) was used as loading control. Input = 0.25% (MPP6), 0.8% (FLAG, β-actin). (**B**) Representative immunofluorescence images showing the localisation of the indicated 3xFLAG-MINA constructs in subconfluent and confluent conditions. Expression of 3xFLAG-MINA was induced for 48 h using 0.1 µg/mL doxycycline. Cells were fixed with PFA and stained for MINA (magenta) and nucleolin (NCL, cyan). Scale bars represent 15 µm. Nuclei were visualised with DAPI. Images were acquired using a Zeiss LSM 880 confocal system equipped with a 40x C-Apochromat 1.2 W Korr M27 objective and ZEN black software.

et al., 2014; Figure 3.11A). To determine whether these residues are also important for interaction with MPP6, we replaced D333 and M405 with alanine. Consistent with the literature, mutation of D333/M405 reduced RPL27A binding (Figure 3.11B). Interestingly, these substitutions also reduced binding of endogenous MPP6, although not to the same extent as their effect on RPL27A binding, or the effect of MINA H179 mutation (H179A; Figure 3.11B).

Next, we assessed the effect of cofactor presence on binding. It is well established that 2OG oxygenases require Fe(II), oxygen and 2OG as cofactors for catalytic activity. For this reason, HEK293T cells expressing HA-tagged MINA were treated for 15 hours with iron-chelator desferrioxamine (DFO) or dimethyloxalylglycine (DMOG), a cell-permeable precursor of the competitive 2OG inhibitor N-oxalylglycine (NOG; Jaakkola et al., 2001). The effectiveness of drug treatment was validated by immunoblotting for HIF1α stabilisation (due to HIF prolyl hydroxylase inhibition, see Chapter 1). Surprisingly, treatment with DMOG completely abrogated both RPL27A and MPP6 binding. Iron chelation, in contrast, did not noticeably affect binding of RPL27A, nor MPP6 (Figure 3.11C).

The effect of DMOG on MPP6/RPL27A binding was unexpected as DMOG usually locks a substrate in the catalytic domain, thereby increasing the interaction between enzyme and substrate and facilitating detection of the interaction (Cockman et al., 2006; Coleman et al., 2007; Markolovic et al., 2018). To test whether the effect observed might be caused by indirect effects of prolonged treatment, a DMOG time course was performed. HEK293T cells expressing both HA-tagged MPP6 and FLAG-tagged MINA were treated with DMOG for 0, 10, 60 or 480 minutes. Surprisingly, a decrease in MPP6 binding was noted in as little as 10 minutes (Figure 3.11D). Although the effect of DMOG and iron chelations were unexpected, they were consistent between RPL27A and MPP6. Combined with the mutation analysis the results in this section are still supportive of MPP6 as a potential novel MINA substrate.

Next, we sought to assess the specificity of the interaction between MINA and MPP6. It was previously reported that there is no cross-reactivity between MINA and

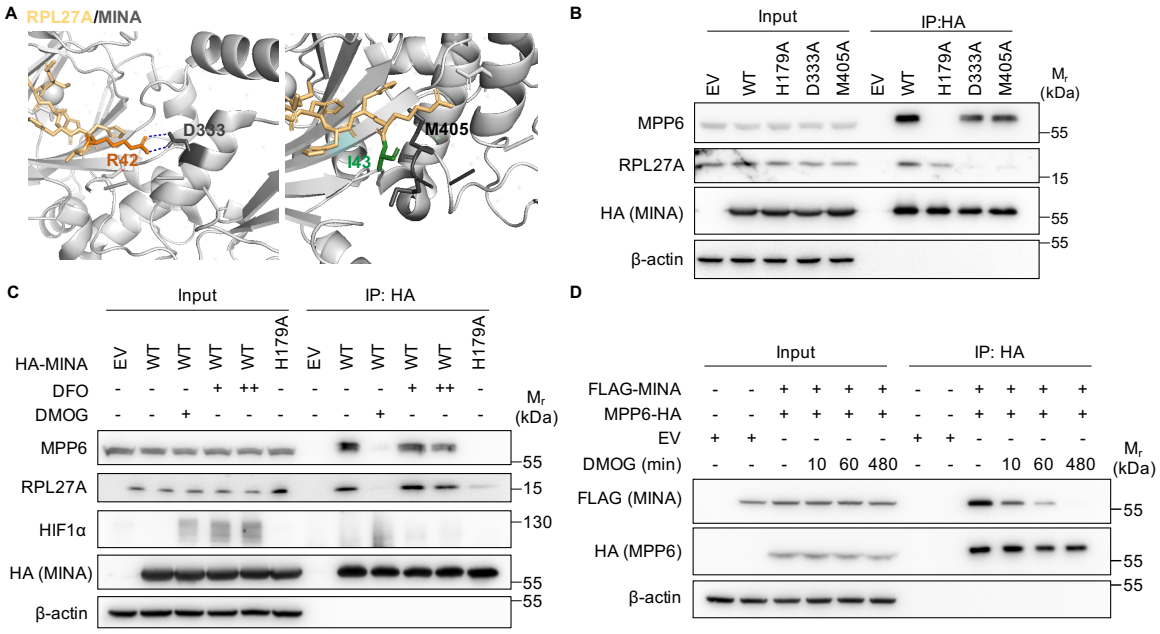
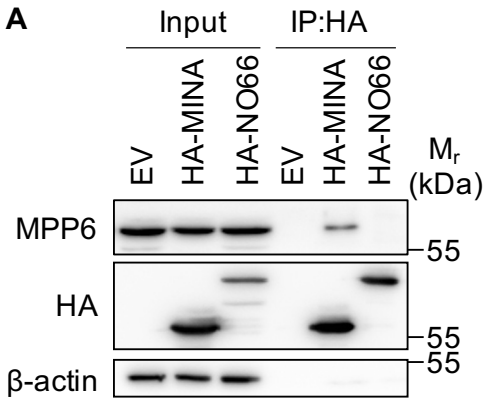


Figure 3.11: MPP6 binds MINA in a substrate-like manner. (**A**) Ribbon representations of a MINA monomer showing the salt bridge interaction between MINA asparagine-333, located in the dimerisation domain, and RPL27A arginine-42 (left panel) and the hydrophobic interaction between MINA methionine-405, located in the winged-helix (WH) domain, and RPL27A isoleucine-43 (right panel). PDB ID = 4BXF. Structures were visualised using PyMOL. (**B**) Coprecipitation of MPP6 and RPL27A with HA-MINA is affected by mutation. Anti-HA immunoprecipitates from cell extracts of HEK293T cells transiently expressing an empty vector (EV) or the indicated HA-tagged MINA variants were immunoblotted for HA (MINA, 53 kDa) and MPP6 (61 kDa, Atlas Antibodies). Input = 2.5% (MPP6), 1% (RPL27A), 50% (HA, β-actin). (**C**) DMOG and DFO affect coprecipitation of MPP6 and RPL27A with HA-MINA in a similar manner. Anti-HA immunoprecipitates from cell extracts of HEK293T cells expressing empty vector (EV), wild-type (WT) HA-MINA or the catalytically dead H179A mutant were immunoblotted for MPP6 (61 kDa, Atlas Antibodies), RPL27A (17 kDa), HIF1α (93 kDa) and HA (MINA, 53 kDa). Cells were either untreated or treated with 1 mM DMOG, 100 µM (+) or 250 µM (++) DFO for 16 hours before harvesting. Input = 1.25% (MPP6, HIF1α), 0.3 % (RPL27A), 12.5% (HA, β-actin). (**D**) DMOG rapidly disrupts the interaction between FLAG-MINA and MPP6-HA. Anti-HA immunoprecipitates from cell extracts of HEK293T cells expressing empty vector (EV) or FLAG-MINA and MPP6-HA were immunoblotted for FLAG (MINA, 53 kDa) and HA (MPP6, 61 kDa). Cells were either untreated or treated with 1 mM DMOG for 10, 60 or 480 minutes before harvesting. Input = 10% (FLAG, β-actin), 33% (HA). (**B-D**) β-actin was used as loading control.

NO66 with respect to their respective substrates RPL27A and RPL8 (Ge et al., 2012). Indeed, a coprecipitation experiment confirmed that MPP6 coprecipitates with MINA and not with NO66 (Figure 3.12A). The membrane palmitoylated protein (MPP) subfamily of MAGUKs, to which MPP6 belongs, consists of 7 proteins (MPP1-7) that share significant sequence similarity. A sequence alignment of the human MPPs is presented in Appendix B. MPP2, with 65% sequence identity, is the most closely related to MPP6 (Figure 3.12B). However, as shown in Figure 3.12C, MINA binds strictly to MPP6, and not MPP2.

3.2.3.2 Mapping the domains in MPP6 that are necessary and sufficient for activity-dependent MINA binding

As scaffold proteins, MAGUK proteins are characterised by the presence of protein-protein interaction modules. These include a characteristic PSD-95/DLG/ZO-1 (PDZ) - Src homology 3 (SH3) - guanylate kinase (GUK) tandem, but many MAGUKs contain additional domains. MPPs, with the exception of MPP1, also share two L27 domains. An overview of the domain organisation of MAGUK proteins is presented in Figure 3.13. In order to test the domain requirements for binding of MINA to MPP6, a set of HA-tagged MPP6 truncation mutants was generated, each missing different domains of the protein (Figure 3.14A). Each deletion mutant was then co-overexpressed with FLAG-tagged MINA in HEK293T cells. Next, HA-tagged MPP6 was immunoprecipitated and the interaction with MINA was evaluated by western blot. As shown in Figure 3.14B, removing the GUK ($MPP6^{1\text{-}306Fs}$) and (part of) the SH3 ($MPP6^{1\text{-}222}$) domains results in partial ($MPP6^{1\text{-}306Fs}$) or complete ($MPP6^{1\text{-}222}$) loss of MINA binding. To distinguish between the SH3 and the GUK domains, two additional mutants were generated, $MPP6^{285\text{-}540}$ and $MPP6^{338\text{-}540}$ (Figure 3.14A). Whereas $MPP6^{285\text{-}540}$ still successfully bound MINA, further truncation to also remove the small domain between the SH3 and GUK domains ($MPP6^{338\text{-}540}$), prevented MINA from binding (Figure 3.14B), suggesting that this region is critical for the interaction. Subsequently, the localisation of all mutants was assessed to test whether loss of MINA binding to $MPP6^{338\text{-}540}$ might



B

MPP	Sequence identity with MPP6 (%)
MPP1	34.4%
MPP2	**65.2%**
MPP3	31.3%
MPP4	26.5%
MPP5	28.0%
MPP7	33.9%

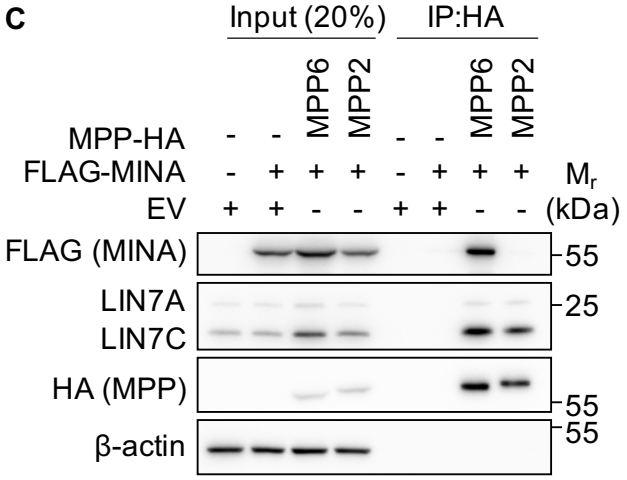


Figure 3.12: Interaction between MINA and MPP6 is not conserved between ribosomal oxygenases or MPP family members. (**A**) MPP6 binds MINA but not NO66. Anti-HA immunoprecipitates from extracts of HEK293T cells transiently expressing an empty vector (EV), HA-MINA or HA-NO66 were immunoblotted for MPP6 (61 kDa, GeneTex antibody) and HA. Input = 1.25% (MPP6), 12.5% (HA, β-actin). (**B**) Sequence alignment revealed MPP2 as having the highest sequence similarity to MPP6. (**C**) MINA binds MPP6 but not MPP2. Anti-HA immunoprecipitates from extracts of HEK293T cells transiently expressing the indicated constructs were immunoblotted for FLAG (MINA, 53 kDa), LIN7A/C (26/22 kDa) and HA. (**A,C**) β-actin (42 kDa) was used as loading control.

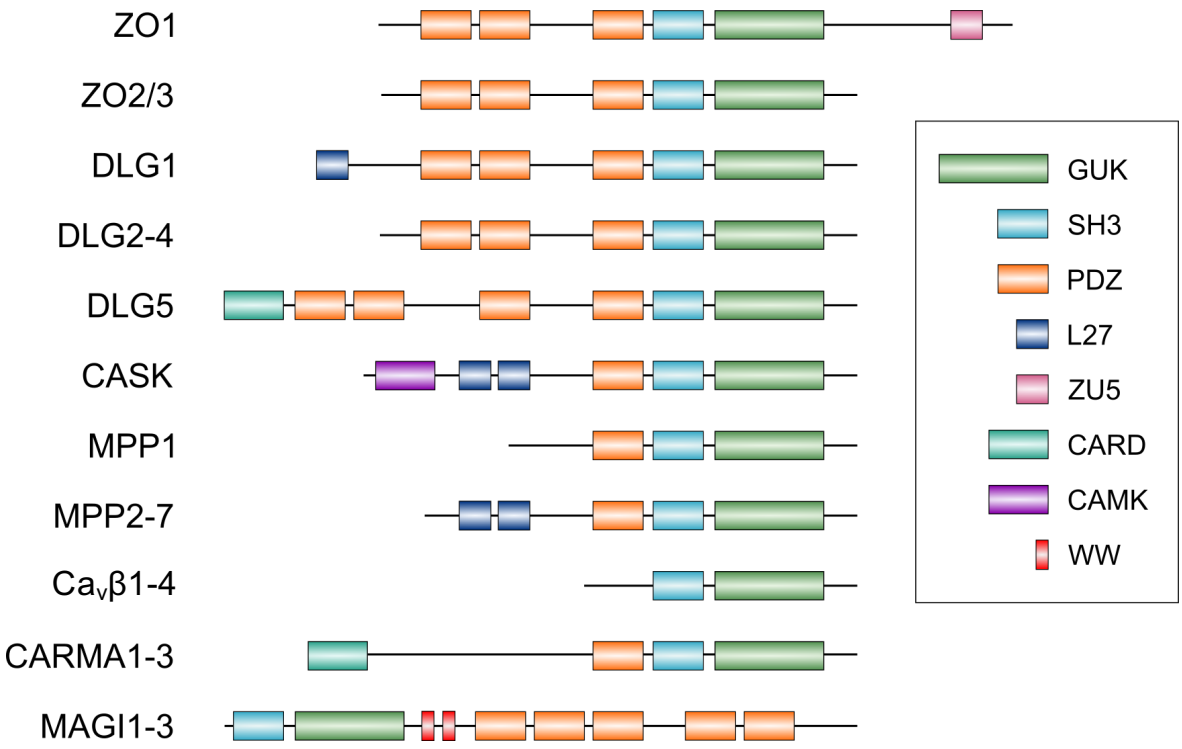


Figure 3.13: Domain organisation of MAGUK proteins. With the exception of the $Ca_v\beta$ proteins, all MAGUKs contain (at least one) PSD-95/DLG/ZO-1 (PDZ), src homology 3 (SH3) and guanylate kinase (GUK) domain. The membrane palmitoylated proteins (MPPs), except MPP1, contain two additional L27 domains. Abbreviations: ZO = zona occludens, DLG = discs large, CASK = calcium/calmodulin-dependent serine protein kinase, $Ca_v\beta$ = voltage-gated calcium channel β subunit, CARMA = caspase recruitment domain-containing MAGUK, MAGI = membrane-associated guanylate kinase inverted.

simply be explained by this mutant being excluded from the nucleus (Figure 3.14C). Importantly, although the localisation of all the truncation mutants was affected relative to full-length MPP6, they all showed some level of nucleoplasmic distribution, which we demonstrated previously (Figure 3.9) is the likely site of the MINA:MPP6 interaction. Overall therefore, our data would suggest that amino acids 285-338 are required for MINA binding. Importantly, it would appear that this domain (in the context of the $MPP6^{285\text{-}540}$ mutant) may be sufficient for activity-dependent MINA interaction: $MPP6^{285\text{-}540}$ binds wild-type (WT) MINA but not the catalytically inactive Fe(II)-binding mutant (H179A, Figure 3.14D).

Next, we addressed whether amino acids 285-338 are also sufficient for MINA binding. In order to explore this, we took advantage of the fact that MPP2 does not bind MINA, despite the significant primary sequence and structural conservation between

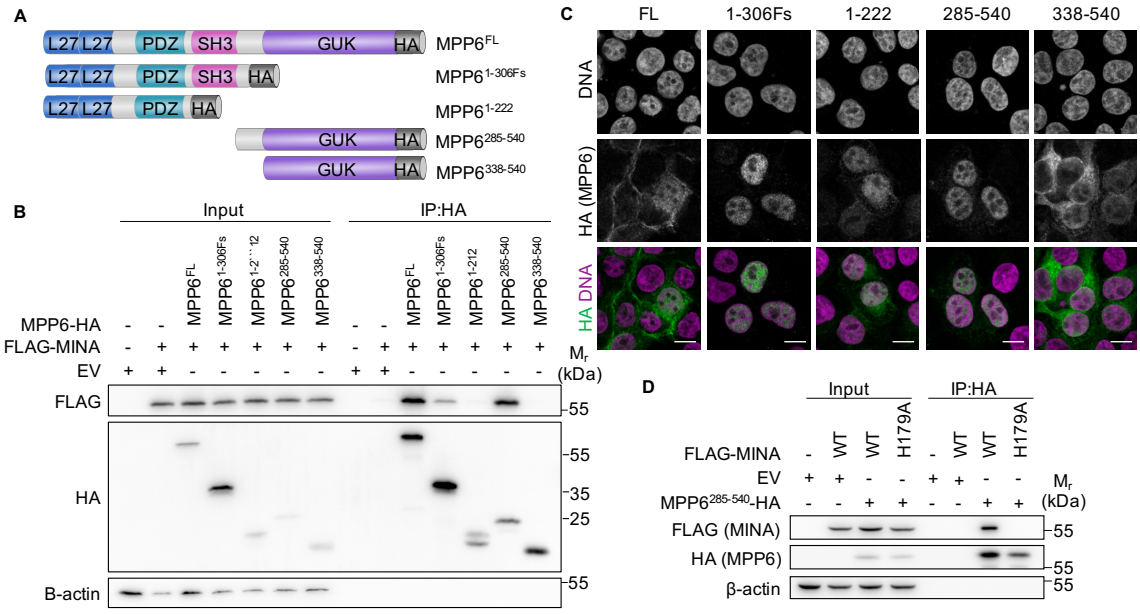


Figure 3.14: MPP6 amino acids 285-338 are required for activity-dependent MINA binding. (**A**) Domain structures of MPP6 mutants used in (B-D). FL = full-length, 306Fs = cancer mutant, frame shift mutation at amino acid 306. (**B**) MPP6 amino acids 285-338 are required for coprecipitation of FLAG-MINA. Anti-HA immunoprecipitates from cell extracts of HEK293T cells expressing an empty vector (EV) or the indicated FLAG-MINA and MPP6-HA constructs were immunoblotted for FLAG (MINA, 53 kDa) and HA (MPP6). (**C**) Localisation of MPP6 truncation mutants in HEK293T cells. HEK293T cells transiently expressing the indicated MPP6-HA constructs were fixed with PFA and stained for HA (MPP6, green). Nuclei were visualised with DAPI (magenta). Scale bars represent 10 µm. Single focal plane images were acquired using a Zeiss LSM 780 confocal microscope equipped with a 40x C-Apochromat 1.2 W Korr M27 objective and ZEN black software. (**D**) MPP6-HA$^{285\text{-}540}$ coprecipitates wild-type (WT), but not catalytically inactive (H179A) FLAG-MINA. Anti-HA immunoprecipitates from cell extracts of HEK293T cells expressing the indicated constructs were immunoblotted as indicated. (**B,D**) Input = 10% (FLAG, β-actin), 20% (HA). β-actin (42 kDa) was used as loading control.

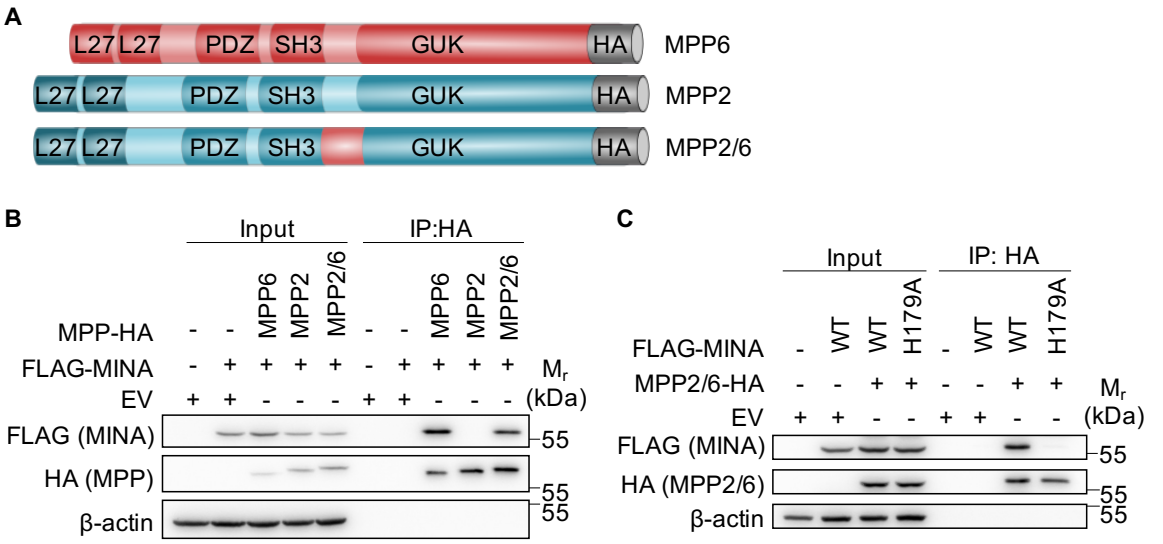


Figure 3.15: MPP6 amino acids 285-338 are sufficient for activity-dependent MINA binding. (**A**) Graphical representation of the constructs used in (B,C). (**B**) An MPP2 mutant that contains amino acids 285-338 of MPP6 (MPP2/6), but not wild-type MPP2, coprecipitates FLAG-MINA. Anti-HA immunoprecipitates from extracts of HEK293T cells expressing the indicated constructs were immunoblotted for FLAG and HA. Input = 10% (FLAG, β-actin), 20 % (HA). (**C**) MPP2/6 coprecipitates FLAG-MINA in an activity-dependent manner. Anti-HA immunoprecipitates from extracts of HEK293T cells expressing the indicated constructs were immunoblotted for FLAG and HA. Input = 10% (FLAG, β-actin), 100% (HA). (**B,C**) β-actin (42 kDa) was used as loading control.

MPP2 and MPP6. We generated an MPP2 mutant 'hybrid', where the amino acids between the SH3 and GUK domains of MPP2 were replaced with those of MPP6 (Figure 3.15A). Consistent with our hypothesis that AAs 285-338 of MPP6 are sufficient for MINA binding, FLAG-MINA coprecipitated with the MPP2/6 hybrid (Figure 3.15B). Importantly, the binding of FLAG-MINA to the MPP6/2 hybrid retains its activity-dependence (Figure 3.15C).

In an attempt to narrow down the binding region even further, we next focussed on the differences in primary sequence between MPP2 and MPP6 in this region. To our surprise, the sequence identity of this region was 67.9% (Figure 3.16A), suggesting that the strikingly different MINA binding profiles might be determined by the relatively few regions of low homology. To test the importance of these regions we swapped some of the residues within them (Figure 3.16A), and analysed whether they affect MINA binding in the context of the MPP2/6 hybrid. As shown in Figure 3.16B, mutation of

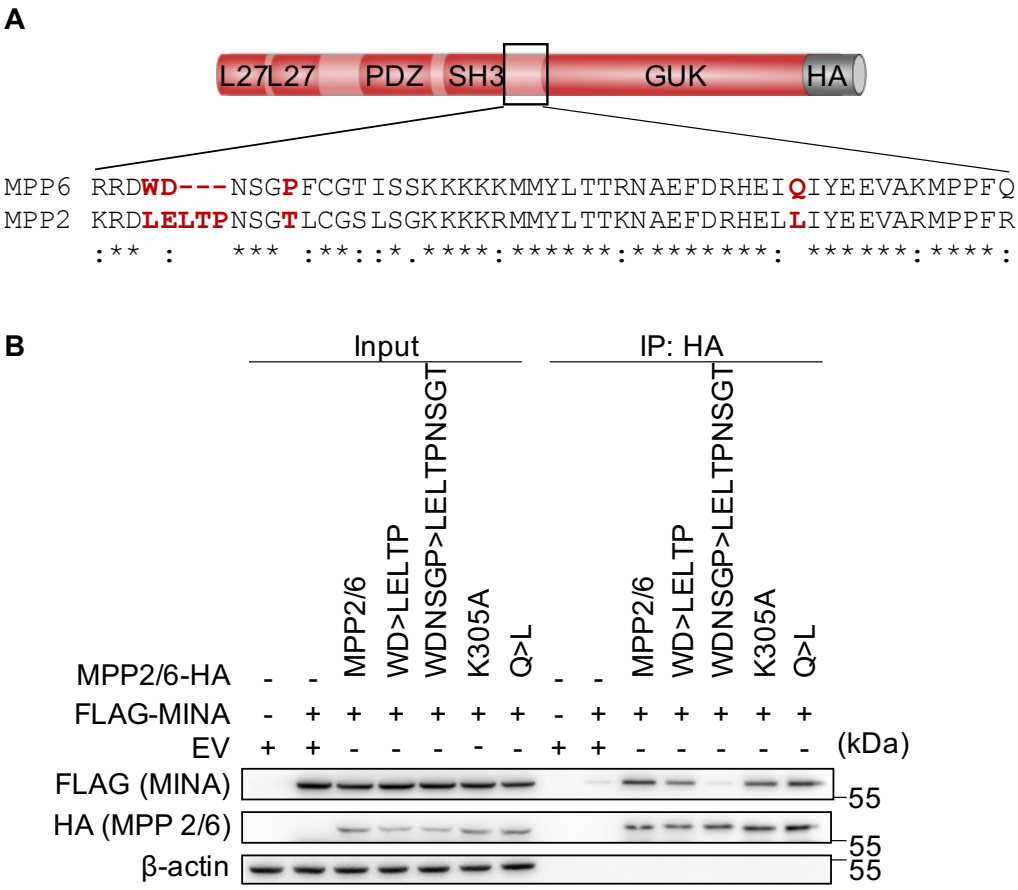


Figure 3.16: MINA binds to the N-terminal end of the MPP6 SH3-GUK interdomain. (**A**) Graphical representation of the mutated residues used in (B). (**B**) Anti-HA immunoprecipitates from extracts of HEK293T cells expressing the indicated constructs were immunoblotted for FLAG (MINA, 53 kDa) and HA (MPP2/6). Input = 50 % (FLAG, β-actin), 40% (HA). β-actin (42 kDa) was used as loading control.

W291/D292 (as in MPP6) to LELPT (as in MPP2) modestly affected FLAG-MINA binding. However, extending this insertion from LELPT to LELPTNSGT completely abolished the interaction with MINA (Figure 3.16B).

Based on these data, we tested whether introducing a proline and phenylalanine (as in MPP6 P296/F297) at the respective amino acid positions 332 and 333 in MPP2 (T332P/L333F) was sufficient to gain MINA binding. However, as indicated in Figure 3.17, having just a proline and phenylalanine at those locations is not sufficient, raising the possibility that the presence of other residues is also required.

Overall, our data indicate that the SH3-GUK interdomain is responsible for the activity-dependent interaction between MINA and MPP6. Moreover, our results in-

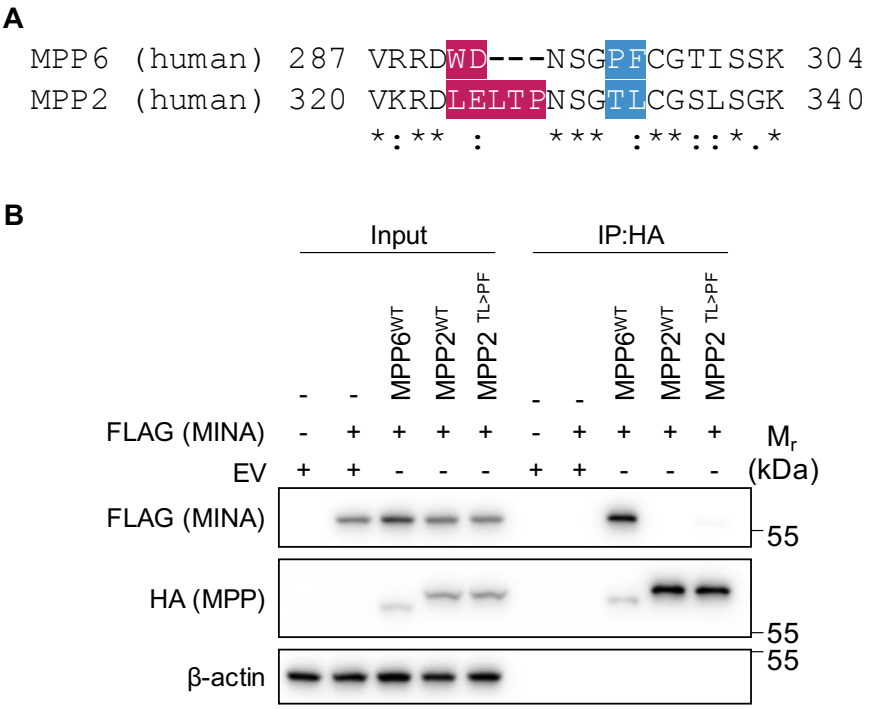


Figure 3.17: MPP6 P296 and F297 are not sufficient for MINA binding. (**A**) Sequence alignment of human MPP6 and MPP2. (**B**) Anti-HA immunoprecipitates from extracts of HEK293T cells transiently expressing the indicated constructs were immunoblotted for FLAG (MINA, 53 kDa) and HA (MPP2/MPP6). Input = 10% (FLAG, β-actin), 20% (HA). β-actin (42 kDa) was used as loading control.

dicate that the short insertion at AAs 326-328 (LTP) at the N-terminal end of the interdomain contributes to the fact that MPP2 cannot bind MINA, suggesting that the region spanning this sequence in MPP6 may be important. Therefore, it was of interest to investigate whether any of the residues in this region are targeted by MINA for hydroxylation.

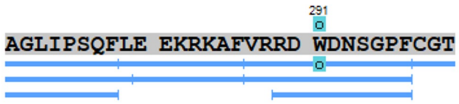
3.2.3.3 Mass spectrometry analyses of MPP6 oxidation

As MPP6 was identified as interacting with MINA in an activity-dependent manner, suggesting it is a potential substrate, we aimed to identify the residue that might be targeted by MINA for hydroxylation. For this reason, we analysed MPP6-FLAG immunoprecipitates from HEK293T cells by LC-MS/MS which can identify proteins and their post-translational modifications. In an attempt to help support the identification of a MINA-dependent MPP6 oxidation, MPP6 was overexpressed in the presence or absence of overexpressed MINA. Following immunoprecipitation, the samples were subjected

to in-solution chymotrypsin digest before analysis by LC-MS/MS (Oxford Advanced MS Facility). Chymotrypsin was used because it has a broader cleavage specificity compared to conventional trypsin (which only cuts after lysine and arginine), which we considered might improve the sequence coverage of the minimal MINA-binding domain (the SH3-GUK 'interdomain'), which is relatively lysine/arginine rich. Following LC-MS/MS, the data were processed using PEAKS X software which identified 92% sequence coverage of MPP6 in each sample. The data were then filtered to remove methionine oxidations and those with an A-score of <20 (an A-score of 20 corresponds to a modification correctly localised with 99% certainty). This identified a single high scoring (A-score 1000) oxidised residue in MPP6 (W291) in the absence and presence of overexpressed MINA (Figures 3.18 and 3.19, respectively). Although the abundance of oxidised W291 increased in the presence of MINA, the overall stoichiometry of the modification was very low (0.04% under endogenous MINA levels, 0.44% in the presence of overexpressed HA-MINA; Figure 3.19D). Oxidised tryptophan (+16 Da) can spontaneously dehydrate (-18 Da), yielding a 'didehydro' form (-2 Da): consistent with increased W291 oxidation in the presence of overexpressed MINA we also identified didehydro-W291 in this samples (0.19%, A-score of 1000; Figure 3.19C,D). Interestingly, W291 resides within the N-terminal domain of the SH3-GUK 'interdomain' identified above as important for activity-dependent MINA binding (Figures 3.14 and 3.15), raising the possibility that it might be a novel MINA-dependent oxidation event. Although we note that tryptophan can undergo spontaneous chemical oxidation as an artefact of sample preparation for MS, it is interesting to note that none of the other four tryptophan residues in MPP6 were identified as oxidised in these samples.

Next, we sought to determine whether the apparent MINA-dependent MPP6 W291 oxidation described above was reproducible. In doing so we took the opportunity to explore whether the very low stoichiometry of the modification might be increased by two other conditions in addition to MINA overexpression. Firstly, we tested whether proteasomal inhibition with MG132 might protect oxidised MPP6 from degradation. Secondly, we tested whether the modification might be boosted by increasing the op-

A



B

#	b	b-H2O	b-NH3	b (2+)	Seq	y	y-H2O	y-NH3	y (2+)	#
1	100.08	82.07	83.05	50.54	V					11
2	256.18	238.17	239.15	128.59	R	1265.57	1247.56	1248.54	633.28	10
3	412.28	394.27	395.25	206.64	R	1109.46	1091.45	1092.44	555.23	9
4	527.30	509.29	510.28	264.15	D	953.36	935.35	936.34	477.18	8
5	729.40	711.37	712.35	365.19	W(+15.99)	838.34	820.33	821.31	419.67	7
6	844.40	826.40	827.38	422.70	D	636.26	618.25	619.24	318.63	6
7	958.45	940.44	941.42	479.72	N	521.24	503.22	504.21	261.09	5
8	1045.48	1027.47	1028.45	523.24	S	407.19	389.18	390.17	204.10	4
9	1102.50	1084.49	1085.48	551.75	G	320.16	302.15	303.13	160.58	3
10	1199.56	1181.55	1182.53	600.30	P	263.14	245.13	246.11	132.10	2
11					F	166.09	148.08	149.06	83.54	1

C

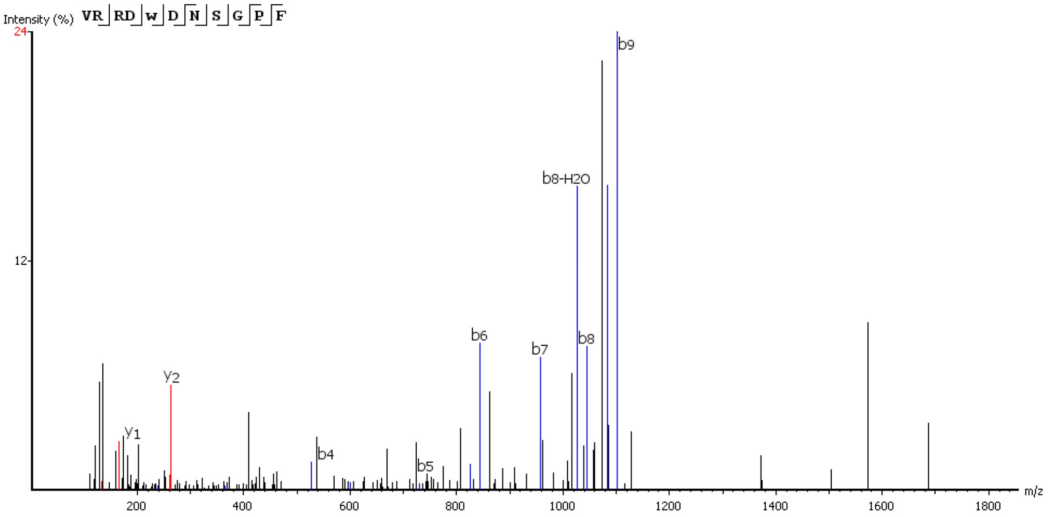
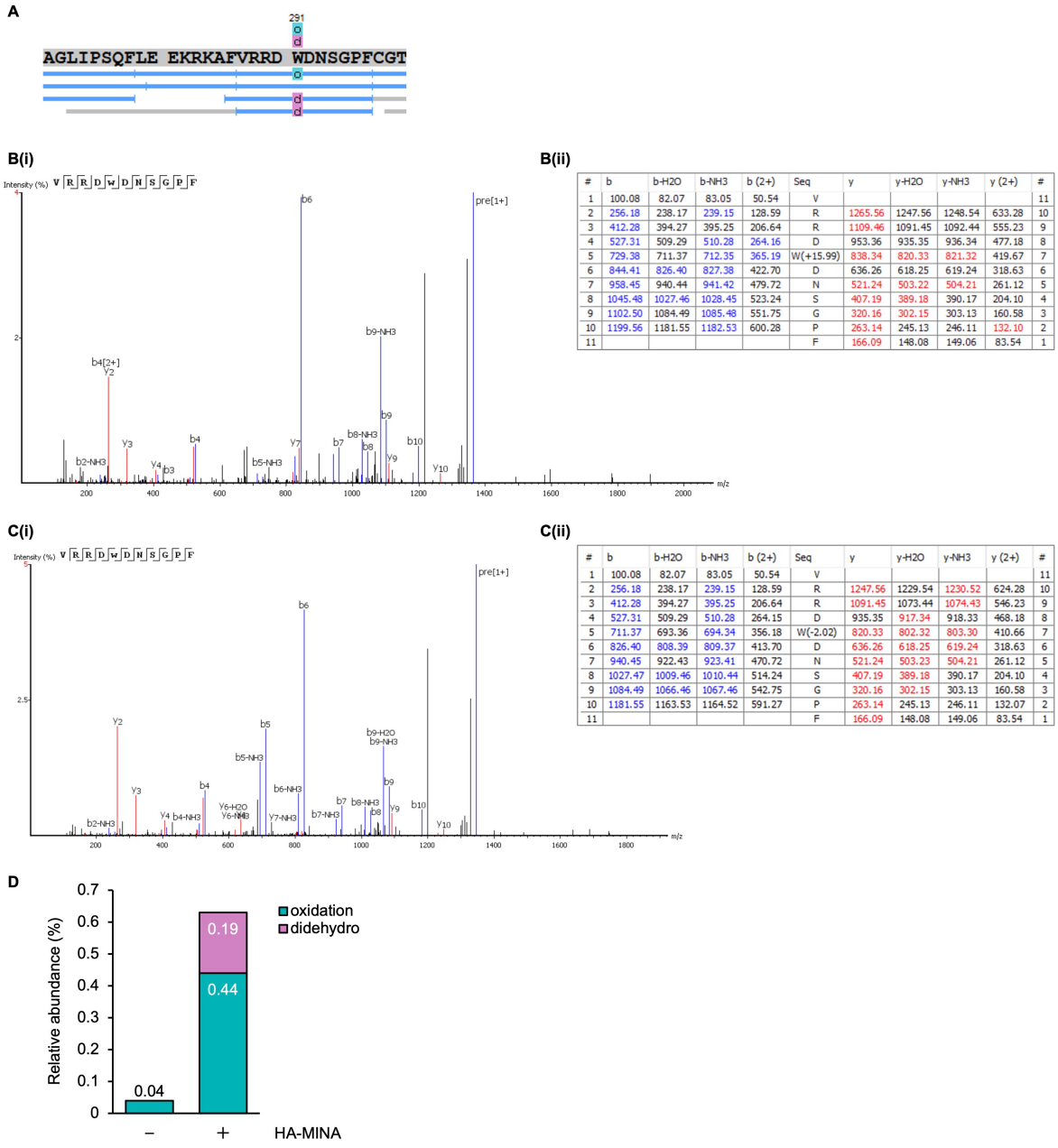


Figure 3.18: Preliminary MS analysis of MPP6 oxidations in the minimal binding domain. MPP6-FLAG immunoprecipitates from extracts of transiently transfected HEK293T cells were digested with chymotrypsin and analysed for the presence of oxidation or oxidation/dehydration by LC-MS/MS. Immunoprecipitations were carried out by Uncaar Boora. (**A**) Identified peptide fragments and modifications (o = oxidation). (**B**) Ion tables of the chymotryptic peptide VRRDWDNSGPF showing theoretical (black) and identified (blue/red) ion species. A mass identical to a hydroxytryptophan-containing fragment is observed in the b ion series at b5. (**C**) Corresponding MS/MS spectra assigning oxidation at W291.



B(ii)

#	b	b-H2O	b-NH3	b (2+)	Seq	y	y-H2O	y-NH3	y (2+)	#
1	100.08	82.07	83.05	50.54	V					11
2	256.18	238.17	239.15	128.59	R	1265.56	1247.56	1248.54	633.28	10
3	412.28	394.27	395.25	206.64	R	1109.46	1091.45	1092.44	555.23	9
4	527.31	509.29	510.28	264.16	D	953.36	935.35	936.34	477.18	8
5	729.38	711.37	712.35	365.19	W(+15.99)	838.34	820.33	821.32	419.67	7
6	844.41	826.40	827.38	422.70	D	636.26	618.25	619.24	318.63	6
7	958.45	940.44	941.42	479.72	N	521.24	503.22	504.21	261.12	5
8	1045.48	1027.46	1028.45	523.24	S	407.19	389.18	390.17	204.10	4
9	1102.50	1084.49	1085.48	551.75	G	320.16	302.15	303.13	160.58	3
10	1199.56	1181.55	1182.53	600.28	P	263.14	245.13	246.11	132.10	2
11					F	166.09	148.08	149.06	83.54	1

C(ii)

#	b	b-H2O	b-NH3	b (2+)	Seq	y	y-H2O	y-NH3	y (2+)	#
1	100.08	82.07	83.05	50.54	V					11
2	256.18	238.17	239.15	128.59	R	1247.56	1229.54	1230.52	624.28	10
3	412.28	394.27	395.25	206.64	R	1091.45	1073.44	1074.43	546.23	9
4	527.31	509.29	510.28	264.15	D	935.35	917.34	918.33	468.18	8
5	711.37	693.36	694.34	356.18	W(-2.02)	820.33	802.32	803.30	410.66	7
6	826.40	808.39	809.37	413.70	D	636.26	618.25	619.24	318.63	6
7	940.45	922.43	923.41	470.72	N	521.24	503.23	504.21	261.12	5
8	1027.47	1009.46	1010.44	514.24	S	407.19	389.18	390.17	204.10	4
9	1084.49	1066.46	1067.46	542.75	G	320.16	302.15	303.13	160.58	3
10	1181.55	1163.53	1164.52	591.27	P	263.14	245.13	246.11	132.07	2
11					F	166.09	148.08	149.06	83.54	1

Figure 3.19: Preliminary MS analysis of MINA-dependent oxidations in the minimal binding domain. Parallel MS/MS assignment of W291 oxidation in MPP6-FLAG immunoprecipitated from HEK293T cells cotransfected with HA-MINA. (**A**) Identified peptide fragments and modifications (o = oxidation; d = dehydration). (**B,C**) MS/MS spectra (i) and ion tables (ii) of the chymotryptic peptide VRRD-WDNSGPF showing theoretical (black) and identified (blue/red) ion species. (**B**) A mass identical to a hydroxytryptophan-containing fragment is observed in the b and y ion series at b5 and y7, respectively. (**C**) A mass identical to a didehydrotryptophan-containing fragment is observed in the b and y ion series at b5 and y7, respectively. (**D**) Relative abundance of oxidation/didehydration at W291 in the presence or absence of MINA overexpression.

portunity for MINA and MPP6 to interact: cells were rendered subconfluent after transient transfection in order to try and recreate conditions previously identified as being favourable for complex formation (Figures 3.8, 3.9 and 3.10). Samples were prepared and analysed by mass spectrometry as described previously. Unfortunately, the basal level of W291 oxidation detected in the control samples (-MINA) in this experiment were already similar to that detected in the +MINA sample in the previous experiment (approximately 0.4%), and did not increase in response to MINA overexpression (Figure 3.20). Consistent perhaps with a higher background level of protein oxidation in this experiment, oxidation of all five tryptophan residues in MPP6 was detected (data not shown), which is at odds with the results of the first experiment (see above). Furthermore, we did not observe an increase in MPP6 W291 oxidation in response to either proteasome inhibition or subconfluence under the conditions tested here (Figure 3.20). Overall, the data are not strongly supportive of a robust (high stoichiometry) and reproducible MINA-dependent W291 oxidation.

Mutation of target residues in other JmjC hydroxylase substrates prevents their association (Cockman et al., 2006; Markolovic et al., 2018). As the results of the preliminary MS analysis were inconclusive, we tested whether alanine substitution of W291 blocked the association of MINA and MPP6. However, no significant alterations were noted (Figure 3.21A). We then extended this approach to the other residues in the W291-containing chymotryptic peptide identified above. Interestingly, MINA binding to MPP6 was significantly affected or completely lost upon mutation of G295, P296 and F297, respectively (Figure 3.21A/B). We further expanded our alanine scanning to identify any other residues required for MINA binding: individual point mutations of MPP6 amino acids 298-303 were made and interaction with MINA was analysed by immunoprecipitation and western blot. As shown in Figure 3.21B/C, we found that C298 and G299 are also essential for MINA binding. The region responsible and required for MINA binding was therefore narrowed down to five amino acids. Whether any of these residues could be candidate hydroxylation targets is not yet clear.

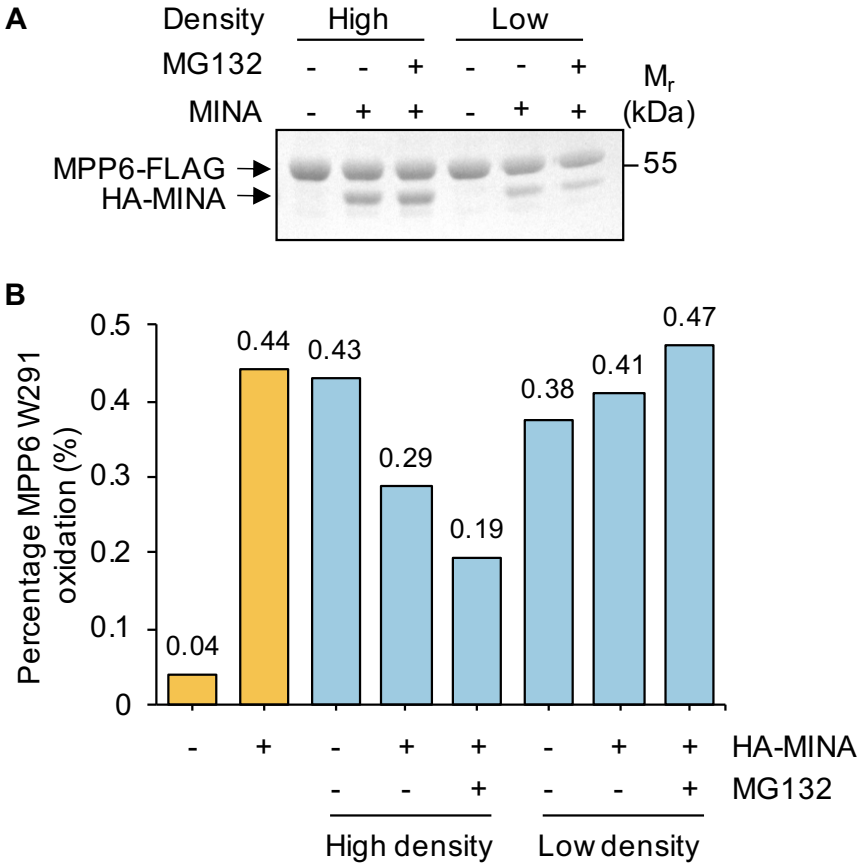


Figure 3.20: MPP6 oxidation in response to MINA overexpression, proteasome inhibition and confluence. (**A**) Coomassie Brilliant Blue staining of samples submitted for LC-MS/MS analysis shows efficient precipitation of MPP6 (upper band) and MINA (lower band). (**B**) Bars indicate the percentage of MPP6 oxidation at W291 in the various samples. Yellow bars represent the percentage oxidation identified in the previous experiment.

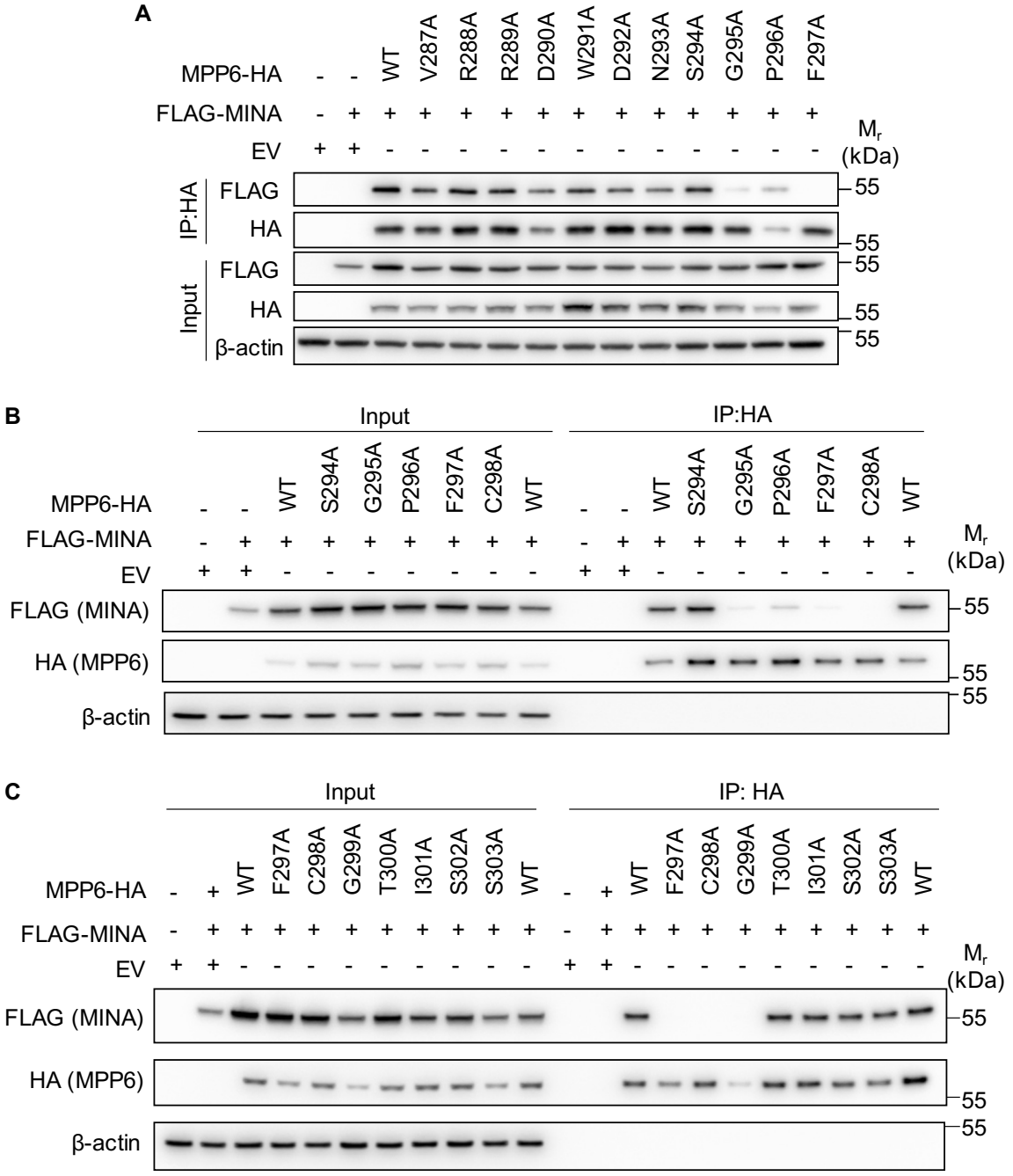


Figure 3.21: MPP6 G295, P296 and F297, C298 and G299 are required for binding to MINA. (**A-C**) Anti-HA immunoprecipitates from extracts of HEK293T cells expressing the indicated constructs were immunoblotted for FLAG (MINA, 53 kDa) and HA (MPP6, 61 kDa). β-actin (42 kDa) was used as loading control. Input = 10% (FLAG, β-actin), 20% (HA).

3.3 Discussion

In this Chapter, a proteomic screen was performed to identify extra-nucleolar interactors of MINA, with a particular focus on proteins that associate with wild-type MINA, but not a catalytically inactive mutant. Using this method, a membrane-associated scaffold protein, MPP6, was identified. The association between exogenous, tagged MINA and endogenous MPP6 was validated in multiple cell lines, and the interaction was confirmed at endogenous levels (Figures 3.3, 3.4 and 3.5). Moreover, we showed that the interaction is specific, with no redundancy observed between NO66 and MINA, or between MPP6 and the closely related protein MPP2 (Figure 3.12). Interestingly, the binding profile of MPP6 to MINA is strikingly similar to that of RPL27A, being affected by MINA mutations and the 2OG oxygenase inhibitor DMOG in a similar fashion (Figure 3.11). Although this raises the possibility that MPP6 is a novel MINA substrate (as discussed below), an alternative explanation could be that MPP6 binding is indirect, via RPL27A. However, we believe this is highly unlikely considering the fact that the NoLS mutant efficiently interacts with MPP6, whereas it is unable to capture RPL27A (Figure 3.4C). Overall, our data still supports MPP6 being a novel MINA substrate, although more work is required to understand the nature of the potential modification.

The N-terminal region of the MPP6 minimal binding domain (herein referred to as the SH3/GUK interdomain) that confers activity-dependent association with MINA does not contain any histidine residues, nor does the primary sequence resemble RPL27A. Whether it contains a non-canonical hydroxylation site is not clear. Alanine scanning identified specific G/P/F/C residues that when mutated blocked MINA binding, raising the possibility that these could be a site for hydroxylation. Although MINA has been reported to catalyse histidyl hydroxylation (Ge et al., 2012), this does not exclude that it might be able to also hydroxylate other residues. Interestingly, if true, this would not be the first report of a JmjC oxygenase with substrate specificity towards multiple residues. Factor-inhibiting HIF (FIH) shows activity towards multiple

residues, including asparagine, aspartate, histidine and leucine (Cockman et al., 2006; Coleman et al., 2007; Yang et al., 2011a,b, 2013; Choi et al., 2020).

Despite considerable evidence supporting a substrate-like interaction between MINA and MPP6, the identification of a substrate residue in MPP6 has proved challenging. Initial LC-MS/MS analysis of MPP6-FLAG immunoprecipitates identified oxidation of one MPP6 peptide, on W291. Moreover, and importantly, oxidation of this site was possibly regulated by MINA. However, whether the W291 oxidation identified here represents a bona fide hydroxylation is not clear. The stoichiometry of W291 oxidation observed was very low (0.04 - 0.44%) and caution is warranted when assigning oxidation to a tryptophan residue. Certain amino acids, including methionine and tryptophan residues, often acquire artificial oxidations as a result of the mass spectrometry sample preparation process. Artificial oxidations have potentially led to the misassignment of several non-HIF prolyl hydroxylase substrates, as discussed by Cockman and colleagues (Cockman et al., 2019). Although we did not find evidence of any other tryptophan or methionine oxidations in our sample, at this point we cannot exclude that the W291 hydroxylation was not a technical artefact. Another possibility could be that the identified W291 might be a consequence of close proximity to the potentially oxidising environment of the MINA catalytic domain. Although we set out to repeat the LC-MS/MS analysis using new samples, the basal level of oxidation observed was higher and this was not evidently regulated by MINA. In these samples, we also observed substantial levels of artificial oxidations on residues including methionines and tryptophans, which possibly explains why no regulation by MINA was noted. Future studies will aim at reducing the artificial background oxidations by ensuring that the samples are processed quickly and analysed by MS in a timely manner. This might increase the sensitivity of detecting a low level of MINA-specific tryptophan oxidation.

We should also consider that other mechanisms could explain the low levels of oxidised peptide identified in our sample. For example, perhaps the oxidised form is being degraded, or further processed by other post-translational modifications. We already considered the involvement of proteasomal degradation, but inhibition with MG132 did

not increase the detection of oxidised W291 in our samples. However, it is possible that proteasome-independent proteolytic pathways may be involved. Moreover, the modification could be restricted to a specific context. Our data showing that both MINA and MPP6 are present in distinctive subcellular locations at certain times could be consistent with this hypothesis. In most cell lines tested so far (including HEK293T), RPL27A H39 is hydroxylated >90% (Ge et al., 2012). In future experiments, we could therefore consider whether inhibiting ribosome biogenesis might stimulate MPP6 hydroxylation.

The unique effect of DMOG, as well as the absence of a major effect of DFO, on the MINA:RPL27A and MINA:MPP6 interactions observed here are not clear. We speculate that it could be an indirect effect: both DMOG and DFO potentially target all 2OG oxygenases (and other iron-dependent enzymes in the case of DFO) so the observed effects could therefore be independent of MINA's activity. Alternatively, it could reflect a specific feature of MINA biology, including the structure of its catalytic domain and/or 2OG/iron binding. In the case of the latter, we could also speculate that unique enzyme-substate binding specificities might explain why W291 substitution does not interfere with the interaction between MINA and MPP6.

Although mutation of W291 did not affect MINA binding, we did identify five residues in the vicinity of W291 that are critical for the interaction between MINA and MPP6. Members of the MAGUK family of membrane proteins are characterised by the presence of a conserved PDZ-SH3-GUK protein-protein interaction module. Each of these domains can interact with proteins individually, or they can form structural and functional supramodules with distinct binding properties (Ye et al., 2018). Important for formation of supramodules is the flexible linker region between the SH3 and GUK domains. Interestingly, this linker region or 'interdomain' was identified here as the minimal domain required for MINA binding (Figure 3.14). Moreover, deletion of the PDZ/SH3 domains did not affect the interaction with MINA, indicating it is residues within the interdomain itself, rather than its function in formation of a supramodule, that mediate MINA binding. Within this interdomain MAGUKs contain a short

sequence, known as the HOOK domain, which can mediate protein binding and contains a polybasic stretch that has been reported to target MAGUKs to the membrane (Hanada et al., 2003). An intriguing possibility, explored further in Chapter 5, would be that hydroxylation of MPP6 by MINA causes a conformational change of the SH3-GUK module that regulates MPP6 membrane targeting, possibly through binding of other proteins. Furthermore, the HOOK domain has also implicated in regulation of ubiquitination and subsequent proteasomal degradation of MAGUK proteins (Moreno-García et al., 2010).

A key question arising from the identification of peripheral membrane proteins as MINA-interacting proteins, is where in a cellular context this complex might form. Indeed, whereas our investigations into the subcellular localisation of MINA suggest that MINA predominantly resides in the nucleolus/nucleus (Chapter 2), so far, MPP6 has mainly been described in association with the membrane (Kamberov et al., 2000; Kamijo et al., 2016). However, our indirect immunofluorescence, PLA, cellular fractionation and immunoprecipitation analyses in Caco-2 indicate that a cellular context exists where MINA and MPP6 are both localised to the nucleoplasm, where the interaction occurs (Figures 3.9, 3.8).

To our knowledge, we provide the first evidence of a potential nuclear localisation of MPP6 (Figure 3.8B). Moreover, we found that MPP6 is excluded from the membrane in HeLa cells, and is instead enriched in the nucleus/cytoplasm (Figure 3.8D/E). Nuclear retention of polarity proteins has previously been described and is reported to exert signalling roles. One well-known example of this is the adherens junctions-associated protein β-catenin. In response to Wnt signalling, the E-cadherin-associated protein β-catenin is dissociated from the membrane and translocates to the nucleus to regulate gene expression (Nelson and Nusse, 2004). Nuclear accumulation of β-catenin is widely implicated in cancer, including colorectal cancer (Shang et al., 2017). Our observation therefore raises the possibility of a nuclear, possibly oncogenic, role for MPP6. Consistent with this, the MPP6$^{1\text{-}306Fs}$ mutant, used in Figure 3.14 as part of our domain mapping analysis, is in fact a recurrent cancer mutant. As shown in

Figure 3.14C, MPP6$^{1\text{-}306Fs}$ localises exclusively to the nucleus and binds MINA less well in HEK293T. Similar observations regarding the localisation of this mutant have been made in stable Caco-2 cells (data not shown). Based on these data, one could speculate that perhaps MINA functions as a tumour suppressor through suppression or inactivation of nuclear MPP6. This hypothesis will be explored further in Chapter 5 of this thesis.

Given the observations discussed in the previous paragraph, it was of interest to search the literature for what is currently known about the role of MPP6, and by extension LIN7, in cancer. Unfortunately only a few studies so far have focussed on characterising the role of MPP6 and LIN7 proteins in cancers. Studies on MPP6 are currently limited to a single report describing an inverse association between MPP6 expression and ovarian cancer progression (Xu et al., 2019). Reduced expression of LIN7C in oral squamous cell carcinoma was found associated with increased metastatic potential (Onda et al., 2007). Our own investigations into *MPP6* and *LIN7* mutations across the 33 studies included in The Cancer Genome Atlas (TCGA) project have however revealed that MPP6 and LIN7 mutations are found in a variety of cancer types (Figure 3.22A). These mutations include truncating mutations and deletions, including in colorectal cancer (Figure 3.22B,C). Interestingly, the mutations are not limited to (potential) loss-of-function mutations, but also include gene amplifications (Figure 3.22C), perhaps consistent with an oncogenic role. In addition, our analysis of the TCGA data suggests that MINA, MPP6 and LIN7 gene mutations may be mostly mutually exclusive, suggesting they may function in a pathway (Figure 3.22D).

In conclusion, the data described in this chapter suggest that the interaction between MINA and MPP6 is specific and possibly regulated depending on the context. The context could relate to the physiological state of the cell (e.g. confluence, ribosome biogenesis) and/or an underlying pathology, such as cancer. Considering the known roles of MINA and MAGUK proteins such as MPP6 in tumourigenesis, it is therefore of interest to further explore the roles of MINA and MPP6 in cell polarity and/or epithelial morphogenesis. This will be the focus of the next chapters.

A

Gene	Cancer type	Frequency
MPP6	Melanoma	7.21%
	Endometrial carcinoma	6.83%
	Bladder urothelial carcinoma	5.35%
	Oesophageal squamous cell carcinoma	5.26%
	Esophagogastric adenocarcinoma	3.89%
	Adrenocortical carcinoma	3.30%
	Sarcoma	2.75%
	Non-small cell lung cancer	2.66%
	Head and neck squamous cell carcinoma	2.29%
	Cervical adenocarcinoma	2.17%
	Colorectal adenocarcinoma	2.02%
	Ovarian epithelial tumour	1.71%
	Pancreatic adenocarcinoma	1.63%
	Prostate adenocarcinoma	1.62%
	Seminoma	1.95%
	Invasive breast carcinoma	1.38%
	Hepatocellular carcinoma	1.36%
	Cervical squamous cell carcinoma	1.20%
LIN7C	Oesophageal squamous cell carcinoma	3.16%
	Endometrial carcinoma	2.39%
	Esophagogastric adenocarcinoma	2.14%
	Mature B-cell neoplasms	2.08%
	Bladder urothelial carcinoma	1.22%

Gene	Cancer type	Frequency
LIN7C (cont.)	Ovarian epithelial tumour	1.20%
	Pancreatic adenocarcinoma	1.09%
	Non-small cell lung cancer	1.04%
	Invasive breast carcinoma	1.01%
	Colorectal adenocarcinoma	1.01%
	Non-small cell lung cancer	1.04%
	Invasive breast carcinoma	1.01%
	Colorectal adenocarcinoma	1.01%
LIN7A	Sarcoma	6.67%
	Melanoma	4.95%
	Esophagogastric adenocarcinoma	3.50%
	Adrenocortical carcinoma	3.30%
	Endometrial carcinoma	3.24%
	Oesophageal squamous cell carcinoma	2.11%
	Cervical squamous cell carcinoma	1.99%
	Non-small cell lung cancer	1.80%
	Bladder urothelial carcinoma	1.70%
	Prostate adenocarcinoma	1.42%
	Invasive breast carcinoma	1.38%
	Head and neck squamous cell carcinoma	1.34%
	Colorectal adenocarcinoma	1.18%
	Pleural mesothelioma	1.15%
	Pancreatic adenocarcinoma	1.09%



Figure 3.22: Genetic alterations of MPP6 and LIN7 in cancer. (**A**) Frequency of gene alteration of the indicated genes as per The Cancer Genome Atlas (TCGA) study. Table shows frequencies $\geq 1\%$. (**B**) Distribution of gene alterations of the indicated genes found in all TCGA studies. (**C**) Distribution of gene alterations of the indicated genes found in colorectal cancer samples (n = 594). (**D**) Oncoprint representing alterations in MINA (RIOX2), MPP6, LIN7A and LIN7C genes identified across TCGA studies. Oncoprint was generated using the ComplexHeatmap R package. (**A-D**) Data source: cBioportal (https://www.cbioportal.org).

Chapter 4: Role of MINA in epithelial morphogenesis

4.1 Introduction

In the preceding chapter, we identified MPP6 as a novel extra-nucleolar interactor of MINA. MPP6 belongs to the MAGUK family of membrane-associated scaffold proteins, members of which have been heavily implicated in epithelial biology and polarity. As such, MPP6 could represent a good candidate to explain the downstream effects of MINA's reported role in cancer and epithelial-mesenchymal transition. In this chapter, we further define the role of MINA in epithelial morphogenesis and cell polarity using loss-of-function and rescue models in two- and three dimensional culture. In order to put this in context, we provide a brief overview of the major protein complexes involved in establishing and maintaining cell polarity.

Epithelial tissues outline all compartments within the human body and provide a physical barrier against the environment. During development, tight regulation of epithelial cell proliferation, differentiation and death allows epithelial tissues to expand and organise into structures such as tubes (Bryant and Mostov, 2008). Some epithelia develop to perform specialised functions, including absorption by the intestinal epithelium and secretion by glandular epithelia. Epithelia consist of highly polarised epithelial cells, characterised by asymmetrically distributed proteins and distinct mem-

brane compartments. This physical and functional asymmetry is crucial to form an intact barrier, but also allows for selective transport of molecules. Loss of epithelial integrity has been associated with diseases such as cancer (Bulgakova and Knust, 2009; Halaoui and McCaffrey, 2015).

Polarised epithelial cells are defined by apico-basal asymmetry: the apical surface faces the external, luminal environment, whereas the basal membrane connects to the extracellular matrix (ECM; Figure 4.1). Neighbouring cells are connected to each other laterally by a set of cellular junctions, including tight junctions, adherens junctions, desmosomes and gap junctions (Figure 4.1). Tight junctions regulate the transport between cells (paracellular transport) and are characterised by the presence of transmembrane proteins occludin and claudin (Zihni et al., 2016). Desmosomes and adherens junctions are responsible for adhesion between neighbouring cells. Epithelial adherens junctions consist of epithelial cadherin (E-cadherin) and intracellular α- and β-catenin and are reported to link to the cytoskeleton (Hartsock and Nelson, 2008). In addition to the prototypical tight and adherens junction components, other transmembrane proteins including junctional adhesion molecules (JAMs) and nectins (Figure 4.1), assemble at the membrane during the early stages of cell:cell adhesion and are important for the formation of junctions (Campbell et al., 2017; Takai et al., 2008). At the basal membrane, hemidesmosomes, characterised by the presence of integrins, another family of transmembrane proteins, provide a link between the cell and the extracellular matrix (Harburger and Calderwood, 2009). Intracellularly, transmembrane proteins are linked to cytoplasmic proteins that regulate signalling pathways that control proliferation, differentiation, survival and apoptosis (Halaoui and McCaffrey, 2015; Harburger and Calderwood, 2009).

The establishment of polarity and cell junctions is a complex, coordinated event that involves a large number of proteins and signalling pathways. Three protein complexes, partitioning-defective (PAR), Crumbs (CRB) and Scribble complexes, originally identified and extensively studied in *Caenorhabditis elegans* (*C. elegans*) and *Drosophila melanogaster*, play pivotal roles in this process (Figure 4.1). Par and Crumbs localise

to the apical membrane where they regulate apical membrane and junctional complex formation (Assémat et al., 2008). Members of the Scribble complex, comprising Scribble, the Discs large (DLG) and Lethal giant larvae (LGL) proteins, localise to adherens junctions where they define and stabilise the basolateral membrane (Assémat et al., 2008). As discussed by Rodriguez-Boulan and Macara (2014), in the early stages of mesenchymal-epithelial transition (MET), the Crumbs, Par and Scribble complexes gather at early, immature sites of cell:cell contacts which later segregate into separate tight and adherens junctions. This segregation is in part achieved by exclusion of basal proteins from the apical membrane and vice versa, through mechanisms such as phosphorylation (Rodriguez-Boulan and Macara, 2014). Despite often being viewed as separate complexes, cell polarity/adhesion complexes also communicate internally (Campbell et al., 2017). For instance, integrins can control the formation and stability of cell-cell junctions (Schreider et al., 2002).

Members of the family of membrane-associated guanylate kinases (MAGUKs), to which MPP6 belongs, have reported functions in most of the above described processes. For instance, zona occludens (ZO) proteins are MAGUKs that bind to the intracellular domain of tight junction-associated transmembrane proteins, linking them with the actin cytoskeleton (Fanning et al., 1998). Correct localisation of ZO-1 is often used as an indicator for tight junction integrity. Moreover, ZO-1 also directly binds afladin and thereby physically links tight and adherens junctions (Figure 4.1; Ooshio et al., 2010). The above mentioned discs large (DLG) is a MAGUK and component of the Scribble polarity complex (Figure 4.1). DLG also interacts with the putative tumour suppressor adenomatous polyposis coli (APC) to control cell proliferation, a function which is thought to be diminished by mutationally activated β-catenin (reviewed by Roberts et al., 2012). Several MAGUKs also interact with each other for stability or to regulate localisation. For example, correct localisation of DLG1 at the basolateral membrane of intestinal epithelial cells has been shown to depend on the expression of the MAGUK CASK (Lozovatsky et al., 2009).

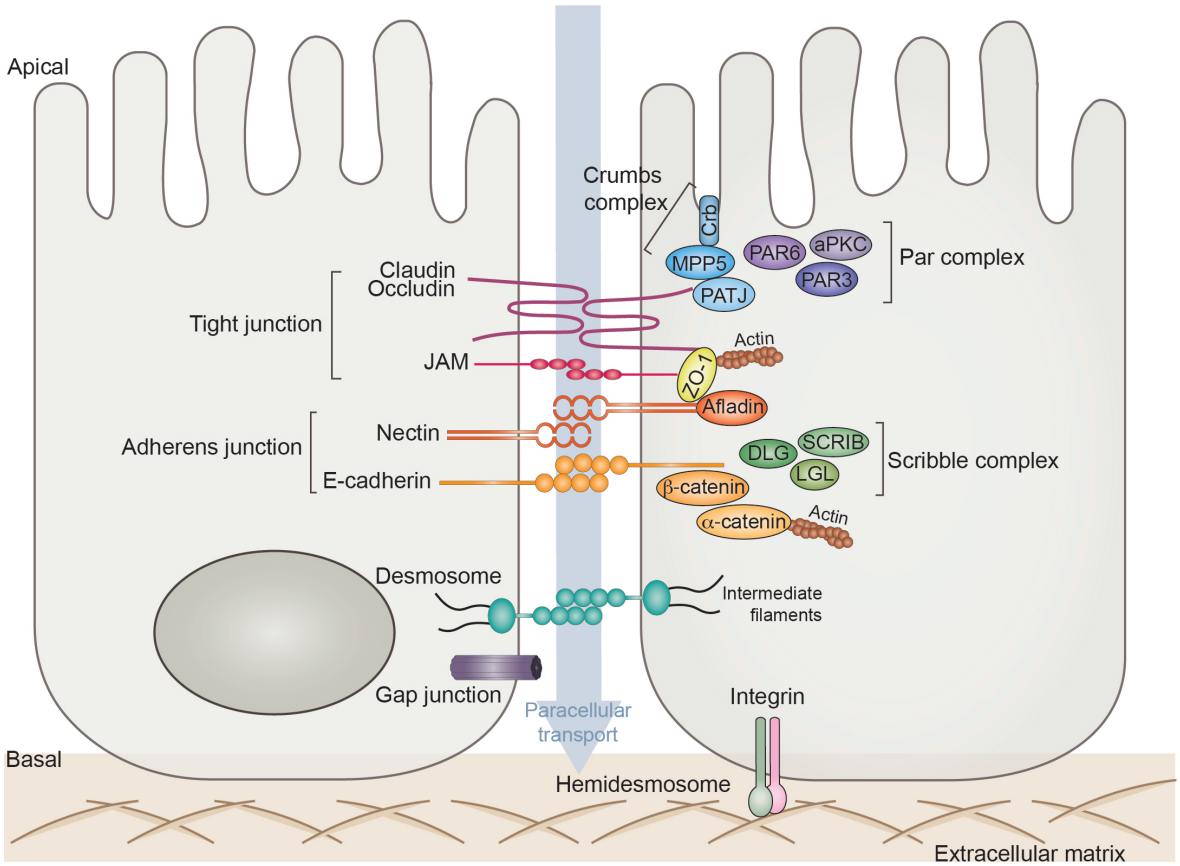


Figure 4.1: Overview of the main cell junctions and core polarity complexes. The main types of cellular junctions are tight junctions, adherens junctions, (hemi)desmosomes and gap junctions. Tight junctions regulate paracellular transport and consist of transmembrane proteins occludin, claudin and junctional adhesion molecules (JAMs). Localised basally from tight junctions are adherens junctions, which consist of E-cadherin and nectin. Crumbs, Par and Scribble polarity complexes localise to early sites of cell:cell adhesion and recruit transmembrane proteins. Intracellularly, polarity and adaptor proteins (such as ZO-1) connect to the cytoskeleton. At the basal membrane, integrin complexes at hemidesmosomes link with the extracellular matrix. Figure was created using Adobe Illustrator.

MPP6 belongs to the palmitoylated membrane protein (MPP) subfamily of MAGUKs, which comprises 7 members (MPP1-7; Chytła et al., 2020). Despite high sequence similarity (a sequence alignment of all MPPs is presented in Appendix B), members of this family exert diverse functions with regards to membrane biology. **MPP1** (also called p55) was first identified in erythrocytes, where it functions in a complex with the transmembrane protein glycophorin C and 4.1R to link the membrane with the cytoskeleton, thereby stabilising and ensuring elasticity of the membrane (Alloisio et al., 1993). Defects in this complex have been associated with abnormal, elliptically shaped red blood cells (Gallagher, 2004). **MPP2** is reported to bind to and suppress kinase activity of the proto-oncogene c-Src in epithelial cells: expression of MPP2 was shown to prevent the pro-migratory reorganisation of the cortical actin cytoskeleton in cells made to overexpress c-Src (Baumgartner et al., 2009). **MPP3** and **MPP4** have been extensively investigated with respect to their role in the retina (Dudok et al., 2013; Stöhr and Weber, 2001; Yang et al., 2007; Kantardzhieva et al., 2005). Moreover, MPP3 localises to the lateral membrane in epithelial cells, where it interacts with cell adhesion molecule 1 (CADM1) and has a reported tumour suppressor role in lung cancer (Fukuhara et al., 2003). **MPP5** (also known as protein associated with Lin-7 1, PALS1) is probably the most well-characterised of the MPPs. It was first identified in a study aimed at characterising novel interactors of mammalian LIN7 (Kamberov et al., 2000). MPP5 localises to the apical membrane and mediates the interaction between CRB and PATJ (Roh et al., 2002; Figure 4.1). Consequently, MPP5 depletion in MDCK cells causes tight junction and polarity defects, but also mistargeting of E-cadherin (Straight et al., 2004; Wang et al., 2007). **MPP7** is targeted to the lateral surface of epithelial cells through interactions with DLG1 and MPP5-CRB3 and functions in formation and maintenance of tight junctions (Stucke et al., 2007; Bohl et al., 2007).

MPP6 was first identified in the same study that identified MPP5 (resulting in its subsequent assignment as PALS2; Kamberov et al., 2000). However, in contrast to MPP5, which localises to the apical membrane, MPP6 was shown to localise to

the basolateral membrane in MDCK cells (Kamberov et al., 2000). Interestingly, and perhaps consistent with our localisation data presented in Chapter 3, analysis of the subcellular localisation of MPP6 in epithelial cells of the mouse small intestine indicated that the staining pattern differed slightly between the proliferating crypt cells and terminally differentiated cells within the villi, with more diffuse cytoplasmic localisation observed in crypt cells (Kamijo et al., 2016).

Aside from its subcellular localisation, not much is currently known about the function of MPP6. Nonetheless, it was shown to be recruited to early stage cell-cell adhesion sites in mouse epithelial MTD-1A cells (Shingai et al., 2003). Based on these data and our data indicating that MINA and MPP6 preferentially interact in low density culture conditions, one might hypothesise that the MINA-MPP6 'pathway' could play a role during the early stages of epithelial morphogenesis, cell:cell adhesion or polarity. In this chapter, we begin to test this hypothesis by characterising a series of phenotypes observed following reduced MINA expression.

4.2 Results

4.2.1 Caco-2 as a model to study epithelial morphogenesis/cell polarity

Cultured caco-2 cells show several morphological and functional features of polarised intestinal cells and are therefore suitable as a model to study cell polarity: these cells grow in a monolayer with microvilli on the apical side and tight junctions between neighbouring cells (Lechanteur et al., 2017; an image of a caco-2 monolayer showing asymmetrical distribution and apical localisation of tight junction protein ZO-1 is presented in Figure 4.2A). When grown on plastic, functional polarity of differentiated monolayers is evidenced by the formation of 'domes'. Domes are the result of unidirectional transport of ions and water from the apical to the basolateral site which leads to lifting of the cells (Figure 4.2B; MacCallum et al., 2005).

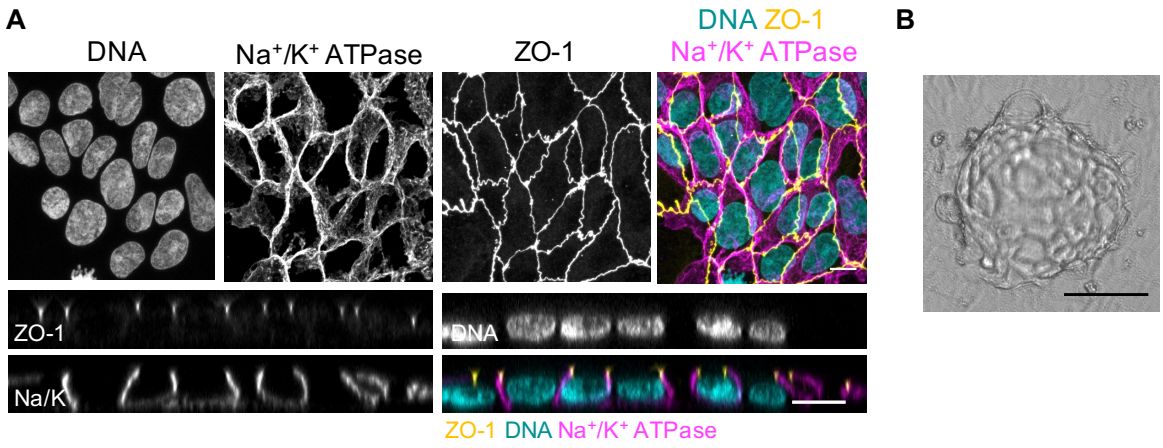


Figure 4.2: Caco-2 cells spontaneously polarise in two-dimensional cell culture. (**A**) Caco-2 cells grown to a confluent monolayer on glass coverslips were fixed with PFA and stained for the apical tight junction protein Zona Occludens-1 (ZO-1, yellow) and the lateral sodium potassium pump (Na^+/K^+ ATPase, magenta). Consecutive images were taken from the basal to the apical side and presented as a maximum projection image (top panels) or orthogonal view (rectangular bottom panels). Orthogonal views show the basal side at the bottom and apical side (as indicated by ZO-1) at the top. Nuclei were visualised with DAPI (cyan). Scale bars represent 10 µm. Z-stack images were acquired using a Zeiss LSM 780 confocal system equipped with a 40x C-Apochromat 1.2 W Korr M27 objective and ZEN black software. (**B**) Phase-contrast image of a dome, acquired using an EVOS inverted microscope equipped with a 10x objective. Scale bar represents 100 µm.

Whereas two-dimensional cell culture has long been the gold standard to study the behaviour of human cells *in vitro*, it is argued that monolayers do not always appropriately reflect what occurs *in vivo*. Therefore, in recent years a shift to using three-dimensional cell culturing techniques has occurred, particularly for studies concerning cell polarity and differentiation. Here, cells are provided with extracellular matrix to generate a more physiological environment. Marked differences have been observed regarding cell proliferation, differentiation and metabolism between cells cultured in two and three dimensions (Lagies et al., 2020). Caco-2 cells have the ability to form 'spheroids' or 'cysts' from single cells when grown in a three-dimensional extracellular matrix. As in monolayers, differentiation and subsequent ion and water transport results in the formation of a central, fluid-filled lumen (Figure 4.3A). Polarised cysts are characterised by accumulation of filamentous actin (F-actin) at the apical site facing the lumen (Figure 4.3B). The asymmetrical distribution of proteins along the apico-basal axis is further evidenced by the presence of distinct tight and adherens junctions, as visualised by ZO-1 and E-cadherin, respectively (Figure 4.3C, Jaffe et al., 2008).

4.2.2 Loss of MINA interferes with Caco-2 spheroid growth and lumen formation without affecting apico-basal polarity

To investigate the role of MINA in epithelial morphogenesis *in vitro*, we generated stable Caco-2 cell lines expressing doxycycline-inducible short hairpin RNA (shRNA). pZIP-TRE3G-ZsGreen-Puro lentiviral vectors containing two different shRNA sequences targeting MINA and a non-targeting control shRNA sequence were obtained from TransOMIC. These vectors contain a puromycin resistance gene allowing for antibiotic selection of successfully transduced cells. A schematic of the pZIP-TRE3G-ZsGreen-Puro vector is shown in Appendix A. Following selection with puromycin, MINA depletion was confirmed at the protein level by western blot (Figure 4.4A,B). In addition to the shRNA, the pZIP-TRE3G-ZsGreen-Puro vector contains a green fluorescent

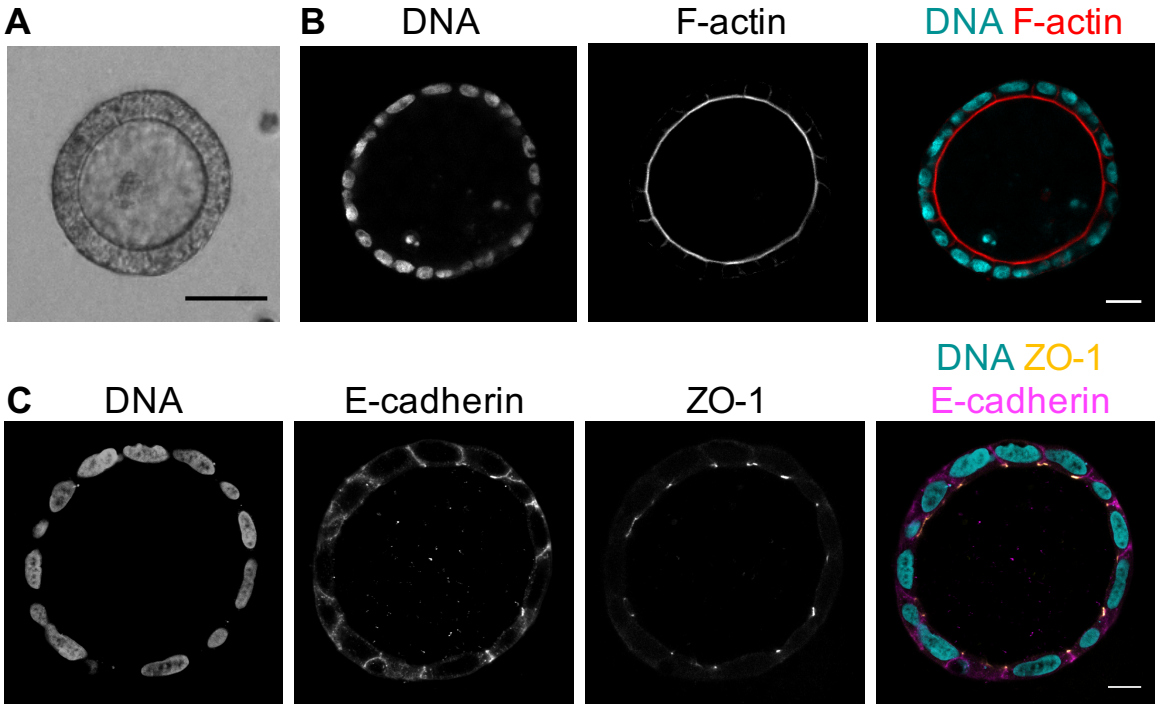


Figure 4.3: Caco-2 cells spontaneously polarise in three-dimensional cell culture. Caco-2 cells were plated as a single cell suspension in chamber slides coated with extracellular matrix (Matrigel) and left to grow for 7 days. The culture medium containing 4% matrigel was refreshed every 72 hours. Images represent single focal sections through the middle of the spheroid. (**A**) Phase-contrast image acquired using an EVOS inverted microscope equipped with a 10x objective. Scale bar represents 50 µm. (**B**) Caco-2 spheroid stained with phalloidin (F-actin, red). (**C**) Caco-2 spheroid stained for E-cadherin (magenta) and ZO-1 (yellow). (**B-C**) The fixation medium (4% (w/v) PFA) was supplemented with 5% (v/v) sucrose in order to keep the three-dimensional structure intact. Nuclei were visualised with DAPI (cyan). Scale bars represent 10 µm. Images were acquired using a Zeiss LSM 880 confocal system equipped with a 40x C-Apochromat 1.2 W Korr M27 objective and ZEN black software.

protein (ZsGreen) reporter gene under control of the same promoter to visualise expression of the shRNA. As shown in Figure 4.4C, the large majority of cells showed expression of GFP following induction with doxycycline, albeit heterogeneously. To further characterise the dynamics of the shRNA system, we performed a doxycycline titration and time course. Whereas shRNA expression resulted in reduced MINA protein levels after just 24 hours, more significant MINA knockdown was obtained at 72 hours post-treatment. Furthermore, similar levels of knockdown were obtained using reduced concentrations of doxycycline of 0.25 or 0.5 µg/mL, when compared to 1 µg/mL (Figure 4.4D).

Next, we set out to explore whether MINA is required for epithelial morphogenesis *in vitro*. Knockdown was induced by doxycycline for 72 hours before the cells were seeded either in two dimensions on plastic or in three dimensions in Matrigel. After 5 or 7 days, respectively, gross morphology was analysed. Interestingly, we noted substantial defects in the morphology of the MINA-depleted 3D spheroids. Whereas 44-47% of spheroids expressing control shRNA had formed a single, central lumen after 7 days, a lumen could only be detected in 19% or 13% of spheroids expressing MINA shRNA #1 or #3, respectively (Figure 4.5B). Furthermore, overall, MINA-depleted spheroids tended to be smaller than control spheroids (Figure 4.5C) and fewer in number (data not shown).

Based on the observation that MINA suppression affects spheroid diameter and number, we speculated that cell growth might be affected in these spheroids. To explore this possibility, we employed a CellTiter-Glo® Luminescent Cell Viability Assay (Promega). This assay quantifies the number of viable cells based on the amount of ATP present in culture, an indicator of metabolic (mitochondrial) activity. Upon addition of the reagent, a luminescent signal proportional to the amount of ATP is generated. As shown in Figure 4.6, we indeed noted a significant reduction in cell proliferation upon MINA knockdown.

This effect of MINA knockdown appeared specific to the 3D growth of Caco-2 cells, because MINA depletion in 2D cultures did not induce a reduction in cell proliferation,

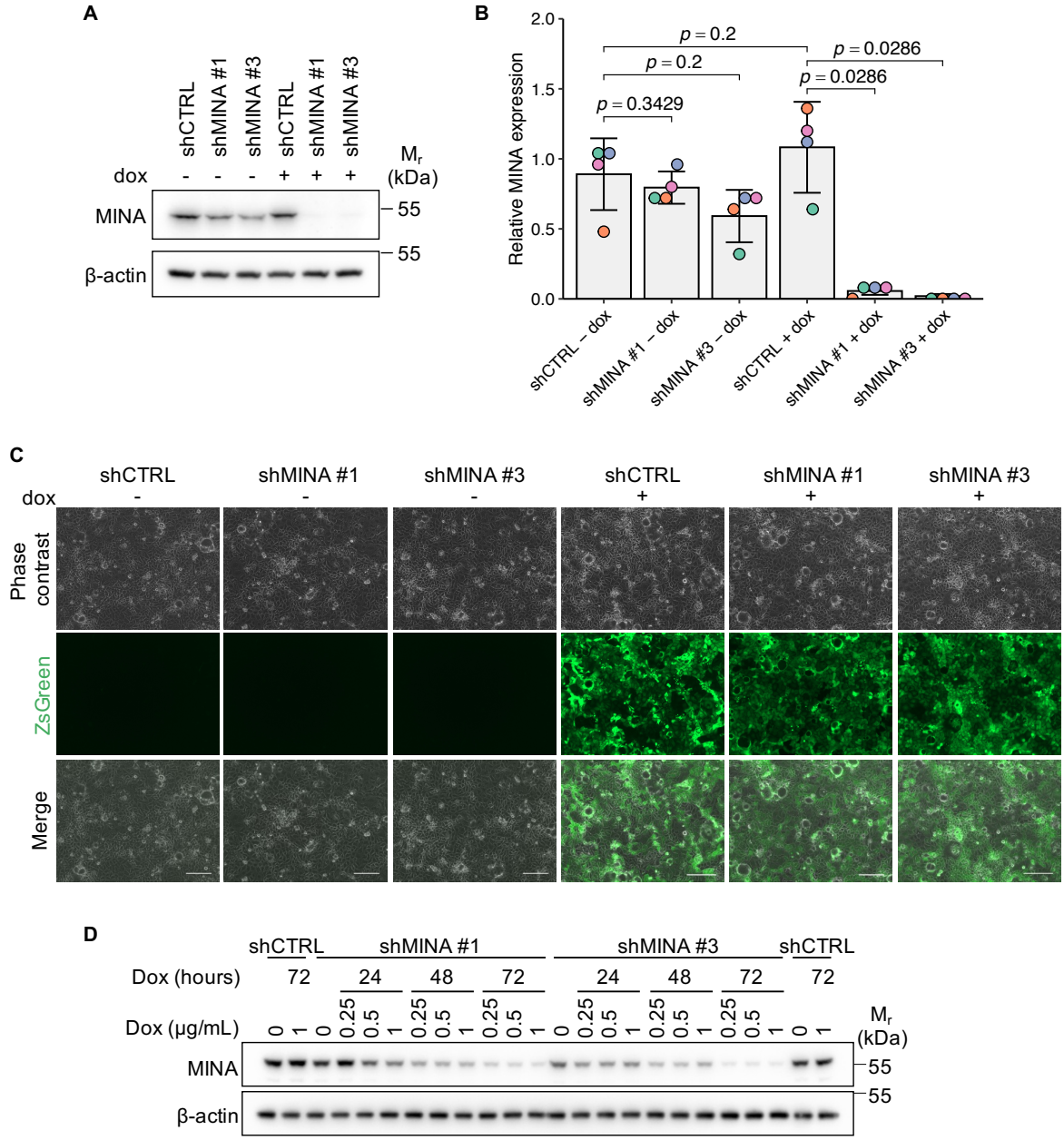


Figure 4.4: MINA expression in stable Caco-2 cell lines expressing inducible shRNA against MINA. (**A**) Representative immunoblot validating knockdown of MINA (53 kDa) in stable Caco-2 cell lines expressing doxycycline-inducible control (shCTRL) or MINA-targeting (shMINA #1/#3) shRNAs. Cells were either untreated or treated with 1 µg/mL doxycycline (dox) for 72 hours prior to immunoblotting. β-actin (42 kDa) was used as loading control. (**B**) Quantification of MINA protein levels following 72 hours of shRNA induction. Bars represent averages from n = 4 biological replicates. Each replicate is colour-coded. Statistical significance was determined using a Kruskal-Wallis rank sum test and p values were calculated using a post-hoc pairwise Wilcoxon test. (**C**) Expression of green fluorescent protein (GFP) was analysed 72 hours after induction with 1 µg/mL doxycycline (dox). Images were acquired using an EVOS inverted microscope equipped with a 10x objective. (**D**) MINA (53 kDa) expression levels were analysed by immunoblotting after 0, 24, 48 or 72 hours of shRNA induction with respectively 0, 0.25, 0.5 or 1 µg/mL doxycycline (dox). β-actin (42 kDa) was used as loading control.

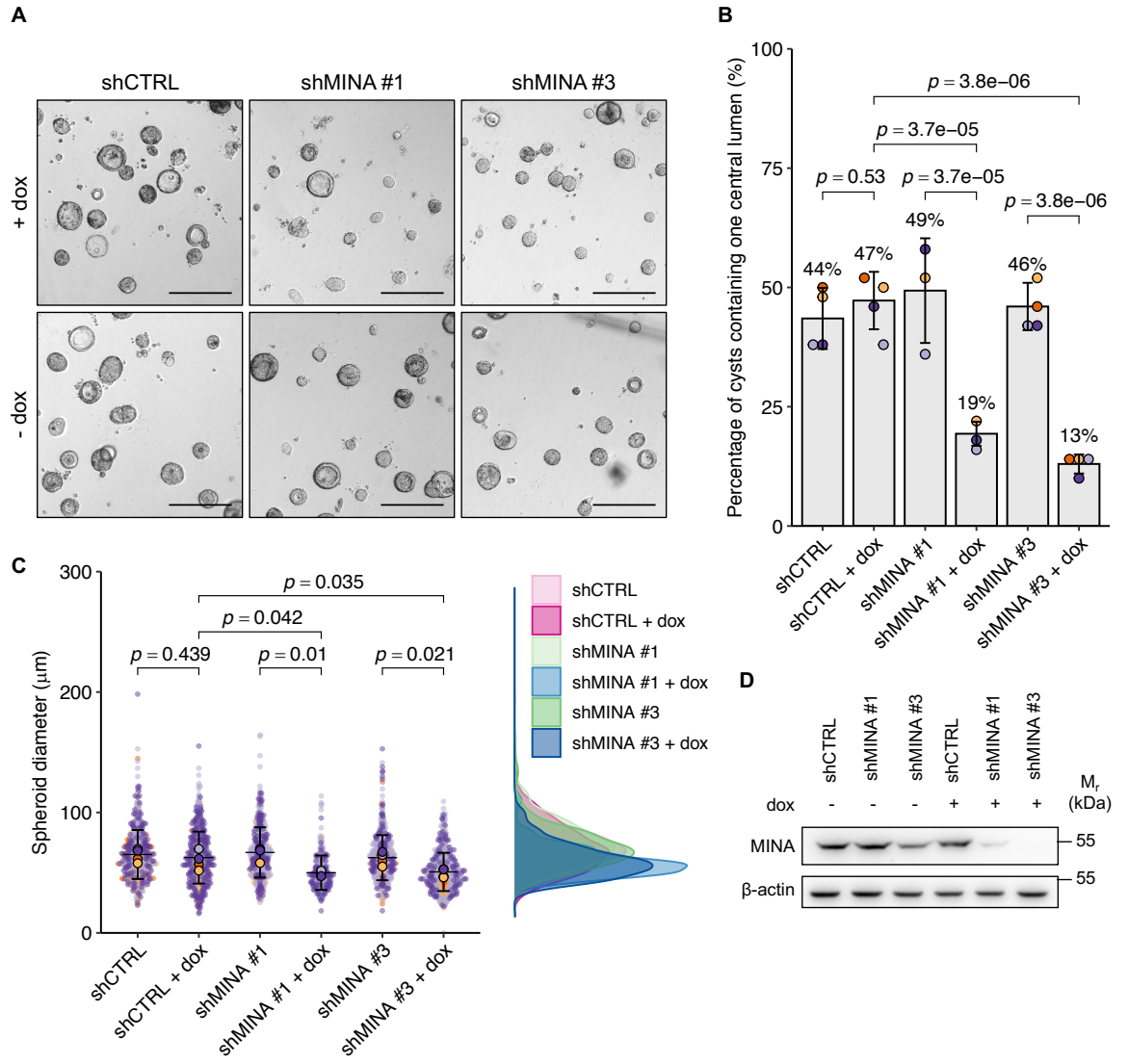


Figure 4.5: MINA depletion affects 3D spheroid growth and lumen formation. (**A-D**) Caco-2 cells stably expressing inducible shRNA against control (shCTRL) or MINA (shMINA) sequences were treated with 1 µg/mL doxycycline (dox) for 72 hours before seeding. Once seeded, the cells were grown for 7 days in 0.5 µg/mL dox before the presence of a central lumen (B) and spheroid diameter (C) were assessed and MINA depletion was confirmed (D). Fresh dox was added every 72 h. (**A**) Representative phase-contrast images acquired using an EVOS inverted microscope equipped with a 10x objective. Scale bars represent 200 µm. At least 10 random images were taken per condition for analysis. (**B**) MINA depletion affects lumen formation. Bars represent averages from n $\geq$ 3 biological replicates. The average of each replicate is colour-coded. (**C**) Beeswarm (left) and density (right) plots quantifying spheroid diameter. Individual data points and the average values are colour-coded according to biological replicate. (**B,C**) Data are mean ± SD of replicate averages. A total of 648 (shCTRL), 646 (shCTRL + dox), 483 (shMINA #1), 285 (shMINA #1 + dox), 540 (shMINA #3) and 690 (shMINA #3 + dox) spheroids were counted across all replicates. Statistical significance was determined using one-way ANOVA and p values were calculated using pairwise t tests. P values were adjusted for multiple testing using the Benjamini-Hochberg method. Analysis of lumen presence and spheroid diameter was performed manually using Fiji. Acquired images were blinded prior to analysis. (**D**) Representative immunoblot validating knockdown of MINA (53 kDa) in 3D on day 7. β-actin (42 kDa) was used as loading control.

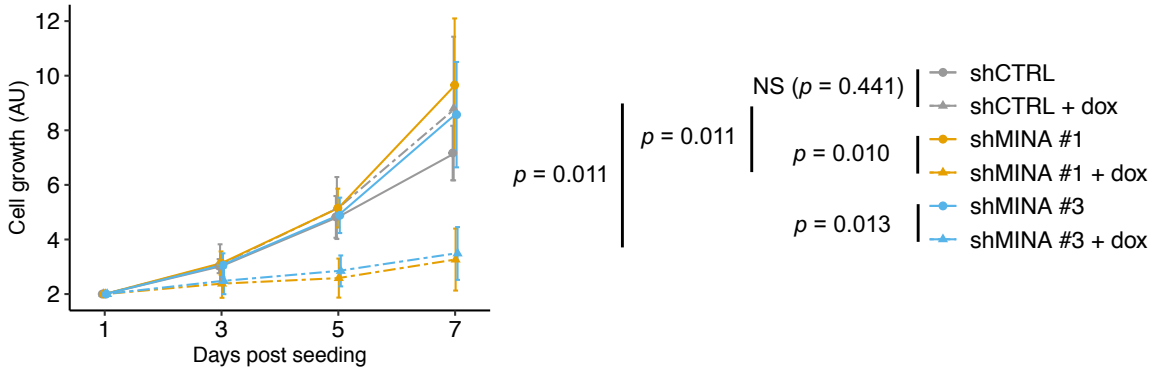


Figure 4.6: Loss of MINA expression inhibits Caco-2 cell proliferation in 3D. Cells were seeded in 96-well plates coated with Matrigel in the presence or absence of 1 µg/mL doxycycline (dox) and cell viability was assayed by a CellTiter-Glo® Luminescent Cell Viability Assay on the indicated days. Cell culture medium was refreshed and fresh dox was added every 72 hours. AU = arbitrary unit. Values represent averages from n = 3 biological replicates. NS = not significant. Error bars represent SD. Statistical significance on day 7 was determined using one-way ANOVA and p values were calculated using a pairwise t test. P values were adjusted for multiple testing using the Benjamini-Hochberg method. A representative immunoblot validating suppression of MINA protein expression is shown in Figure 4.5.

as monitored with a resazurin reduction assay (Figure 4.7A). Similar to the CellTiter-Glo® assay used for 3D cultures, resazurin is an indicator of metabolic activity. In viable cells, resazurin is reduced by the mitochondria, causing a colourimetric change. Furthermore, we did not observe obvious alterations in the gross morphology of the 2D monolayer, as assessed by phase-contrast microscopy (Figure 4.7B). However, we did note that the cells' ability to form domes was affected (Figure 4.7C). As mentioned above, domes are thought to be the result of fluid transport following the formation of functional tight junctions in a monolayer. To explore the possibility that MINA might regulate tight junction formation, cells grown on a semi-permeable support for 14 days were stained with an antibody for the tight junction protein zona occludens 1 (ZO-1). Concurrently, the cells were also stained for adherens junction protein E-cadherin. Although cell polarity *per se* did not appear to be affected, as ZO-1 and E-cadherin correctly localised to the apical and lateral membrane sections, respectively, MINA-depleted cells appeared flatter and larger, indicating a reduction of the lateral membrane and expansion of the apical and basal membranes (Figure 4.8A). In 3D, analogous to 2D, ZO-1 and E-cadherin remained asymmetrically distributed in MINA-

depleted cysts. However, the apical membrane appeared distorted, as indicated by the diffuse membrane staining of ZO-1 (Figure 4.8B). A similar staining pattern was seen in a fraction of control shRNA-expressing cysts that were smaller and had not yet formed a lumen, suggesting that MINA-depleted cysts remain in an immature state. No effect was noted on global expression levels of cell junction proteins in 2D or 3D, however (Figure 4.8C). Taken together, our results thus far would therefore indicate that MINA depletion does not interfere with cell polarity as such, but might instead affect the stability or functionality of certain cell junctions, ultimately resulting in a defect in dome and lumen formation.

4.2.3 Stable re-expression of MINA in inducible knockdown cell lines

The data obtained so far suggest that MINA may have a role in epithelial morphogenesis *in vitro*. In light of the results presented in the previous chapters, we were interested to determine whether the phenotypes observed are dependent on the catalytic activity and/or nucleolar localisation of MINA. To this end, we aimed to re-introduce MINA variants into the inducible MINA shRNA background by using specific cDNA sequences predicted to be resistant to the corresponding shRNA. Moreover, such 'rescue' experiments can validate whether the observed shRNA effects are in fact specific to the loss of MINA, rather than off-target effects of the short hairpin RNA (as discussed by Kaelin, 2017).

Six silent mutations were introduced into the target site of MINA shRNA#1 to generate shRNA-resistant MINA that was either wild-type (WT), catalytically inactive (H179A), defective in nucleolar localisation (NoLS), or a double mutant (NoLS/H179A). Subsequently, these sequences were cloned into the QM800A vector (systemBIO). Here, gene expression is induced by cumate rather than doxycycline, allowing us to control re-expression levels of shRNA-resistant MINA following transduction of the doxycycline-inducible MINA shRNA cell lines. Because these cells are already puromycin-resistant

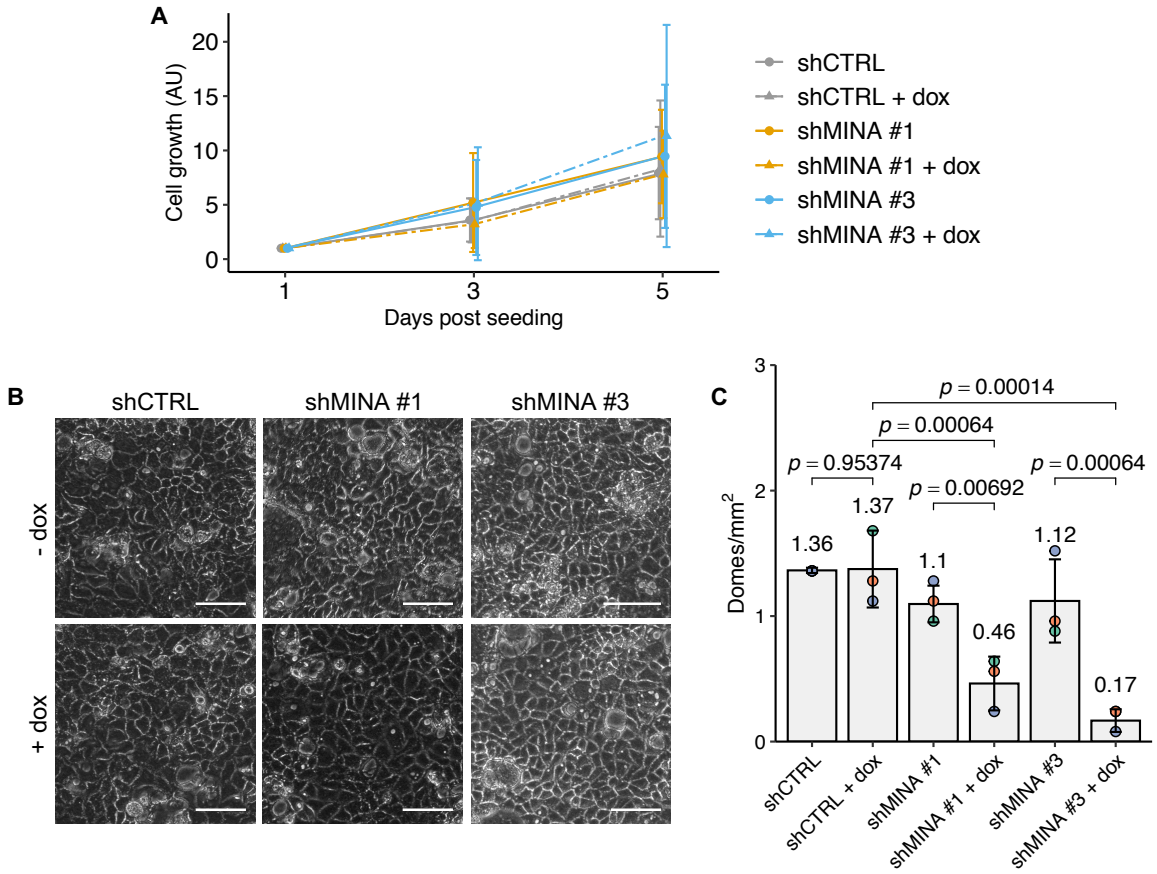


Figure 4.7: MINA depletion affects dome formation in Caco-2 monolayers. Expression of control (shCTRL) or MINA-targeting (shMINA) shRNA was induced in stable Caco-2 cell lines by incubation with 1 µg/mL doxycycline (dox) for 72 hours before cells were seeded. Once seeded, knockdown was maintained by incubation with 0.5 µg/mL doxycycline. The culture medium was refreshed every 72 hours after seeding. (**A**) MINA depletion does not affect cell growth in 2D. Cell growth in 2D was monitored with resazurin. Data presented are the mean ± SD of 4 biological replicates. Four technical replicates of each sample were used in each experiment. No significant differences in average growth were observed. AU = arbitrary unit. (**B**) MINA depletion does not affect the gross morphology of Caco-2 monolayers, as assessed by phase-contrast microscopy. Images were taken 5 days after seeding using an Evos microscope (Thermo) equipped with a 10x objective. (**C**) MINA depletion affects dome formation. A total of 30 random phase-contrast images were taken per condition, five days after seeding, using an Evos microscope (Thermo) equipped with a 10x objective, after which domes were quantified (for an example of a dome, see Figure 4.2A). Bars represent the average number of domes per mm^2 of three independent experiments. The average of each biological replicate is colour-coded. Error bars represent the SD. Statistical significance was determined using one-way ANOVA and p values were calculated using a pairwise t test. P values were adjusted for multiple testing using the Benjamini-Hochberg method.

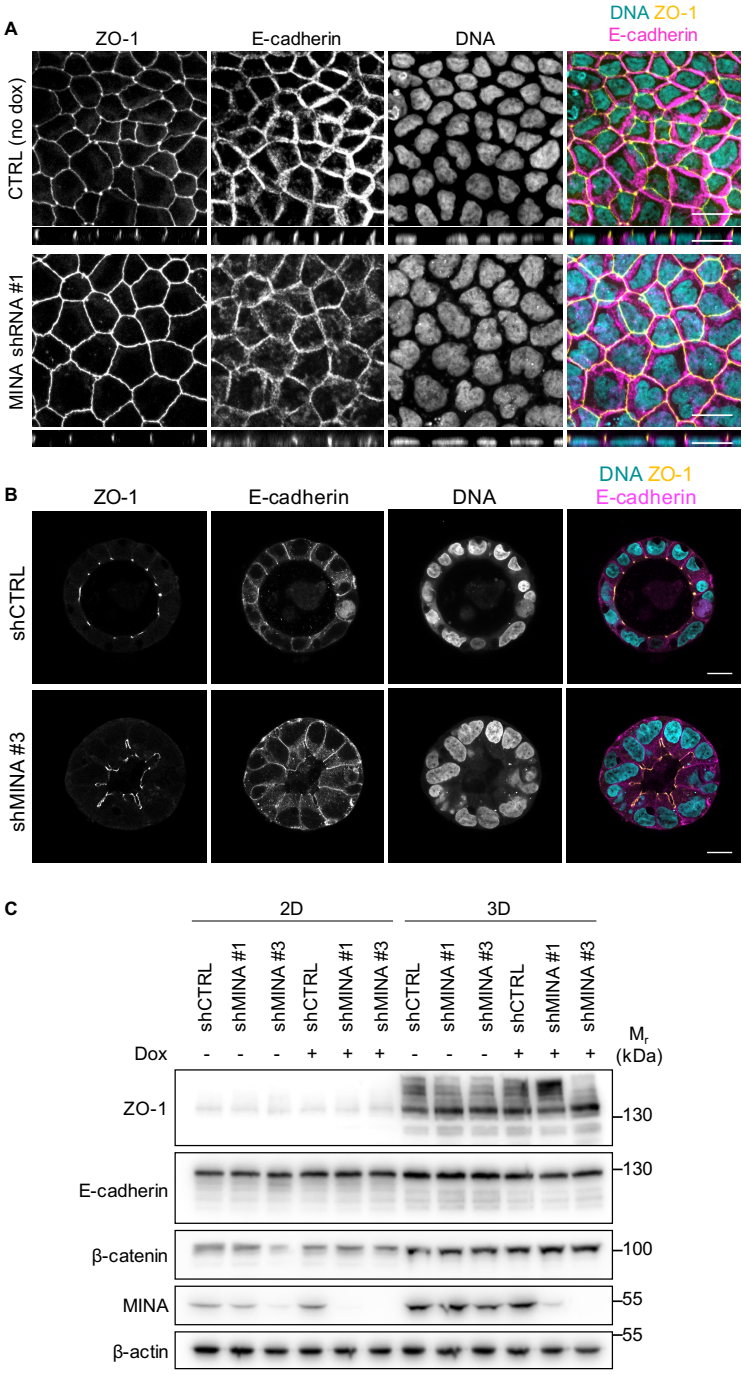


Figure 4.8: MINA is dispensable for the establishment of apico-basal polarity in Caco-2 cells. (**A**) Caco-2 cells were that were either untreated or treated with 1 µg/mL doxycycline to induce expression of MINA-targeting shRNA were grown on a semi-permeable membrane for 14 days. Consecutive images were taken from the basal to the apical side and presented as a maximum projection image (top panels) or orthogonal view (rectangular bottom panels). (**B**) Expression of either non-targeting control or MINA-targeting shRNA cells was induced with 1 µg/mL doxycycline and cells were grown for 10 days in 3D. (**A,B**) Cells were fixed with PFA and stained for tight junction protein zona occludens 1 (ZO-1, yellow) and adherens junction protein E-cadherin (magenta) to mark the apical and basolateral surfaces, respectively. Nuclei were visualised with DAPI (cyan). Images were acquired using a Zeiss LSM 780 (A) or 880 (B) confocal microscope equipped with a 40x C-Apochromat 1.2 W Korr M27 objective and ZEN black software. (**C**) Cell lysates from 2D or 3D cultures grown for 7 days with or without 1 µg/mL doxycycline (dox) were probed for MINA (53 kDa) and polarity markers ZO-1 (195 kDa), E-cadherin (97 kDa) and β-catenin (85 kDa). β-actin (42 kDa) was used as loading control.

(because of the presence of the pZIP shRNA vectors), the puromycin resistance cassette in the QM800A vector was replaced with a blasticidin resistance cassette (QM800A-Blast), to allow for antibiotic selection. A schematic of this vector is shown in Appendix A. Following viral transduction and selection using 10 µg/mL blasticidin, expression of the exogenous shRNA-resistant untagged MINA constructs was analysed. Induction of an empty vector or shRNA-resistant MINA was induced by the recommended concentration of 30 µg/mL for 72 hours. In parallel, expression of either non-targeting control or MINA-targeting shRNA was induced by 1 µg/mL doxycycline. As shown in Figure 4.9A, a low level of apparent 'leaky' MINA expression was observed in the absence of cumate when compared to MINA knockdown cells minus re-expression (compare lanes 5, 7, 9, and 11 to lanes 3 and 4). Unfortunately, although the leaky expression of exogenous MINA could be modestly increased by the addition of cumate (e.g. compare lanes 7 and 8), the induced levels were still lower than the endogenous MINA levels in control shRNA cells (shCTRL; compare lanes 5, 7, 9, and 11 to lanes 1 and 2). Next, a cumate titration was performed, aiming to increase the expression of exogenous MINA to endogenous levels. For this purpose, the cells were incubated for 72 hours with 1 µg/mL doxycycline and 0, 30, 60, 300 or 600 µg/mL cumate. Unfortunately, however, expression of exogenous MINA was not significantly increased beyond 30 µg/mL cumate (Figure 4.9B). Lastly, rather than adding one dose of cumate on day 0, fresh cumate was added every 24 hours for 0–5 days, to ensure the lack of induction observed in Figure 4.9B was not a result of the cumate concentration dropping over time. However, as shown in Figure 4.9C-E, we again observed insufficient levels of induced exogenous MINA. We therefore concluded that the inducible cumate system is not suitable for re-expression experiments, at least not as a stable model in this cell type.

Next we considered a non-inducible transient approach in Caco-2 cells as an alternative. cDNA sequences encoding 3xFLAG-tagged MINA that was either wild-type, catalytically inactive (Fe(II)-binding mutant H179A), defective in nucleolar localisation (NoLS) or a double mutant (NoLS/H179A), were cloned into the pIHZ lentiviral

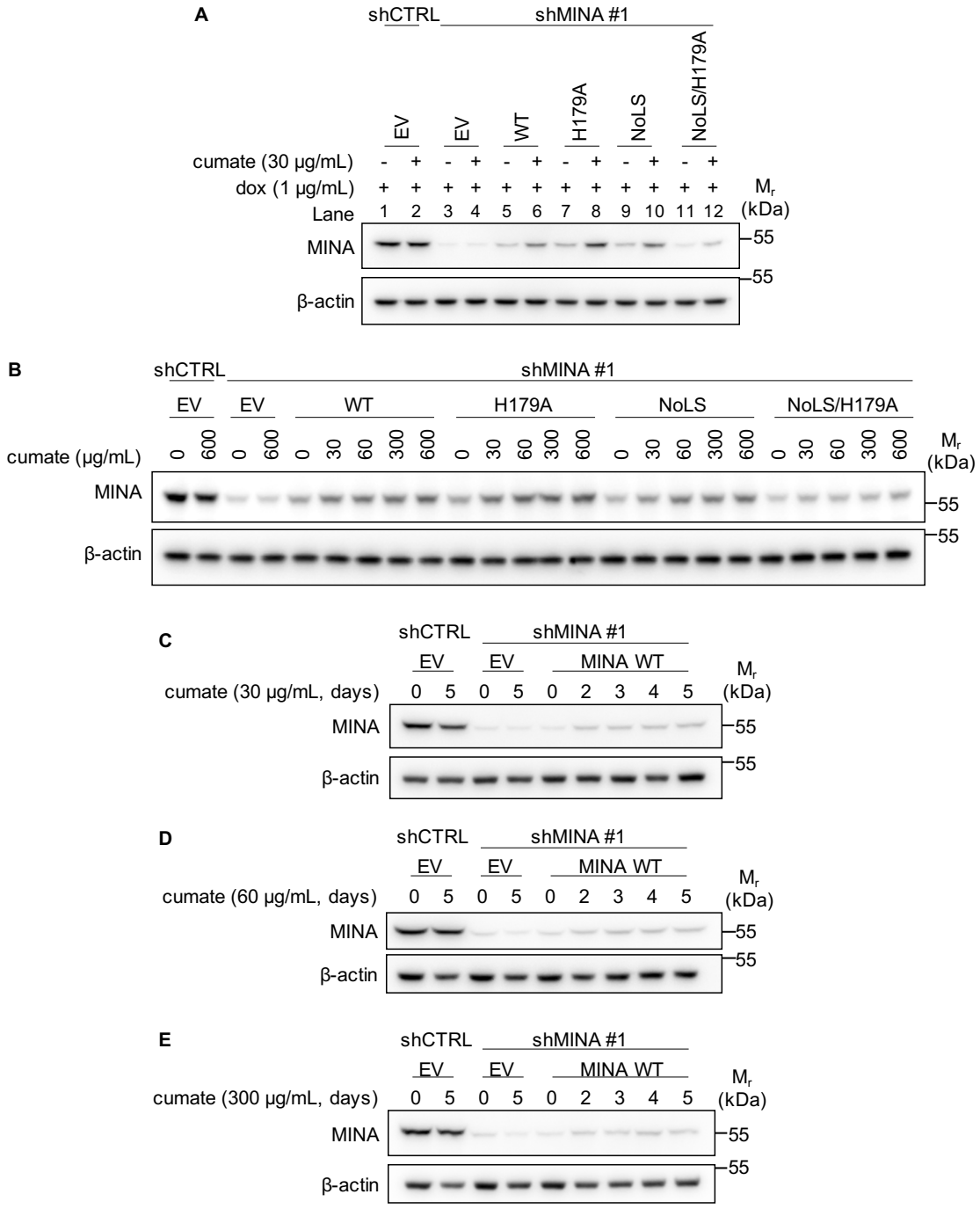


Figure 4.9: Characterisation of Caco-2 cells stably expressing cumate-inducible untagged MINA. (**A-E**) Unless otherwise indicated, Caco-2 cells stably expressing doxycycline-inducible shRNA and cumate-inducible shRNA-resistant untagged MINA were treated with 1 µg/mL doxycycline (dox) and/or the indicated concentrations of cumate for 72 hours. Cell extracts were immunoblotted for MINA (53 kDa). β-actin (42 kDa) was used as loading control. shCTRL = non-targeting control shRNA. EV = empty vector. WT = wild-type, NoLS = nucleolar localisation mutant, H179A = catalytically inactive mutant. (**A**) Low levels of exogenous MINA are expressed following induction with cumate. (**B**) Increased concentrations of cumate do not increase expression of exogenous MINA. (**C-E**) Increasing the frequency of cumate addition does not increase the expression of exogenous MINA. Cell culture medium was refreshed and fresh cumate at the indicated concentrations was added every 24 hours for the indicated amount of days.

vector for constitutive expression. The pIHZ vector is a derivative of the pGIPZ vector (Open Biosystems) that lacks the green fluorescent protein (GFP) reporter and contains a hygromycin rather than a puromycin resistance cassette. A schematic of this vector is shown in Appendix A. Initially, pZIP shMINA #1 cells were transduced with lentiviruses encoding the pIHZ 3xFLAG-MINA vectors described above. Because our intention was to test this as an acute intervention, as opposed to antibiotic selection and creation of a stable cell line, we did not treat the cells with hygromycin. Instead, cells were immediately seeded in 2D and 3D to analyse dome and lumen formation, respectively, in order to assess the potential success of the approach. Using this method, expression levels of exogenous FLAG-MINA were obtained that were the same (NoLS and NoLS/H179A), or slightly higher (WT and H179A), than the endogenous protein (Figure 4.10A). Because the cells had not been selected with hygromycin, and we could expect <100% viral infection efficiency, we next checked the frequency of FLAG-MINA expression in the cell populations prior to phenotyping experiments. As shown in Figure 4.10B, the majority of cells expressed FLAG-MINA, with expression levels being modestly heterogeneous across the populations. Next, we proceeded to undertake some preliminary assays to determine whether the exogenous FLAG-MINA was capable of rescuing the MINA shRNA knockdown phenotypes described above. Importantly, introducing exogenous wild-type FLAG-MINA into a MINA-depleted background (shMINA #1) restored dome formation towards control levels (Figure 4.10C). Interestingly, the phenotype was also rescued with expression of the MINA mutant defective in nucleolar localisation (NoLS), consistent with the role of MINA in dome formation being related to its extra-nucleolar function(s). The results with respect to MINA activity were less clear however. Expression of exogenous 3xFLAG-MINA H179A and NoLS/H179A partially restored dome formation (compared to the EV control). Importantly however, these inactive mutants did not fully rescue the phenotype to wild-type or NoLS levels (Figure 4.10C). Whether this reflects a partial activity-dependence, or a technical limitation of the approach, is not yet clear. We highlight that the values shown are of a single experiment, which may have contributed to the re-

sult not being clearer. In parallel to the 2D dome assays described above, cells were also seeded for 3D spheroid growth and lumen formation assays. Unfortunately, in contrast to growth in 2D, very few 3D cysts showed noticeable expression of 3xFLAG-MINA, complicating the analysis (Figure 4.11).

In an attempt to increase the percentage of cells expressing 3xFLAG-MINA in 3D, we selected successfully transduced cells with 100 µg/mL hygromycin B before seeding the experiments. However, although hygromycin-resistant, we were surprised to discover that Caco-2 cells cultured and seeded in hygromycin B fail to functionally polarise, as observed by the absence of domes (Figure 4.12). For this reason, hygromycin B was removed from the culturing medium 72 hours before seeding of subsequent experiments.

During the period of hygromycin depletion, doxycycline was added to induce shRNA expression. In a pilot experiment we observed that wild-type 3xFLAG-MINA re-expression fully restored the frequency of lumen-containing cysts in MINA knockdown cells (Figure 4.13A). In a subsequent expanded experiment, we observed a similar relationship between MINA expression, nucleolar localisation, activity, and dome formation as described above (Figure 4.13B): 3xFLAG-MINA restored normal dome formation in a manner that was independent of nucleolar expression and partially activity-dependent. Unfortunately however, a rapid decline in expression of exogenous MINA was noted, possibly due to negative selection of MINA-overexpressing cells, which prevented further analyses within the timeframe of this thesis (Figure 4.13C).

4.3 Discussion

Following the results described in Chapter 3, we hypothesised that MINA regulates epithelial morphogenesis/polarity in a manner that depends on its localisation, activity, and interaction with MPP6. To explore this, the aims of this Chapter were to study the phenotypes in loss-of-function systems, and to undertake structure-function analyses in these using the nucleolar (NoLS) and catalytic (H179A) mutants characterised in Chapters 2 and 3.

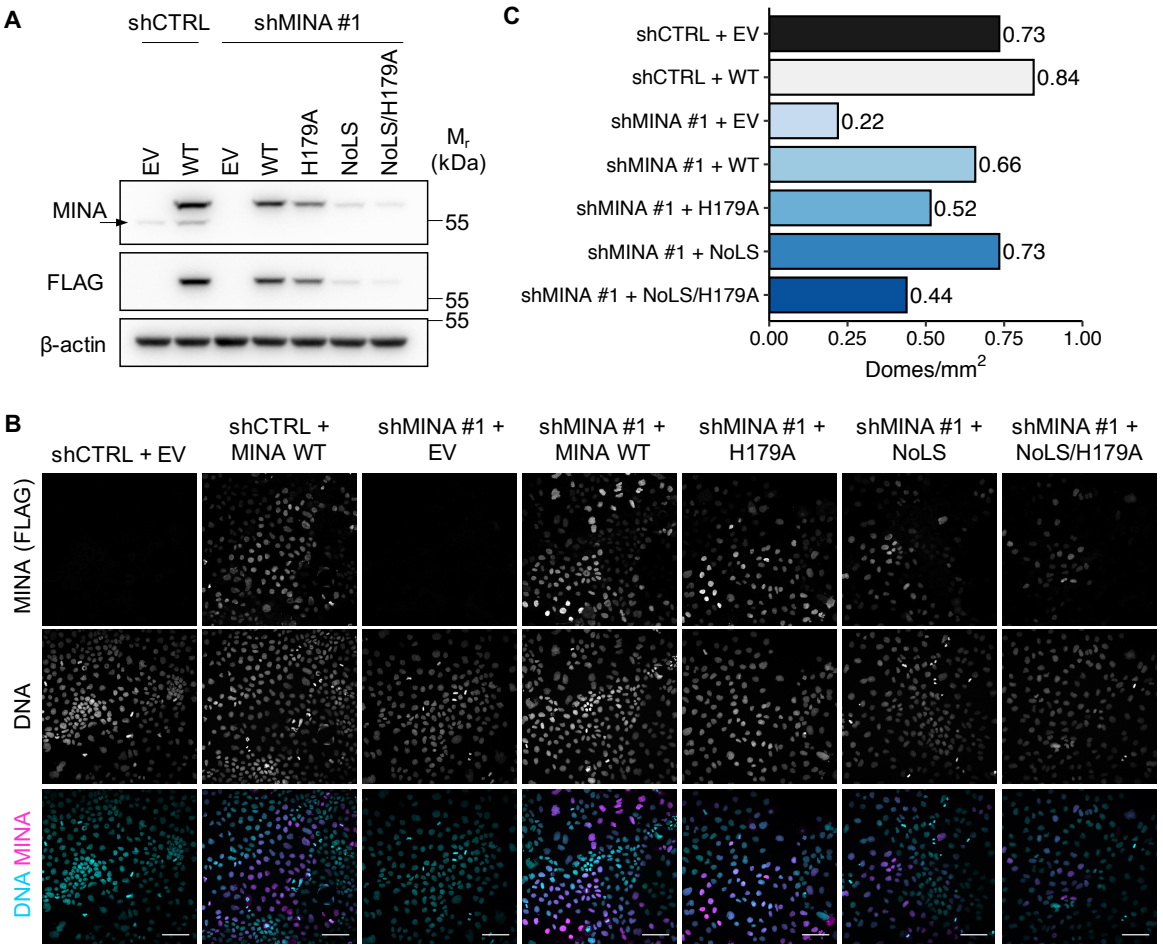


Figure 4.10: Transient re-expression of 3xFLAG-tagged MINA in doxycycline-inducible shRNA cell lines: 2D dome assays. Caco-2 cells expressing either control (shCTRL) or MINA-targeting (shMINA #1) shRNA were transduced with lentivirus encoding an empty vector (EV) or the indicated 3xFLAG-MINA constructs. shRNA expression was induced with 1 µg/mL doxycycline 48 h before transduction. 48 h after transduction, the cells were seeded and grown for 5 days before protein expression was analysed by immunoblot (A), immunofluorescence (B) and the presence of domes was assessed (C). The culture medium was refreshed and fresh dox (0.5 µg/mL) was added every 72 hours. (**A**) Cell extracts were immunoblotted for MINA (53 kDa) and FLAG, confirming endogenous MINA knockdown and expression of exogenous 3xFLAG-MINA. Black arrow indicates endogenous MINA. β-actin (42 kDa) was used as loading control. (**B**) Representative immunofluorescence images showing expression of 3xFLAG-MINA. Cells were fixed with PFA and stained with an anti-FLAG antibody (magenta). Nuclei were stained with DAPI (cyan). Scale bars represent 100 µm. Images were acquired using a Zeiss LSM 880 confocal microscope equipped with a 20x C-Apochromat 1.2 W Korr M27 objective and ZEN black software. (**C**) Bar graph shows the average number of domes per mm^2, calculated from 30 random images taken using an EVOS microscope equipped with a 10x objective. Values are data from n = 1 experiment. Images were blinded prior to analysis.

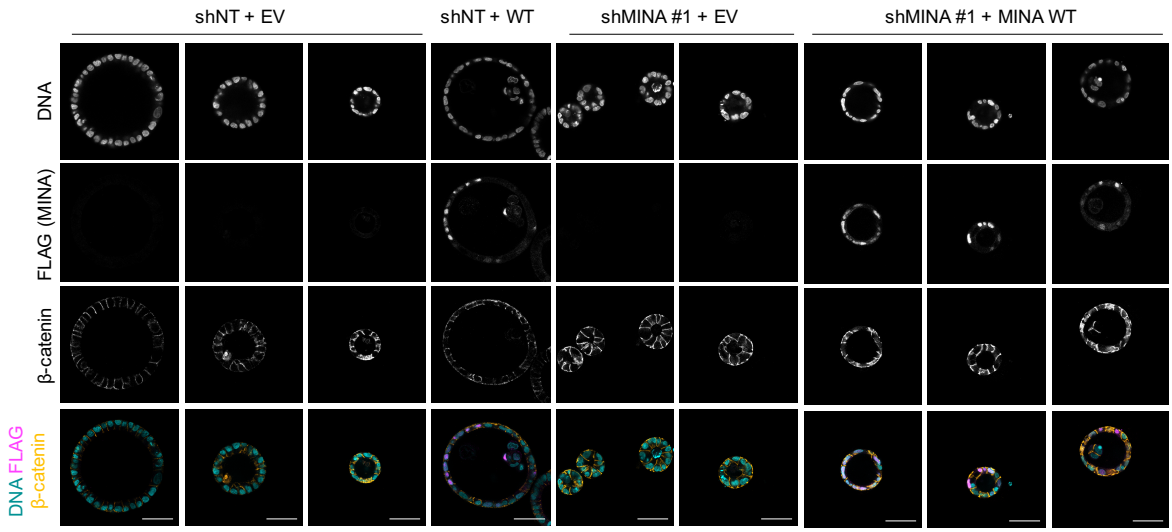


Figure 4.11: Transient re-expression of 3xFLAG-tagged MINA in doxycycline-inducible shRNA cells lines: 3D spheroid assays. Heterogeneous expression of 3xFLAG-MINA in transiently transduced Caco-2 cells grown in 3D. Caco-2 cells expressing either control (shCTRL) or MINA-targeting (shMINA #1) shRNA were transduced with lentivirus encoding an empty vector (EV) or wild-type (WT) 3xFLAG-MINA. shRNA expression was induced with 1 µg/mL doxycycline 48 h before transduction. 48 h after transduction, the cells were seeded in 3D. Fresh doxycycline (0.5 µg/mL) was added every 72 hours. Expression of 3xFLAG-MINA was assessed by indirect immunofluorescence on day 7. Spheroids were fixed and stained for FLAG (MINA, magenta) and β-catenin (yellow). Nuclei were visualised with DAPI (cyan). Scale bars represent 50 µm. Images were acquired using a Zeiss LSM 880 confocal microscope equipped with a 40x C-Apochromat 1.2 W Korr M27 objective and ZEN black software.

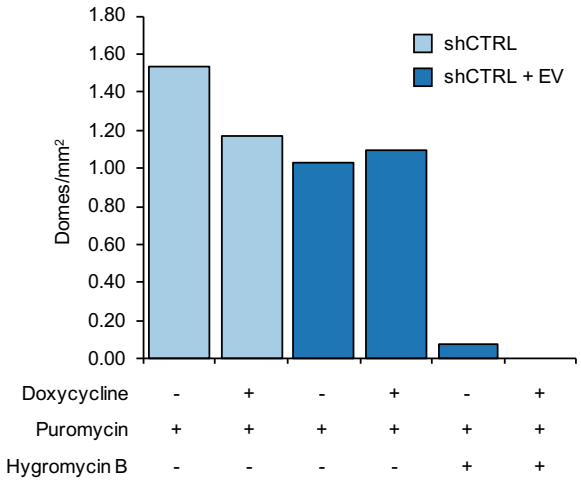


Figure 4.12: Effect of hygromycin B on Caco-2 dome formation. Caco-2 cells transduced once (light blue) or twice (dark blue) were seeded in puromycin-containing medium with or without 1 µg/mL doxycycline and/or 100 µg/mL hygromycin B and grown to confluence for 5 days before the presence of domes was assessed. A total of 30 random images were taken per condition using an EVOS microscope equipped with a 10x objective. Values represent data from n = 1 experiment.

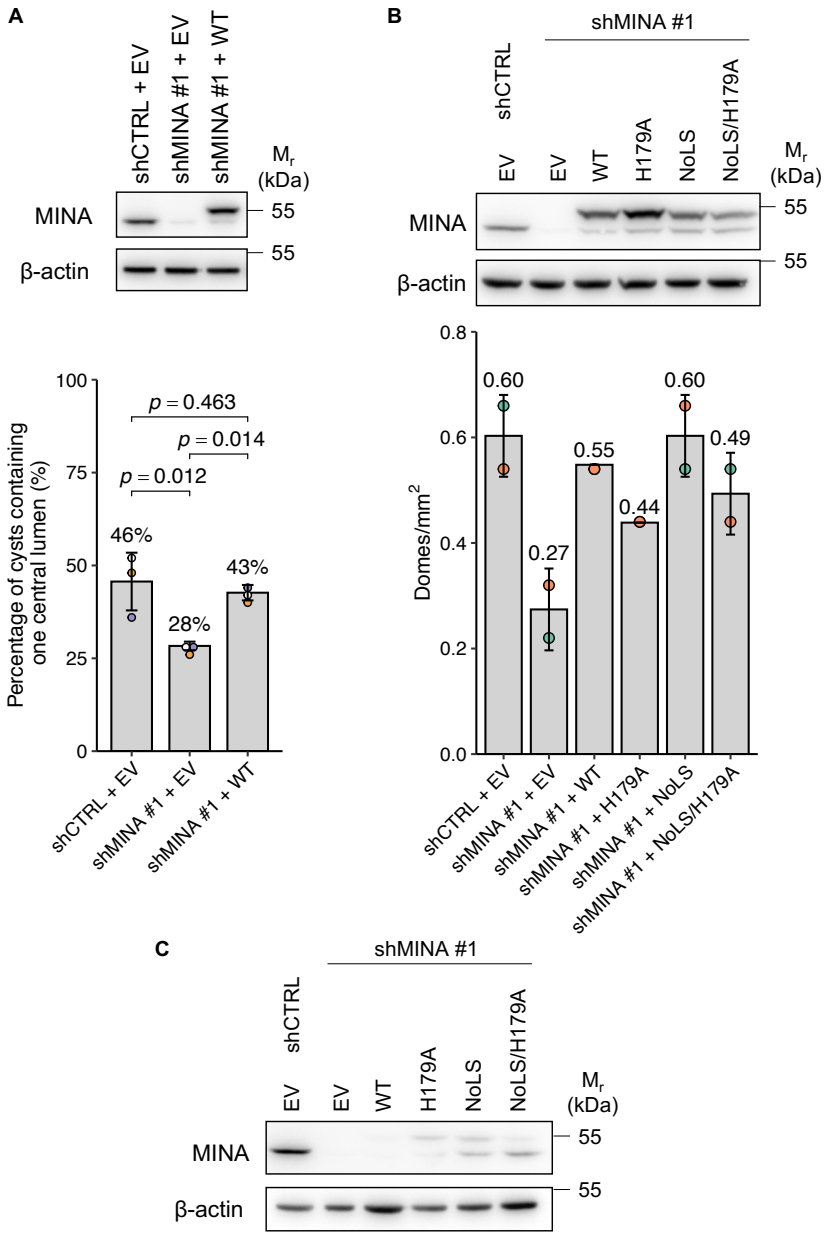


Figure 4.13: Re-expression of 3xFLAG-tagged MINA in doxycycline-inducible shRNA cells lines: dome and lumen formation assays following hygromycin selection. Caco-2 cells co-expressing either non-targeting control (shCTRL) or MINA-targeting (shMINA #1) shRNA and either an empty vector (EV) or the indicated 3xFLAG-MINA constructs were grown in 3D (A) or 2D (B,C). shRNA expression was induced with 1 µg/mL doxycycline (dox) for 72 hours before seeding. The culture medium was refreshed and fresh dox (0.5 µg/mL) was added every 72 hours. Cell extracts were immunoblotted for MINA (53 kDa). β-actin was used as loading control. (**A**) Bar graph shows the percentage of 3D spheroids containing one central lumen after 7 days in culture. Bars represent the average of 3 biological replicates. Statistical significance was determined using one-way ANOVA and p values were calculated using a post-hoc pairwise t test. P values were adjusted for multiple testing using the Benjamini-Hochberg method. (**B**) Bar graph showing the average number of domes per mm^2 after 5 days of culture. 30 random images were taken per condition per biological replicate using an Evos microscope equipped with a 10x objective. Bars represent the average of 2 biological replicates. (**A,B**) Dots represent replicate averages, colour-coded according to the replicate. Images were blinded prior to analysis. (**C**) Immunoblots showing that expression of 3xFLAG-MINA decreases after prolonged culturing (approximately 4 weeks). Cell extracts were collected 5 days after seeding.

The generation of a 'tuneable' depletion and reconstitution system for such studies proved technically challenging and our attempts were only partly successful. Initial efforts aimed at reconstituting MINA through transduction with cumate-inducible vectors in doxycycline-inducible shRNA cell lines were unsuccessful. We observed that this system was somewhat leaky, consistent with the observation made by others (Dr Norma Masson, Ratcliffe laboratory, University of Oxford), and more importantly, that it was not very inducible by cumate. We believe this might be, in part, a limitation of the Caco-2 cell line, as we observed increased levels of cumate-induced MINA when this approach was tested in HeLa cells (data not shown, experiment performed by Dr Regina Andrijes). Technical limitations of an alternative, constitutive system using a vector that contained a hygromycin resistance gene included persistent sensitivity to hygromycin B, rapid negative selection of MINA-overexpressing cells, and heterogeneity (particularly in 3D). Nonetheless, ultimately some preliminary positive results were obtained (discussed below). In the future, we intend to repeat these experiments using the constitutive expression model in order to finalise the existing datasets, but also to develop other potentially more stable models: in collaboration with Dr Regina Andrijes, we are in the process of deriving CRISPR-Cas9 knockouts for MINA and MPP6, which would provide a 'clean' stable background in which to restore expression with our existing and well-characterised doxycycline-inducible 3xFLAG-MINA constructs.

The effect of MINA depletion with respect to epithelial morphogenesis, cell polarity and cell growth was studied in two- and three-dimensional Caco-2 cell culture. We noted an impaired ability of MINA-depleted monolayers and spheroids to form domes or a central lumen, respectively. Apico-basal polarity was not apparently severely affected by MINA knockdown, as indicated by the asymmetrical distribution of cell polarity markers ZO-1 and E-cadherin (Figure 4.8A and B). Therefore, the observed phenotype may be the result of defective cell-cell adhesion or impaired barrier function. The phenotypes observed in MINA-depleted monolayers and spheroids are consistent with a range of reported defects: whereas dome formation and barrier function have historically been attributed to tight junction integrity (MacCallum et al., 2005; Sambuy

et al., 2005; Zihni et al., 2016), we also observed cell flattening in 2D, indicative of a reduced lateral membrane (Laprise et al., 2009). It is becoming increasingly evident, however, that cell polarity complexes should not be viewed as separate complexes with distinctive functions (Campbell et al., 2017). For example, the Scribble polarity complex and E-cadherin are required for the timely formation of tight junctions (Qin et al., 2005). To begin to clarify the mechanism(s) by which MINA contributes to epithelial morphogenesis, it will be interesting to investigate if, and which of, the observations made following MINA depletion are phenocopied by MPP6. We will begin to explore this in the next Chapter.

MINA depletion in 3D spheroids also caused a delay in cell proliferation, which may be consistent with our hypothesis that in the early, proliferative stage of epithelial morphogenesis, nucleolar MINA might support cell growth. However, if this were the case, we would also expect to see reduced proliferation in 2D. Therefore, we suspect that other mechanisms might be responsible for the reduced growth in 3D. Interestingly, some polarity proteins have reported tumour suppressing as well as promoting roles. One example of this is Par3: loss of Par3 in a mouse skin cancer model was previously associated with mislocalised Ras and disrupted Ras signalling, resulting in a reduction in cell growth (Iden et al., 2012). To confirm whether the observed growth defect is associated with extra-nucleolar functions of MINA, it will be of interest to analyse whether re-expression of exogenous MINA defective in nucleolar localisation (NoLS) is able to rescue this phenotype.

Despite the limitations with the rescue approaches described above, our initial results suggest that the knockdown phenotypes are likely on target, and independent of nucleolar localisation of MINA. Moreover, our preliminary results suggest that the observed phenotypes might be partially dependent on the catalytic activity of MINA. It is tempting to speculate that, in addition to MPP6, MINA possibly regulates epithelial morphogenesis through other proteins. Perhaps consistent with this, several other polarity proteins (including MPP7, DLG3 and LLGL1) were identified as interacting with MINA in Chapter 3 (Table 3.1 and Figure 3.2). Although these interactions have

not yet been validated, this would be of interest and it might be important to do so, particularly given the observations made in this chapter.

Polarised epithelia are fundamental for development and organ function. On a cellular level, cell polarity complexes 'read' the environment and initiate signalling cascades that ultimately control cell proliferation, differentiation, apoptosis, motility and metabolism (Halaoui and McCaffrey, 2015). A common feature of epithelial cancers is the loss of apico-basal polarity, resulting in loss of differentiation, uncontrolled growth and increased motility (Halaoui and McCaffrey, 2015; Dongre and Weinberg, 2019). Interestingly, loss of MINA expression was previously reported to induce epithelial-mesenchymal transition (EMT) in the non-small cell lung cancer cell line A549 (Geng et al., 2017). In this study, upregulation of mesenchymal markers (N-cadherin, vimentin), and downregulation of epithelial markers (including E-cadherin, claudin-1, integrin β1/4) was noted following MINA depletion. Furthermore, MINA depletion was associated with increased invasion/migration potential, whereas overexpression decreased the number of migrating and invading cells. Conversely, overexpression of MINA increased the expression of epithelial markers E-cadherin, claudin-1, integrin β1/4 and ZO-1 in both A549 and human umbilical vein endothelial cells (HUVECs). Although we have not yet carefully addressed whether MINA depletion in Caco-2 initiates EMT, we did not observe reduced expression of E-cadherin or ZO-1 following MINA knockdown in 2D or 3D cultures. Differences like these may highlight the context-dependency of MINA's function. As shown in Chapter 2, MINA is highly enriched in the nucleoli of A549 cells (Figure 2.1). We could speculate that MINA knockdown in cells that already have most MINA sequestered in the nucleoli, may more efficiently deplete any remaining protein from the nucleoplasm, and therefore induce a more severe phenotype. The concept of the nucleoli and ribosome biogenesis acting as a 'sink' for MINA will be further addressed in the Final Discussion (Ch.6).

In light of the results described in this chapter and the discussion presented above, we hypothesise that at least part of the role of MINA in epithelial morphogenesis might be driven by MPP6 regulation. If this is true, we propose that MPP6 loss-of-function

might cause similar effects on epithelial morphogenesis to those seen by MINA, and that MPP6 mutants with altered MINA interaction or localisation might be unable to rescue the phenotypes observed. In the next Chapter we begin to test these hypotheses.

Chapter 5: Role of MPP6 and the MPP6:MINA complex in epithelial morphogenesis

5.1 Introduction

In the previous Chapter, we described a series of observations related to epithelial morphogenesis, cell polarity and proliferation of Caco-2 cells in 2D and 3D following MINA depletion. Although our observations are similar to those made by others following depletion of proteins with recognised functions in membrane biology or polarity (Laprise et al., 2009; Durgan et al., 2011), the mechanisms are yet to be elucidated. In light of the results of our proteomic screen, that identified MPP6 as an activity-dependent MINA interactor, we hypothesise that this mechanism might involve MPP6, and that an MPP6 loss-of-function model may phenocopy the observations made following MINA knockdown.

In Chapter 3, we characterised the interaction between MINA and MPP6 biochemically. The region of interaction was narrowed down to the N-terminal end of the SH3-GUK interdomain of MPP6. In other MAGUKs, this region has been shown to mediate protein:protein interactions (Marfatia et al., 1995) and deletion of the HOOK domain (which is part of the SH3-GUK interdomain) in MAGUKs DLG1, DLG4 and

CARMA1 was sufficient to induce polyubiquitination (Moreno-García et al., 2010). Furthermore, the HOOK domain of the MPP6 *Drosophila* homologue, Varicose, has been shown to be essential for membrane recruitment (Wu et al., 2007). Interestingly, we found that alanine substitution of single amino acids in a five amino acid region (AAs 295-299) within the HOOK domain of MPP6 was sufficient to interfere with MINA binding. In this chapter, we employ one of these MINA-binding mutants to begin to explore the potential functional consequences of the MINA:MPP6 complex.

5.2 Results

5.2.1 Effect of MPP6 depletion on Caco-2 spheroid development

In order to investigate the effect of MPP6 depletion on epithelial morphogenesis and cell polarity, pZIP-TRE3G-ZsGreen-Puro lentiviral vectors containing three independent shRNA sequences against MPP6 were obtained from transOMIC and stable doxycycline-inducible MPP6 knockdown Caco-2 cell lines were generated. Following puromycin selection of successfully transduced cells, a doxycycline time course was performed to assess the dynamics of MPP6 knockdown. Cells were harvested at 24, 48 and 72 hours post addition of doxycycline. Concurrently, cells were fixed to analyse expression of the green fluorescent protein (GFP) reporter gene. Albeit heterogeneously, the vast majority of cells showed expression of GFP 24 hours after doxycycline was added (Figure 5.1A). However, a slight delay in the reduction of MPP6 protein expression was noted and satisfactory knockdown levels were observed at 48-72 hours post expression of all three MPP6 shRNAs (Figure 5.1B).

Subsequently, the effects of MPP6 depletion on spheroid growth and lumen formation were investigated. Interestingly, the effects observed in MINA-depleted spheroids were phenocopied by MPP6 knockdown. Specifically, depletion of MPP6 in 3D, as validated in Figure 5.2A, induced a reduction in the percentage of spheroids with a

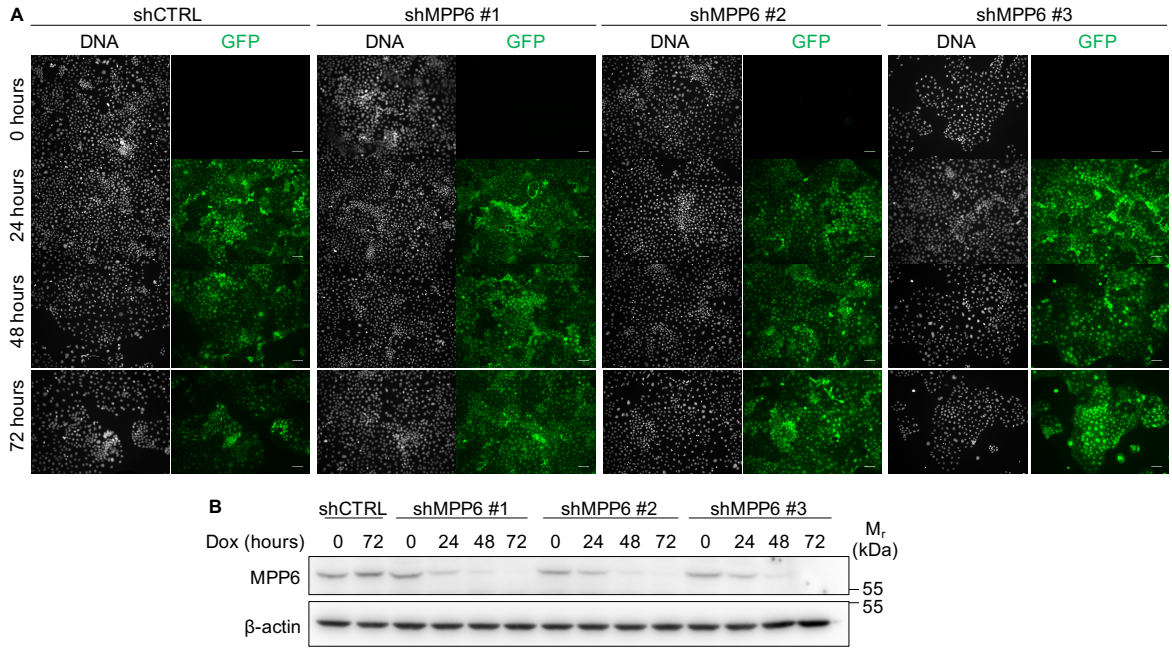


Figure 5.1: Characterisation of stable Caco-2 cell lines expressing doxycycline-inducible MPP6-targeting shRNA sequences. (**A**) Expression of the indicated shRNA sequences was induced with 1 µg/mL doxycycline for 0, 24, 48 or 72 hours and expression of green fluorescent protein (GFP) was analysed. Nuclei were visualised with DAPI (grey). Scale bars represent 100 µm. Single-plane images were acquired using a Leica DM6000 epifluorescence microscope and LAS X software. (**B**) Cell extracts from (A) were immunoblotted for MPP6 (61 kDa, GeneTex antibody) to validate knockdown of MPP6 at protein level. β-actin (42 kDa) was used as loading control.

lumen, as well as spheroid diameter (Figures 5.2C and D, respectively). In addition, like MINA, MPP6 knockdown induced a cell growth delay (Figure 5.2E). It should be noted that, although data from only one biological replicate is shown in Figure 3.7B-D, repeats of this experiment were performed by Dr Regina Andrijes with similar results.

Similar to MINA depletion, no major alterations in expression (Figure 5.3A) or localisation (Figure 5.3B) of the tight junction marker ZO-1 and adherens junction markers β-catenin and E-cadherin were observed following shRNA-mediated MPP6 depletion. Nonetheless, ZO-1 appeared more diffusely distributed at the apical membrane (Figure 5.3B, right panel), analogous to MINA-depleted spheroids (Figure 4.8). Moreover, although β-catenin was still enriched at the lateral membrane in MPP6-depleted cells, it also appeared to be diffusely distributed in the cytoplasm and nuclei (Figure 5.3B, left panel).

5.2.2 Effect of MINA on MPP6 expression and localisation

In order to begin to explore the functional consequences of the MINA:MPP6 complex, cell lines constitutively expressing C-terminally HA-tagged wild-type (WT) MPP6 or MPP6 defective in MINA-binding (C298A, as identified in Chapter 3) were generated. Specifically, the MPP6 sequences were cloned into the pIHZ lentiviral vector described in section 4.2.3 and transduced into Caco-2 cells. Following selection of successfully transduced cells with hygromycin, the expression of both constructs was assessed. Interestingly, MPP6-HA C298A expression was apparently lower than wild-type MPP6 (Figure 5.4A). Based on this observation, the effect of MINA depletion on endogenous MPP6 expression in Caco-2 was analysed. In 2D, like MPP6 C298A, we noted decreased MPP6 expression (Figure 5.4B). While this effect appeared inconsistent between shMINA #1 and #3, this is possibly a consequence of higher levels of residual MINA present in shMINA #1-expressing cells, as we have seen before (e.g. Figure 4.5D), but further research is required to confirm whether this is indeed the case, or whether the observed effect is off-target. To assess whether the C298A mutant

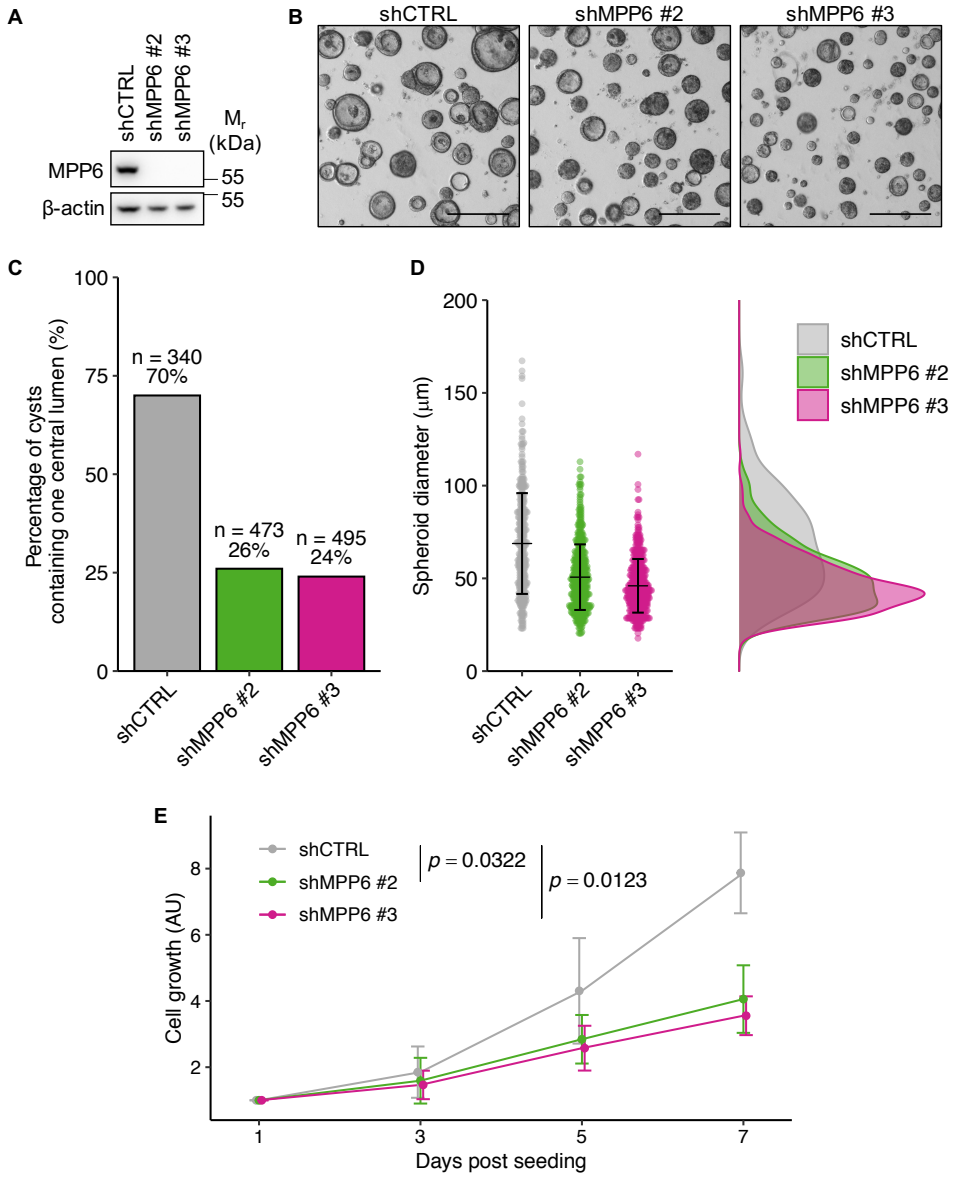


Figure 5.2: Effect of MPP6 depletion on Caco-2 spheroid growth and lumen formation. Stable Caco-2 cells were treated for 72 hours with 1 µg/mL doxycycline to induce expression of non-targeting control (shCTRL) or MPP6-targeting shRNA (shMPP6 #2/#3) and subsequently seeded in 3D to analyse lumen formation (C), spheroid diameter (D) and cell proliferation (E). Fresh doxycycline was added every 72 hours. (**A**) Cell extracts from (B-D), grown for 7 days, were immunoblotted for MPP6 (61 kDa, Atlas Antibodies) to confirm MPP6 knockdown. β-actin (42 kDa) was used as loading control. (**B**) Representative phase-contrast images of 7 day old Caco-2 spheroids expressing the indicated shRNAs. Scale bars represent 200 µm. Images were acquired using an EVOS microscope equipped with a 10x objective. (**C,D**) Quantification of (B). At least 10 random images were taken per condition and analysed manually using Fiji (ImageJ). Images were blinded prior to analysis. (**C**) Percentage of spheroids containing one central lumen after 7 days in culture. Data presented are of n = 1 experiment. (**D**) Spheroid diameter after 7 days in culture. Values represent mean + SD from n = 1 experiment. (**E**) Cell growth of 3D spheroids was analysed using a CellTiter-Glo® Luminescent Cell Viability Assay kit after 3, 5 and 7 days in culture. Presented values are relative to day 1 and represent mean + SD of n = 4 biological replicates. Statistical significance was determined using one-way ANOVA and p values were calculated using Tukey's test. AU = arbitrary unit. This experiment was performed in collaboration with Dr Regina Andrijes, who provided data for 3 of 4 replicates.

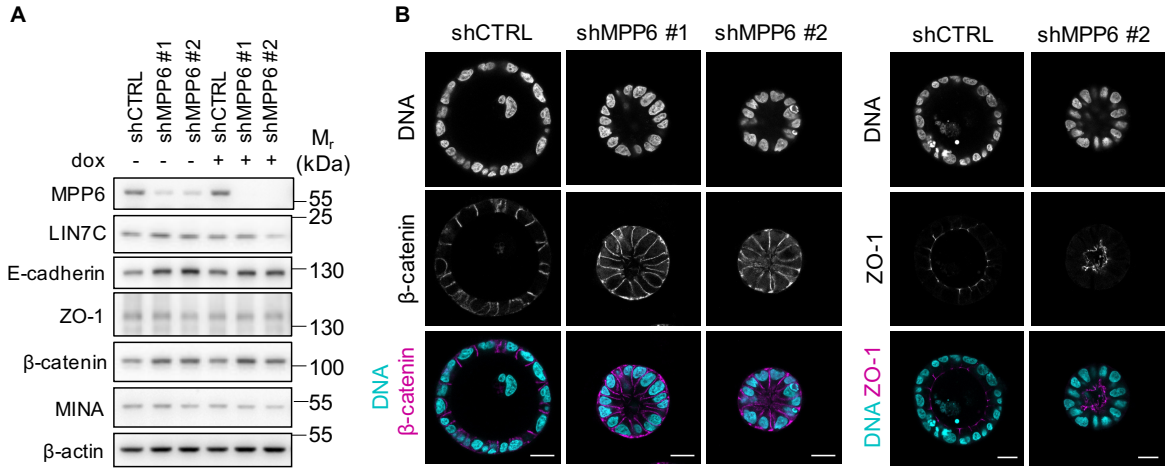


Figure 5.3: Expression and localisation of cell junction proteins in MPP6-depleted Caco-2 cells. (**A**) Cell extracts from the indicated Caco-2 cell lines grown in 2D for 7 days were immunoblotted for MPP6 (61 kDa, Atlas Antibodies), LIN7C (22 kDa), E-cadherin (97 kDa), Zona occudens 1 (ZO-1, 195 kDa), β-catenin (85 kDa) and MINA (53 kDa). β-actin (42 kDa) was used as loading control. (**B**) Caco-2 cells expressing control (shCTRL) or MPP6-targeting (shMPP6 #1/#2) shRNAs, grown for 7 days in Matrigel-coated chamber slides, were fixed with PFA supplemented with sucrose and stained for β-catenin (left panel, magenta) and ZO-1 (right panel, magenta). Scale bars represent 20 µm. Nuclei were visualised with DAPI (cyan). Single-plane images shown were acquired using a Zeiss LSM 880 confocal system equipped with a 40x C-Apochromat 1.2 W Korr M27 objective and ZEN black software. (**A-B**) Unless otherwise indicated, expression of shRNA was induced with 1 µg/mL doxycycline (dox). The culture medium was refreshed and fresh doxycycline was added every 72 hours.

is potentially unstable and degraded by the proteasome, MPP6 wild-type or C298A-expressing cells were treated with proteasome inhibitor MG132. However, although a slight increase in expression of MPP6 C298A was noted in response to MG132, a similar increase in expression of wild-type MPP6 was observed (Figure 5.4C), suggesting that the decrease caused by the mutation is unlikely to be specifically due to increased proteasomal turnover.

Next, we aimed to investigate the subcellular localisation of MPP6^{C298A}. For this purpose, we first assessed the localisation of wild-type exogenous MPP6 in more detail by indirect immunofluorescence. Based on a previous publication reporting basolateral localisation of MPP6 in the mouse intestine (Kamijo et al., 2016), consecutive images were taken from the basal to the apical side of a monolayer, and the MPP6-HA signal was compared to ZO-1 which is known to localise apically at tight junctions (Fanning et al., 1998). As shown in Figure 5.5A, although some overlap with ZO-1 was noted, MPP6-HA localised more broadly along the apical-basal axis, indicating lateral membrane localisation in a confluent monolayer. Similarly, in 3D, lateral membrane localisation of MPP6-HA was observed (Figure 5.5B). Interestingly, MPP6 localises to sites of cell-cell contacts in 3D as early as the two-cell stage (Figure 5.5). Next, the localisation of wild-type MPP6 and MPP6^{C298A} was compared in 2D and 3D. Interestingly, in contrast to wild-type MPP6, no membrane localisation of MPP6^{C298A} was noted. Instead, MPP6^{C298A} was found in the nucleus and/or cytoplasm (Figure 5.6). Moreover, we also noticed that none of the MPP6^{C298A}-expressing spheroids had successfully formed a lumen and they appeared smaller. Overall, these preliminary phenotypic observations are not inconsistent with those we observed in Chapter 4 following MINA loss of function.

5.3 Discussion

In this Chapter, we presented preliminary data suggesting that MPP6 depletion in Caco-2 cells phenocopies the effects on spheroid growth and lumen formation that

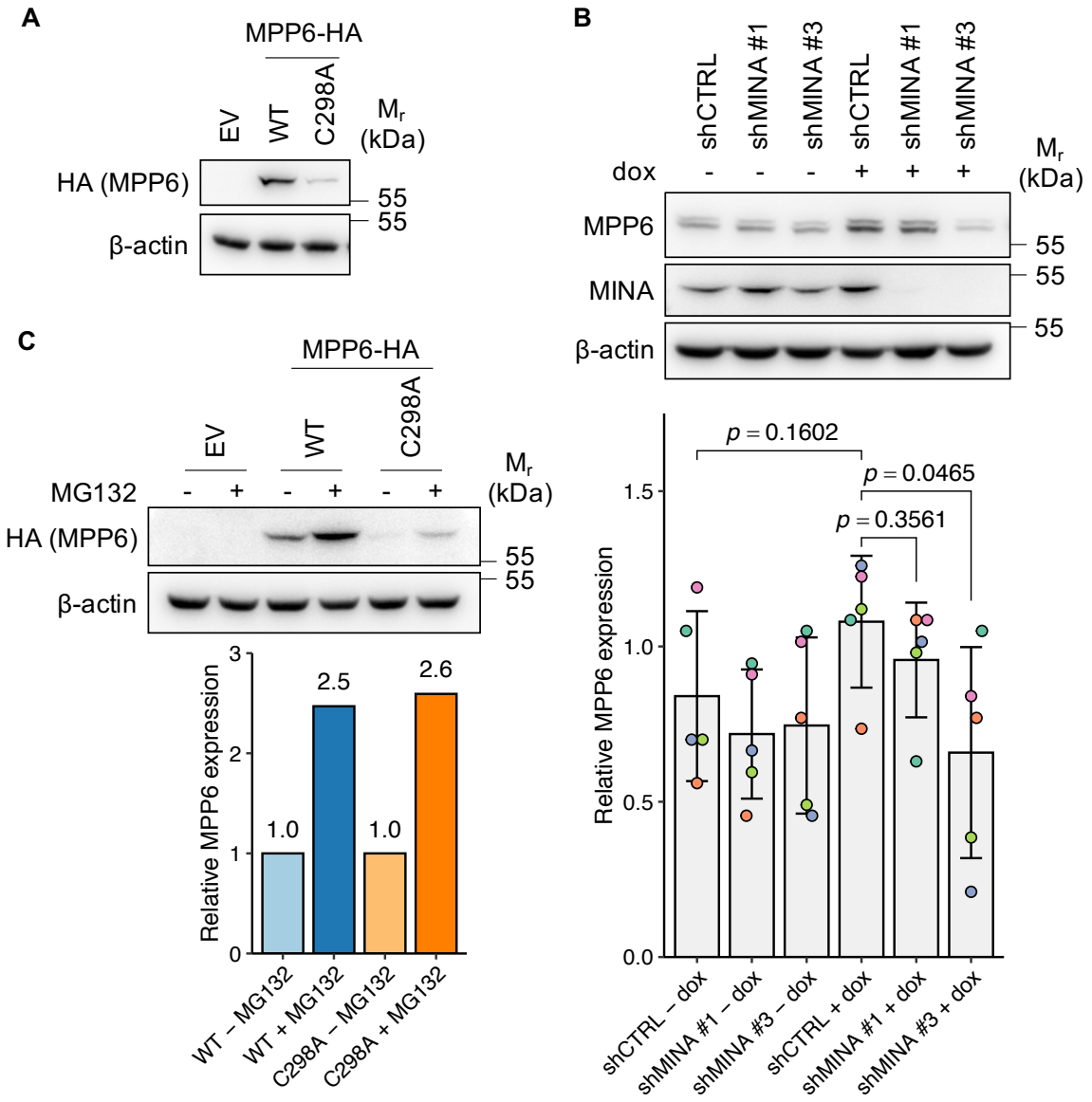


Figure 5.4: Effect of mutation or MINA depletion on MPP6 expression. (**A**) Cell extracts from stable Caco-2 cells constitutively expressing an empty vector (EV), wild-type (WT) MPP6-HA or MPP6-HA C298A were immunoblotted for HA (MPP6, 61 kDa). (**B**) Cell extracts from Caco-2 cells expressing control shRNA (shCTRL) or MINA-targeting shRNA (shMINA #1 and #3) that were either untreated or treated with 1 µg/mL doxycycline for 7 days to induce expression of the indicated shRNAs were immunoblotted for MPP6 (61 kDa, Atlas Antibodies) and MINA (53 kDa). Bar graph represents the average MPP6 expression levels (quantified using Fiji) of 5 independent biological replicates. Each replicate is colour-coded. (**C**) Caco-2 cells constitutively expressing an empty vector (EV), wild-type (WT) MPP6-HA or MPP6-HA C298A were either untreated (-) or treated with 10 µM MG132 (+) for 4 hours and cell extracts were immunoblotted for HA (MPP6, 61 kDa, top panel). Protein expression levels were quantified using Fiji (bottom panel). The increase in expression following MG132 treatment, relative to the untreated control is presented in the bar graph. (**A-C**) β-actin (42 kDa) was used as loading control.

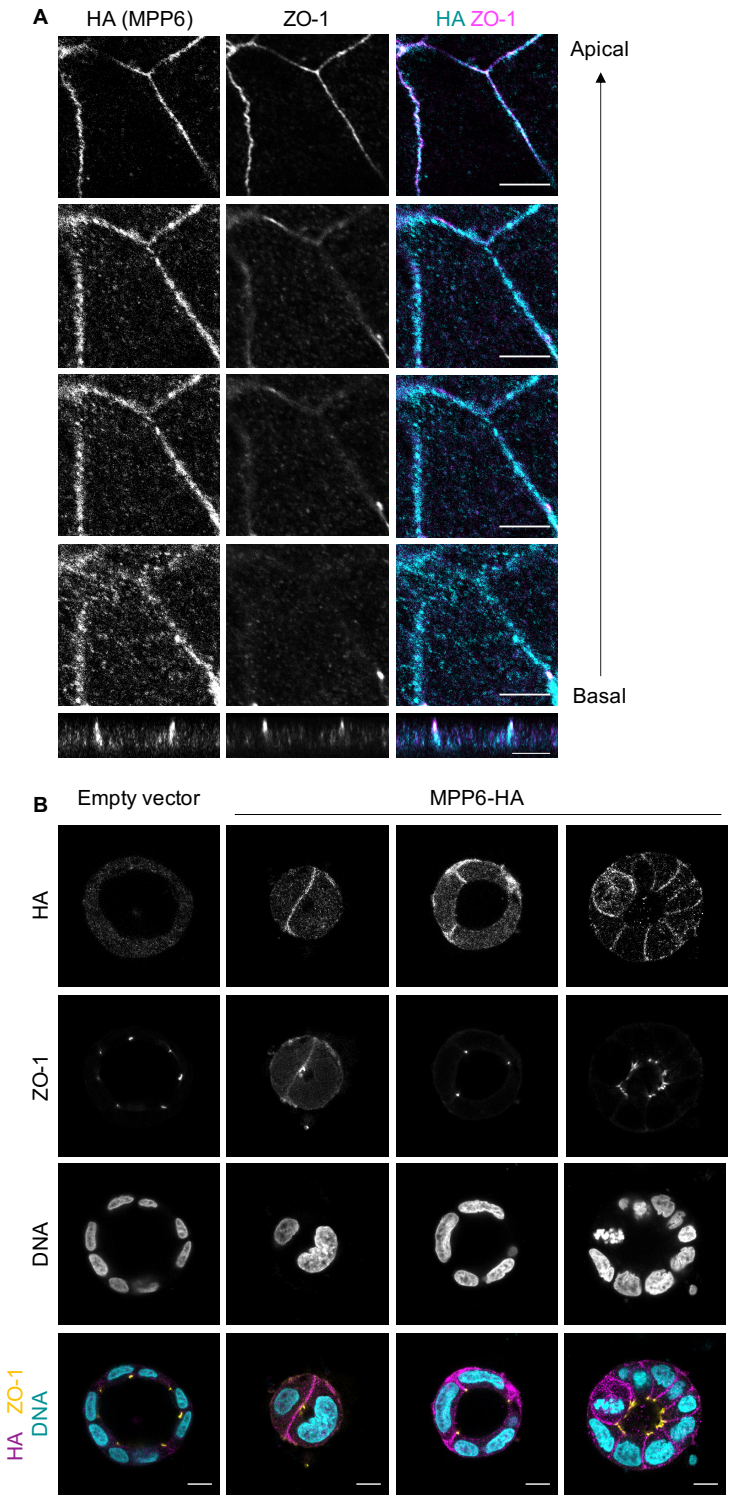


Figure 5.5: Localisation of MPP6-HA in Caco-2 monolayers and spheroids. Caco-2 cells constitutively expressing wild-type MPP6-HA were grown in 2D on glass coverslips as a monolayer (A) or in 3D on matrigel-coated chamber slides (B). (**A**) MPP6-HA localises to the lateral membrane in 2D. Once grown to a confluent monolayer, cells were fixed and stained for HA (MPP6, cyan) and ZO-1 (magenta). Consecutive images were taken from the basal to the apical side and presented as an orthogonal view (rectangular bottom panels). (**B**) MPP6-HA localises to areas of cell-cell contact in 3D. Single cells were grown to spheroids for 7 days, fixed and stained for HA (MPP6, magenta) and tight junction marker ZO-1 (yellow). Nuclei were visualised with DAPI (cyan). (**A,B**) Scale bars represent 10 µm. Images were acquired using a Zeiss LSM 880 confocal system equipped with a 40x C-Apochromat 1.2 W Korr M27 objective and ZEN black software.

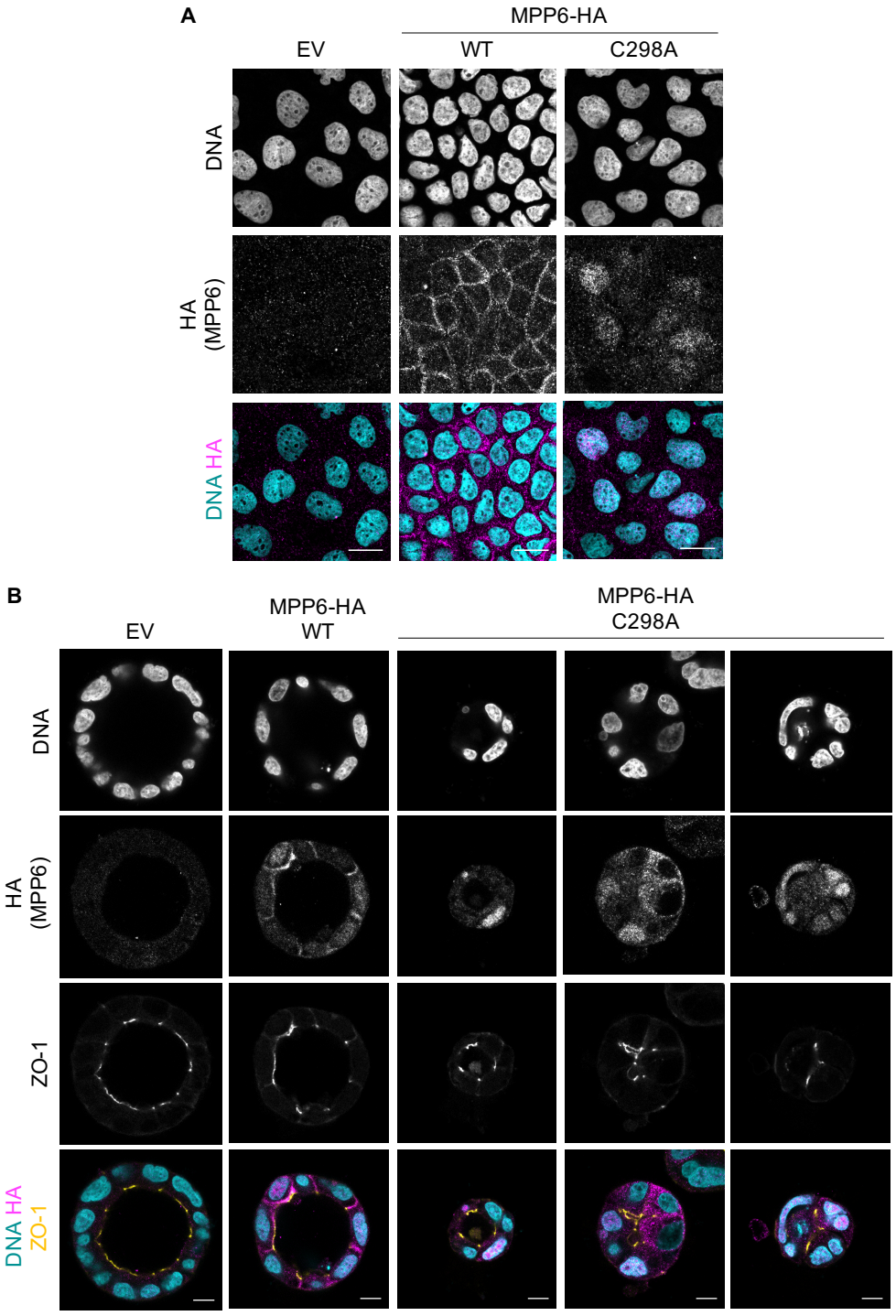


Figure 5.6: Localisation of MPP6-HA C298A in Caco-2 monolayers and spheroids. Caco-2 cells constitutively expressing wild-type MPP6-HA or MPP6-HA C298A were grown in 2D on glass coverslips as a monolayer (A) or in 3D on matrigel-coated chamber slides (B). (**A**) Nuclear localisation of MPP6-HA C298A in 2D. Once grown to a confluent monolayer, cells were fixed and stained for HA (MPP6, cyan). Scale bars represent 20 µm. (**B**) MPP6-HA C298A fails to concentrate at the cell membrane in 3D. Single cells were grown to spheroids for 7 days, fixed and stained for HA (MPP6, magenta) and tight junction marker ZO-1 (yellow). Scale bars represent 10 µm. (**A,B**) Nuclei were visualised with DAPI (cyan). Single-plane images shown were acquired using a Zeiss LSM 880 confocal system equipped with a 40x C-Apochromat 1.2 W Korr M27 objective and ZEN black software.

were described in Chapter 4 following MINA knockdown. Although this line of inquiry requires further work to explore just how closely these phenotypes align, and the mechanisms involved, the observations might support MINA and MPP6 having a common function in a shared pathway.

Although depletion of MPP6 or MINA in Caco-2 cells negatively affects lumen formation, we did not observe significant mislocalisation of tight or adherens junction markers. This may not be surprising as similar observations were made previously, including in MPP7, Scribble and Par3-depleted cells (Stucke et al., 2007; Qin et al., 2005; Xue et al., 2013). As discussed by Stucke and colleagues, this may suggest that these proteins are not primarily involved in the assembly of cell junctions, but rather in ensuring and maintaining functionality. Future efforts will aim to investigate this possibility in more detail. Nonetheless, defective junction functionality may contribute to a malignant phenotype (Xue et al., 2013). Alternatively, the absence of severe alterations in expression and localisation of polarity markers may be the result of redundancy between MPP6 and other MPPs. Such functional compensation has been associated with several polarity proteins. For instance, increased expression of LIN7C has been reported in LIN7A/B knockout mice (Misawa et al., 2001). Moreover, whereas single knockouts of LIN7A, LIN7B or LIN7C produce live and fertile mice, triple knockouts are perinatally lethal (Olsen et al., 2005). Furthermore, even E-cadherin was shown to be dispensable for the maintenance of cell polarity after initial junctional formation, possibly due to compensation by other polarity proteins (Capaldo and Macara, 2007). Consistent with this, significant overlap in binding partners exists between MPPs (reviewed in Chytła et al., 2020).

The observed effects of MPP6 depletion on Caco-2 spheroid formation may be consistent with the reported function of the *Drosophila* homologue of MPP6, Varicose (vari). Vari is required for assembly and function of septate junctions in epithelial cells (Wu et al., 2007; Moyer and Jacobs, 2008). Septate junctions are thought to be the functional equivalent of vertebrate tight junctions, although several homologues of septate junction components in fact localise to the basolateral membrane in vertebrates

(Wu and Beitel, 2004). Whereas Vari was not essential for the asymmetric distribution of key cell polarity markers, including DPatJ (PATJ) and DE-cadherin (E-cadherin), *vari* mutation caused barrier defects, leading the authors to conclude that Vari is required for septate junction formation and cell-cell adhesion, but not for polarity (Wu et al., 2007). Phenotypically, drosophila *vari* mutants show defects in tracheal tube formation (Beitel and Krasnow, 2000; Wu et al., 2007).

A first hint at a potential functional consequence of the association between MINA and MPP6 came from the observation that MINA knockdown possibly affects MPP6 expression (Figure 5.4B). Whilst the observed reduction may be an indirect, transcriptional effect, it could be direct and regulated at the post-translational level. In support of the latter, reduced expression of a MINA-binding mutant, MPP6^{C298A}, was noted in stable Caco-2 cell lines (Figure 5.4A). Although this reduced expression was not seen when MPP6^{C298A} was transiently overexpressed in HEK293T (Figure 3.21), there are significant differences in the methodologies (i.e. transient versus stable expression) as well as the cell types, that could be responsible. The lack of effect of the C298A mutation on MPP6 expression in HEK293Ts is in some ways reassuring, as it might suggest that the C>A mutation is unlikely to induce major changes in protein folding that would lead to decreased stability independent of MINA. However, further work is required to investigate whether the reduced expression of MPP6^{C298A} in Caco-2 cells is the result of increased degradation/protein turnover. Treatment with cycloheximide or a pulse-chase experiment could clarify whether this is the case. Our results suggest that the decreased expression was not proteasome-dependent (Figure 5.4C), but other proteolytic pathways, such as lysosomal degradation (Shen et al., 2008), could be involved. If true, it would be of interest to clarify the mechanism by which MINA regulates MPP6 expression. The most obvious hypothesis would be that this is the consequence of a hydroxylation event, or an additional post-translational modification that follows hydroxylation. This would be analogous to the oxygen sensing pathway, where prolyl hydroxylation of HIF results in VHL-mediated degradation (Maxwell et al., 1999; Ohh et al., 2000; Ivan et al., 2001; Jaakkola et al., 2001). Alternatively, the effect of MINA

on MPP6 may be structural in nature. For example, a structural change could affect protein-protein interactions, which is of interest given that the PDZ-SH3-GUK tandem can form a supramodule that is known to mediate protein interactions (Ye et al., 2018). Furthermore, it is not unprecedented that the stability of polarity proteins depends on the formation of complexes with other polarity proteins (Ahmed and Macara, 2016). For instance, pulse-chase experiments indicated reduced stability of MPP5 in the absence of LIN7 binding (Straight et al., 2006). Hydroxylation-mediated regulation of protein-protein interactions also has a precedent. As mentioned in the Chapter 1, hydroxylation of HIF Asn-803 by FIH prevents association with co-activator p300 (Lando et al., 2002; Hewitson et al., 2002). Similarly, FIH-mediated hydroxylation of ankyrinR reduces its interaction with the cytoplasmic domain of band 3 (CDB3; Yang et al., 2011b).

To explore the possibility of MINA regulating the interaction between MPP6 and its binding partners further, it would be of interest to study differences in interaction profiles between wild-type MPP6 and MPP6^{C298A}, as well as to compare MPP6 interactions in control versus MINA-depleted cells. Reported interactors of MPP6 in epithelial cells include LIN7 (Kamberov et al., 2000; Tseng et al., 2001), CASK (Kamijo et al., 2016) and CADM1 (Shingai et al., 2003). In neuronal cells, MPP6 was also reported to interact with 4.1G (Terada et al., 2012), CADM1/3 (Kakunaga et al., 2005) and CASPR2 (Horresh et al., 2008). Interestingly, membrane localisation of MPP6 was previously reported to depend on the interaction with CADM1, and binding of MPP6 to CADM1 was shown to be mediated through the PDZ domain of MPP6 (Shingai et al., 2003). Given our data, suggesting that the SH3-GUK interdomain is also required for membrane recruitment, it is possible that additional interactions may also be required for membrane recruitment and/or retention of MPP6. A multiple interaction membrane recruitment mechanism has been reported for other MAGUKs, including MPP7 and DLG1 (Stucke et al., 2007; Thomas et al., 2000). Interestingly, both MPP7 and DLG1 were identified in our proteomic screen as MINA interactors (Chapter 3). Alternatively, we could speculate that CADM1 binding and membrane localisation of

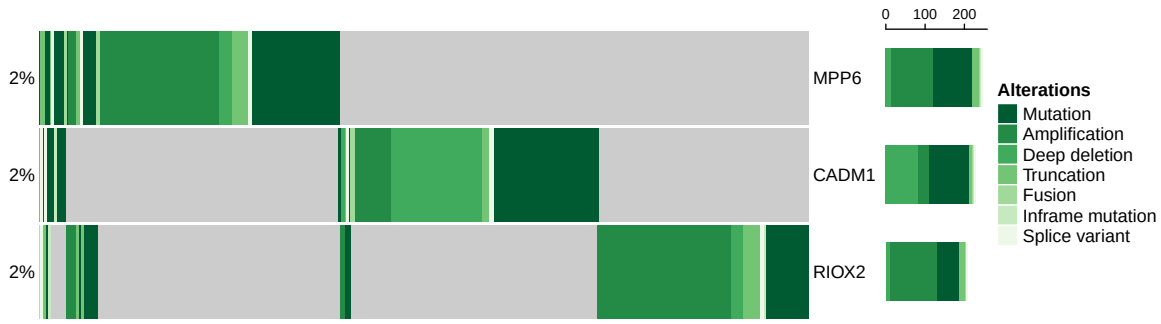


Figure 5.7: OncoPrint analysis of MPP6, CADM1 and MINA mutations across cancer types. Oncoprint representing alterations in MPP6, CADM1 and MINA (RIOX2) genes identified in TCGA studies. Samples that did not contain any mutations in MPP6, MINA or CADM1 are not shown. Data source = cBioportal (https://www.cbioportal.org). OncoPrint was generated using the ComplexHeatmap R package.

MPP6 is dependent on the formation of a PDZ-SH3-GUK supramodule. The affinity with which Crumbs binds MPP5$^{\text{PDZ-SH3-GUK}}$ was previously reported to be approximately 100 times stronger than binding to the isolated MPP5$^{\text{PDZ}}$ domain (Li et al., 2014). It would be of interest therefore to test whether the MPP6-CADM1 interaction depends on C298, as, like MINA and MPP6, CADM1 is a potential tumour suppressor (You et al., 2014; Zeng et al., 2016; Vallath et al., 2016; Zhang et al., 2016; Qian et al., 2017; Saito et al., 2018; Kanke et al., 2019; Ito et al., 2019; Si et al., 2020). Therefore, one might hypothesise that deletion or mutation of CADM1 in cancer may prevent membrane retention of MPP6, possibly triggering its nuclear translocation. Interestingly, oncoprint analysis of the TCGA dataset indicates that MINA, MPP6 and CADM1 mutations in cancer are mutually exclusive (Figure 5.7), suggesting that they might act in a common pathway.

In Chapter 3, we discussed the possibility of MPP6 having a role in the nucleus, based on the observation of differential localisation in subconfluent and confluent cell culture conditions. Furthermore, we hypothesised that nuclear MPP6 could be oncogenic, as no membranous MPP6 can be observed in HeLa cells, and a recurrent cancer mutant (K306Fs) exclusively resides in the nucleus. In this chapter, we expanded the characterisation of MPP6 localisation in 3D and noted nuclear localisation, to some extent, of wild-type MPP6-HA in Caco-2 spheroids (Figure 5.6B). Moreover, im-

munofluorescence studies of the MINA binding mutant MPP6^{C298A} revealed that this mutant does not localise to the membrane, but is instead enriched in the nucleus and/or cytoplasm (Figure 5.6). In light of this observation, we speculate that extra-nucleolar MINA could be involved in promoting the membrane localisation of MPP6, thus suppressing its nuclear localisation and function. It will be interesting to further explore the effect of MINA depletion on MPP6 localisation in the future.

Chapter 6: Final discussion

In this thesis, we set out to expand our understanding of the functions and regulation of the 2OG oxygenase MINA. Based on the available literature, we hypothesised that MINA might exert roles that are independent of its role in ribosome biogenesis, and that these might be related to extra-nucleolar localisation. We show that active rRNA transcription is sufficient to retain MINA in the nucleolus, and furthermore, that MINA is apparently released when the translation or proliferation rate decreases. We identified MPP6 as an extra-nucleolar candidate substrate, and characterised the function of MINA and MPP6 in epithelial morphogenesis using loss-of-function and reconstitution models. In this Chapter, we attempt to discuss the implications of the findings in the wider context and consider the future directions.

6.1 MPP6 as a candidate MINA substrate

In Chapter 3, MPP6 was identified as a novel MINA interactor, the binding profile of which bore a striking resemblance to that of the substrate RPL27A, including effects of MINA mutation and response to 2OG oxygenase inhibitors. Furthermore, the phenotypes observed following MINA depletion were rescued by extra-nucleolar MINA in a partially activity-dependent manner (Chapter 4). Taken together, these data might be supportive of a substrate-like role for MPP6. Indeed, in the first MPP6 mass spectrometry experiment presented in Chapter 3, low level oxidation was identified only on W291, with high confidence and no evidence of other artificial oxidations. Unfortu-

nately however, subsequent experiments were unable to confidently assign an abundant MINA-dependent oxidation of MPP6. Perhaps consistent with this, the region identified as necessary and sufficient for activity-dependent MINA binding, including the residues in proximity of a candidate hydroxylation site (W291), did not resemble the amino acids surrounding H39 in RPL27A. Overall therefore, further studies are required to elucidate whether or not MPP6 is in fact a substrate. A starting point for such studies could be to test whether MINA is able to hydroxylate residues other than histidine. This could be done by replacing H39 in RPL27A with other residues, including tryptophan and the residues identified as required for MINA binding (glycine, proline, phenylalanine and cysteine; Chapter 3). If such studies reveal that MINA accepts other AAs as substrates, in a similar fashion to FIH (Yang et al., 2011a; Choi et al., 2020), it might help direct future studies on MPP6. For example, the possibilities that hydroxylated MPP6 is not present in the cell anymore (i.e. the product is degraded), or that the modification is masked, for instance by subsequent modifications, should be reconsidered.

If MPP6 is not a true substrate of MINA, how might we rationalise its unique activity-dependent binding profile and the findings from our functional studies? Is it possible that the observed MPP6 W291 oxidation is simply an indication that this residue is located within or in close proximity to the oxidising environment of the catalytic site? The observed oxidation could be an artefact of the environment, rather than a classical hydroxylation event. Perhaps consistent with this, we have observed that MINA's catalytic residues can become auto-oxidised (Dr Mathew Coleman, personal communication). If this is hypothesis is correct, it would place MPP6 binding directly at the MINA catalytic pocket, but without a PTM resulting from the interaction. This scenario is analogous to 'pseudosubstrates', which are well-characterised in other fields such as kinases or ubiquitin ligases (House and Kemp, 1987; Miller et al., 2006), but are not yet described for 2OG oxygenases.

Regardless of whether or not MPP6 is a genuine substrate, our data would suggest that the interaction between MINA and MPP6 is probably physiologically relevant,

possibly regulated by the availability of cofactors and/or the catalytic pocket, and that MINA may act as a tumour suppressor at least partly through its interaction with MPP6 (further discussed below).

6.2 Could defective MINA activity contribute to altered epithelial morphogenesis in response to changes in nutrient availability or metabolism?

The activity of some 2OG oxygenases is regulated by the availability of their cofactors 2-oxoglutarate, iron and oxygen. Therefore, reduced availability of these cofactors, or increased concentrations of their respective competitors, can inhibit 2OG oxygenase function.

The loss of cell polarity and cell:cell adhesion is a hallmark of the transition from an epithelial to a mesenchymal phenotype in cancer (Halaoui and McCaffrey, 2015). Changes in cellular metabolism, induced by mutations including in the Krebs' cycle enzymes succinate dehydrogenase (SDH), isocitrate dehydrogenase (IDH) and fumarate hydrogenase (FH), have been associated with induction of EMT (Sciacovelli and Frezza, 2017; Colvin et al., 2016). Mutations in these enzymes lead to accumulation of intermediates including fumarate, succinate and 2-hydroxyglutarate (often referred to as oncometabolites) that compete with 2-oxoglutarate and thereby inhibit some 2OG oxygenases (Fletcher and Coleman, 2020). Importantly, it is not yet known how many 2OG oxygenases are inhibited by oncometabolites, or to what extent. Indeed, studies investigating the relation between inhibition of 2OG oxygenases by alterations in cellular metabolism and epithelial-mesenchymal transition have mainly focussed on the histone lysine demethylase (KDM) and ten-eleven translocation (TET) DNA demethylase subfamilies (Sciacovelli and Frezza, 2017). Whether oncometabolites such as fumarate might also target other 2OG oxygenases to contribute to the observations described is not known, but is pertinent to the work undertaken here. For example, it is in-

teresting to speculate that oncometabolites could interfere with functions of MPP6 in membrane biology and EMT by targeting MINA. Oncometabolites could act on MINA in the classical sense, by competing with 2OG and inhibiting an MPP6 hydroxylase activity. Alternatively, they could block the catalytic pocket and prevent MPP6 binding as a pseudosubstrate. Of interest with respect to the latter hypothesis is our unusual observation in Chapter 3 that treatment with a 2OG competitive inhibitor (DMOG) rapidly prevents the MINA:MPP6 interaction. It will be of interest to test the effect of cell permeable oncometabolites on the MINA:MPP6 complex in the future.

Hypoxia has been extensively studied in relation to cancer, and has been shown to mediate EMT in a HIF-dependent manner (Haase, 2009). Nonetheless, as above, hypoxia may inhibit other 2OG oxygenases which in turn, can favourably regulate EMT-inducing signalling pathways. For example, the TET hydroxylases are inhibited at pathological oxygen levels (Thienpont et al., 2016). Whether MINA activity is regulated by oxygen in the pathological context, is not yet clear. Many 2OG oxygenases, including MINA, have been shown to retain significant activity in hypoxic conditions (Ge et al., 2012; Feng et al., 2014; Tian et al., 2011). Nonetheless, it would be of interest to study the behaviour of these hydroxylases in severe, prolonged hypoxic conditions, as is often observed in tumours, as well as chronic inflammatory conditions, such as inflammatory bowel disease (Taylor and Colgan, 2007).

In contrast to the above described inhibition of 2OG oxygenases through pathological changes, physiological changes in cofactor availability have also been observed that might favour epithelial morphogenesis. One example that is relevant here and that was already briefly mentioned in Chapter 2, is the intestinal epithelium. Differentiated, post-mitotic cells face the intestinal lumen and specialise in secretion or absorption. Most distant from the lumen, the intestinal epithelium consists of proliferating progenitor and stem cells (Beumer and Clevers, 2021). Oxygen levels gradually decrease from the well-vascularised site of cell proliferation to the more luminal, differentiated villi, and can be as low as 0.04% in the distal colon (He et al., 1999). One could therefore speculate whether these changes in oxygen availability could induce a shift from

a proliferative towards a differentiated phenotype. In support of this hypothesis, tight junction protein claudin-1 was found to be a transcriptional target of HIF and defects in barrier function were observed following depletion of HIF1α in T84 intestinal epithelial cells (Saeedi et al., 2015). Considering our observation that MINA is sequestered in the nucleolus of proliferating cells, but nucleoplasmic in polarised monolayers (Chapter 2), and given that nucleolar retention is partly dependent on its catalytic activity (Chapter 2), it is interesting to speculate whether changes in oxygen levels could contribute to the translocation of MINA. It is not currently clear whether changes in oxygen levels in a physiological context could induce translocation of MINA: a pilot experiment did not support a role for hypoxia in regulating MINA localisation (Chapter 2), although it is possible that the level of hypoxia employed was not severe enough. The intestinal epithelium can be subjected to prolonged periods in hypoxia, and nitric oxide (NO) is a cell-permeable oxygen competitor that is produced from dietary nitrate by certain bacteria in the intestinal lumen (Tiso and Schechter, 2015). These factors might need to be considered before drawing conclusions and planning future studies.

6.3 Nucleolar sequestration as a mechanism of hydroxylase signalling and tumour suppression

Whereas reversible PTMs are fundamental to dynamic signalling in cells, no enzyme that catalyses the reverse reaction of stable hydroxylation has thus far been identified. Presuming that enzymatic reversal of stable hydroxylation does not exist and removal of hydroxylation (the 'OFF' reaction) solely depends on turnover of the substrate, we could speculate that regulation of the 'ON' modification might become more critical. This can be achieved by restricting the function of the enzyme itself, i.e. through transcription/translation of the enzyme, post-translational modifications, metabolism and cofactor availability (see above) or subcellular localisation. For instance, transcription of histone demethylases as well the collagen prolyl and lysyl hydroxylases is induced in hypoxia in a HIF-dependent manner (Pollard et al., 2008; Gilkes et al., 2013), and

phosphorylation of PHDs can alter substrate specificity (Ortmann et al., 2016). Based on the data presented in this thesis, we hypothesise that MINA's function might, at least in part, be regulated by restricting its subcellular localisation: Consistent with previous reports that MINA is highly enriched in nucleoli of proliferating tumour cells (Tsuneoka et al., 2002; Teye et al., 2004; Zhang et al., 2005), we have shown that enrichment of MINA is evident in the nucleoli of Caco-2 cells in low density cultures that have space to grow and divide (Chapter 2). Moreover, in an otherwise confluent monolayer, where MINA is predominantly nucleoplasmic, nucleolar localisation was triggered by introducing a scratch to disrupt the confluent cell monolayer and stimulate growth and migration. We demonstrated that MINA nucleolar localisation was dependent on ongoing rRNA transcription, associated with nascent protein synthesis, and partly dependent on MINA hydroxylase activity. Overall therefore, we propose that ribosome biogenesis acts as a 'sink' for MINA, inhibiting its alternative functions by retaining it in the nucleolus.

Traditionally, in addition to being the site of ribosome biogenesis, the nucleolus has been described as a 'prison' for some proteins, that captures them in an inactive state until released. This has mostly been studied in relation to proteins involved in cell cycle regulation and mitosis (Visintin and Amon, 2000). A renowned example of this principle is the inhibitor of p53, MDM2, which is sequestered in the nucleolus by $p19^{Arf}$ in response to DNA damage, thereby allowing stabilisation of p53 (Weber et al., 1999; Tao and Levine, 1999). Moreover, proteomic studies of the nucleolus revealed the presence of several proteins involved in transcription (Andersen et al., 2005). Nucleolar release of the transcription factor Hand1 was reported to initiate stem cell fate determination and differentiation (Martindill et al., 2007).

The work in this thesis suggests that the nucleolus might also act as a sink for proteins controlling cell:cell junction biology and epithelial morphogenesis. To our knowledge this is not a possibility that has been widely appreciated previously. That being said, there are some indications in the literature to support it. For example, it was recently reported that overexpression of the rRNA transcription initiation factor RRN3

is sufficient to upregulate rRNA synthesis and block normal lumen formation when non-tumourigenic mammary epithelial HME1 cells were grown in 3D (Rossetti et al., 2016). Whereas the absence of a central lumen was attributed to increased cell proliferation, one might speculate that a loss of functional cell-cell contacts and/or polarity would also be necessary, consistent perhaps with a role for increased ribosome biogenesis in interfering with such processes. The mechanisms involved in this phenotype have not yet been elucidated, so it remains possible that the nucleolar retention of MINA could at least be a contributing factor.

Normal barrier function, cell:cell junctions and apico-basal polarity are critical determinants of epithelial homeostasis that are suppressed during tumourigenesis. Therefore, the disruption of these by MINA loss of function would be consistent with a novel tumour suppressor (TS) role for MINA. Extending this hypothesis in line with the structure:function analyses presented here, we suggest that it is specifically the extra-nucleolar localisation and function(s) of MINA that relate to its TS activity. It is interesting to speculate that this TS activity is reduced or lost in tumour cells that have high ribosome biogenesis that acts as a sink to restrict MINA to the nucleolus. It has long been appreciated that increased size and number of nucleoli in tumour cells is common and strongly associated with tumour proliferation and poor prognosis (Ruggero, 2012; Derenzini et al., 2009). This raises the intriguing possibility that inactivation of MINA's TS activity by ribosome-driven nucleolar sequestration could be a frequent event in cancer. If true, this would represent a novel mechanism of TS inactivation that does not involve mutation or gene silencing and that would not be apparent from standard transcriptomic or genetic analysis. As such, the relatively low frequency of MINA gene mutation in cancer (1-2%, see Chapter 3) might significantly underestimate the true extent to which MINA's TS activity is compromised. Our results suggest that future cancer pathology studies should not only consider the expression level of MINA relative to normal tissue (which has been the almost singular focus of all the studies thus far), but also the relative distribution of MINA between the nucleoplasm and nucleolus. We would predict that high MINA levels correlate with

nucleolar localisation, and that it is this nucleolar localisation and lost TS activity, as opposed to increased expression and a gain in oncogenic activity (as discussed in the literature), that may be more relevant to the role of MINA in cancer.

It would be of interest to explore whether our hypothesis that ribosome biogenesis may act as a sink for MINA TS activity may extend to other proteins with known functions in ribosome biogenesis or translation. This would be of particular interest for proteins that, like MINA, have apparently complex and paradoxical roles in cancer biology. Interestingly, a dual function was also reported for $p19^{Arf}$: in addition to sequestering MDM2 in the nucleolus upon DNA damage, $p19^{Arf}$ was shown to function in ribosome biogenesis (Sugimoto et al., 2003; Lessard et al., 2010). With respect to related protein hydroxylases, a clear example could be the ribosomal hydroxylase NO66 which, as described in Chapter 1, has also been reported in extra-nucleolar compartments, including in nucleoplasmic dots (Eilbracht et al., 2004). Moreover, it was shown that nucleolar enrichment of NO66 depends on ongoing transcription, as its localisation was altered following treatment with RNase (Eilbracht et al., 2004).

6.4 The relationship between MINA and MPP6 in cancer

It will also be of interest to elucidate how the TS function of MINA relates to the potential role of MPP6 in cancer. We would predict that the TS function of MPP6 relates to its membrane functions, yet our data suggests that MINA does not interact with it there. Rather, our data suggest that MPP6 can also reside in the nucleoplasm, and that this is where it likely interacts with MINA. We speculate that MINA modifies or interacts with MPP6 in the nucleoplasm in a way that supports the normal membrane function of MPP6 (Figure 6.1A). Mechanistically, MINA could promote or interfere with protein:protein interactions involving MPP6. This regulation would be reduced or lost when MINA is sequestered in the nucleolus in response to physiological (Figure

6.1B and C) or pathological (Figure 6.1D) cues. Further work is required to understand whether MINA inhibition negatively effects the membrane localisation and function of MPP6. Potentially consistent with the hypothesis however, our preliminary analysis suggests that an MPP6 mutant defective in MINA binding is expressed at lower levels and is mislocalised from the membrane to the cytoplasm and/or nucleus (Chapter 5).

An alternative hypothesis regarding the relationship between MINA and MPP6 in tumourigenesis relates to the possibility that MPP6 has alternative functions in the nucleus that are more oncogenic in nature, and that MINA inhibits this in some way. Interestingly, it is not unprecedented for tumour suppressor membrane and polarity proteins to translocate to the nucleus where they undertake other functions, including those involved in driving cell growth and proliferation. Examples of these include β-catenin, DLG and CASK (Valenta et al., 2012; Roberts et al., 2007; Hsueh et al., 2000). Potentially consistent with nuclear functions of MPP6 in tumour cells, we observed exclusively nuclear/cytoplasmic localisation of MPP6 in HeLa cervical carcinoma cells (Chapter 3). Furthermore, a recurrent MPP6 cancer mutant (Figure 6.2) which we employed to model loss of the GUK domain in our early domain mapping experiments (Chapter 3), was almost exclusively nuclear.

Further investigations into the potential nuclear function of MPP6 could also help to clarify whether any of the previously reported effects of MINA expression (or lack thereof) can be explained via its interaction with MPP6. These include changes in histone methylation and gene expression regulation of genes involved in cell cycle progression (Zhang et al., 2005; Ma et al., 2015; Aziz et al., 2020). Although we have not yet begun to explore if MPP6 has a nuclear function and what this may be, we could speculate based on what is known about β-catenin, CASK and DLG. For instance, nuclear β-catenin regulates transcription through the association with the T-cell factor (TCF) / lymphoid enhancer factor (LEF) transcription factors (Cadigan and Waterman, 2012). Interestingly, nuclear translocation of β-catenin also induces changes in histone modifications (Cadigan and Waterman, 2012). Similar to β-catenin, CASK was found to interact with the transcription factor Tbr-1 upon nuclear translocation (Hsueh

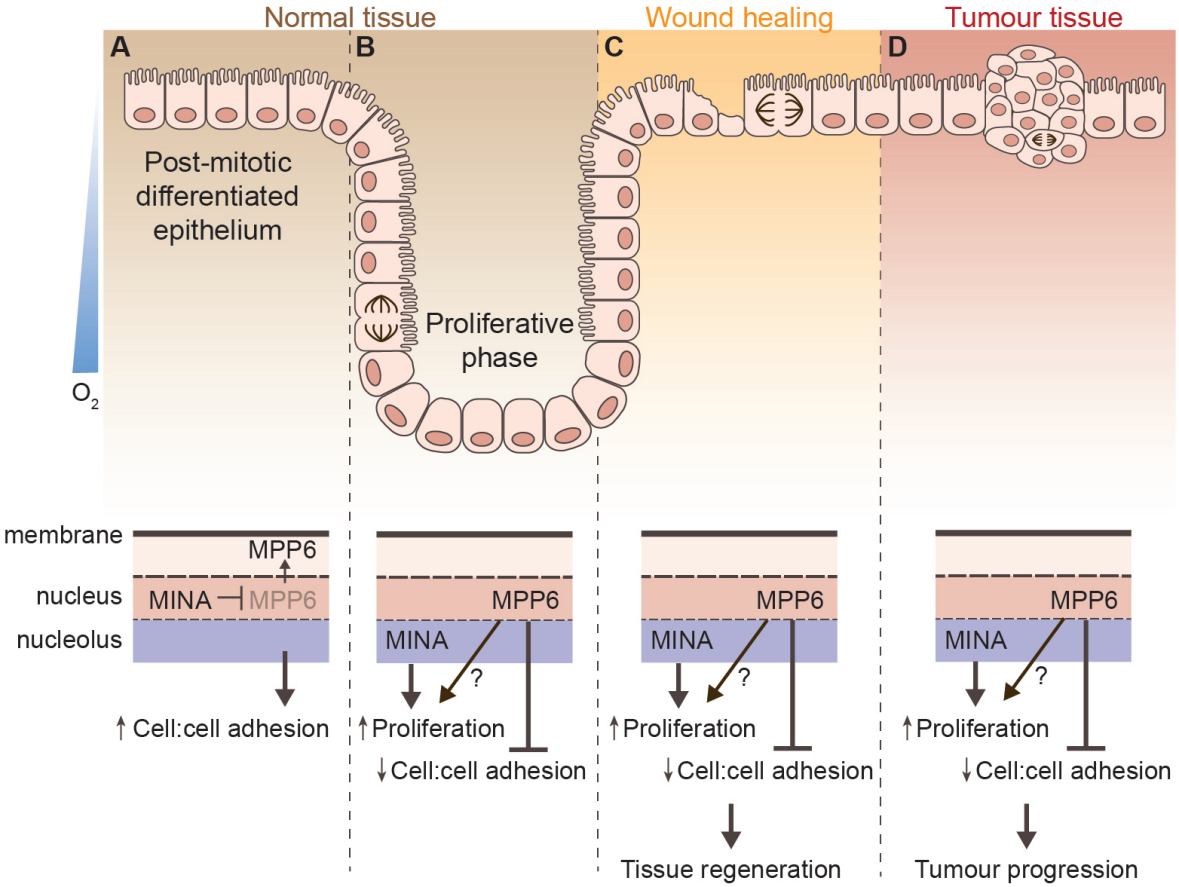


Figure 6.1: Current working hypothesis. (**A**) In a normal, differentiated epithelium cells have basal levels of ribosome biogenesis and MINA is mostly nucleoplasmic. Nuclear MINA hydroxylates or binds MPP6 and subsequently promotes nuclear removal and/or membrane retention of MPP6, thereby promoting its membrane function and cell:cell adhesion, and/or inhibiting its nuclear (oncogenic) function. (**B-C**) To maintain tissue homeostasis (B) or upon injury (C) cells can (re)enter the cell cycle. Increased ribosome biogenesis retains MINA in the nucleolus, where it promotes cell growth. The absence of MINA from the nucleoplasm promotes the nuclear localisation of MPP6 and inhibits its membrane function, thereby inhibiting cell:cell adhesion and possibly promoting cell motility and proliferation. (**D**) Similar to a proliferative epithelium, as shown in (B) and (C), pathogenic signals trigger nucleolar and nuclear (re)localisation of MINA and MPP6, respectively, thereby promoting tumour progression. (**A-D**) It should be noted that the intestinal epithelium is presented in this figure purely as an example, and this hypothesis extends to other tissue types.

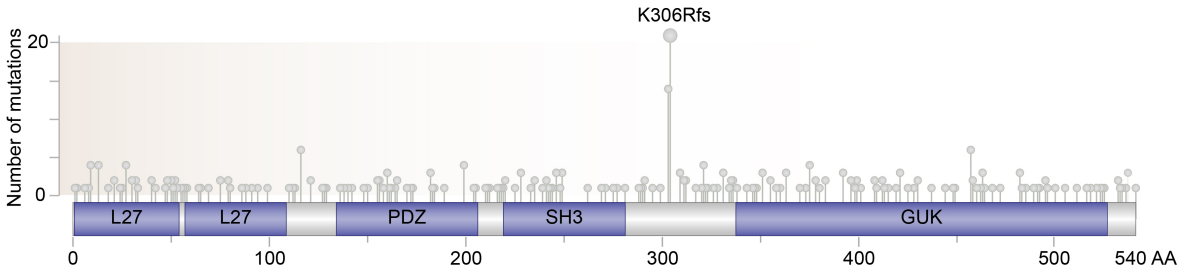


Figure 6.2: Distribution of mutations in MPP6. Lollipop plot showing the distribution of mutation in the MPP6 gene as identified across 254 studies available on cBioPortal. K306R frameshift (fs) mutation is annotated.

et al., 2000). Nuclear DLG1 may also control gene expression through regulation of mRNA processing, as it was shown to interact with the polypyrimidine tract-binding protein-associated splicing factor (PSF; Sabio et al., 2010).

6.5 Conclusion

In conclusion, the findings presented in this thesis provide new insights into the regulation and tumour suppressor role of MINA. Moreover, our results indicate that MINA may act as a link between cell proliferation and adhesion. The identification of MPP6 as a novel MINA interactor, as well as the preliminary loss-of-function analyses, provide a basis for future investigations into the mechanisms by which MINA functions in epithelial morphogenesis. Finally, the data in this thesis support the intriguing possibility that upregulation of ribosome biogenesis may act as a mechanism to inhibit polarity-associated pathways.

Chapter 7: Materials and methods

7.1 Molecular biology techniques

7.1.1 Plasmid constructs and cloning procedures

Coding sequences of MINA, MPP6, LIN7C and NO66 were PCR cloned from plasmid DNA or cDNA into pFLAG (Sigma), pEF6 (Invitrogen), QM800A-Blast (System Biosciences), pTIPZ, pTIBZ, pIPZ or pIHZ vectors. pIPZ, pTIPZ are derivatives of the pGIPZ and pTRIPZ lentiviral vectors (Open Biosystems) that lack the green fluorescent protein (GFP) and red fluorescent protein (RFP), respectively. The pTIBZ and pIHZ vectors are identical to the pTIPZ and pIPZ vectors, respectively, except for the blasticidin and hygromycin resistance genes which have replaced the puromycin resistance gene, respectively. The coding sequences of MPP2, MPP2$^{\mathrm{TPLF}}$ and the MPP2/6 hybrids containing C-terminal HA-tags and restriction sites required for cloning into the pIPZ vector were obtained from Thermo Scientific as a GeneArt String Fragment. MINA and MPP6 shRNA sequences in pZIP-TRE3G vectors were obtained from TransOMIC and are listed in Table 7.1.

Target	Catalogue number	Sequence (5' to 3')
Non-targeting control	ULTRA-NT#4	TGCTGTTGACAGTGAGCGAAGGCAGAAGTATGCAA AGCATTAGTGAAGCCACAGATGTAATGCTTTGCATA CTTCTGCCTGTGCCTACTGCCTCGGA
MINA #1	ULTRA-3406274	TGCTGTTGACAGTGAGCGCCCCTCTGGACAGAATG TTTAATAGTGAAGCCACAGATGTATTAAACATTCTG TCCAGAGGGAT GCCTACTGCCTCGGA
MINA #3	ULTRA-3406273	TGCTGTTGACAGTGAGCGCCCCAGAGGAACCATTC ATCAATGAAGCCACAGATGTATTGATGAATGGTTCC TCTGGGATGCCTACTGCCTCGGA
MPP6 #1	ULTRA-3337605	TGCTGTTGACAGTGAGCGCAGACATCACTCCTCTA ATAAATAGTGAAGCCACAGATGTATTTATTAGAGGA GTGATGTCTTTGCCTACTGCCTCGGA
MPP6 #2	ULTRA-3337606	TGCTGTTGACAGTGAGCGCATGGAGAATCCTATTG TAAAATAGTGAAGCCACAGATGTATTTTACAATAGG ATTCTCCATATGCCTACTGCCTCGGA
MPP6 #3	ULTRA-3337607	TGCTGTTGACAGTGAGCGCCCGACTCTGACTTGAA GAAAATAGTGAAGCCACAGATGTATTTTCTTCAAGT CAGAGTCGGTTGCCTACTGCCTCGGA

Table 7.1: shRNA sequences.

PCR reactions were driven by the Phusion High Fidelity DNA polymerase (New England Biolabs (NEB), M0530). Primers were designed to contain a C- or N-terminal tag and the required restriction sites for subsequent ligations. All primers are listed in Table 7.2. The amplified DNA was recovered using a GenElute gel purification kit (Sigma) after electrophoresis on a 1% (w/v) agarose gel, digested with the appropriate restriction enzymes and subsequently ligated using T4 DNA ligase (NEB, M0202) into the vector of interest. All vectors were pre-treated with calf intestinal alkaline phosphatase (CIP, NEB, 0290S) to prevent re-ligation of the linearised plasmid DNA. The ligated DNA was then transformed into *Escherichia coli* DH5α bacterial cells (NEB, C29872). Once grown, the DNA was purified using a GeneElute Miniprep Kit (Sigma-Aldrich). All constructs were confirmed by sequencing, carried out by Source Bioscience.

For nucleotide exchanges, site-directed mutagenesis was performed using a Phusion Site-directed Mutagenesis kit (Thermo, F541). 5' termini of the primers were phosphorylated using T4 polynucleotide kinase (PNK, Thermo, EK0031) prior to the reaction. Primer sequences are listed in Table 7.3. All constructs were confirmed by sequencing.

Construct	**Primers (5' to 3')**
pTIPZ 3xFLAG-MINA	forward: GCGTTTGGCGCGCCATGGACTACAAAGACCATGATGGTGA TTATAAAGATCATGACATCGATTACAAGGATGACGATGATA AGCCAAAGAAAGCAAAGCCT
	reverse: AAAATACCTGCAGGCTAGACTACTTGAATTAAACATTC
QM800A MINA	forward: GCGTTTTTCGAAATGCCAAAGAAAGCAAAGC
	reverse: AAAATAGCGGCCGCCTAGACTACTTGAATTAAACATTCTGT
QM800A MINA ($sh3^{resistant}$)	forward: GCGTTTTTCGAAATGCCAAAGAAAGCAAAGC
	reverse: AAAATAGCGGCCGCTAGACTACTTGAATCAAGCACT
pIHZ 3xFLAG-MINA	forward: GCGTTTATCGATATGGACTACAAAGACCATGATGGTGATT ATAAAGATCATGACATTGATTACAAGGATGACGATGATAA GCCAAAGAAAGCAAAGCCTACA
	reverse: AAAATAGCGGCCGCCTAGACTACTTGAATTAAACATTCTGTC
pIHZ 3xFLAG-MINA ($sh3^{resistant}$)	forward: GCGTTTATCGATATGGACTACAAAGACCATGATGGTGATT ATAAAGATCATGACATTGATTACAAGGATGACGATGATAA GCCAAAGAAAGCAAAGCCTACA
	reverse: AAAATAGCGGCCGCCTAGACTACTTGAATTAAGCACTCTG
pIPZ/pIHZ MPP6-HA	forward: TTTATCATCGATATGCAGCAAGTCTTGGAA
	reverse: CCAATCAGCTGGGTTTACGATTACCCATACGATGTTCCAGA TTACGCTTGAGCGGCCGCTATGCA
pTIBZ MPP6-3xFLAG	forward: TTTATCACCGGTATGCAGCAAGTCTTGGAAAA
	reverse: TGCATAATCGATTCACTTATCATCGTCATCCTTGTAATCAA TGTCATGATCTTTATAATCACCATCATGGTCTTTGTAGTCG TAAACCCAGCTGATTGGG
$MPP6^{110-541}$ -HA	forward: TTTATCATCGATATGAGCCCAGAAATGAATAATTCT
	reverse: TGCATAGCGGCCGCTCAAGCGTAATCTGGAACATCGTATGG GTAATCGTAAACCCAGCTGATTGG
$MPP6^{210-541}$ -HA	forward: TTTATCATCGATATGAGAGATACCATTACTCCTCAACA
	reverse: GCATAGCGGCCGCTCAAGCGTAATCTGGAACATCGTATGGG TAATCGTAAACCCAGCTGATTGG
$MPP6^{1-212}$ -HA	forward: TTTATCATCGATATGCAGCAAGTCTTGGAA
	reverse: TGCATAGCGGCCGCTCAAGCGTAATCTGGAACATCGTATGG GTAATCGGTATCTCTATAACTTGGTAAGATTTT

Table 7.2: List of primers used for cloning.

Mutation	Primers (5' to 3')
MPP6 V287A	forward: AGAAAGGCATTTGCTAGAAGAGACTGGG
	reverse: CTTCTCTTCCAGGAACTGGCTTGG
MPP6 R288A	forward: GAAAGGCATTTGTTGCAAGAGACTGGGAC
	reverse: TCTTCTCTTCCAGGAACTGGCTTG
MPP6 R289A	forward: AGGCATTTGTTAGAGCAGACTGGGACAATTC
	reverse: TTCTCTTCTCTTCCAGGAACTGGCT
MPP6 D290A	forward: ATTTGTTAGAAGAGCCTGGGACAATTCAGG
	reverse: GCCTTTCTCTTCTCTTCCAGGAACTG
MPP6 W291A	forward: TGTTAGAAGAGACGCGGACAATTCAGGA
	reverse: AATGCCTTTCTCTTCTCTTCCAGGA
MPP6 D292A	forward: GAAGAGACTGGGCCAATTCAGGACC
	reverse: TAACAAATGCCTTTCTCTTCTCTTCCAGG
MPP6 N293A	forward: AGAGACTGGGACGCTTCAGGACCTTT
	reverse: TCTAACAAATGCCTTTCTCTTCTCTTCCAG
MPP6 S294A	forward: AGACTGGGACAATGCAGGACCTTTTTG
	reverse: CTTCTAACAAATGCCTTTCTCTTCTCTTCCA
MPP6 G295A	forward: TGGGACAATTCAGCACCTTTTTGTGGAA
	reverse: GTCTCTTCTAACAAATGCCTTTCTCTTCTCTT
MPP6 P296A	forward: AGAGAAAGGCATTTGTTAGAAGAGACTG
	reverse: CAGTCTCTTCTAACAAATGCCTTTCTCT
MPP6 F297A	forward: ACAATTCAGGACCTGCTTGTGGAACTATAAG
	reverse: CCCAGTCTCTTCTAACAAATGCCTTT
MPP6 C298A	forward: CAATTCAGGACCTTTTGCGGGAACTATAAGTAGC
	reverse: TCCCAGTCTCTTCTAACAAATGCCT
MPP6 G299A	forward: CAGGACCTTTTTGTGCAACTATAAGTAGCAA
	reverse: AATTGTCCCAGTCTCTTCTAACAAATGC
MPP6 T300A	forward: GGACCTTTTTGTGGAGCTATAAGTAGCAAAA
	reverse: TGAATTGTCCCAGTCTCTTCTAACAAATG
MPP6 I301A	forward: CCTTTTTGTGGAACTGCAAGTAGCAAAAAAAAG
	reverse: TCCTGAATTGTCCCAGTCTCTTCTAAC
MPP6 S302A	forward: TGTGGAACTATAGCTAGCAAAAAAAAGAAA
	reverse: AAAAGGTCCTGAATTGTCCCAGTCTCT
MINA H179A	forward: TCGAGGTTTTCATCCTGCAGCTG
	reverse: CATCATCATAAGCGGGCGGC
MINA D333A	forward: GACTCCCCCCTTACTCTGCG
	reverse: TGTGCATAATAAAAGCCTTCTTCATGT
MINA M405A	forward: GAGGAGGAAACAGAGTTTCATGGACTTC
	reverse: ATTTCCCATCGCGTGTGTCTCTC
MINA R125G/ K125G	forward: CACTTTCTTCAGCTGGGAGGAGATTTTGATCAGAAAAGG GCAACGATTC
	reverse: CTGATCAAAATCTCCTCCCAGCTGAAGAAAGTGTGCTTTG CCATC

Continued on next page

Table 7.3: Primers used for site-directed mutagenesis.

Mutation	Primers (5' to 3')
MINA S455S/ L456L/E459E/ C460C	forward: GAGTGCTTAATTCAAGTAGTCTAGAAGCTTCC reverse: GTCCAAAGTGATAATACCAGGCTTTCC
MINA T457T/ L461L	forward: GCTTGATTCAAGTAGTCTAGAAGCTTCCC reverse: CTCGGTCCAAAGTGATAATACCAGG

Table 7.3: Primers used for site-directed mutagenesis.

7.2 Cell biology techniques

7.2.1 Cell culture

HEK293T, Caco-2, SW620, U2OS, HeLa and A549 cells were cultured in Dulbecco's Modified Eagle Medium (DMEM, Gibco) supplemented with 10% (v/v) foetal bovine serum (FBS, Sigma) and 100 international units/mL (IU/mL) penicillin and 100 µg/mL streptomycin (Gibco). Cell culture medium for stable cell lines was supplemented with 1 µg/mL puromycin (Gibco), 100 µg/mL hygromycin B (Invitrogen) and/or 5 µg/mL blasticidin S (Gibco). All cell lines were grown at 37 °C in a humidified atmosphere with 5% (v/v) CO_2. For 3D spheroid cultures, culturing medium was supplemented with 4% (v/v) Matrigel (Corning, 356231). All cell lines were routinely tested for mycoplasma contamination.

7.2.2 Transient transfection

Plasmid DNA transfections were performed using FuGENE® 6 transfection reagent (Promega). Briefly, the transfection mix was made up in Opti-MEM™ (Gibco, cat. no. 31985070) using a ratio of DNA to transfection reagent of 1:3, and incubated for 15-30 min at room temperature (RT) before the complexes were added to the cells. 500 ng of DNA was used per mL of culturing medium. Cells were seeded 24 h prior to transfection and harvested 48 h after transfection.

7.2.3 Generation of stable cell lines

Stable expression cell lines were generated by transduction with lentivirus. For lentivirus production, HEK293T cells were transfected with the plasmid of interest (50%), the packaging vector psPAX2 (35%) and envelope vector pMD2.G (15%) as described above. The lentivirus-containing supernatant was collected 48 h after transfection, passed through a 0.45 µM polyethersulfone (PES) filter, diluted 1:1 with fresh medium and added to the recipient cells for 48 h. Thereafter, transduced cells were selected using puromycin (2 µg/mL final concentration, Gibco), hygromycin B (200 µg/mL, Invitrogen) or blasticidin S (10 µg/mL, Gibco).

7.2.4 Cell treatments

A list of all chemicals can be found in Table 7.4. Hypoxia was achieved by incubating cells at 1% oxygen for 16 hours in a H35 Hypoxystation (Don Whitley Scientific), set at 37°C, 75% humidity, 5% CO_2 and balanced with N_2.

7.2.5 Cell viability assays

To monitor cell proliferation of 2D cultures, cells were seeded in clear, flat bottom, white or black 96-well plates (Corning, CLS3610) at a density of 2,500 cells/well and cell viability was monitored by incubation with resazurin at a final concentration of 0.025 mg/mL (Sigma-Aldrich, #R7017) for 2 h. For 3D growth assays, cells were seeded on Matrigel-coated clear, flat bottom, white or black 96-well plates (Corning, CLS3610) at a density of 4,000 cells/well and cell viability was measured using a CellTiter-Glo® Luminescence Assay kit (Promega), according to the manufacturer's instructions.

Chemical	Final concentration	Company	Cat. no.	Effect
Actinomycin D	40 ng/mL	Sigma-Aldrich	A9415	Inhibition of RNA polymerase I
Cumate	30-300 µg/mL	System Biosciences	QM150 A-1	Induction of gene expression
CX-5461	50 nM	APExBIO	A8337	Inhibition of RNA polymerase I
Cycloheximide	100 µg/mL	Sigma-Aldrich	C4859	Inhibition of translation
Desferrioxamine (DFO)	100 - 250 µM	Sigma-Aldrich	D9533	Iron chelation
Dimethyl-N-oxalylglycine (DMOG)	1 mM	Sigma-Aldrich	D3695	Inhibition of 2OG-oxygenases
Doxycycline	0.05 - 1 µg/mL	Sigma-Aldrich	D9891	Induction of gene expression
MG132	10 µM	Alfa Aesar	J6350	Inhibition of the proteasome
ML-60218	25 µM	Focus Biomolecules	10-181	Inhibition of RNA polymerase III
N-oxalylglycine (NOG)	1 mM	Sigma-Aldrich	O9390	Inhibition of 2OG-oxygenases

Table 7.4: List of chemicals.

7.2.6 Metabolic labelling of newly synthesised proteins

Protein synthesis was monitored with L-azidohomoalanine (AHA) using a Click-iT™ Nascent Protein Synthesis kit (Thermo Scientific), according to the instructions of the manufacturer. Briefly, cells were incubated with methionine-free medium for 1 h before AHA was added at a final concentration of 50 µM. After 1 h, cells were fixed and permeabilised as described in section 7.2.8. Next, Alexa Fluor 595 Alkyne diluted in Click-iT® Cell Reaction Buffer (Thermo Scientific) at a final concentration of 2.5 µM was conjugated to any incorporated AHA.

7.2.7 Proximity ligation assay

Duolink® proximity ligation assay kits were purchased from Sigma-Aldrich and performed according to the manufacturer's instructions. Briefly, samples were fixed and permeabilised as in section 7.2.8 and subsequently blocked for 1 h at 37°C using Duolink® blocking solution before primary antibody incubation under standard conditions (see section 7.2.8). Next, the samples were incubated for 1 h at 37°C with Duolink® MINUS and PLUS secondary antibody probes conjugated to oligonucleotides that were subsequently ligated for 30 min at 37°C, forming a closed circle if in close proximity to each other. Finally, the samples were incubated for 100 min at 37°C with a polymerase that amplifies the signal of any existing closed oligonucleotide circles. Detection was achieved using complementary, fluorescently labelled oligonucleotides. Coverslips were mounted using Duolink® Mounting Media with DAPI (cat. no. DUO82040). Confocal images were acquired as described in section 7.2.8.

7.2.8 Immunofluorescence staining and image acquisition

For immunofluorescence studies of 2D cultures, cells were grown on poly-D-lysine-coated or uncoated glass coverslips and fixed with methanol for 10 min at -20°C or 4% (w/v) paraformaldehyde (PFA) in phosphate-buffered saline (PBS, Sigma) for 15 min

at RT. Cells fixed with PFA were subsequently permeabilised using 0.1% (v/v) Triton in PBS for 10 min at RT. Next, cells were blocked with 1% (w/v) bovine serum albumin (BSA) in PBS for 1 h and subsequently incubated overnight (ON) at 4°C with primary antibodies in 1% BSA/PBS. The next day, coverslips were washed with 1% (w/v) BSA/PBS and incubated with secondary antibodies in 1% (w/v) BSA/PBS for one hour at RT. Secondary antibodies were purchased from Invitrogen and used at a final concentration of 1:1,000. Where indicated, secondary antibody incubation was followed by a 1 h incubation at RT with Texas Red®-X phalloidin (Thermo Scientific, T7471) at a concentration of 1:500 to visualise F-actin. Nuclei were stained by incubation with 0.5 - 1 µg/mL 4',6-diamidino-2-phenylindole (DAPI, D1306, Invitrogen) in PBS for 10 min at RT, and the coverslips were mounted with Prolong Gold antifade mountant (Molecular Probes) onto microscope slides. For long-term storage, the coverslips were sealed with nail varnish and kept at -20°C.

Caco-2 cells grown as 3D cultures were fixed with 4% (w/v) PFA/5% (w/v) sucrose in PBS for 20 min at RT, washed three times with PBS and incubated with 100 mM glycine in PBS for 20 min at RT to quench unreacted aldehydes. After three washes in PBS, cells were permeabilised with 0.1% (v/v) Triton X-100 in PBS for 5 min at RT, washed 3 times with PBS, blocked with 1% (w/v) BSA/PBS at RT for 1 h and subsequently stained as described above.

Confocal images were acquired with a Zeiss LSM 780 or 880 laser scanning confocal system equipped with a 20x, 40x or 60x C-Apochromat 1.2 W Korr M27 objective. Epifluorescence images were acquired using an EVOS inverted microscope (Life Technologies) or a Leica DM6000. Immunofluorescence images of similarly stained experiments were acquired with identical illumination settings. Images were processed with Fiji. Brightness and contrast were adjusted using only linear operations applied to the entire image. Final images were assembled using Microsoft PowerPoint.

7.3 Biochemical techniques

7.3.1 Whole cell extracts

2D cultures were washed and harvested in ice-cold PBS, pelleted by centrifugation at 234 x g and lysed by rotation at 4°C for 1 h in JIES buffer (100 mM NaCl, 20 mM Tris-HCl [pH 7.4], 5 mM $MgCl_2$, 0.5% (v/v) NP-40) containing 1x SIGMAFAST™ protease inhibitor cocktail (Sigma-Aldrich, S8830). Subsequently, cell debris was pelleted by centrifugation (10 min at 21,910 x g at 4°C) and the supernatant was collected.

Spheroids were collected and washed two times with ice-cold PBS containing 1x SIGMAFAST™ protease inhibitor cocktail (Sigma-Aldrich, S8830). Cells were pelleted by centrifugation for 15 seconds at 21,910 x g in between washes. Subsequently, the cell pellet was resuspended in 1x Laemmli Loading Buffer (6x: 125 mM Tris-HCl [pH 6.8], 6% (w/v) SDS, 50% (v/v) glycerol, 225 mM dithiotheitol (DTT), 0.1% (w/v) bromophenol blue), vortexed, boiled for 5 min and sonicated.

7.3.2 Immunoprecipitation

For immunoprecipitations, cells were harvested on ice and lysed by rotation for 1 h at 4°C in JIES buffer (see section 7.3.1) containing 1x SIGMAFAST™ protease inhibitor cocktail (Sigma-Aldrich, S8830). Subsequently, cell debris was pelleted by centrifugation (10 min at 21,910 x g at 4°C) and the supernatant was incubated with anti-FLAG® M2 Magnetic Beads (Sigma-Aldrich, M8823) or anti-hemagglutinin (HA) agarose beads (Sigma-Aldrich, A2095) overnight at 4°C. The next day, beads were washed 6 times with JIES buffer before the immunoprecipitates were boiled for 5 min in 1x Laemmli Loading Buffer or eluted using 100 µg/mL HA (Thermo Scientific, 26184) or 40 ng/mL FLAG (Generon, A6001) peptide in JIES for 15 min at 1,400 rpm at RT.

7.3.3 SDS-PAGE and Western blot analysis

Where indicated, proteins were separated and detected by sodium dodecyl sulfate-polyacrylamide gel electrophoresis (SDS-PAGE). Protein samples were prepared in Laemmli Loading Buffer, boiled for 5 min at 95°C and loaded onto either 10%, 12% or 15% (v/v) polyacrylamide gels made in-house, Novex™ WedgeWell™ 8-16% gels (cat. no. XP08165BOX, Invitrogen) or NuPAGE™ 4-12% Bis-Tris Midi gels (cat. no. WG1403A, Invitrogen). Electrophoresis was performed in Tris/Glycine/SDS (National diagnostics) or NuPAGE™ MOPS SDS (Invitrogen, cat. no. NP0001) running buffer. Following SDS-PAGE, the samples were electroblotted onto methanol-activated Amersham™ Hybond™ P0.45 polyvinylidene difluoride (PVDF) membranes (GE Healthcare) in Tris/Glycine transfer buffer (National diagnostics). Following transfer, the membrane was blocked with 5% (w/v) milk powder dissolved in PBS/0.1% (v/v) Tween-20 (PBS-T) and incubated with primary antibody for 1 h at RT or overnight at 4°C. Where unconjugated primary antibodies were used, immunoblots were subsequently incubated with horseradish peroxidase (HRP)-conjugated secondary antibodies purchased from Cell Signaling. Signals were visualised using Clarity Western ECL reagent (Bio-Rad) or Femto (Thermo Scientific) using a Vilber Fusion Fx. A detailed list of the antibodies and dilutions used in this thesis are given in Tables 7.5, 7.6 and 7.7.

7.3.4 Mass Spectrometry

For identification of interacting proteins or post-translational modification analysis, the protein of interest was immunoprecipitated as described in section 7.3.2 and eluted using peptide in tris-buffered saline (TBS). Subsequently, eluates were submitted to the Target Discovery Institute at the University of Oxford for further processing.

Antigen	Host species	Clonality	Used dilution	Company	Cat. no.
E-cadherin	Rabbit	Monoclonal	WB 1:1000 IF 1:500	Cell Signaling Technology	3195
FLAG	Mouse	Monoclonal	IF 1:1000	Sigma-Aldrich	F1804
FLAG	Rabbit	Monoclonal	IF 1:800	Cell Signaling Technology	14793S
HA	Mouse	Monoclonal	IF 1:500	Covance	MMS-101P
HA	Rabbit	Monoclonal	IF 1:500	Cell Signaling Technology	C29F4
LIN7C	Rabbit	Polyclonal	WB 1:500	Proteintech	14656-1-AP
MINA	Mouse	Monoclonal	WB 1:40	DSHB	6C6
MINA	Mouse	Monoclonal	IF 1:100	Invitrogen	39-7300
MPP6	Rabbit	Polyclonal	WB 1:500	GeneTex	GTX108010
MPP6	Rabbit	Polyclonal	WB 1:500 IF 1:500	Atlas Antibodies	HPA019085
Na^+/K^+ ATPase α-1	Rabbit	Polyclonal	WB 1:1000	Cusabio	CSB-PA 18129A0Rb
Na^+/K^+ ATPase α-1	Rabbit	Monoclonal	IF 1:500	Abcam	ab76020
Nucleolin	Rabbit	Polyclonal	IF 1:200 - 1:1000	Santa Cruz Biotechnology	sc-13056
Nucleo-phosmin	Rabbit	Polyclonal	IF 1:200	Santa Cruz Biotechnology	sc-6013-R
PARP	Rabbit	Monoclonal	WT 1:1000	Cell Signaling Technology	95425
RPL27A	Rabbit	Polyclonal	WB 1:500	Abcam	ab74731
ZO-1	Mouse	Monoclonal	WB 1:1000 IF 1:500	Invitrogen	33-9100
α-tubulin	Rabbit	Polyclonal	IF 1:500	GeneTex	GTX113098
α-tubulin	Mouse	Monoclonal	IF 1:2500	Sigma-Aldrich	T6199
β-catenin	Mouse	Monoclonal	WB 1:1000 IF 1:500	BD Biosciences	610153
β-tubulin	Rabbit	Polyclonal	WB 1:500	Abcam	ab6046

Table 7.5: List of unconjugated primary antibodies.

Antigen	Host species	Clonality	Used dilution	Company	Cat. no.
FLAG	Mouse	Monoclonal	WB 1:10,000	Sigma-Aldrich	A8592
HA	Rat	Monoclonal	WB 1:1,000 - 1:5,000	Roche	12013819001
β-actin	Mouse	Monoclonal	WB 1:25,000	Abcam	ab-49900

Table 7.6: List of horseradish peroxidase (HRP)-conjugated primary antibodies.

Antigen	Host species	Clonality	Conjugate	Used dilution	Company	Cat. no.
anti-mouse	Horse	Polyclonal	Horseradish Peroxidase (HRP)	WB 1:2,500	Cell Signaling Technology	7076
anti-rabbit	Goat	Polyclonal	Horseradish Peroxidase	WB 1:2,500	Cell Signaling Technology	7074
anti-rabbit	Mouse	Monoclonal	Horseradish Peroxidase	WB 1:2,500	Rockland	18-8816-31
anti-mouse	Goat	Polyclonal	Alexa-Fluor (AF) 488	IF 1:1,000	Invitrogen	A11029
anti-mouse	Goat	Polyclonal	AF 555	IF 1:1,000	Invitrogen	A31570
anti-mouse	Goat	Polyclonal	AF 633	IF 1:1,000	Invitrogen	A21053
anti-rabbit	Goat	Polyclonal	AF 488	IF 1:1,000	Invitrogen	A11070
anti-rabbit	Goat	Polyclonal	AF 555	IF 1:1,000	Invitrogen	A21430

Table 7.7: List of secondary antibodies.

7.3.5 *In vitro* hydroxylation assays

For *in vitro* hydroxylation assays, HA-tagged MINA was overexpressed and purified from HEK293T cells, as described in sections 7.2.2 and 7.3.2. Following immunoprecipitation, the purified protein was eluted using 2 mg/mL HA peptide (Thermo Scientific, 26184) in 50 mM HEPES, 50 mM NaCl. Purified enzyme was then incubated with RPL27A peptide (GRGNAGGLHHhINFDKYHP) at a final concentration of 100 µM in 50 mM Tris [pH 7.5], 150 mM NaCl, 1 mM DTT for 5 min at 37°C in the presence of 200 µM 2OG, 100 µM Fe(II) and 100 µM ascorbate (final volume 20 µL). Thereafter, the reaction was quenched with 10 µL of 1% (v/v) formic acid (HCOOH) in H_2O. The presence of hydroxylation was subsequently analysed using a Succinate-Glo™ JmjC Demethylase/Hydroxylase Assay kit (Promega). For detection using a Succinate-Glo™ JmjC Demethylase/Hydroxylase Assay kit, the samples were diluted 1:10 in H_2O and 5 µL of the diluted reaction was mixed with an equal volume of Succinate-Glo™ detection reagent 1 and incubated for 1 h at RT in a clear bottom 384-well plate. Each reaction was performed in triplicate. Subsequently, 10 µL of Succinate-Glo™ detection reagent 2 was added, mixed and incubated for 10 min at RT, before luminescence was analysed.

7.3.6 Subcellular fractionation

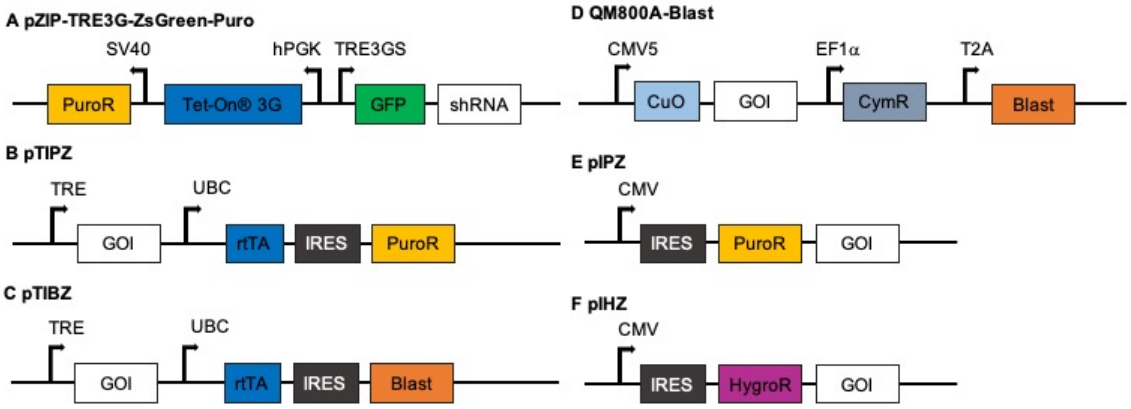
Subcellular fractionation was achieved with a Subcellular Protein Fractionation Kit for Cultured Cells purchased from Thermo Scientific (cat. no. 78840), according to the instructions of the manufacturer. Briefly, Caco-2 cells were collected with TrypLE™ Express Enzyme (Gibco, 12604013), counted, and incubated with cytoplasmic extraction buffer (CEB) for 10 min at 4°C with gentle mixing before the lysate was pelleted by centrifugation at 500 x g for 5 min, and the supernatant was transferred into a fresh tube. Next, the pellet was resuspended with ice-cold membrane extraction buffer (MEB) containing protease inhibitor, vortexed for 5 sec and incubated for 10 min at 4°C with gentle mixing. Afterwards, the extract was centrifuged for 5 min at 3,000 x

g and the supernatant (containing the membrane extract) was transferred to a clean tube. Finally, the pellet was resuspended in ice-cold nuclear extraction buffer (NEB) containing protease inhibitor, vortexed for 15 sec, mixed for 30 min at 4°C, and the supernatant containing the nuclear extract was transferred to a clean tube. The volume of extraction buffers added was in accordance to the packed cell volume, as outlined in the manufacturer's protocol.

7.4 Illustration plotting, statistical analysis and reproducibility

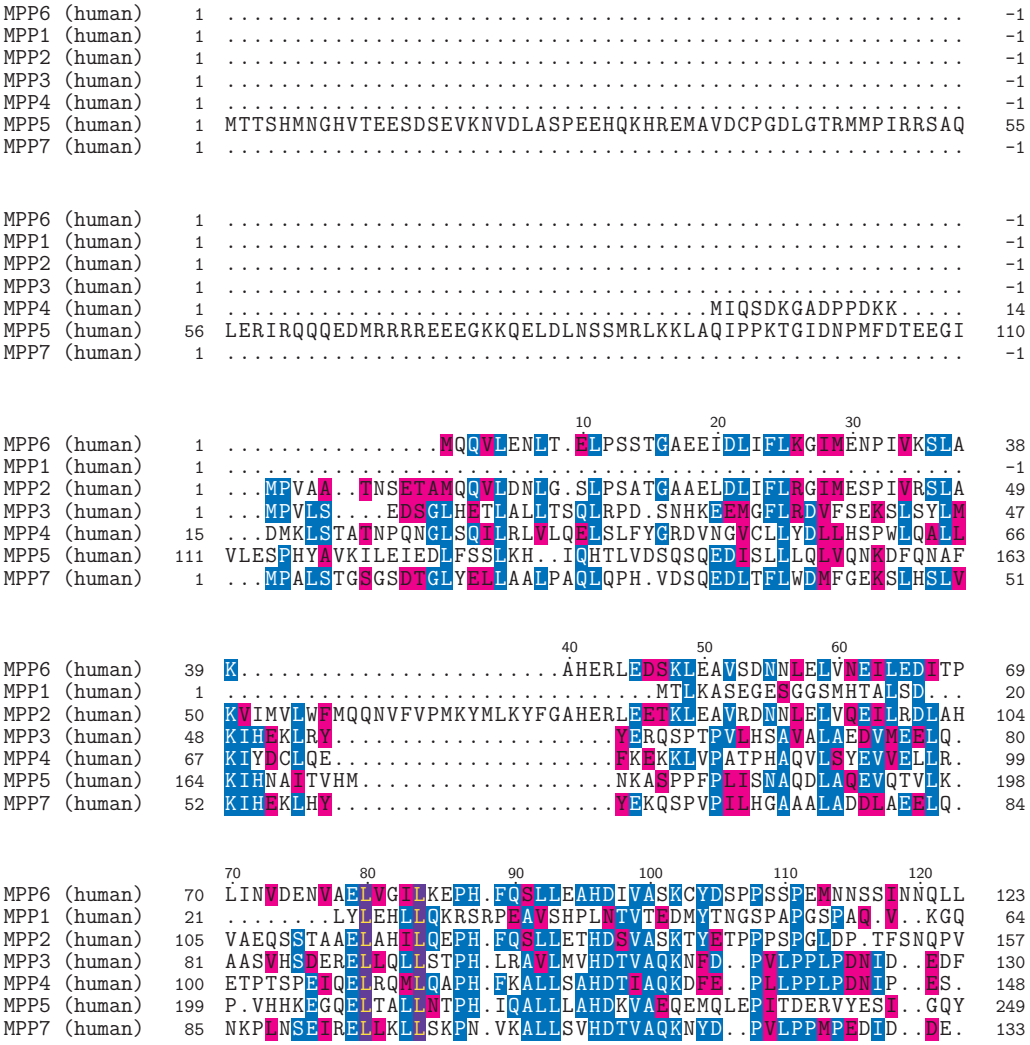
Statistical analyses were performed in R using a one-way ANOVA or non-parametric Kruskal–Wallis rank sum test. Post-hoc pairwise comparisons were performed using the pairwise t or Wilcoxon tests. Differences were considered significant at $p<0.05$. Western blot quantifications were performed with ImageJ (National Institutes of Health, USA). Graphs and plots were created using the ggplot2 R package. Oncoprints were generated with the ComplexHeatmap R package. Chemical structures were drawn using ChemDraw (PerkinElmer). Illustrations were generated using Adobe Illustrator or Inkscape. Sequence alignments were generated using multiple sequence alignment (msa) R and texshade LaTeX packages.

Appendix A

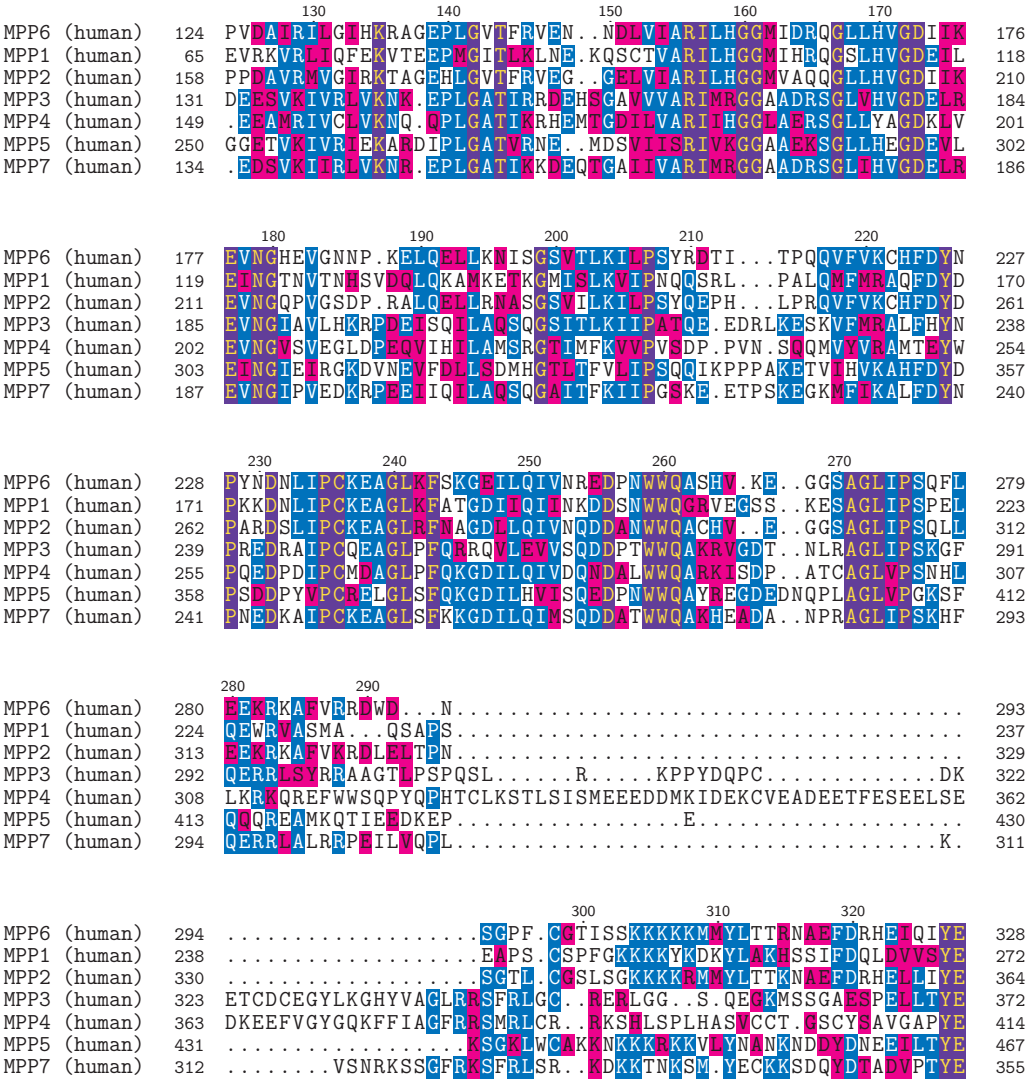


Appendix A: Schematics of the lentiviral vectors used in this thesis. (**A**) pZIP is a lentiviral Tet-On vector for doxycycline-inducible short hairpin RNA (shRNA) expression. In the presence of doxycycline. the Tet-On® 3G reverse tetracycline transactivator activates the tetracycline-inducible promoter (TRE3GS) which in turn drives expression of the shRNA and green fluorescent protein (GFP) reporter genes. Constitutive expression of the Tet-On® 3G and puromycin resistance (PuroR) genes is driven by the human phosphoglycerate kinase and SV40 promoters, respectively (**B**) The pTIPZ vector is a derivative of the commercially available pTRIPZ™ vector. In the presence of doxycycline, the reverse tetracycline transactivator (rtTA) binds to and thereby activates the tetracycline-inducible promotor (TRE), which in turn induces expression of the gene of interest (GOI). Constitutive expression of the rtTA as well as the puromycin resistance (PuroR) genes is driven by the human ubiquitin C (UBC) promoter. The internal ribosomal entry site (IRES) allows expression of rtTA and the puromycin resistance genes in a single transcript. (**C**) The pTIBZ vector is identical to the pTIPZ vector except for the blasticidin resistance gene which has replaced the puromycin resistance gene. (**D**) The QM800A-Blast lentiviral vector contains a constitutively expressed repressor (CymR), driven by the EF1αpromoter, that binds to the cumate operator sequence (CuO). Addition of cumate results in release of the CymR molecules, activation of the cumate inducible promoter and expression of the GOI. Constitutive expression of a blasticidin resistance gene (Blast) is driven by the T2A promoter. (**E**) The pIPZ vector is a derivative of the commercially available pGIPZ lentiviral vector. Constitutive expression of the GOI and puromycin resistance (PuroR) gene is driven by the human cytomegalovirus (CMV) promoter. (**F**) The pIHZ vector is identical to the pIPZ vector except for the hygromycin resistance (HygroR) gene which has replaced the puromycin resistance gene.

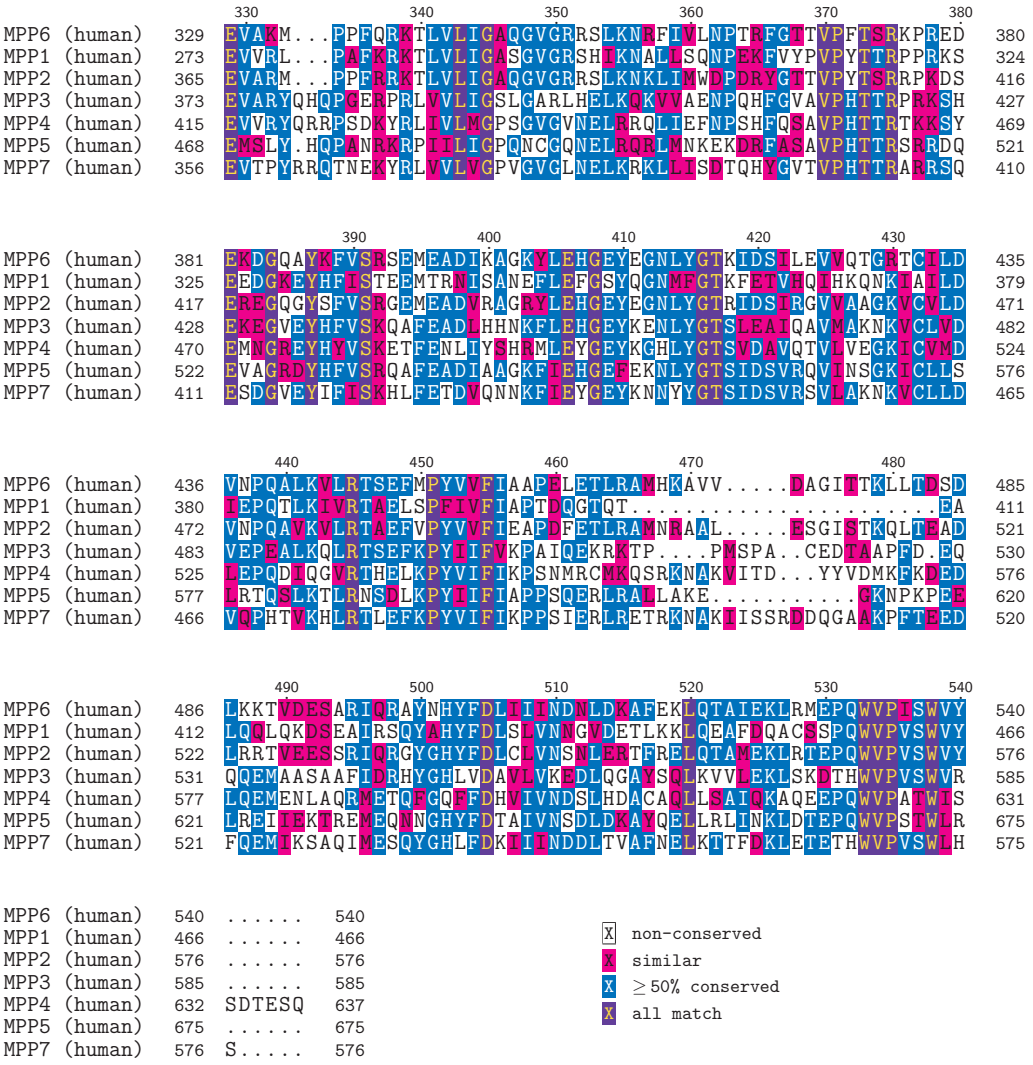
Appendix B



Appendix B: Sequence alignment of human MPPs. Amino acid alignment of human MPP6 (Q9NZW5), MPP1 (Q00013), MPP2 (Q14168), MPP3 (Q13368), MPP4 (Q96JB8), MPP5 (Q8N3R9) and MPP7 (Q5T2T1) – continued on next page.

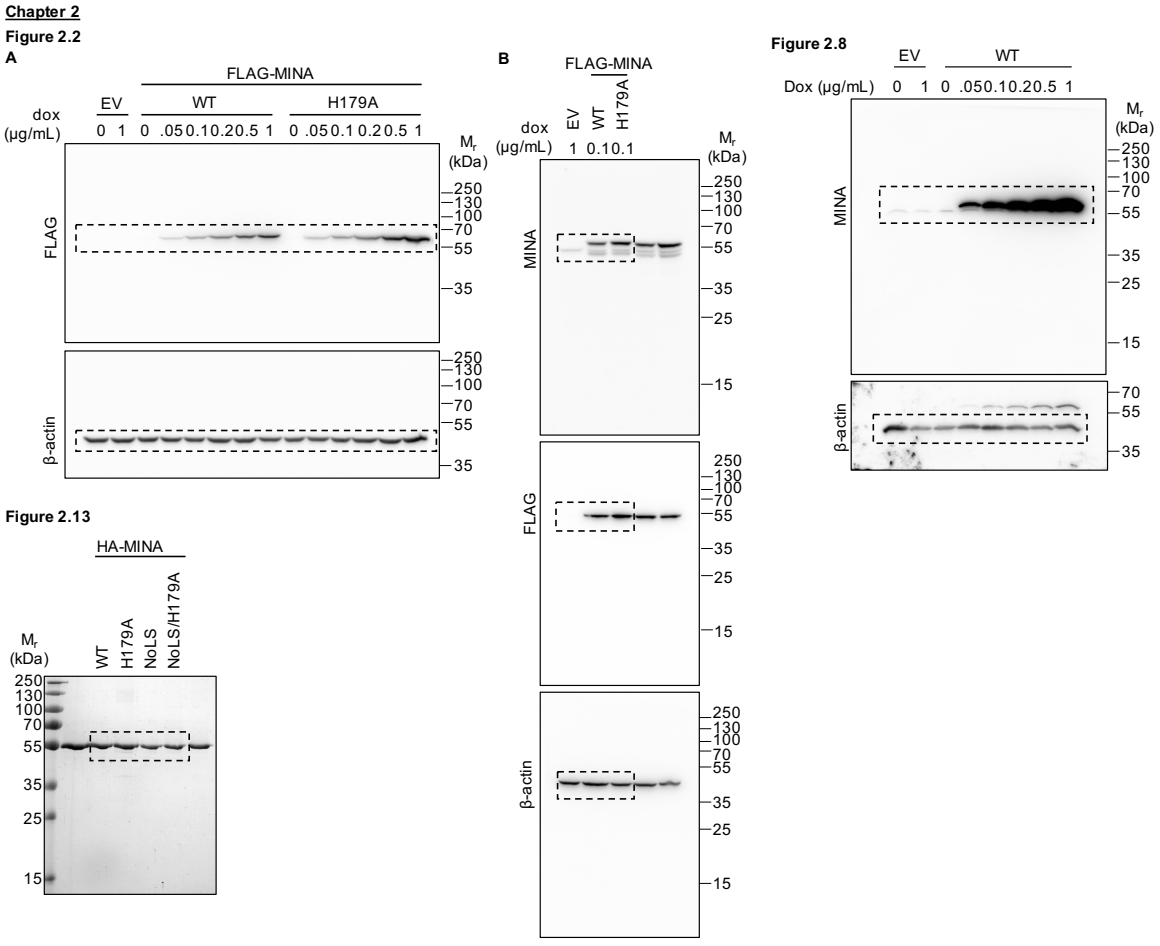


Appendix B: Sequence alignment of human MPPs – continued from previous page. Amino acid alignment of human MPP6 (Q9NZW5), MPP1 (Q00013), MPP2 (Q14168), MPP3 (Q13368), MPP4 (Q96JB8), MPP5 (Q8N3R9) and MPP7 (Q5T2T1) – continued on next page.

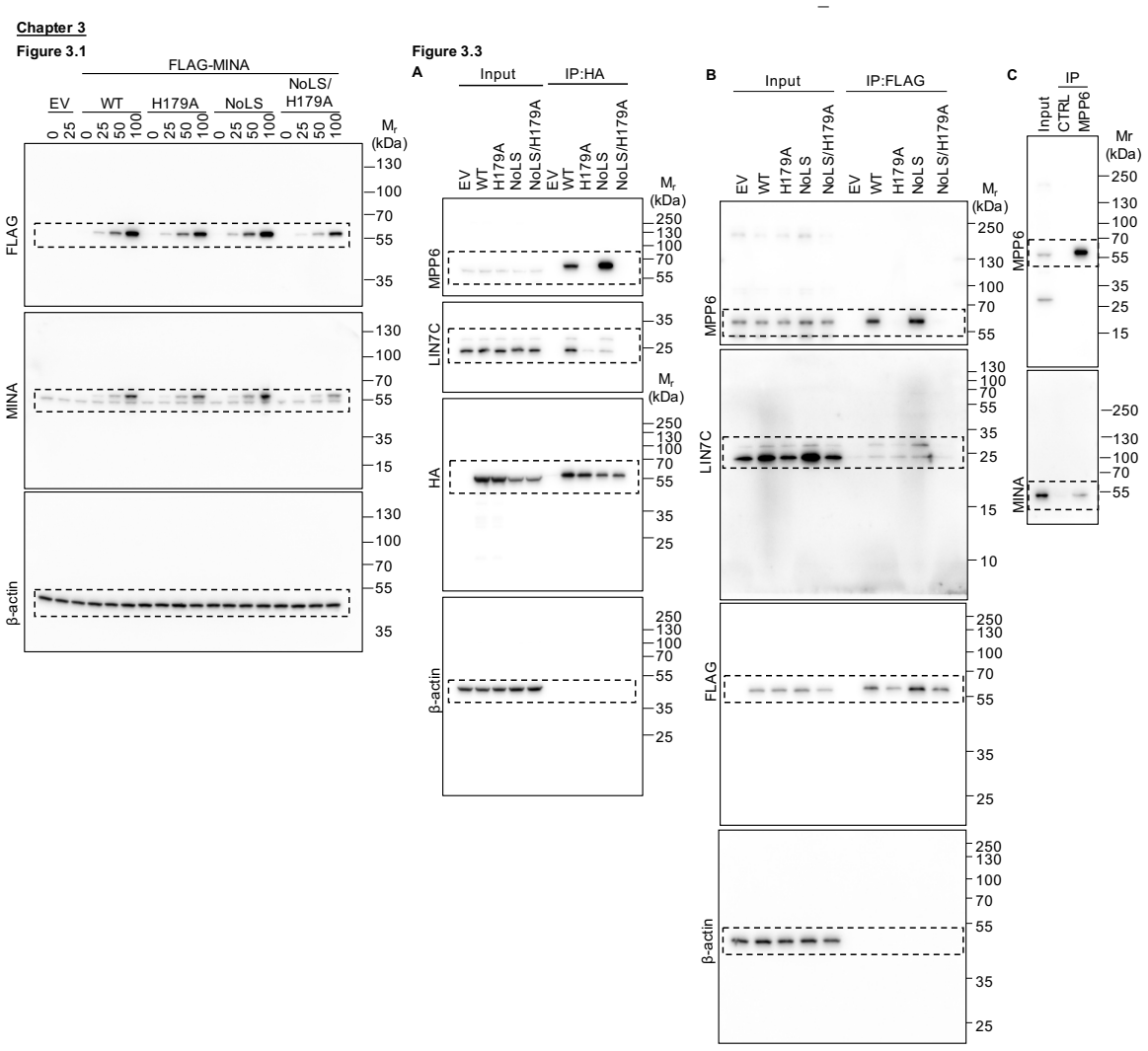


Appendix B: Sequence alignment of human MPPs – continued from previous page. Amino acid alignment of human MPP6 (Q9NZW5), MPP1 (Q00013), MPP2 (Q14168), MPP3 (Q13368), MPP4 (Q96JB8), MPP5 (Q8N3R9) and MPP7 (Q5T2T1).

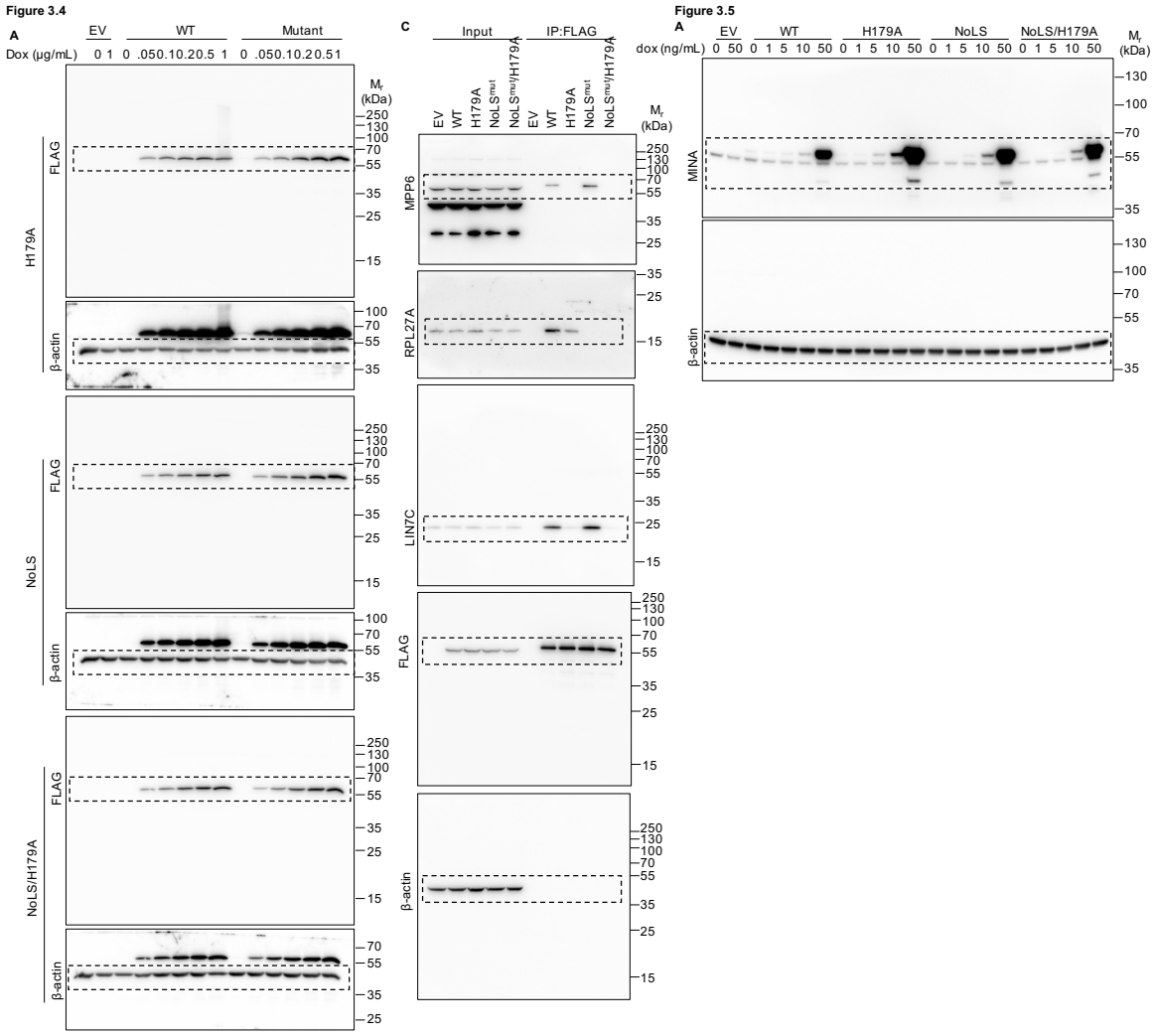
Appendix C



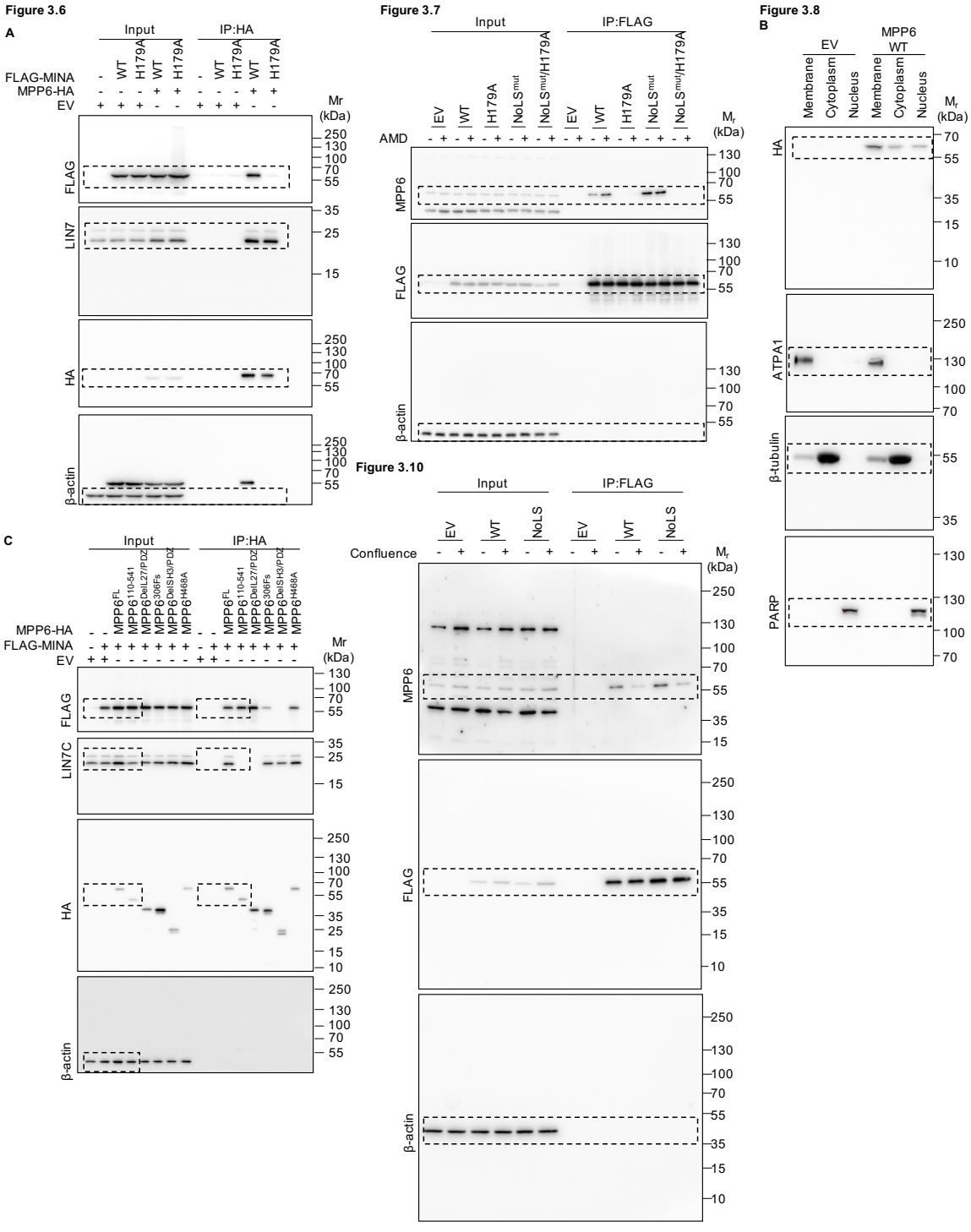
Appendix C: Uncropped western blot images.



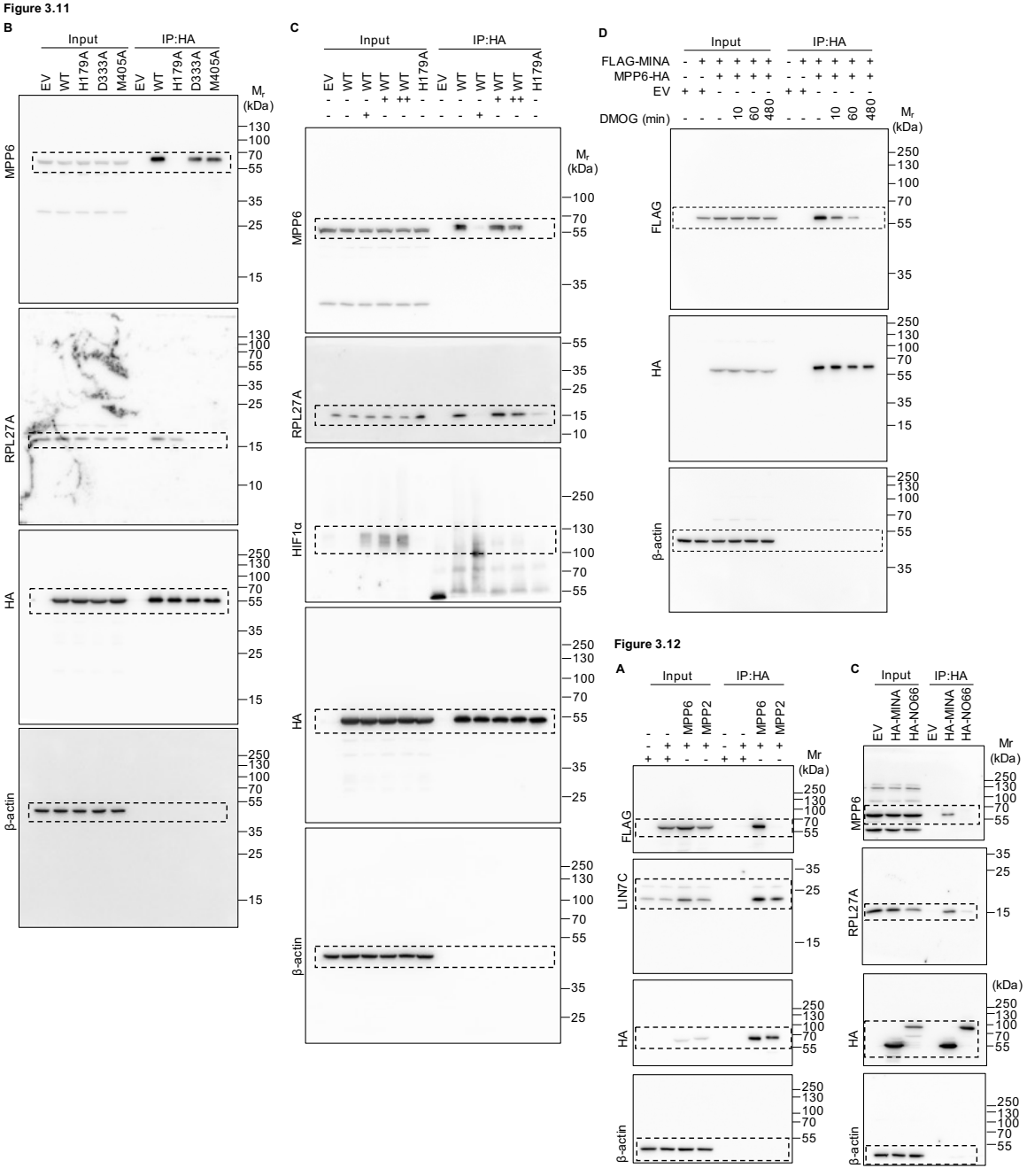
Appendix C: Uncropped western blot images.



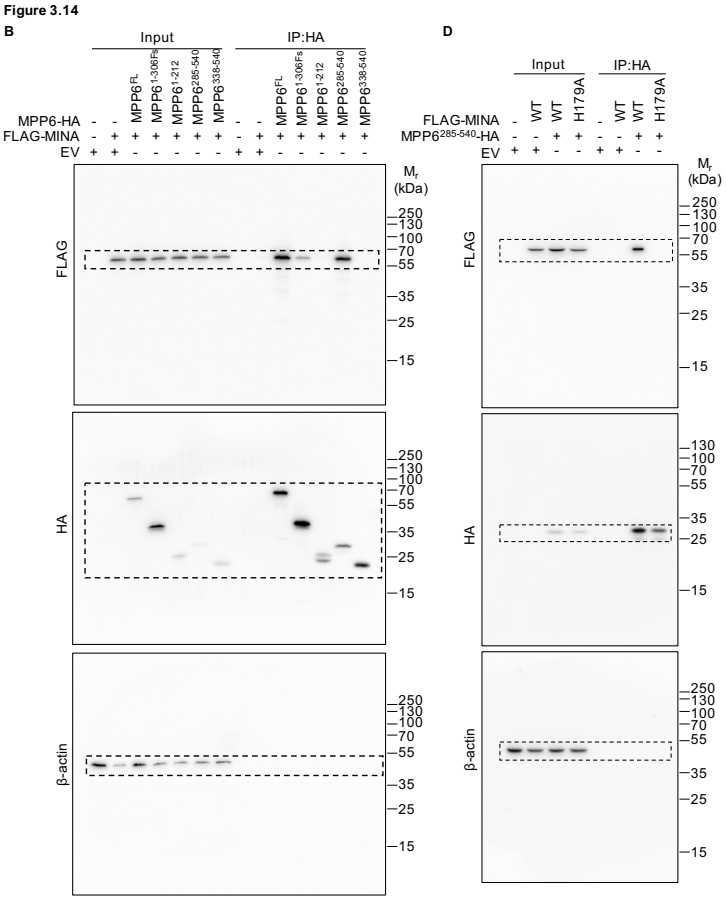
Appendix C: Uncropped western blot images.

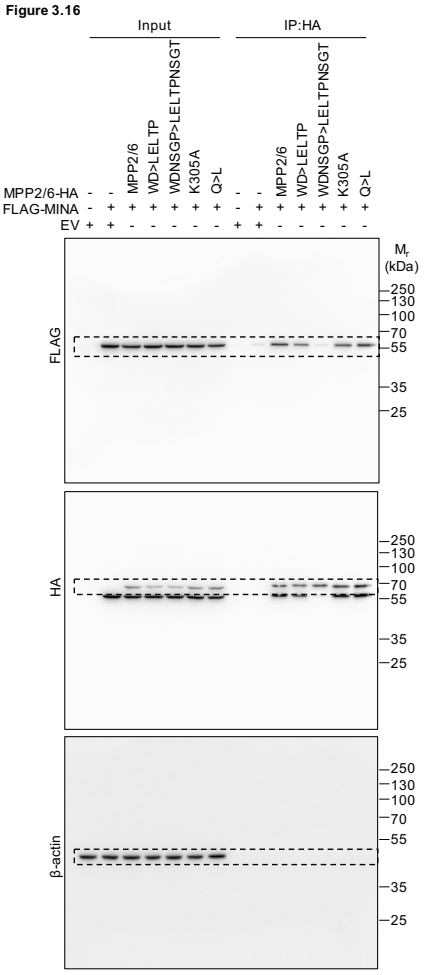


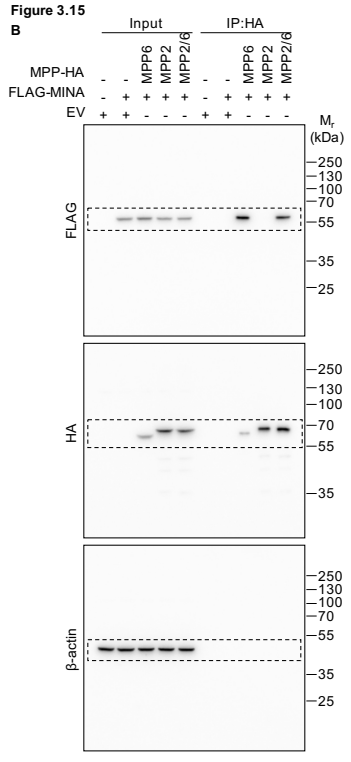
Appendix C: Uncropped western blot images.

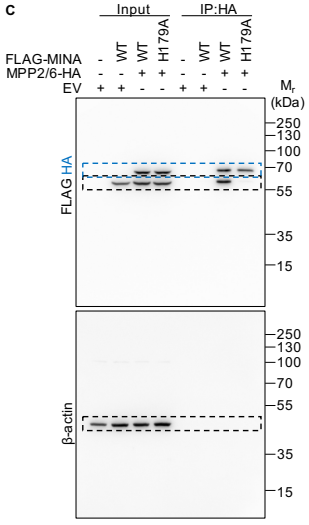


Appendix C: Uncropped western blot images.

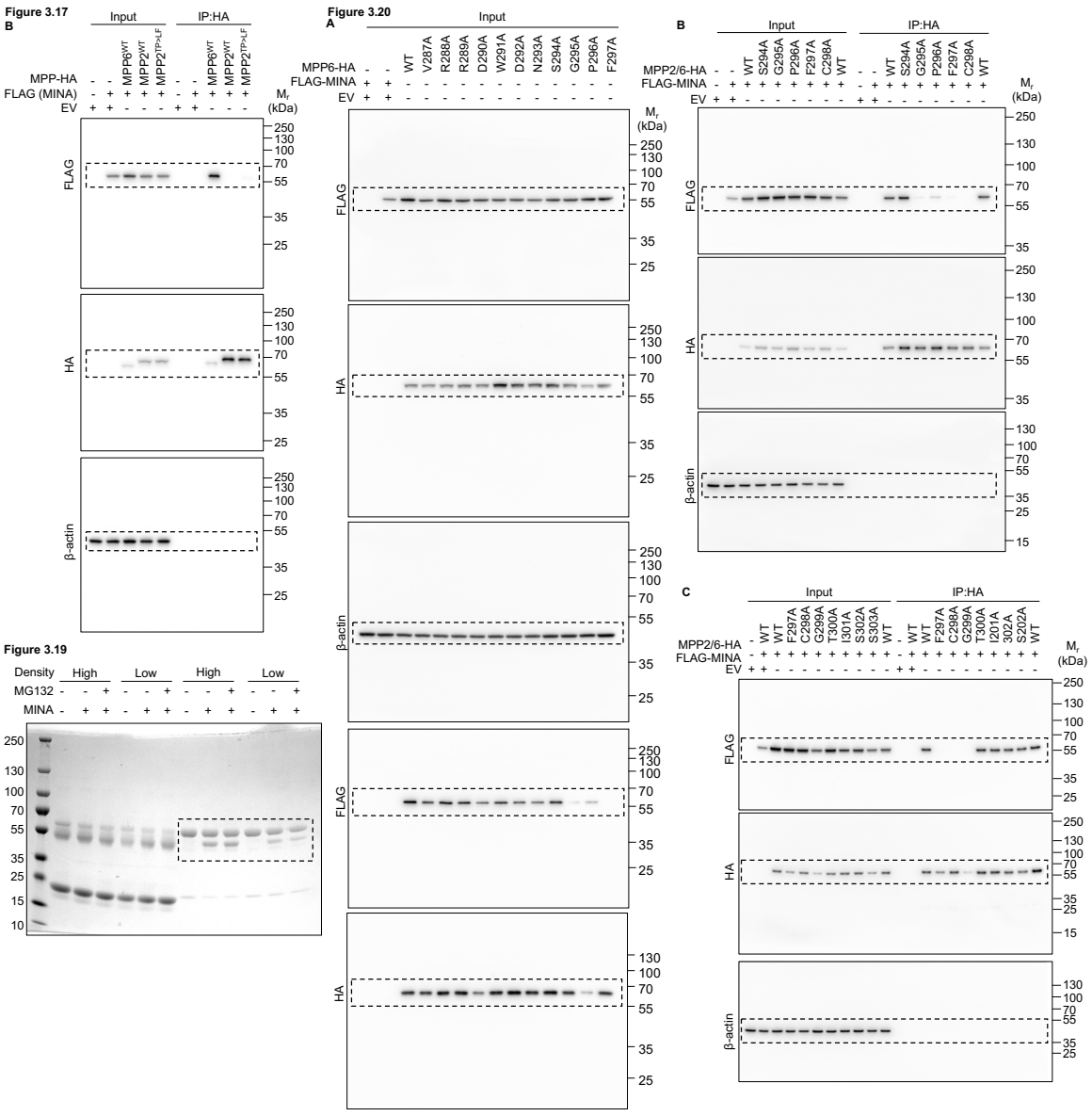








Appendix C: Uncropped western blot images.



Appendix C: Uncropped western blot images.

Figure 4.4

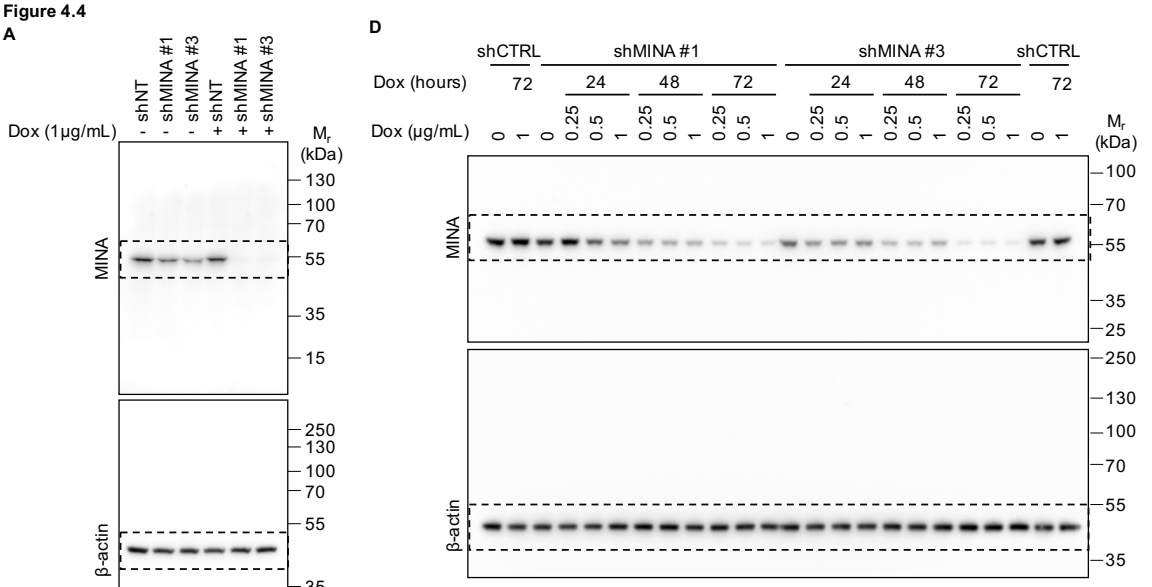


Figure 4.5

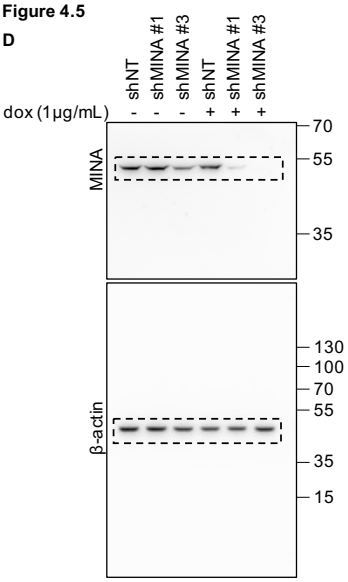
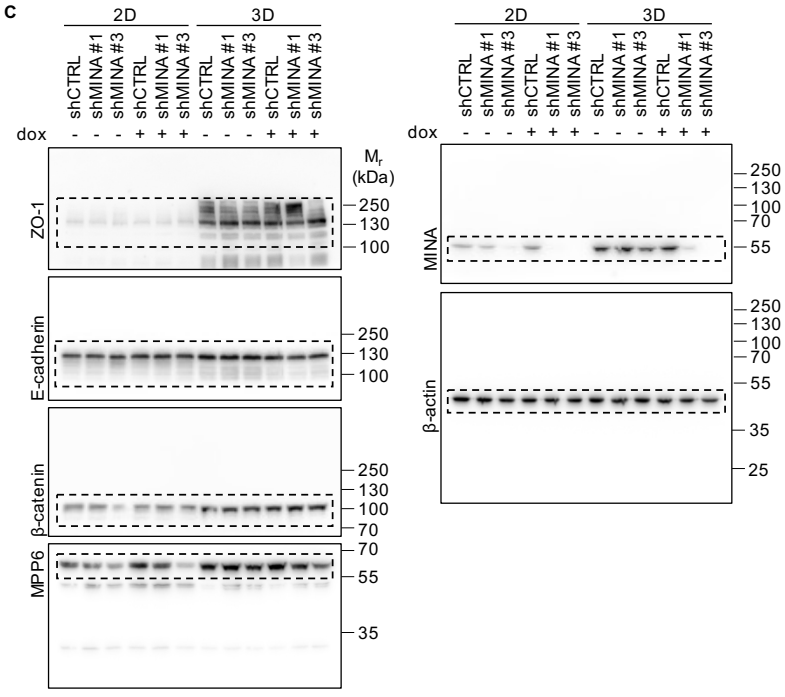
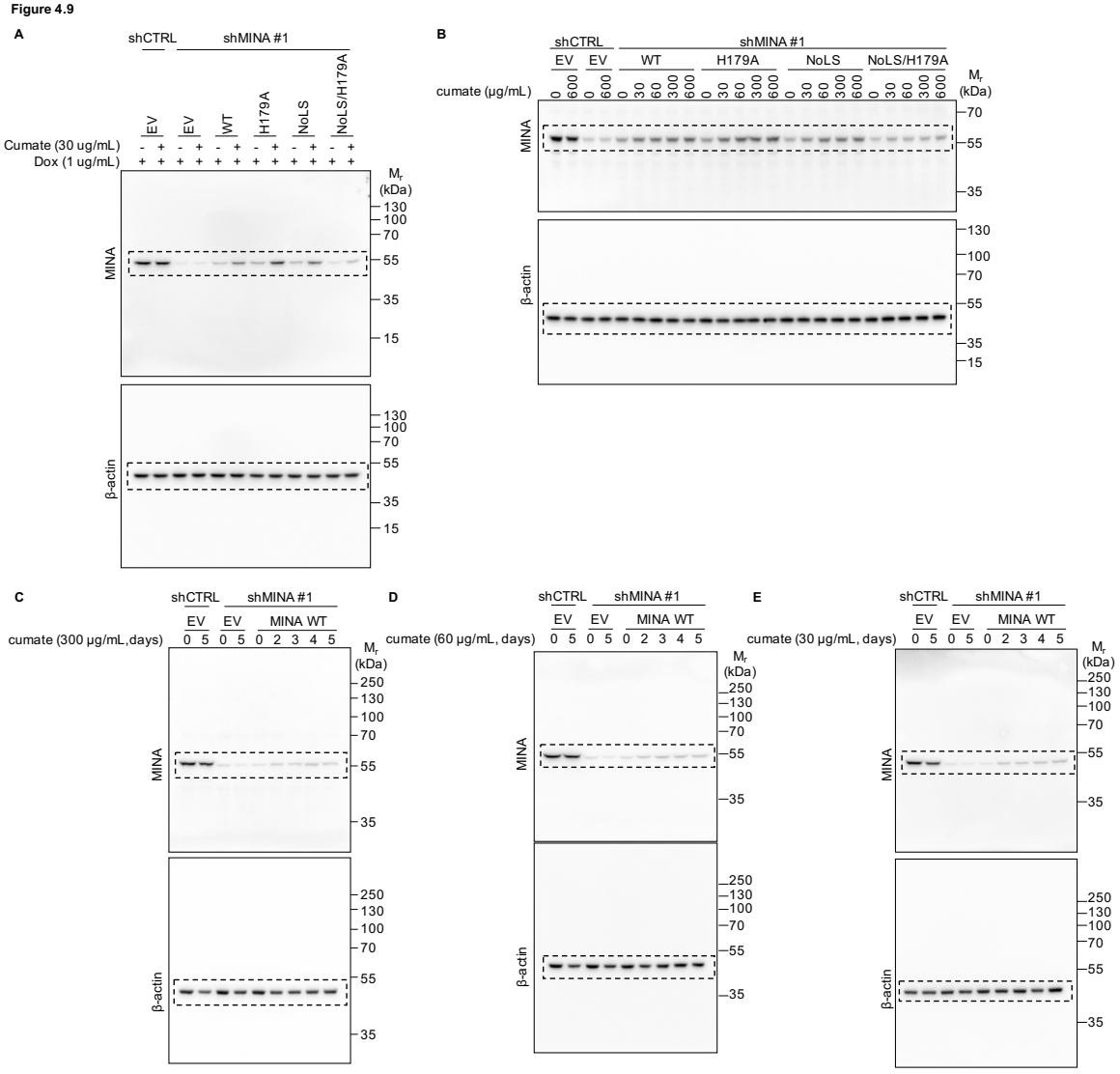


Figure 4.8



Appendix C: Uncropped western blot images.



Appendix C: Uncropped western blot images.

Figure 4.10

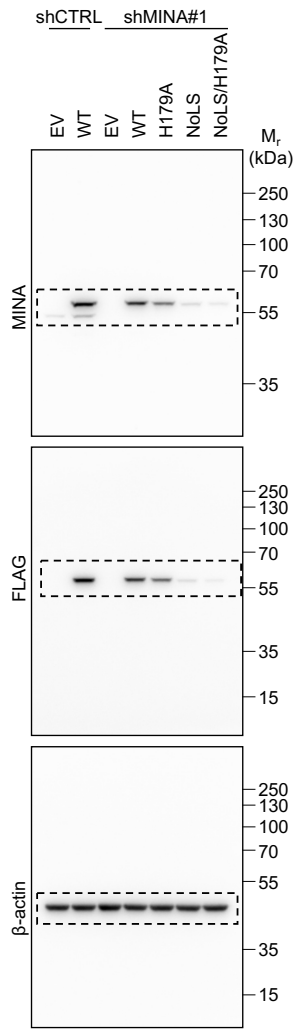
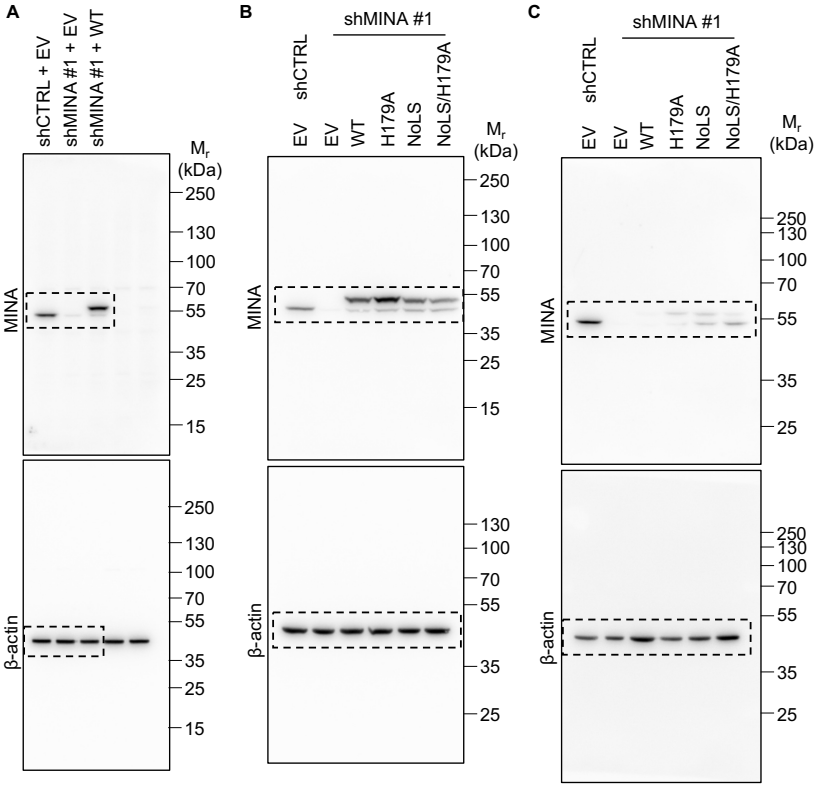
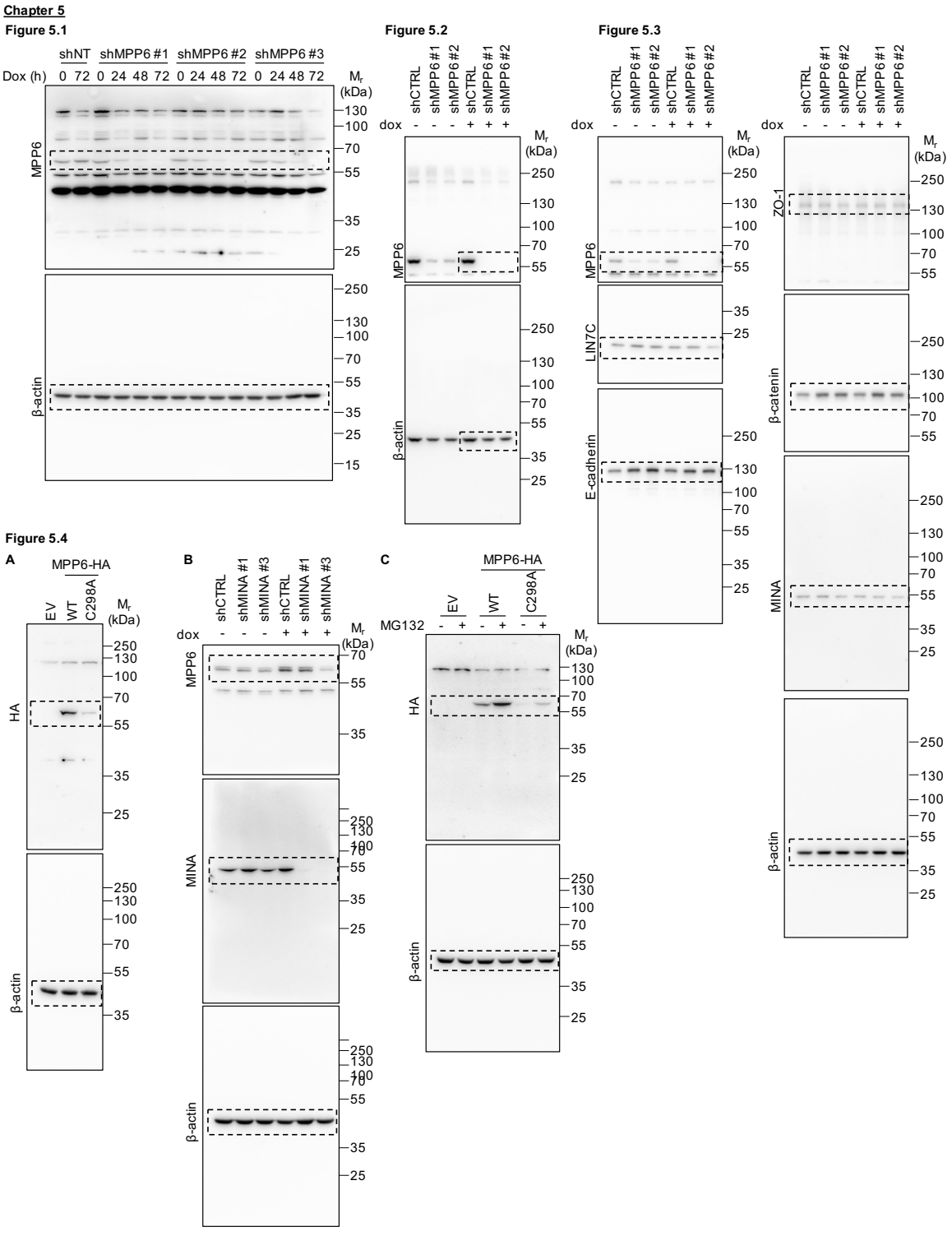


Figure 4.13



Appendix C: Uncropped western blot images.



Appendix C: Uncropped western blot images.

Bibliography

S. M. Ahmed and I. G. Macara. Mechanisms of polarity protein expression control. *Current Opinion in Cell Biology*, 42:38–45, 2016.

S. Alahari, M. Post, and I. Caniggia. Jumonji domain-containing protein 6: a novel oxygen sensor in the human placenta. *Endocrinology*, 156(8):3012–3025, 2015.

S. Alahari, M. Post, A. Rolfo, R. Weksberg, and I. Caniggia. Compromised JMJD6 histone demethylase activity affects VHL gene repression in preeclampsia. *Journal of Clinical Endocrinology and Metabolism*, 103(4):1545–1557, 2018.

E. Z. Alkalaeva, A. V. Pisarev, L. Y. Frolova, L. L. Kisselev, and T. V. Pestova. In vitro reconstitution of eukaryotic translation reveals cooperativity between release factors eRF1 and eRF3. *Cell*, 125(6):1125–1136, 2006.

N. Alloisio, N. Dalla Venezia, A. Rana, K. Andrabi, P. Texier, F. Gilsanz, J. P. Cartron, J. Delaunay, and A. H. Chishti. Evidence that red blood cell protein p55 may participate in the skeleton-membrane linkage that involves protein 4.1 and glycophorin C. *Blood*, 82:1323–1327, 1993.

P. G. Amendola, N. Zaghet, J. J. Ramalho, J. J. Vilstrup, M. Boxem, and A. E. Salcini. JMJD-5/KDM8 regulates H3K36me2 and is required for late steps of homologous recombination and genome integrity. *PLoS Genetics*, 13(2), 2017.

J. S. Andersen, Y. W. Lam, A. K. L. Leung, S. Ong, C. E. Lyon, A. I. Lamond, and M. Mann. Nucleolar proteome dynamics. *Nature*, 433(7021):77–83, 2005.

O. Aprelikova, K. Chen, L. H. El Touny, C. Brignatz-Guittard, J. Han, T. Qiu, H. H. Yang, M. P. Lee, M. Zhu, and J. E. Green. The epigenetic modifier JMJD6 is amplified in mammary tumors and cooperates with c-Myc to enhance cellular transformation, tumor progression, and metastasis. *Clinical Epigenetics*, 8(38), 2016.

E. Assémat, E. Bazellières, E. Pallesi-Pocachard, A. Le Bivic, and D. Massey-Harroche. Polarity complex proteins. *Biochimica et Biophysica Acta*, 1778(3):614–630, 2008.

N. Aziz, Y. H. Hong, M. Jo, J. K. Kim, K. Kim, D. T. Smoot, H. Hur, B. C. Yoo, and J. Y. Cho. Molecular signatures of JMJD10/MINA53 in gastric cancer. *Cancers*, 12 (5), 2020.

N. Ban, R. Beckmann, J. H. Cate, J. D. Dinman, F. Dragon, S. R. Ellis, D. L. Lafontaine, L. Lindahl, A. Liljas, J. M. Lipton, M. A. McAlear, P. B. Moore, H. F. Noller, J. Ortega, V. G. Panse, V. Ramakrishnan, C. M. Spahn, T. A. Steitz,

M. Tchorzewski, D. Tollervey, A. J. Warren, J. R. Williamson, D. Wilson, A. Yonath, and M. Yusupov. A new system for naming ribosomal proteins. *Current Opinion in Structural Biology*, 24:165–169, 2014.

A. Bannister and T. Kouzarides. Regulation of chromatin by histone modifications. *Cell Research*, 21:381–395, 2011.

M. Baumgartner, A. Weiss, T. Fritzius, J. Heinrich, and K. Moelling. The PDZ protein MPP2 interacts with c-Src in epithelial cells. *Experimental Cell Research*, 315(17): 2888–2898, 2009.

G. J. Beitel and M. A. Krasnow. Genetic control of epithelial tube size in the Drosophila tracheal system. *Development*, 127(15):3271–3282, 2000.

J. Beumer and H. Clevers. Cell fate specification and differentiation in the adult mammalian intestine. *Nature Reviews Molecular Cell Biology*, 22(1):39–53, 2021.

J. Boeckel, A. Derlet, S. F. Glaser, A. Luczak, T. Lucas, A. W. Heumüller, M. Krüger, C. M. Zehendner, D. Kaluza, A. Doddaballapur, K. Ohtani, K. Treguer, and S. Dimmeler. JMJD8 regulates angiogenic sprouting and cellular metabolism by interacting with pyruvate kinase M2 in endothelial cells. *Arteriosclerosis, Thrombosis, and Vascular Biology*, 36(7):1425–1433, 2016.

J. N. Boeckel, V. Guarani, M. Koyanagi, T. Roexe, A. Lengeling, R. T. Schermuly, P. Gellert, T. Braun, A. Zeiher, and S. Dimmeler. Jumonji domain-containing protein 6 (Jmjd6) is required for angiogenic sprouting and regulates splicing of VEGF-receptor 1. *Proceedings of the National Academy of Sciences*, 108(8):3276–3281, 2011.

J. Bohl, N. Brimer, C. Lyons, and S. B. Vande Pol. The stardust family protein MPP7 forms a tripartite complex with LIN7 and DLG1 that regulates the stability and localization of DLG1 to cell junctions. *Journal of Biological Chemistry*, 282(13): 9392–9400, 2007.

J. Böse, A. D. Gruber, L. Helming, S. Schiebe, I. Wegener, M. Hafner, M. Beales, F. Köntgen, and A. Lengeling. The phosphatidylserine receptor has essential functions during embryogenesis but not in apoptotic cell removal. *Journal of Biology*, 3 (4):15, 2004.

S. Boulon, B. J. Westman, S. Hutten, F. M. Boisvert, and A. I. Lamon. The nucleolus under stress. *Molecular Cell*, 40(2):P216–227, 2010.

K. E. Bräuer, K. Brockers, J. Moneer, A. Feuchtinger, E. Wollscheid-lengeling, A. Lengeling, and A. Wolf. Phylogenetic and genomic analyses of the ribosomal oxygenases Riox1 (No66) and Riox2 (Mina53) provide new insights into their evolution. *BMC Developmental Biology*, 18(96), 2018.

G. L. Brien, G. Gambero, D. J. O'Connell, E. Jerman, S. A. Turner, C. M. Egan, E. J. Dunne, M. C. Jurgens, K. Wynne, L. Piao, A. J. Lohan, N. Ferguson, X. Shi, K. M. Sinha, B. J. Loftus, G. Cagney, and A. P. Bracken. Polycomb PHF19 binds H3K36me3 and recruits PRC2 and demethylase NO66 to embryonic stem cell genes during differentiation. *Nature Structural and Molecular Biology*, 19(12):1273–1281, 2012.

R. K. Bruick and S. L. McKnight. A conserved family of prolyl-4-hydroxylases that modify HIF. *Science*, 294(55545):1337–1340, 2001.

D. M. Bryant and K. E. Mostov. From cells to organs: building polarized tissue. *Nature Reviews Molecular Cell Biology*, 9(11):887–901, 2008.

N. A. Bulgakova and E. Knust. The Crumbs complex: from epithelial-cell polarity to retinal degeneration. *Journal of Cell Science*, 122(15):2587–2596, 2009.

J. R. Bundred, E. Hendrix, and M. L. Coleman. The emerging roles of ribosomal histidyl hydroxylases in cell biology, physiology and disease. *Cellular and Molecular Life Sciences*, 75(22):4093–4105, 2018.

K. M. Cadigan and M. L. Waterman. TCF/LEFs and Wnt signaling in the nucleus. *Cold Sping Harbor Perspectives in Biology*, 4(11):a007906, 2012.

H. K. Campbell, J. L. Maiers, and K. A. DeMali. Interplay between tight junctions and adherens junctions. *Experimental Cell Research*, 358(1):39–44, 2017.

I. D. Campbell and P. Bork. Epidermal growth factor-like modules. *Current Opinion in Structural Biology*, 3:385–392, 1993.

C. T. Capaldo and I. G. Macara. Depletion of E-cadherin disrupts establishment but not maintenance of cell junctions in Madin-Darby Canine Kidney epithelial cells. *Molecular Biology of the Cell*, 18:189–200, 2007.

P. Chandramouli, M. Topf, J. Ménétret, N. Eswar, J. J. Cannone, R. R. Gutell, A. Sali, and C. W. Akey. Structure of the mammalian 80S ribosome at 8.7 A resolution. *Structure*, 16(4):535–548, 2008.

B. Chang, Y. Chen, Y. Zhao, and R. K. Bruick. Jmjd6 is a histone arginine demethylase. *Science*, 317:444–447, 2007.

C. F. Chen, X. Feng, H. Y. Liao, W. J. Jin, J. Zhang, Y. Wang, L. L. Gong, J. J. Liu, X. H. Yuan, B. B. Zhao, D. Zhang, G. F. Chen, Y. Wan, J. Guo, H. P. Yan, and Y. W. He. Regulation of T cell proliferation by JMJD6 and PDGF-BB during chronic hepatitis B infection. *Scientific Reports*, 4(6359), 2014.

Y. Chen, X. Yang, Y. Huang, E. Liu, and L. Wang. Normal associations of the single-nucleotide polymorphisms of the mina gene with the development of asthma in Chinese Han children: A case–control study. *Genetic Testing and Molecular Biomarkers*, 15(7-8):531–536, 2011.

H. Choi, A. P. Hardy, T. M. Leissing, R. Chowdhury, Y. Nakashima, W. Ge, M. Markoulides, J. S. Scotti, P. A. Gerken, H. Thorbjornsrud, D. Kang, S. Hong, J. Lee, M. A. McDonough, H. Park, and C. J. Schofield. A human protein hydroxylase that accepts *D*-residues. *Communications Chemistry*, 3(52), 2020.

R. Chowdhury, R. Sekirnik, N. C. Brissett, T. Krojer, C. Ho, S. S. Ng, I. J. Clifton, W. Ge, N. J. Kershaw, G. C. Fox, J. R. C. Muniz, M. Vollmar, C. Phillips, E. S. Pilka, K. L. Kavanagh, F. von Delft, U. Oppermann, M. A. McDonough, A. J. Doherty, and C. J. Schofield. Ribosomal oxygenases are structurally conserved from prokaryotes to humans. *Nature*, 510:422–426, 2014.

A. Chytła, W. Gajdzik-Nowak, P. Olszewska, A. Biernatowska, A. F. Sikorski, and A. Czogalla. Not just another scaffolding protein family: the multifaceted MPPs. *Molecules*, 25(21):4954, 2020.

M. Cikala, O. Alexandrova, C. N. David, M. Pröschel, B. Stiening, P. Cramer, and A. Böttger. The phosphatidylserine receptor from Hydra is a nuclear protein with potential Fe(II)-dependent oxygenase activity. *BMC Cell Biology*, 5(26), 2004.

I. J. Clifton, M. A. H. McDonough, Michael A, D. Ehrismann, N. J. Kershaw, N. Granatino, and C. J. Schofield. Structural studies on 2-oxoglutarate oxygenases and related double-stranded beta-helix fold proteins. *Journal of Inorganic Biochemistry*, 100(4):644–669, 2006.

M. E. Cockman, D. E. Lancaster, I. P. Stolze, K. S. Hewitson, M. A. McDonough, M. L. Coleman, C. H. Coles, K. Yu, R. T. Hay, S. C. Ley, C. W. Pugh, N. J. Oldham, N. Masson, C. J. Schofield, and P. J. Ratcliffe. Posttranslational hydroxylation of ankyrin repeats in IκB proteins by the hypoxia-inducible factor (HIF) asparaginyl hydroxylase, factor inhibiting HIF (FIH). *Proceedings of the National Academy of Sciences*, 103(40):14767–14772, 2006.

M. E. Cockman, J. D. Webb, H. B. Kramer, B. M. Kessler, and P. J. Ratcliffe. Proteomics-based identification of novel factor inhibiting hypoxia-inducible factor (FIH) substrates indicates widespread asparaginyl hydroxylation of ankyrin repeat domain-containing proteins. *Molecular and Cellular Proteomics*, 8(3):535–546, 2009.

M. E. Cockman, K. Lippl, Y. Tian, H. B. Pegg, W. D. J. Figg, M. I. Abboud, R. Heilig, R. Fischer, J. Myllyharju, C. J. Schofield, and P. J. Ratcliffe. Lack of activity of recombinant HIF prolyl hydroxylases (PHDs) on reported non-HIF substrates. *eLife*, 8:e46490, 2019.

M. L. Coleman, M. A. McDonough, K. S. Hewitson, C. Coles, J. Mecinović, M. Edelmann, K. M. Cook, M. E. Cockman, D. E. Lancaster, B. M. Kessler, N. J. Oldham, P. J. Ratcliffe, and C. J. Schofield. Asparaginyl hydroxylation of the notch ankyrin repeat domain by factor inhibiting hypoxia-inducible factor. *Journal of Biological Chemistry*, 282(33):24027–24038, 2007.

H. Colvin, N. Nishida, M. Konno, N. Haraguchi, H. Takahashi, J. Nishimura, T. Hata, K. Kawamoto, A. Asai, K. Tsunekuni, J. Koseki, T. Mizushima, T. Satoh, Y. Doki, M. Mori, and H. Ishii. Oncometabolite d-2-hydroxyglurate directly induces epithelial-mesenchymal transition and is associated with distant metastasis in colorectal cancer. *Scientific Reports*, 6:36289, 2016.

Ş. Comşa, A. M. Cîmpean, and M. Raica. The story of MCF-7 breast cancer cell line: 40 years of experience in research. *Anticancer research*, 35(6):3147–3154, 2015.

T. R. Cox. The matrix in cancer. *Nature Reviews Cancer*, 2021.

P. Cui, B. Qin, N. Liu, G. Pan, and D. Pei. Nuclear localization of the phosphatidylserine receptor protein via multiple nuclear localization signals. *Experimental Cell Research*, 293:154–163, 2004.

S. M. de la Monte, S. Tamaki, M. C. Cantarini, N. Ince, M. Wiedmann, J. J. Carter, S. A. Lahousse, S. Califano, T. Maeda, T. Ueno, A. D'Errico, F. Trevisani, and J. R. Wands. Aspartyl-(asparaginyl)-beta-hydroxylase regulates hepatocellular carcinoma invasiveness. *Journal of Hepatology*, 44(5):971–983, 2006.

P. A. Del Rizzo, S. Krishnan, and R. C. Trievel. Crystal structure and functional analysis of JMJD5 indicate an alternate specificity and function. *Molecular and Cellular Biology*, 32(19):4044–4052, 2012.

M. Derenzini, L. Montanaro, and D. Treré. What the nucleolus says to a tumour pathologist. *Histopathology*, 54(6):753–762, 2009.

J. Dinchuk, R. Focht, J. Kelley, N. Henderson, N. Zolotarjova, R. Wynn, N. Neff, J. Link, R. Huber, T. Burn, M. Rupar, M. Cunningham, B. Selling, J. Ma, A. Stern, G. Hollis, R. Stein, and P. Friedman. Absence of post-translational aspartyl β-hydroxylation of epidermal growth factor domains in mice leads to developmental defects and an increased incidence of intestinal neoplasia. *Journal of Biological Chemistry*, 277(15):12970–12977, 2002.

X. Ding, H. Pan, J. Li, Q. Zhong, X. Chen, S. M. Dry, and C. Wang. Epigenetic activation of AP1 promotes squamous cell carcinoma metastasis. *Science Signaling*, 6(273), 2013.

X. Dong, Q. Lin, A. Aihara, Y. Li, C. Huang, W. Chung, Q. Tang, X. Chen, R. Carlson, C. Nadolny, G. Gabriel, M. Olsen, and J. R. Wands. Aspartate β-Hydroxylase expression promotes a malignant pancreatic cellular phenotype. *Oncotarget*, 6(2): 1231–1248, 2015.

A. Dongre and R. A. Weinberg. New insights into the mechanisms of epithelial-mesenchymal transition and implications for cancer. *Nature Reviews Molecular Cell Biology*, 20(2):69–84, 2019.

D. Drygin, A. Linm, J. Bliesath, C. B. Ho, S. E. O'Brien, C. Proffitt, M. Omori, M. Haddach, M. K. Schwaebe, A. Siddiqui-Jain, N. Streiner, J. E. Quin, E. Sanij, M. J. Bywater, R. D. Hannan, D. Ryckman, K. Anderes, and W. G. Rice. Targeting RNA polymerase I with an oral small molecule CX-5461 inhibits ribosomal RNA synthesis and solid tumor growth. *Cancer Research*, 71(4):1418–1430, 2011.

J. J. Dudok, A. S. Sanz, D. M. Lundvig, V. Sothilingam, M. Garcia Garrido, J. Klooster, M. W. Seeliger, and J. Wijnholds. MPP3 regulates levels of PALS1 and adhesion between photoreceptors and Müller cells. *Glia*, 61(10):1629–1644, 2013.

M. Duechler, G. Leszczyńska, E. Sochacka, and B. Nawrot. Nucleoside modifications in the regulation of gene expression: focus on tRNA. *Cellular and Molecular Life Sciences*, 73:3075–3095, 2016.

T. Duncan, S. C. Trewick, K. Pertti, P. A. Bates, T. Lindahl, and B. Sedgwick. Reversal of DNA alkylation damage by two human dioxygenases. *Proceedings of the National Academy of Sciences*, 99(26):16660–16665, 2002.

J. Durgan, N. Kaji, D. Jin, and A. Hall. Par6B and atypical PKC regulate mitotic spindle orientation during epithelial morphogenesis. *Journal of Biological Chemistry*, 286(14):12461–12474, 2011.

K. T. Ebata, K. Mesh, S. Liu, M. Bilenky, A. Fekete, M. G. Acker, M. Hirst, B. A. Garcia, and M. Ramalho-Santos. Vitamin C induces specific demethylation of H3K9me2 in mouse embryonic stem cells via Kdm3a/b. *Epigenetics Chromatin*, 10(36), 2017.

J. Eilbracht, M. Reichenzeller, M. Hergt, M. Schnölzer, H. Heid, M. Stöhr, W. W. Franke, and M. S. Schmidt-Zachmann. NO66, a highly conserved dual location protein in the nucleolus and in a special type of synchronously replicating chromatin. *Molecular Biology of the Cell*, 15:1816–1832, 2004.

J. Eilbracht, S. Kneissel, A. Hofmann, and M. S. Schmidt-Zachmann. Protein NO52-a constitutive nucleolar component sharing high sequence homologies to protein NO66. *European Journal of Cell Biology*, 84(2-3):279–294, 2005.

A. C. Epstein, J. M. Gleadle, L. A. McNeill, K. S. Hewitson, J. O'Rourke, D. R. Mole, M. Mukherji, E. Metzen, M. I. Wilson, A. Dhanda, Y. M. Tian, N. Masson, D. L. Hamilton, P. Jaakkola, R. Barstead, J. Hodgkin, P. H. Maxwell, C. W. Pugh, C. J. Schofield, , and P. J. Ratcliffe. C. elegans EGL-9 and mammalian homologs define a family of dioxygenases that regulate HIF by prolyl hydroxylation. *Cell*, 197:43–54, 2001.

V. A. Fadok, D. L. Bratton, D. M. Rose, A. Pearson, R. A. Ezekewitz, and P. M. Henson. A receptor for phosphatidylserine-specific clearance of apoptotic cells. *Nature*, 405:85–90, 2000.

P. O. Falnes, R. F. Johansen, and E. Seeberg. AlkB-mediated oxidative demethylation reverses DNA damage in Escherichia coli. *Nature*, 419(6903):178–182, 2002.

A. S. Fanning, B. J. Jameson, L. A. Jesaitis, and J. M. Anderson. The tight junction protein ZO-1 establishes a link between the transmembrane protein occludin and the actin cytoskeleton. *Journal of Biological Chemistry*, 273(45):29745–29753, 1998.

T. Feng, A. Yamamoto, S. E. Wilkins, E. Sokolova, L. A. Yates, M. Münzel, P. Singh, R. J. Hopkinson, R. Fischer, M. E. Cockman, J. Shelley, D. C. Trudgian, J. Schödel, J. S. McCullagh, W. Ge, B. M. Kessler, R. J. Gilbert, L. Y. Frolova, E. Alkalaeva, P. J. Ratcliffe, C. J. Schofield, and M. L. Coleman. Optimal translational termination requires C4 lysyl hydroxylation of eRF1. *Molecular Cell*, 53:645–654, 2014.

W. Feng, M. Yonezawa, J. Ye, T. Jenuwein, and I. Grummt. PHF8 activates transcription of rRNA genes through H3K4me3 binding and H3K9me1/2 demethylation. *Nature Structural and Molecular Biology*, 17(4):445–450, 2010.

J. E. Ferguson, Y. Wu, K. Smith, P. Charles, K. Powers, H. Wang, and C. Patterson. ASB4 is a hydroxylation substrate of FIH and promotes vascular differentiation via an oxygen-dependent mechanism. *Molecular and Cellular Biology*, 27(18):6407–6419, 2007.

S. C. Fletcher and M. L. Coleman. Human 2-oxoglutarate-dependent oxygenases: nutrient sensors, stress responders, and disease mediators. *Biochemical Society Transactions*, 48(5):1843–1858, 2020.

D. Frescas, D. Guardavaccaro, F. Bassermann, R. Koyama-Nasu, and M. Pagano. JHDM1B/FBXL10 is a nucleolar protein that represses transcription of ribosomal RNA genes. *Nature*, 450(7167):309–313, 2007.

Y. Fu, Q. Dai, W. Zhang, J. Ren, T. Pan, and C. He. The AlkB domain of mammalian ABH8 catalyzes hydroxylation of 5-methoxycarbonylmethyluridine at the wobble position of tRNA. *Angewandte Chemie International Edition*, 49(47):8885–8888, 2010.

D. Fuhrmann, M. Mernberger, A. Nist, T. Stiewe, and H. P. Elsässer. Miz1 controls Schwann cell proliferation via H3K36me2 demethylase Kdm8 to prevent peripheral nerve demyelination. *Journal of Neuroscience*, 38(4):858–877, 2018.

S. Fukahori, H. Yano, M. Tsuneoka, Y. Tanaka, M. Yagi, M. Kuwano, T. Tajiri, T. Taguchi, M. Tsuneyoshi, and M. Kojiro. Immunohistochemical expressions of Cap43 and Mina53 proteins in neuroblastoma. *Journal of Pediatric Surgery*, 42(11): 1831–1840, 2007.

H. Fukuhara, M. Masuda, M. Yageta, T. Fukami, M. Kuramochi, T. Maruyama, T. Kitamura, and Y. Murakami. Association of a lung tumor suppressor TSLC1 with MPP3, a human homologue of Drosophila tumor suppressor Dlg. *Oncogene*, 22(40): 6160–6165, 2003.

L. Funke, S. Dakoji, and D. S. Bredt. Membrane-associated guanylate kinases regulate adhesion and plasticity at cell junctions. *Annual Review of Biochemistry*, 74:219–245, 2005.

P. G. Gallagher. Hereditary elliptocytosis: Spectrin and protein 4.1R. *Seminars in Hematology*, 41(2):142–164, 2004.

W. W. Gao, R. Q. Xiao, B. L. Peng, H. T. Xu, H. F. Shen, M. F. Huang, T. T. Shi, J. Yi, W. J. Zhang, X. N. Wu, X. Gao, X. Z. Lin, P. C. Dorrestein, M. G. Rosenfeld, and W. Liu. Arginine methylation of HSP70 regulates retinoid acid-mediated RARβ2 gene activation. *Proceedings of the National Academy of Sciences*, 112(26):E3327–36, 2015.

W. Ge, A. Wolf, T. Feng, C. Ho, R. Sekirnik, A. Zayer, N. Granatino, M. E. Cockman, C. Loenarz, N. D. Loik, A. P. Hardy, T. D. W. Claridge, R. B. Hamed, R. Chowdhury, L. Gong, C. V. Robinson, D. C. Trudgian, M. Jiang, M. M. Mackeen, J. S. Mccullagh, Y. Gordiyenko, A. Thalhammer, A. Yamamoto, M. Yang, P. Liu-Yi, Z. Zhang, M. Schmidt-Zachmann, B. M. Kessler, P. J. Ratcliffe, G. M. Preston, M. L. Coleman, and C. J. Schofield. Oxygenase-catalyzed ribosome hydroxylation occurs in prokaryotes and humans. *Nature Chemical Biology*, 8:960–962, 2012.

F. Geng, Z. Jiang, X. Song, H. Zhou, and H. Zhao. Mdig suppresses epithelial-mesenchymal transition and inhibits the invasion and metastasis of non-small cell lung cancer via regulating GSK-3β/β-catenin signaling. *International Journal of Oncology*, 51(6):1898–1908, 2017.

E. R. Gibney and C. M. Nolan. Epigenetics and gene expression. *Heredity*, 105:4–13, 2010.

D. M. Gilkes, S. Bajpai, P. Chaturvedi, D. Wirtz, and G. L. Semenza. Hypoxia-inducible factor 1 (HIF-1) promotes extracellular matrix remodeling under hypoxic conditions by inducing *P4HA1, P4HA2* and *PLOD2* expression in fibroblasts. *Journal of Biological Chemistry*, 288(15):10819–10829, 2013.

R. A. F. Gjaltema and R. A. Bank. Molecular insights into prolyl and lysyl hydroxylation of fibrillar collagens in health and disease. *Critical Reviews in Biochemistry and Molecular Biology*, 52(1):74–95, 2017.

M. V. C. Greenberg and D. Bourc'his. The diverse roles of DNA methylation in mammalian development and disease. *Nature Reviews Molecular Cell Biology*, 20: 590–606, 2019.

V. H. Haase. Oxygen regulates epithelial-to-mesenchymal transition: insights into molecular mechanisms and relevance to disease. *Kidney International*, 76(5):P492–499, 2009.

P. Hahn, I. Wegener, A. Burrells, J. Böse, A. Wolf, C. Erck, and D. Butler. Analysis of Jmjd6 cellular localization and testing for its involvement in histone demethylation. *PLoS ONE*, 5(10):e13769, 2010.

R. Halaoui and L. McCaffrey. Rewiring cell polarity signaling in cancer. *Oncogene*, 34 (8):939–950, 2015.

T. Hanada, A. Takeuchi, G. Sondarva, and A. H. Chishti. Protein 4.1-mediated membrane targeting of human Discs Large in epithelial cells. *Journal of Biological Chemistry*, 278(26):34445–34450, 2003.

D. S. Harburger and D. A. Calderwood. Integrin signalling at a glance. *Journal of Cell Science*, 122:159–163, 2009.

A. Hartsock and W. J. Nelson. Adherens and tight junctions: Structure, function and connection to the actin cytoskeleton. *Biochimica et Biophysica Acta*, 1776(3): 660–669, 2008.

G. He, R. A. Shankar, M. Chzhan, A. Samouilov, P. Kuppusamy, and J. L. Zweier. Noninvasive measurement of anatomic structure and intraluminal oxygenation in the gastrointestinal tract of living mice with spatial and spectral EPR imaging. *Proceedings of the National Academy of Sciences*, 96(8):4586– 4591, 1999.

Z. He, J. Wu, X. Su, Y. Zhang, L. Pan, H. Wei, Q. Fang, H. Li, D. L. Wang, and F. L. Sun. JMJD5 (Jumonji Domain-containing 5) associates with spindle microtubules and is required for proper mitosis. *Journal of Biological Chemistry*, 291(9):4684–4697, 2016.

A. Heim, C. Grimm, U. Müller, S. Häußler, M. M. Mackeen, J. Merl, S. M. Hauck, B. M. Kessler, C. J. Schofield, A. Wolf, and A. Böttger. Jumonji domain containing protein 6 (Jmjd6) modulates splicing and specifically interacts with arginine–serine-rich (RS) domains of SR- and SR-like proteins. *Nucleic Acids Research*, 42(12): 7833–7850, 2014.

K. S. Hewitson, L. A. McNeill, M. V. Riordan, Y. M. Tian, A. N. Bullock, R. W. Welford, J. M. Elkins, N. J. Oldham, S. Bhattacharya, J. M. Gleadle, P. J. Ratcliffe, C. W. Pugh, and C. J. Schofield. Hypoxia-inducible factor (HIF) asparagine hydroxylase is identical to factor inhibiting HIF (FIH) and is related to the cupin structural family. *Journal of Biological Chemistry*, 277(29):26351–26355, 2002.

K. S. Hewitson, S. L. Holmes, D. Ehrismann, A. P. Hardy, R. Chowdhury, C. J. Schofield, and M. A. McDonough. Evidence that two enzyme-derived histidine ligands are sufficient for iron binding and catalysis by factor inhibiting HIF (FIH). *Journal of Biological Chemistry*, 283(38):25971–25978, 2008.

X. Hong, J. Zang, J. White, C. Wang, C. H. Pan, R. Zhao, R. C. Murphy, S. Dai, P. Henson, J. W. Kappler, J. Hagman, and G. Zhang. Interaction of JMJD6 with single-stranded RNA. *Proceedings of the National Academy of Sciences*, 107(33): 14568–14572, 2010.

S. Horita, J. S. Scotti, C. Thinnes, Y. S. Mottaghi-Taromsari, A. Thalhammer, W. Ge, W. Aik, C. Loenarz, C. J. Schofield, and M. A. McDonough. Structure of the ribosomal oxygenase OGFOD1 provides insights into the regio- and stereoselectivity of prolyl hydroxylases. *Structure*, 23(4):639 – 652, 2015.

I. Horresh, S. Poliak, S. Grant, D. Bredt, M. N. Rasband, and E. Peles. Multiple molecular interactions determine the clustering of Caspr2 and Kv1 channels in myelinated axons. *Journal of Neuroscience*, 28(52):14213–22, 2008.

C. House and B. E. Kemp. Protein kinase C contains a pseudosubstrate prototope in its regulatory domain. *Science*, 238(4834):1726–1728, 1987.

D. A. Hsia, C. G. Tepper, M. R. Pochampalli, E. Y. Hsia, C. Izumiya, S. B. Huerta, M. Wright, H. Chen, H. Kung, and Y. Izumiya. KDM8, a H3K36me2 histone demethylase that acts in the cyclin A1 coding region to regulate cancer cell proliferation. *Proceedings of the National Academy of Sciences*, 107(21):9671–9676, 2010.

Y. P. Hsueh, T. F. Wang, F. C. Yang, and M. Sheng. Nuclear translocation and transcription regulation by the membrane-associated guanylate kinase CASK/LIN-2. *Nature*, 404(6775):298–302, 2000.

H. S. Huang, P. Pozarowski, Y. Gao, Z. Darzynkiewicz, and E. Y. Lee. Protein phosphatase-1 inhibitor-3 is co-localized to the nucleoli and centrosomes with PP1gamma1 and PP1alpha, respectively. *Archives of Biochemistry and Biophysics*, 443(1-2):33–44, 2005.

X. Huang, L. Zhang, H. Qi, J. Shao, and J. Shen. Identification and functional implication of nuclear localization signals in the n-terminal domain of JMJD5. *Biochimie*, 95(11):2114–2122, 2013.

X. Huang, S. Zhang, H. Qi, Z. Wang, H. W. Chen, J. Shao, and J. Shen. JMJD5 interacts with p53 and negatively regulates p53 function in control of cell cycle and proliferation. *Biochimica et Biophysica Acta*, 1853(10 Pt A):2286–2295, 2015.

Q. Huo, C. Ge, H. Tian, J. Sun, M. Cui, H. Li, F. Zhao, T. Chen, H. Xie, Y. Cui, M. Yao, and J. Li. Dysfunction of IKZF1/MYC/MDIG axis contributes to liver cancer progression through regulating H3K9me3/p21 activity. *Cell Death and Disease*, 8(5), 2017.

S. Iden, W. E. van Riel, R. Schäfer, Y. Song, and Y. Hirose. Tumor type-dependent function of the Par3 polarity protein in skin tumorigenesis. *Cancer Cell*, 22(3): P389–403, 2012.

K. Imami, M. Milek, B. Bogdanow, T. Yasuda, N. Kastelic, H. Zauber, Y. Ishihama, M. Landthaler, and M. Selbach. Phosphorylation of the ribosomal protein RPL12/uL11 affects translation during mitosis. *Molecular Cell*, 72(1):84–98, 2018.

Y. Ishihama, Y. Oda, T. Tabata, T. Sato, T. Nagasu, J. Rappsilber, and M. Mann. Exponentially modified protein abundance index (emPAI) for estimation of absolute protein amount in proteomics by the number of sequenced peptides per protein. *Molecular and Cellular Proteomics*, 4(9):1265 – 1272, 2005.

K. Ishikawa, S. Azuma, S. Ikawa, Y. Morishita, J. Gohda, T. Akiyama, K. Semba, and J. i. Inoue. Cloning and characterization of Xenopus laevis drg2, a member of the developmentally regulated GTP-binding protein subfamily. *Gene*, 322:105–112, 2003.

A. Ishimura, K. Minehata, M. Terashima, G. Kondoh, T. Hara, and T. Suzuki. Jmjd5, an H3K36me2 histone demethylase, modulates embryonic cell proliferation through the regulation of Cdkn1a expression. *Development*, 139(4):749–759, 2012.

A. Ishimura, M. Terashima, S. Tange, and T. Suzuki. Jmjd5 functions as a regulator of p53 signaling during mouse embryogenesis. *Cell and Tissue Research*, 363(3): 723–733, 2016.

H. Ishizaki, H. Yano, M. Tsuneoka, S. Ogasawara, J. Akiba, N. Nishida, S. Kojiro, S. Fukahori, F. Moriya, K. Matsuoka, and M. Kojiro. Overexpression of the myc target gene Mina53 in advanced renal cell carcinoma. *Pathology International*, 57 (10):672–680, 2007.

S. Islam, T. M. Leissing, R. Chowdhury, R. J. Hopkinson, and C. J. Schofield. 2-oxoglutarate-dependent oxygenases. *Annual Review of Biochemistry*, 87(15):1–36, 2018.

S. Islam, M. A. McDonough, R. Chowdhury, J. Gault, A. Khan, E. Pires, and C. J. Schofield. Biochemical and structural investigations clarify the substrate selectivity of the 2-oxoglutarate oxygenase JMJD6. *Journal of Biological Chemistry*, 294(30): 11637–11652, 2019.

S. Ito, L. Shen, Q. Dai, S. C. Wu, L. B. Collins, J. A. Swenberg, C. He, and Y. Zhang. Tet proteins can convert 5-methylcytosine to 5-formylcytosine and 5-carboxylcytosine. *Science*, 333(6047):1300–1303, 2011.

T. Ito, A. Nakamura, I. Tanaka, Y. Tsuboi, T. Morikawa, J. Nakajima, D. Takai, M. Fukayama, Y. Sekido, T. Niki, D. Matsubara, and Y. Murakami. CADM1 associates with Hippo pathway core kinases; membranous co-expression of CADM1 and LATS2 in lung tumors predicts good prognosis. *Cancer Science*, 110(7):2284–2295, 2019.

M. Ivan, K. Kondo, H. Yang, W. Kim, J. Valiando, M. Ohh, A. Salic, J. M. Asara, W. S. Lane, and W. G. Kaelin. HIFα targeted for VHL-mediated destruction by proline hydroxylation: Implications for O2 sensing. *Science*, 292(5516):464–468, 2001.

P. Jaakkola, D. R. Mole, Y. M. Tian, M. I. Wilson, J. Gielbert, S. J. Gaskell, A. von Kriegsheim, H. H. F, M. Mukherji, C. J. Schofield, P. H. Maxwell, C. W. Pugh, and R. P. J. Targeting of HIFα to the von Hippel-Lindau ubiquitylation complex by O2-regulated prolyl hydroxylation. *Science*, 292(5516):468–472, 2001.

K. Jack, C. Bellodi, D. M. Landry, R. O. Niederer, A. Meskauskas, S. Musalgaonkar, N. Kopmar, O. Krasnykh, A. M. Dean, S. R. Thompson, D. Ruggero, and J. D. Dinman. rRNA pseudouridylation defects affect ribosomal ligand binding and translational fidelity from yeast to human cells. *Molecular Cell*, 44(4):660–666, 2011.

A. B. Jaffe, N. Kaji, J. Durgan, and A. Hall. Cdc42 controls spindle orientation to position the apical surface during epithelial morphogenesis. *Journal of Cell Biology*, 183(4):625–633, 2008.

M. Jarvius, J. Paulsson, I. Weibrecht, K. Leuchowius, A. Andersson, C. Wählby, M. Gullberg, J. Botling, T. Sjöblom, B. Markova, A. Östman, U. Landegren, and O. Söderberg. *In situ* detection of phosphorylated platelet-derived growth factor receptor β using a generalized proximity ligation method. *Molecular and Cellular Proteomics*, 6(9):P1500–1509, 2007.

G. Jia, Y. Fu, X. Zhao, Q. Dai, G. Zheng, Y. Yang, C. Yi, T. Lindahl, T. Pan, Y. G. Yang, and C. He. N6-methyladenosine in nuclear RNA is a major substrate of the obesity-associated FTO. *Nature Chemical Biology*, 7(12):885–887, 2011.

M. Jiang, Y. Ma, H. Cheng, X. Ni, L. Guo, Y. Xie, and Y. Mao. Molecular cloning and characterization of a novel human gene (HSPBAP1) from human fetal brain. *Cytogenetic and Genome Research*, 95(1-2):48–51, 2001.

C. Johansson, A. Tumber, K. Che, P. Cain, R. Nowak, C. Gileadi, and U. Oppermann. The roles of Jumonji-type oxygenases in human disease. *Epigenomics*, 6(1):89–120, 2014.

M. A. Jones, M. F. Covington, L. DiTacchio, C. Vollmers, S. Panda, and S. L. Harmer. Jumonji domain protein JMJD5 functions in both the plant and human circadian systems. *Proceedings of the National Academy of Sciences*, 107(50):21623–21628, 2010.

W. G. Kaelin. Common pitfalls in preclinical cancer target validation. *Nature Reviews Cancer*, 17(7):441–450, 2017.

S. Kakunaga, W. Ikeda, S. Itoh, M. Deguchi-Tawarada, T. Ohtsuka, A. Mizoguchi, and Y. Takai. Nectin-like molecule-1/TSLL1/SynCAM3: A neural tissue-specific immunoglobulin-like cell-cell adhesion molecule localizing at non-junctional contact sites of presynaptic nerve terminals, axons and glia cell processes. *Journal of Cell Science*, 118(6):1267–1277, 2005.

E. Kamberov, O. Makarova, M. Roh, A. Liu, D. Karnak, S. Straight, and B. Margolis. Molecular cloning and characterization of Pals, proteins associated with mLin-7. *Journal of Biological Chemistry*, 275(15):11425–11431, 2000.

A. Kamijo, Y. Saitoh, N. Ohno, S. Ohno, and N. Terada. Immunohistochemical study of the membrane skeletal protein, membrane protein palmitoylated 6 (MPP6), in the mouse small intestine. *Histochemistry and Cell Biology*, 145(1):81–92, 2016.

Y. Kanke, M. Saito, N. Abe, K. Saito, A. Goto, T. Ohtake, Y. Murakami, and K. Kono. Expression profile of CADM1 and CADM4 in triple negative breast cancer with primary systemic therapy. *Oncology Letters*, 17(1):921–926, 2019.

A. Kantardzhieva, I. Gosens, S. Alexeeva, I. M. Punte, I. Versteeg, E. Krieger, C. A. Neefjes-Mol, A. I. den Hollander, S. J. Letteboer, J. Klooster, F. P. Cremers, R. Roepman, and J. Wijnholds. MPP5 recruits MPP4 to the CRB1 complex in photoreceptors. *Investigative Ophthalmology and Visual Science*, 46(6):2192–2201, 2005.

M. Kato, Y. Araiso, A. Noma, A. Nagao, T. Suzuki, R. Ishitani, and O. Nureki. Crystal structure of a novel JmjC-domain-containing protein, TYW5, involved in tRNA modification. *Nucleic Acids Research*, 39(4):1576–1585, 2011.

M. J. Katz, J. M. Acevedo, C. Loenarz, D. Galagovsky, P. Liu-Yi, M. Pérez-Pepe, A. Thalhammer, R. Sekirnik, W. Ge, M. Melani, M. G. Thomas, S. Simonetta, G. L. Boccaccio, C. J. Schofield, M. E. Cockman, P. J. Ratcliffe, and P. Wappner. Sudestada1, a Drosophila ribosomal prolyl-hydroxylase required for mRNA translation, cell homeostasis, and organ growth. *Proceedings of the National Academy of Sciences*, 111(11):4025–4030, 2014.

M. Kazemie. The importance of Escherichia coli ribosomal proteins L1, L11 and L16 for the association of ribosomal subunits and the formation of the 70-S initiation complex. *European Journal of Biochemistry*, 58:501–510, 1975.

R. Khoueiry, A. Sohni, B. Thienpont, X. Luo, J. Vande Velde, M. Bartoccetti, B. Boeckx, A. Zwijsen, A. Rao, D. Lambrechts, and K. P. Koh. Lineage-specific functions of TET1 in the postimplantation mouse embryo. *Nature Genetics*, 49(7): 1061–1072, 2017.

I. Kim, S. Shin, J. E. Lee, and J. Park. Oxygen sensor FIH inhibits HACE1-dependent ubiquitination of Rac1 to enhance metastatic potential in breast cancer cells. *Oncogene*, 38:3651–3666, 2019.

J. H. Kim, S. M. Lee, J. H. Lee, S. Chun, B. H. Kang, S. Kwak, J. S. Roe, T. W. Kim, H. Kim, W. H. Kim, E. J. Cho, and H. D. Youn. OGFOD1 is required for breast cancer cell proliferation and is associated with poor prognosis in breast cancer. *Oncotarget*, 6(23):19528–19541, 2015.

K. I. Kivirikko and D. J. Prockop. Enzymatic hydroxylation of proline and lysine in protocollagen. *Proceedings of the National Academy of Sciences*, 57(3):782–789, 1967.

R. J. Klose, E. M. Kallin, and Y. Zhang. JmjC-domain-containing proteins and histone demethylation. *Nature Reviews Genetics*, 7:715–727, 2006.

K. Komiya, N. Sueoka-Aragane, A. Sato, T. Hisatomi, T. Sakuragi, M. Mitsuoka, T. Sato, S. Hayashi, H. Izumi, M. Tsuneoka, and E. Sueoka. Expression of Mina53, a novel c-Myc target gene, is a favorable prognostic marker in early stage lung cancer. *Lung Cancer*, 69(2):232–238, 2010.

S. Kumar and P. H. Reddy. MicroRNA-455-3p as a potential biomarker for Alzheimer's Disease: An update. *Frontiers in Aging Neuroscience*, 10(41), 2018.

S. A. Kumar, C. Thakur, L. Li, H. Cui, and F. Chen. Pathological and prognostic role of mdig in pancreatic cancer. *Genes and Cancer*, 8(7-8):650–658, 2017.

K. Kuratomi, H. Yano, M. Tsuneoka, K. Sakamoto, J. Kusukawa, and M. Kojiro. Immunohistochemical expression of Mina53 and Ki67 proteins in human primary gingival squamous cell carcinoma. *Kurume Medical Journal*, 53:71–78, 2006.

S. Lagies, M. Schlimpert, S. Neumann, A. Wäldin, B. Kammerer, C. Borner, and L. Peintner. Cells grown in three-dimensional spheroids mirror in vivo metabolic response of epithelial cells. *Communications Biology*, 3(246), 2020.

D. E. Lancaster, M. A. McDonough, and C. J. Schofield. Factor inhibiting hypoxia-inducible factor (FIH) and other asparaginyl hydroxylases. *Biochemical Society Transactions*, 32(6):943–945, 2004.

D. Lando, D. J. Peet, J. J. Gorman, D. A. Whelan, M. L. Whitelaw, and R. K. Bruick. FIH-1 is an asparaginyl hydroxylase enzyme that regulates the transcriptional activity of hypoxia-inducible factor. *Genes and Development*, 16(12):1466–1471, 2002.

P. Laprise, K. M. Lau, K. P. Harris, N. F. Silva-Gagliardi, S. M. Paul, S. Beronja, G. J. Beitel, C. J. McGlade, and U. Tepass. Yurt, Coracle, Neurexin IV and the Na(+),K(+)-ATPase from a novel group of epithelial polarity proteins. *Nature*, 459 (7250):1141–1145, 2009.

P. Lawrence, J. S. Conderino, and E. Rieder. Redistribution of demethylated RNA helicase A during foot-and-mouth disease virus infection: role of Jumonji C-domain containing protein 6 in RHA demethylation. *Virology*, 452:1–11, 2014.

A. Lechanteur, A. Almeida, and B. Sarmento. Elucidation of the impact of cell culture conditions of Caco-2 cell monolayer on barrier integrity and intestinal permeability. *European Journal of Pharmaceutics and Biopharmaceutics*, 119:137–141, 2017.

C. R. Lee, S. H. Lee, N. K. Rigas, R. H. Kim, M. K. Kang, N. H. Park, and K. H. Shin. Elevated expression of JMJD6 is associated with oral carcinogenesis and maintains cancer stemness properties. *Carcinogenesis*, 37(2):119–128, 2016.

Y. F. Lee, L. D. Miller, X. B. Chan, M. A. Black, B. Pang, C. W. Ong, M. Salto-Tellez, E. T. Liu, and K. V. Desai. JMJD6 is a driver of cellular proliferation and motility and a marker of poor prognosis in breast cancer. *Breast Cancer Research*, 14(3):R85, 2012.

F. Lessard, F. Morin, S. Ivanchuk, F. Langlois, V. Stefanovsky, J. Rutka, and T. Moss. The ARF tumor suppressor controls ribosome biogenesis by regulating the RNA polymerase I transcription factor TTF-I. *Molecular Cell*, 38:539–550, 2010.

P. Li, S. Gao, L. Wang, F. Yu, J. Li, C. Wang, J. Li, and J. Wong. ABH2 couples regulation of ribosomal DNA transcription with DNA alkylation repair. *Cell Reports*, 4(4):817–829, 2013.

Y. Li, Y. Wei, Z. Yan, Q. Du, and M. Zhang. Structure of Crumbs tail in complex with the PALS1 PDZ-SH3-GUK tandem reveals highly specific assembly mechanism for the apical Crumbs complex. *Proceedings of the National Academy of Sciences*, 111 (49):17444–17449, 2014.

C. Liu, R. R. Gilmont, R. Benndorf, and M. J. Welsh. Identification and characterization of a novel protein from Sertoli cells, PASS1, that associates with mammalian small stress protein hsp27. *Journal of Biological Chemistry*, 275(25):18724–18731, 2000.

L. Liu and M. C. Simon. Regulation of transcription and translation by hypoxia. *Cancer Biology and Therapy*, 3(6):492–497, 2004.

X. Liu, W. Si, X. Liu, L. He, J. Ren, Z. Yang, J. Yang, W. Li, S. Liu, F. Pei, X. Yang, and L. Sun. JMJD6 promotes melanoma carcinogenesis through regulation of the alternative splicing of PAK1, a key MAPK signaling component. *Molecular Cancer*, 16(1):175, 2017.

H. Lodish, A. Berk, C. A. Kaiser, M. Krieger, M. P. Scott, A. Bretscher, H. Ploegh, and P. Matsudaira. *Molecular cell biology*. Freeman, W. H., 6th edition, 2007.

C. Loenarz and C. J. Schofield. Physiological and biochemical aspects of hydroxylations and demethylations catalyzed by human 2-oxoglutarate oxygenases. *Trends in Biochemical Sciences*, 36(1):7–18, 2011.

C. Loenarz, R. Sekirnik, A. Thalhammer, W. Ge, E. Spivakovsky, M. M. Mackeen, M. A. McDonough, M. E. Cockman, B. M. Kessler, P. J. Ratcliffe, A. Wolf, and C. J. Schofield. Hydroxylation of the eukaryotic ribosomal decoding center affects translational accuracy. *Proceedings of the National Academy of Sciences*, 111(11): 4019–4024, 2014.

L. Lozovatsky, N. Abayasekara, S. Piawah, and Z. Walther. CASK deletion in intestinal epithelia causes mislocalization of LIN7C and the DLG1/Scrib polarity complex without affecting cell polarity. *Molecular Biology of the Cell*, 20(21):4489–4499, 2009.

D. Ma, D. Guo, W. Li, and H. Zhao. Mdig, a lung cancer-associated gene, regulates cell cycle progression through $p27^{KIP1}$. *Tumor Biology*, 36:6909–6917, 2015.

A. MacCallum, S. P. Hardy, and P. H. Everest. Campylobacter jejuni inhibits the absorptive transport functions of Caco-2 cells and disrupts cellular tight junctions. *Microbiology*, 151:2451–2458, 2005.

P. C. Mahon, K. Hirota, and G. L. Semenza. FIH-1: a novel protein that interacts with HIF-1α and VHL to mediate repression of HIF-1 transcriptional activity. *Genes and Development*, 15(20):2675–2686, 2001.

M. Mantri, T. Krojer, E. A. Bagg, C. Webby, D. S. Butler, G. Kochan, K. Kavanagh, U. Oppermann, M. McDonough, and C. J. Schofield. Crystal structure of the 2-oxoglutarate- and Fe(II)-dependent lysyl hydroxylase JMJD6. *Journal of Molecular Biology*, 401(2):211–222, 2010.

M. Mantri, N. D. Loik, R. B. Hamed, T. D. Claridge, J. S. McCullagh, and C. J. Schofield. The 2-oxoglutarate-dependent oxygenase JMJD6 catalyses oxidation of lysine residues to give 5S-hydroxylysine residues. *Chembiochem*, 12(4):531–434, 2011.

S. M. Marfatia, R. A. Lue, D. Branton, and A. H. Chishti. Identification of the protein 4.1 binding interface on Glycophorin C and p55, a homologue of the *Drosophila discs-large* tumour suppressor protein. *Journal of Biological Chemistry*, 270(2):715–719, 1995.

J. M. Mariadason, D. Arango, G. A. Corner, M. J. Arañes, K. A. Hotchkiss, W. Yang, and L. H. Augenlicht. A gene expression profile that defines colon cell maturation in vitro. *Cancer Research*, 62(16):4791–4804, 2002.

S. Markolovic, T. M. Leissing, R. Chowdhury, S. E. Wilkins, X. Lu, and C. J. Schofield. Structure–function relationships of human JmjC oxygenases—demethylases versus hydroxylases. *Current Opinion in Structural Biology*, 41:62–72, 2016.

S. Markolovic, Q. Zhuang, S. E. Wilkins, C. D. Eaton, M. I. Abboud, M. J. Katz, H. E. Mcneil, R. K. Leśniak, C. Hall, W. B. Struwe, R. Konietzny, S. Davis, M. Yang, W. Ge, J. L. P. Benesch, B. M. Kessler, P. J. Ratcliffe, M. E. Cockman, R. Fischer, P. Wappner, R. Chowdhury, M. L. Coleman, and C. J. Schofield. The Jumonji-C oxygenase JMJD7 catalyzes (3S)-lysyl hydroxylation of TRAFAC GTPases. *Nature Chemical Biology*, 14:688–695, 2018.

D. M. Martindill, C. A. Risebro, N. Smart, M. Del Mar Franco-Viseras, C. O. Rosario, C. J. Swallow, J. W. Dennis, and P. R. Riley. Nucleolar release of hand1 acts as a molecular switch to determine cell fate. *Nature Cell Biology*, 9(10):1131–1141, 2007.

N. Masson, C. Willam, P. H. Maxwell, C. W. Pugh, and P. J. Ratcliffe. Independent function of two destruction domains in hypoxia-inducible factor-α chains activated by prolyl hydroxylation. *EMBO Journal*, 20(18):5197–5206, 2001.

P. H. Maxwell, M. S. Wiesener, G. W. Chang, S. C. Clifford, E. C. Vaux, M. E. Cockman, C. C. Wykoff, C. W. Pugh, E. R. Maher, and P. J. Ratcliffe. The tumour suppressor protein VHL targets hypoxia-inducible factors for oxygen-dependent proteolysis. *Nature*, 399:271–275, 1999.

M. A. McDonough, K. L. Kavanagh, D. Butler, T. Searls, U. Oppermann, and C. J. Schofield. Structure of human phytanoyl-Coa 2-hydroxylase identifies molecular mechanisms of Refsum disease. *Journal of Biological Chemistry*, 280(49):41101–41110, 2005.

K. D. Meyer and S. R. Jaffrey. The dynamic epitranscriptome: N6-methyladenosine and gene expression control. *Nature Reviews Molecular Cell Biology*, 15:313–326, 2014.

J. J. Miller, M. K. Summers, D. V. Hansen, M. V. Nachury, N. L. Lehman, A. Loktev, and P. K. Jackson. Emi1 stably binds and inhibits the anaphase-promoting complex/cyclosome as a pseudosubstrate inhibitor. *Genes and Development*, 20(17): 2410–2420, 2006.

T. E. Miller, B. B. Liau, L. C. Wallace, A. R. Morton, Q. Xie, D. Dixit, D. C. Factor, L. J. Y. Kim, J. J. Morrow, Q. Wu, S. C. Mack, C. G. Hubert, S. M. Gillespie, W. A. Flavahan, T. Hoffmann, R. Thummalapalli, M. T. Hemann, P. J. Paddison, C. M. Horbinski, J. Zuber, P. C. Scacheri, B. E. Bernstein, P. J. Tesar, and J. N. Rich. Transcription elongation factors represent in vivo cancer dependencies in glioblastoma. *Nature*, 546(7663):355–359, 2017.

H. Misawa, Y. Kawasaki, J. Mellor, N. Sweeney, K. Jo, R. A. Nicoll, and D. S. Bredt. Contrasting localizations of MALS/LIN-7 PDZ proteins in brain and molecular compensation in knockout mice. *Journal of Biological Chemistry*, 276(12):9264–92772, 2001.

V. G. Moore, R. E. Atchison, G. Thomas, M. Moran, and H. F. Noller. Identification of a ribosomal protein essential for peptidyl transferase activity. *Proceedings of the National Academy of Sciences*, 72(3):844–848, 1975.

M. E. Moreno-García, K. Sommer, H. Shinohara, A. D. Bandaranayake, T. Kurosaki, and D. J. Rawlings. MAGUK-controlled ubiquitination of CARMA1 modulates lymphocyte NF-ϰB activity. *Molecular and Cellular Biology*, 30(4):922–934, 2010.

T. Mori, K. Okamoto, Y. Tanaka, K. Teye, T. Umata, K. Ohneda, K. Tokuyama, M. Okabe, and M. Tsuneoka. Ablation of mina53 in mice reduces allergic response in the airways. *Cell Structure and Function*, 38(2):155–167, 2013.

K. E. Moyer and J. R. Jacobs. Varicose: a MAGUK required for the maturation and function of Drosophila septate junctions. *BMC Developmental Biology*, 8(99), 2008.

Y. Munehira, Z. Yang, and O. Gozani. Systematic analysis of known and candidate lysine demethylases in the regulation of myoblast differentiation. *Journal of Molecular Biology*, 429(13):2055–2065, 2017.

J. Myllyharju. Prolyl 4-hydroxylases, the key enzymes of collagen biosynthesis. *Matrix Biology*, 22(1):15–24, 2003.

W. J. Nelson and R. Nusse. Convergence of wnt, β-catenin, and cadherin pathways. *Science*, 303(5663):1483–1487, 2004.

Y. Nishizawa, N. Nishida, M. Konno, K. Kawamoto, A. Asai, J. Koseki, H. Takahashi, N. Haraguchi, J. Nishimura, T. Hata, C. Matsuda, T. Mizushima, T. Satoh, Y. Doki, M. Mori, and H. Ishii. Clinical significance of histone demethylase NO66 in invasive colorectal cancer. *Annals of Surgical Oncology*, 24(3):841–849, 2017.

A. Noma, R. Ishitani, M. Kato, A. Nagao, O. Nureki, and T. Suzuki. Expanding the role of the jumonji C domain as an RNA hydroxylase. *Journal of Biological Chemistry*, 285(45):34503–34507, 2010.

T. I. Odintsova, E. C. Muller, A. V. Ivanov, T. A. Egorov, R. Bienert, S. N. Vladimirov, S. Kostka, A. Otto, B. Wittmann-Liebold, and G. G. Karpova. Characterization and analysis of posttranslational modifications of the human large cytoplasmic ribosomal subunit proteins by mass spectrometry and Edman sequencing. *Journal of Protein Chemistry*, 22(3):249–258, 2003.

S. Ogasawara, M. Komuta, O. Nakashima, J. Akiba, M. Tsuneoka, and H. Yano. Accelerated expression of a Myc target gene Mina53 in aggressive hepatocellular carcinoma. *Hepatology Research*, 40(4):330–336, 2010.

S. Oh and R. Janknecht. Histone demethylase JMJD5 is essential for embryonic development. *Biochemical and Biophysical Research Communications*, 420(1):61–65, 2012.

M. Ohh, C. W. Park, M. Ivan, M. A. Hoffman, T. Y. Kim, L. E. Huang, N. Pavletich, V. Chau, and W. G. Kaelin. Ubiquitination of hypoxia-inducible factor requires direct binding to the β-domain of the von Hippel-Lindau protein. *Nature Cell Biology*, 2(7):423–427, 2000.

M. Okamoto, M. Van Stry, L. Chung, M. Koyanagi, X. Sun, Y. Suzuki, O. Ohara, H. Kitamura, A. Hijikata, M. Kubo, and M. Bix. Mina, an Il4 repressor, controls T helper type 2 bias. *Nature Immunology*, 10(8):872–879, 2009.

O. Olsen, K. A. Moore, M. Fukata, J. C. Kazuta, T. Trinidad, F. W. Kauer, M. Streuli, H. Misawa, A. L. Burlingame, R. A. Nicoll, and D. S. Bredt. Neurotransmitter release regulated by a MALS-liprin-α presynaptic complex. *Journal of Cell Biology*, 170(7): 1127–1134, 2005.

T. Onda, K. Uzawa, D. Nakashima, K. Saito, Y. Iwadate, N. Seki, T. Shibahara, and H. Tanzawa. Lin-7C/VELI3/MALS-3: an essential component in metastasis of human squamous cell carcinoma. *Cancer Research*, 67(20):9643–9648, 2007.

T. Ooshio, R. Kobayashi, W. Ikeda, M. Miyata, Y. Fukumoto, N. Matsuzawa, H. Ogita, and Y. Takai. Involvement of the interaction of afadin with ZO-1 in the formation of tight junctions in Madin-Darby canine kidney cells. *Journal of Biological Chemistry*, 285(7):5003–5012, 2010.

B. Ortmann, D. Bensaddek, S. Carvalhal, S. C. Moser, S. Mudie, E. R. Griffis, J. R. Swedlow, A. I. Lamond, and S. Rocha. Cdk-dependent phosphorylation of PHD1 on serine 130 alters its substrate preference in cells. *Journal of Cell Science*, 129(1): 191–205, 2016.

N. A. Paolini, M. Attwood, S. B. Sondalle, C. M. D. S. Vieira, A. M. van Adrichem, F. M. di Summa, M. F. O'Donohue, P. E. Gleizes, S. Rachuri, J. W. Briggs, R. Fischer, P. J. Ratcliffe, M. W. Wlodarski, R. H. Houtkooper, M. von Lindern, T. W. Kuijpers, J. D. Dinman, S. J. Baserga, M. E. Cockman, and A. W. MacInnes. A ribosomopathy reveals decoding defective ribosomes driving human dysmorphism. *American Journal of Human Genetics*, 100(3):506–522, 2017.

M. R. Paule and R. J. White. Transcription by RNA polymerases I and III. *Nucleic Acids Research*, 28(6):1283–1298, 2000.

J. Pelletier, G. Thomas, and S. Volarević. Ribosome biogenesis in cancer: new players and therapeutic avenues. *Nature Reviews Cancer*, 18:51–63, 2017.

I. Pfeffer, L. Brewitz, T. Krojer, S. A. Jensen, G. T. Kochan, N. J. Kershaw, K. S. Hewitson, L. A. McNeill, H. Kramer, M. Münzel, R. J. Hopkinson, U. Oppermann,

P. A. Handford, M. A. McDonough, and C. J. Schofield. Aspartate/asparagine-β-hydroxylase crystal structures reveal an unexpected epidermal growth factor-like domain substrate disulfide pattern. *Nature Communications*, 10(4910):1–16, 2019.

A. Ploumakis and M. L. Coleman. OH, the Places You'll Go! Hydroxylation, Gene Expression, and Cancer. *Molecular Cell*, 58(5):729–741, 2015.

P. J. Pollard, C. Loenarz, D. R. Mole, M. A. McDonough, J. M. Gleadle, C. J. Schofield, and P. J. Ratcliffe. Regulation of Jumonji-domain-containing histone demethylases by hypoxia-inducible factor (HIF)-1α. *Biochemical Journal*, 416(3):387–394, 2008.

C. Poulard, J. Rambaud, N. Hussein, L. Corbo, and M. Le Romancer. JMJD6 regulates ERα methylation on arginine. *PLoS ONE*, 9(2):e87982, 2014.

C. Poulard, J. Rambaud, E. Lavergne, J. Jacquemetton, J. M. Renoir, O. Trédan, S. Chabaud, I. Treilleux, L. Corbo, and M. Le Romancer. Role of JMJD6 in breast tumourigenesis. *PLoS ONE*, 10(5):e0126181, 2015.

J. B. Qian, H. B. Liu, Y. Zhu, F. Lu, Q. C. Yang, and Y. Shen. CADM1 mRNA expression and clinicopathological significance in esophageal squamous cell carcinoma tissue. *Genetics and Molecular Research*, 16(2), 2017.

Y. Qin, C. Capaldo, B. M. Gumbiner, and I. G. Macara. The mammalian Scribble polarity protein regulates epithelial cell adhesion and migration through E-cadherin. *Journal of Cell Biology*, 171(6):1061–1071, 2005.

I. Raphael, S. Nalawade, T. N. Eagar, and T. G. Forsthuber. T cell subsets and their signature cytokines in autoimmune and inflammatory diseases. *Cytokine*, 74(1):5–17, 2016.

T. Ratovitski, N. Arbez, J. C. Stewart, E. Chighladze, and C. A. Ross. PRMT5-mediated symmetric arginine dimethylation is attenuated by mutant huntingtin and is impaired in Huntington's disease (HD). *Cell Cycle*, 14(11):1716–1729, 2015.

J. Ren, Y. Wang, Y. Liang, Y. Zhang, S. Bao, and Z. Xu. Methylation of ribosomal protein S10 by protein-arginine methyltransferase 5 regulates ribosome biogenesis. *Journal of Biological Chemistry*, 285(17):12695–12705, 2010.

P. Reyes-Gutierrez, J. W. Carrasquillo-Rodríguez, and A. N. Imbalzano. Promotion of adipogenesis by JMJD6 requires the AT hook-like domain and is independent of its catalytic function. *PLoS ONE*, 14(8):e0216015, 2019.

S. Roberts, E. Calautti, S. Vanderweil, H. O. Nguyen, A. Foley, H. P. Baden, and A. Viel. Changes in localization of human discs large (hDlg) during keratinocyte differentiation are associated with expression of alternatively spliced hDlg variants. *Experimental Cell Research*, 313:2521–2530, 2007.

S. Roberts, C. Delury, and E. Marsh. The PDZ protein discs-large (DLG): the 'Jekyll and Hyde' of the epithelial polarity proteins. *FEBS Journal*, 279:3594–3558, 2012.

E. Rodriguez-Boulan and I. G. Macara. Organization and execution of the epithelial polarity programme. *Nature Reviews Molecular Cell Biology*, 15:225–242, 2014.

M. H. Roh, O. Makarova, C. J. Liu, K. Shin, S. Lee, S. Laurinec, M. Goyal, R. Wiggins, and B. Margolis. The Maguk protein, Pals1, functions as an adapter, linking mammalian homologues of Crumbs and Discs Lost. *Journal of Cell Biology*, 157(1): 161–172, 2002.

S. Rossetti, A. J. Wierzbicki, and N. Sacchi. Mammary epithelial morphogenesis and early breast cancer. Evidence of involvement of basal components of the RNA Polymerase I transcription machinery. *Cell Cycle*, 15(18):2515–2526, 2016.

D. Ruggero. Revisiting the nucleolus: from marker to dynamic integrator of cancer signaling. *Science Signaling*, 5(241):pe38, 2012.

G. Sabio, M. I. Cerezo-Guisado, P. Del Reino, F. A. Inesta-Vaquera, S. Rousseau, J. S. Arthur, D. G. Campbell, F. Centeno, and A. Cuenda. p38gamma regulates interaction of nuclear PSF and RNA with the tumour-suppressor hDlg in response to osmotic shock. *Journal of Cell Science*, 123:2596–2604, 2010.

K. Saeed, P. Östling, M. Björkman, T. Mirtti, K. Alanen, T. Vesterinen, A. Sankila, J. Lundin, M. Lundin, A. Rannikko, S. Nordling, J. Mpindi, P. Kohonen, K. Iljin, O. Kallioniemi, and J. Rantala. Androgen receptor-interacting protein HSPBAP1 facilitates growth of prostate cancer cells in androgen-deficient conditions. *International Journal of Cancer*, 136(11):2535–2545, 2015.

B. J. Saeedi, D. J. Kao, D. A. Kitzenberg, E. Dobrinskikh, K. D. Schwisow, J. C. Masterson, A. A. Kendrick, C. J. Kelly, A. J. Bayless, D. J. Kominsky, E. L. Campbell, K. A. Kuhn, G. T. Furuta, S. P. Colgan, and L. E. Glover. HIF-dependent regulation of claudin-1 is central to intestinal epithelial tight junction regulation. *Molecular Biology of the Cell*, 26(12):2252–2262, 2015.

M. Saito, A. Goto, N. Abe, K. Saito, D. Maeda, T. Ohtake, Y. Murakami, and S. Takenoshita. Decreased expression of CADM1 and CADM4 are associated with advanced stage breast cancer. *Oncology Letters*, 15(2):2401–2406, 2018.

Y. Sambuy, I. De Angelis, G. Ranaldi, M. L. Scarino, A. Stammati, and F. Zucco. The Caco-2 cell line as a model of the intestinal barrier: influence of cell and culture-related factors on Caco-2 cell functional characteristics. *Cell Biology and Toxicology*, 21(1):1–26, 2005.

J. Schneider, J. Böse, S. D. Bamforth, A. D. Gruber, C. Broadbent, K. Clarke, S. Neubauer, A. Lengeling, and S. Bhattacharya. Identification of cardiac malformations in mice lacking *Ptdsr* using a novel high-throughput magnetic resonance imaging technique. *BMC Developmental Biology*, 4(16), 2004.

C. J. Schofield and P. J. Ratcliffe. Oxygen sensing by HIF hydroxylases. *Nature Reviews Molecular Cell Biology*, 5:343–354, 2004.

C. Schreider, G. Peignon, S. Thenet, J. Chambaz, and M. Pinçon-Raymond. Integrin-mediated functional polarization of Caco-2 cells through E-cadherin–actin complexes. *Journal of Cell Science*, 115(3):543–552, 2002.

M. Sciacovelli and C. Frezza. Metabolic reprogramming and epithelial-to-mensenchymal transition in cancer. *FEBS Journal*, 284(19):3132–3144, 2017.

M. S. Scott, F. M. Boisvert, M. McDowall, A. I. Lamond, and G. Barton. Characterization and prediction of protein nucleolar localization sequences. *Nucleic Acids Research*, 38(21):7388–7399, 2010.

M. S. Scott, P. V. Troshin, and G. Barton. NoD: a nucleolar localization sequence detector for eukaryotic and viral proteins. *BMC Bioinformatics*, 12(317), 2011.

S. Shang, F. Hua, and Z. W. Hu. The regulation of β-catenin activity and function in cancer: therapeutic opportunities. *Oncotarget*, 8(20):33972–33989, 2017.

S. Sharma, T. K. Kelly, and P. A. Jones. Epigenetics and cancer. *Carcinogenesis*, 31 (1):27–36, 2010.

Y. Shen, D. S. Hirsch, C. A. Sasiela, and W. J. Wu. Cdc42 regulates E-cadherin ubiquitination and degradation through an Epithelial Growth Factor Receptor to Src-mediated pathway. *Journal of Biological Chemistry*, 283(8):P5127–5137, 2008.

Y. Shi, F. Lan, C. Matson, P. Mulligan, J. R. Whetstine, P. A. Cole, R. A. Casero, and Y. Shi. Histone demethylation mediated by the nuclear amine oxidase homolog LSD1. *Cell*, 119(7):941–953, 2004.

T. Shingai, W. Ikeda, S. Kakunaga, K. Morimoto, K. Takekuni, S. Itoh, K. Satoh, M. Takeuchi, T. Imai, M. Monden, and Y. Takai. Implications of nectin-like molecule-2/IGSF4/RA175/SgiGSF/TSLC1/SynCAM1 in cell-cell adhesion and transmembrane protein localization in epithelial cells. *Journal of Biological Chemistry*, 278 (37):35421–35427, 2003.

X. Si, F. Xu, F. Xu, M. Wei, Y. Ge, and S. Chenge. CADM1 inhibits ovarian cancer cell proliferation and migration by potentially regulating the PI3K/Akt/mTOR pathway. *Biomedicine and Pharmacotherapy*, 123:109717, 2020.

R. S. Singleton, P. Liu-Yi, F. Formenti, W. Ge, R. Sekirnik, R. Fischer, J. Adam, P. J. Pollard, A. Wolf, A. Thalhammer, C. Loenarz, E. Flashman, A. Yamamoto, M. L. Coleman, B. M. Kessler, P. Wappner, C. J. Schofield, P. J. Ratcliffe, and M. E. Cockman. OGFOD1 catalyzes prolyl hydroxylation of RPS23 and is involved in translation control and stress granule formation. *Proceedings of the National Academy of Sciences*, 111(11):4031–4036, 2014.

K. M. Sinha, H. Yasuda, M. M. Coombes, S. Y. R. Dent, and B. de Crombrugghe. Regulation of the osteoblast-specific transcription factor Osterix by NO66, a Jumonji family histone demethylase. *EMBO Journal*, 29:68–79, 2010.

K. M. Sinha, H. Yasuda, X. Zhou, and B. Decrombrugghe. Osterix and NO66 histone demethylase control the chromatin of osterix target genes during osteoblast differentiation. *Journal of Bone and Mineral Research*, 29(4):855–865, 2014.

A. K. Srivastava, S. R. Renusch, N. E. Naiman, S. Gu, A. Sneh, W. D. Arnold, Z. Sahenk, and S. J. Kolb. Mutant HSPB1 overexpression in neurons is sufficient to cause age-related motor neuronopathy in mice. *Neurobiology of Disease*, 47(2):163–173, 2012.

J. Stenflo, E. Holme, S. Lindstedt, N. Chandramouli, L. H. Huang, J. P. Tam, and R. B. Merrifield. Hydroxylation of aspartic acid in domains homologous to the epidermal growth factor precursor is catalyzed by a 2-oxoglutarate-dependent dioxygenase. *Proceedings of the National Academy of Sciences*, 86(3):444–447, 1989.

H. Stöhr and B. H. Weber. Cloning and characterization of the human retina-specific gene MPP4, a novel member of the p55 subfamily of MAGUK proteins. *Genomics*, 74(3):377–384, 2001.

S. W. Straight, K. Shin, V. C. Fogg, S. Fan, C. J. Liu, M. Roh, and B. Margolis. Loss of PALS1 expression leads to tight junction and polarity defects. *Molecular Biology of the Cell*, 15(4):1981–1990, 2004.

S. W. Straight, J. N. Pieczynski, E. L. Whiteman, C. J. Liu, and B. Margolis. Mammalian lin-7 stabilizes polarity protein complexes. *Journal of Biological Chemistry*, 281(49):37738–37747, 2006.

V. M. Stucke, E. Timmerman, J. Vandekerckhove, K. Gevaert, and A. Hall. The MAGUK protein MPP7 binds to the polarity protein hDlg1 and facilitates epithelial tight junction formation. *Molecular Cell Biology*, 18(5):1744–1755, 2007.

Y. Su and J. Wang. Jmjc domain-containing protein 8 (JMJD8) represses Ku70/Ku80 expression via attenuating AKT/NF-$\varkappa$B/COX-2 signaling. *Biochimica et Biophysica Acta - Molecular Cell Research*, 1866(12), 2019.

M. Sugimoto, M. Kuo, M. F. Roussel, and C. J. Sherr. Nucleolar Arf tumour suppressor inhibits ribosomal RNA processing. *Molecular Cell*, 11:415–424, 2003.

C. Suzuki, K. Takahashi, S. Hayama, N. Ishikawa, T. Kato, T. Ito, E. Tsuchiya, Y. Nakamura, and Y. Daigo. Identification of Myc-associated protein with jmjC domain as a novel therapeutic target oncogene for lung cancer. *Molecular Cancer Therapeutics*, 6(2):542–551, 2007.

T. Suzuki, K. Minehata, K. Akagi, N. A. Jenkins, and N. G. Copelang. Tumor suppressor gene identification using retroviral insertional mutagenesis in Blm-deficient mice. *EMBO Journal*, 25(14):3422–3431, 2006.

D. Szklarczyk, A. L. Gable, D. Lyon, A. Junge, S. Wyder, J. Huerta-Cepas, M. Simonovic, N. T. Doncheva, J. H. Morris, P. Bork, L. J. Jensen, and C. von Mering. STRING v11: protein-protein association networks with increased coverage, supporting functional discovery in genome-wide experimental datasets. *Nucleic Acids Research*, 47:D607–613, 2019.

M. Tahiliani, K. P. Koh, Y. Shen, W. A. Pastor, Y. Brudno, S. Agarwal, L. M. Iyer, R. David, L. Aravind, and A. Rao. Conversion of 5-methylcytosine to 5-hydroxymethylcytosine in mammalian DNA by MLL partner TET1. *Science*, 324 (5929):930–935, 2009.

Y. Takai, J. Miyoshi, W. Ikeda, and H. Ogita. Nectins and nectin-like molecules: roles in contact inhibition of cell movement and proliferation. *Nature Reviews Molecular Cell Biology*, 9:603–615, 2008.

T. Takeuchi, Y. Yamazaki, Y. Katoh-Fukui, R. Tsuchiya, S. Kondo, J. Motoyama, and T. Higashinakagawa. Gene trap capture of a novel mouse gene, jumonji, required for neural tube formation. *Genes and Development*, 9(10):1211–1222, 1995.

X. P. Tan, W. G. Dong, Q. Zhang, Z. R. Yang, X. F. Lei, and M. H. Ai. Potential effects of Mina53 on tumor growth in human pancreatic cancer. *Cell Biochemistry and Biophysics*, 69(3):619–625, 2014.

Y. Tanaka, K. Okamoto, K. Teye, T. Umata, N. Yamagiwa, Y. Suto, Y. Zhang, and M. Tsuneoka. JmjC enzyme KDM2A is a regulator of rRNA transcription in response to starvation. *EMBO Journal*, 29(9):1510–1522, 2010.

W. Tao and A. J. Levine. p19ARF stabilizes p53 by blocking nucleo-cytoplasmic shuttling of Mdm2. *Proceedings of the National Academy of Sciences*, 96(6937-6941), 1999.

C. T. Taylor and S. P. Colgan. Hypoxia and gastrointestinal disease. *Journal of Molecular Medicine*, 85(12):1295–1300, 2007.

M. Teichmann, H. Dumay-Odelot, and S. Fribourg. Structural and functional aspects of winged-helix domains at the core of transcription initiation complexes. *Transcription*, 3(1):2–7, 2012.

N. Terada, Y. Saitoh, N. Ohno, M. Komada, S. Saitoh, E. Peles, and S. Ohno. Essential function of protein 4.1G in targeting of membrane protein palmitoylated 6 into schmidt-lanterman incisures in myelinated nerves. *Molecular and Cellular Biology*, 32(1):199–205, 2012.

K. Teye, M. Tsuneoka, N. Arima, Y. Koda, Y. Nakamura, Y. Ueta, K. Shirouzu, and H. Kimura. Increased expression of a Myc target gene Mina53 in human colon cancer. *American Journal of Pathology*, 164(1):205–216, 2004.

K. Teye, N. Arima, Y. Nakamura, K. Sakamoto, E. Sueoka, H. Kimura, and M. Tsuneoka. Expression of Myc target gene mina53 in subtypes of human lymphoma. *Oncology Reports*, 18(4):841–848, 2007.

C. Thakur, Y. Lu, J. Sun, M. Yu, B. Chen, and F. Chen. Increased expression of mdig predicts poorer survival of the breast cancer patients. *Gene*, 535(2):218–224, 2014.

C. Thakur, M. Wolfarth, J. Y. Sun, Y. D. Zhang, Y. J. Lu, L. Battelli, D. W. Porter, and F. Chen. Oncoprotein mdig contributes to silica-induced pulmonary fibrosis by altering balance between Th17 and Treg T cells. *Oncotarget*, 6(6):3722–3736, 2015.

B. Thienpont, J. Steinbacher, H. Zhao, F. D'Anna, A. Kuchnio, A. Ploumakis, B. Ghesquière, L. Van Dyck, B. Boeckx, L. Schoonjans, E. Hermans, F. Amant, V. N. Kristensen, K. K. Peng, M. Mazzone, M. Coleman, T. Carell, P. Carmeliet, and D. Lambrechts. Tumour hypoxia causes DNA hypermethylation by reducing TET activity. *Nature*, 537(7618):63–68, 2016.

U. Thomas, S. Ebitsch, M. Gorczyca, Y. H. Koh, C. D. Hough, D. Woods, E. D. Gundelfinger, and V. Budnik. Synaptic targeting and localization of discs-large is a stepwise process controlled by different domains of the protein. *Current Biology*, 10: 1108–1117, 2000.

Y. M. Tian, K. K. Yeoh, M. K. Lee, T. Eriksson, B. M. Kessler, H. B. Kramer, M. J. Edelmann, C. Willam, C. W. Pugh, C. J. Schofield, and P. J. Ratcliffe. Differential sensitivity of hypoxia inducible factor hydroxylation sites to hypoxia and hydroxylase inhibitors. *Journal of Biological Chemistry*, 286(15):13041–13051, 2011.

I. Tikhanovich, S. Kuravi, A. Artigues, M. T. Villar, K. Dorko, A. Nawabi, B. Roberts, and S. A. Weinman. Dynamic arginine methylation of tumor necrosis factor (TNF) receptor-associated factor 6 regulates Toll-like receptor signaling. *Journal of Biological Chemistry*, 290(36):22236–49, 2015.

M. Tiso and A. N. Schechter. Nitrate reduction to nitrite, nitric oxide and ammonia by gut bacteria under physiological conditions. *PLoS ONE*, 10(5):e0127490, 2015.

W. C. Tsai, L. C. Reineke, A. Jain, S. Y. Jung, and R. E. Lloyd. Histone arginine demethylase JMJD6 is linked to stress granule assembly through demethylation of the stress granule-nucleating protein G3BP1. *Journal of Biological Chemistry*, 292 (46):18886–18896, 2017.

T. C. Tseng, S. M. Marfatia, P. J. Bryant, S. Pack, Z. Zhuang, J. E. O'Brien, L. Lin, T. Hanada, and A. H. Chishti. VAM-1: a new member of the MAGUK family binds to human Veli-1 through a conserved domain. *Biochimica et Biophysica Acta (BBA) - Gene Structure and Expression*, 1518(3):249–259, 2001.

M. Tsuneoka, Y. Koda, M. Soejima, K. Teye, and H. Kimura. A novel Myc target gene, mina53, that is involved in cell proliferation. *Journal of Biological Chemistry*, 277(38):35450–35459, 2002.

M. Tsuneoka, H. Fujita, N. Arima, K. Teye, T. Okamura, H. Inutsuka, Y. Koda, K. Shirouzu, and H. Kimura. Mina53 as a potential prognostic factor for esophageal squamous cell carcinoma. *Clinical Cancer Research*, 10(21):7347–7356, 2004.

M. Tsuneoka, Y. Nishimune, K. Ohta, K. Teye, H. Tanaka, M. Soejima, H. Iida, T. Inokuchi, H. Kimura, and Y. Koda. Expression of Mina53, a product of a Myc target gene in mouse testis. *International Journal of Andrology*, 29(2):323–330, 2006.

M. Unoki, A. Masuda, N. Dohmae, K. Arita, M. Yoshimatsu, Y. Iwai, Y. Fukui, K. Ueda, R. Hamamoto, M. Shirakawa, H. Sasaki, and Y. Nakamura. Lysyl 5-hydroxylation, a novel histone modification, by Jumonji domain containing 6 (JMJD6). *Journal of Biological Chemistry*, 288(9):6053–6062, 2013.

T. Valenta, G. Hausmann, and K. Basler. The many faces and functions of β-catenin. *EMBO Journal*, 31(12):2714–2736, 2012.

S. Vallath, E. K. Sage, K. K. Kolluri, S. N. Lourenco, V. S. Teixeira, S. Chimalapati, P. J. George, S. M. Janes, and A. Giangreco. CADM1 inhibits squamous cell carcinoma progression by reducing STAT3 activity. *Scientific Reports*, 6:24006, 2016.

E. van den Born, C. B. Vågbø, L. Songe-Møller, V. Leihne, G. F. Lien, G. Leszczynska, A. Malkiewicz, H. E. Krokan, F. Kirpekar, A. Klungland, and P. Ø. Falnes. ALKBH8-mediated formation of a novel diastereomeric pair of wobble nucleosides in mammalian tRNA. *Nature Communications*, 2(172), 2011.

F. M. Vaz and R. J. Wanders. Carnitine biosynthesis in mammals. *Biochemical Journal*, 361(3):417–429, 2002.

N. D. Venezia, A. Vincent, V. Marcel, F. Catez, and J. Diaz. Emerging role of eukaryote ribosomes in translational control. *International Journal of Molecular Sciences*, 20 (5):1226, 2019.

R. Visintin and A. Amon. The nucleolus: the magician's hat for cell cycle tricks. *Current Opinion in Cell Biology*, 12(3):372–377, 2000.

R. M. Voorhees, A. Weixlbaumer, D. Loakes, A. C. Kelley, and V. Ramakrishnan. Insights into substrate stabilization from snapshots of the peptidyl transferase center of the intact 70S ribosome. *Nature Structural and Molecular Biology*, 16(5):528–533, 2009.

J. Wan, H. Liu, L. Yang, L. Ma, J. Liu, and L. Ming. JMJD6 promotes hepatocellular carcinoma carcinogenesis by targeting CDK4. *International Journal of Cancer*, 144 (10):2489–2500, 2019.

C. Wang, Q. Zhang, T. Hang, Y. Tao, X. Ma, M. Wu, X. Zhang, and J. Zang. Structure of the JmjC domain-containing protein NO66 complexed with ribosomal protein Rpl8. *Acta Crystallographica Section D Biological Crystallography*, 71(pt 9):1955–1964, 2015a.

F. Wang, L. He, P. Huangyang, J. Liang, W. Si, R. Yan, X. Han, S. Liu, B. Gui, W. Li, D. Miao, C. Jing, Z. Liu, F. Pei, L. Sun, and Y. Shang. Jmjd6 promotes colon carcinogenesis through negative regulation of p53 by hydroxylation. *PLoS Biology*, 12(3):e1001819, 2014a.

H. J. Wang, Y. J. Hsieh, W. C. Cheng, C. P. Lin, Y. S. Lin, S. F. Yang, C. C. Chen, Y. Izumiya, J. S. Yu, H. Kung, and W. C. Wang. JMJD5 regulates PKM2 nuclear translocation and reprograms HIF-1α-mediated glucose metabolism. *Proceedings of the National Academy of Sciences*, 111(1):279–284, 2014b.

H. J. Wang, M. Pochampalli, L. Y. Wang, J. X. Zou, P. S. Li, S. C. Hsu, B. J. Wang, S. Huang, P. Yang, J. Yang, C. Y. Chu, C. L. Hsieh, S. Y. Sung, C. F. Li, C. G. Tepper, D. K. Ann, A. C. Gao, C. P. Evans, Y. Izumiya, C. P. Chuu, W. C. Wang, H. W. Chen, and H. J. Kung. KDM8/JMJD5 as a dual coactivator of AR and PKM2 integrates AR/EZH2 network and tumor metabolism in CRPC. *Oncogene*, 38(1): 17–31, 2019a.

L. Wang, F. Jiang, F. Ma, and B. Zhang. MiR-873-5p suppresses cell proliferation and epithelial-mesenchymal transition via directly targeting Jumonji domain-containing protein 8 through the NF-ϰB pathway in colorectal cancer. *Journal of Cell Communication and Signaling*, 13(4):549–560, 2019b.

Q. Wang, X. W. Chen, and B. Margolis. PALS1 regulates E-cadherin trafficking in mammalian epithelial cells. *Molecular Biology of the Cell*, 18(3):874–885, 2007.

W. Wang, Y. Lu, P. M. Stemmer, X. Zhang, Y. Bi, Z. Yi, and F. Chen. The proteomic investigation reveals interaction of mdig protein with the machinery of DNA double-strand break repair. *Oncotarget*, 6(29):28269–28281, 2015b.

Y. Wang, L. Liu, F. Ji, J. Jiang, Y. Yu, S. Sheng, and H. Li. Soybean (Glycine max) prevents the progression of breast cancer cells by downregulating the level of histone demethylase JMJD5. *Journal of Cancer Research and Therapeutics*, 14(10):609–615, 2018.

J. D. Webb, A. Murányi, C. W. Pugh, P. J. Ratcliffe, and M. L. Coleman. MYPT1, the targeting subunit of smooth-muscle myosin phosphatase, is a substrate for the asparaginyl hydroxylase factor inhibiting hypoxia-inducible factor (FIH). *Biochemical Journal*, 420(2):327–333, 2009.

C. J. Webby, A. Wolf, N. Gromak, M. Dreger, H. Kramer, B. Kessler, M. L. Nielsen, C. Schmitz, D. S. Butler, J. R. Yates, C. M. Delahunty, P. Hahn, A. Lengeling, M. Mann, N. J. Proudfoot, C. J. Schofield, and A. Böttger. Jmjd6 catalyses lysyl-hydroxylation of U2AF65, a protein associated with RNA splicing. *Science*, 325 (5936):90–93, 2009.

D. J. Weber, L. J. Taylor, M. F. Roussel, C. J. Sherr, and D. Bar-Sagi. Nucleolar Arf sequesters Mdm2 and activate p53. *Nature Cell Biology*, 1:20–25, 1999.

S. E. Wilkins, S. Islam, J. M. Gannon, S. Markolovic, R. J. Hopkinson, W. Ge, C. J. Schofield, and R. Chowdhury. JMJD5 is a human arginyl C-3 hydroxylase. *Nature Communications*, 9(1), 2018.

S. T. Williams, L. J. Walport, R. J. Hopkinson, S. K. Madden, R. Chowdhury, C. J. Schofield, and A. Kawamura. Studies on the catalytic domains of multiple JmjC oxygenases using peptide substrates. *Epigenetics*, 9(12):1596–1603, 2014.

B. Wu, H. Chen, C. M. Cai, J. Z. Fang, C. C. Wu, L. Y. Huang, L. Wang, and Z. G. Han. Epigenetic silencing of JMJD5 promotes the proliferation of hepatocellular carcinoma cells by down-regulating the transcription of CDKN1A 686. *Oncotarget*, 7(6):6847–6863, 2016a.

K. Wu, L. Li, C. Thakur, Y. Lu, X. Zhang, Z. Yi, and F. Chen. Proteomic characterization of the World Trade Center dust-activated mdig and c-myc signaling circuit linked to multiple myeloma. *Scientific Reports*, 6:36305, 2016b.

L. Wu, J. Pan, V. Thoroddsen, D. R. Wysong, R. K. Blackman, C. E. Bulawa, A. E. Gould, T. D. Ocain, L. R. Dick, P. Errada, P. K. Dorr, T. Parkinson, T. Wood, D. Kornitzer, Z. Weissman, I. M. Willis, and K. McGovern. Novel small-molecule inhibitors of RNA polymerase III. *Eukaryotic Cell*, 2(2):256–264, 2003.

T. F. Wu, Y. L. Yao, I. L. Lai, C. C. Lai, P. L. Lin, and W. M. Yang. Loading of PAX3 to mitotic chromosomes is mediated by arginine methylation and associated with Waardenburg syndrome. *Journal of Biological Chemistry*, 290(33):20556–20564, 2015.

V. M. Wu and G. J. Beitel. A junctional problem of apical proportions: epithelial tube-size control by septate junctions in the *Drosophila* tracheal system. *Current Opinion in Cell Biology*, 16(5):493–499, 2004.

V. M. Wu, M. H. Yu, R. Paik, S. Banerjee, Z. Liang, S. M. Paul, M. A. Bhat, and G. J. Beitel. Drosophila Varicose, a member of a new subgroup of basolateral MAGUKs, is required for septate junctions and tracheal morphogenesis. *Development*, 134(5): 999–1009, 2007.

Z. Xi, F. Xiao, J. Yuan, X. Wang, L. Wang, F. Y. Quan, and G. W. Liu. Gene expression analysis on anterior temporal neocortex of patients with intractable epilepsy. *Synapse*, 63(11):1017–1028, 2009.

Z. Q. Xi, J. Sun, X. F. Wang, M. W. Li, X. Z. Liu, L. Wang, X. Zhu, F. Xiao, J. Li, Y. Gong, and L. F. Guan. HSPBAP1 is found extensively in the anterior temporal neocortex of patients with intractable epilepsy. *Synapse*, 61(9):741–747, 2007.

J. Xing, K. Wang, P. W. Liu, Q. Miao, and X. Y. Chen. Mina53, a novel molecular marker for the diagnosis and prognosis of gastric adenocarcinoma. *Oncology Reports*, 31(2):634–640, 2014.

F. Xu, S. Xiaoqiang, J. Du, F. Xu, A. Yang, C. Zhang, X. Zhang, and Y. Yang. Downregulating SynCAM and MPP6 expression is associated with ovarian cancer progression. *Oncology Letters*, 18(3):2477–2483, 2019.

B. Xue, K. Krishnamurthy, D. C. Allred, and S. K. Muthuswamy. Loss of Par3 promotes breast cancer metastasis by compromising cell-cell cohesion. *Nature Cell Biology*, 15 (12):189–200, 2013.

S. Xue and M. Barna. Specialized ribosomes: a new frontier in gene regulation and organismal biology. *Nature Reviews Molecular Cell Biology*, 13:355–369, 2012.

T. Yanagihara, T. Tomino, T. Uruno, and Y. Fukui. Thymic epithelial cell-specific deletion of Jmjd6 reduces Aire protein expression and exacerbates disease development in a mouse model of autoimmune diabetes. *Biochemical and Biophysical Research Communications*, 489(1):8–13, 2017.

J. Yang, B. Pawlyk, X. H. Wen, M. Adamian, M. Soloviev, N. Michaud, Y. Zhao, M. A. Sandberg, C. L. Makino, and T. Li. Mpp4 is required for proper localization of plasma membrane calcium ATPases and maintenance of calcium homeostasis at the rod photoreceptor synaptic terminals. *Human Molecular Genetics*, 16(9):1017–1029, 2007.

M. Yang, R. Chowdhury, W. Ge, R. B. Hamed, M. A. McDonough, T. D. Claridge, B. M. Kessler, M. E. Cockman, P. J. Ratcliffe, and C. J. Schofield. Factor-inhibiting hypoxia-inducible factor (FIH) catalyses the post-translational hydroxylation of histidinyl residues within ankyrin repeat domains. *FEBS Journal*, 278(7):1086–1097, 2011a.

M. Yang, W. Ge, R. Chowdhury, T. D. W. Claridge, B. K. Holger, B. Schmierer, M. A. McDonough, L. Gong, B. M. Kessler, P. J. Ratcliffe, M. L. Coleman, and C. J. Schofield. Asparagine and aspartate hydroxylation of the cytoskeletal ankyrin family is catalyzed by factor-inhibiting hypoxia-inducible factor. *Journal of Biological Chemistry*, 286(9):7648–7660, 2011b.

M. Yang, A. P. Hardy, R. Chowdhury, N. D. Loik, J. S. Scotti, J. S. McCullagh, T. D. Claridge, M. A. McDonough, W. Ge, and C. J. Schofield. Substrate selectivity analyses of factor inhibiting hypoxia-inducible factor. *Angewandte Chemie International Edition*, 52:1700–1704, 2013.

Z. Yang, L. Zhuang, P. Szatmary, L. Wen, H. Sun, Y. Lu, Q. Xu, and X. Chen. Upregulation of heat shock proteins (HSPA12A, HSP90B1, HSPA4, HSPA5 and HSPA6) in tumour tissues is associated with poor outcomes from HBV-related early-stage hepatocellular carcinoma. *International Journal of Medical Sciences*, 12(3): 256–263, 2015.

D. D. Yanshina, K. N. Bulygin, A. Malygin, and G. G. Karpova. Hydroxylated histidine of human ribosomal protein uL2 is involved in maintaining the local structure of 28S rRNA in the ribosomal peptidyl transferase center. *FEBS Journal*, 282(8):1554–1566, 2015.

D. D. Yanshina, A. V. Gopanenko, G. G. Karpova, and A. A. Malygin. Replacement of hydroxylated His39 in ribosomal protein uL15 with Ala or Thr impairs the translational activity of human ribosomes. *Molecular Cell Biology*, 54:449–457, 2020.

F. Ye, M. Zeng, and M. Zhang. Mechanisms of MAGUK-mediated cellular junctional complex organization. *Current Opinion in Structural Biology*, 48:6–15, 2018.

K. S. Yeo, M. C. Tan, W. Y. Wong, S. W. Loh, Y. L. Lam, C. L. Tan, Y. Y. Lim, and C. K. Ea. JMJD8 is a positive regulator of TNF-induced NF-κB signaling. *Scientific Reports*, 6(34125), 2016.

K. S. Yeo, M. C. Tan, Y. Lim, and C. K. Ea. JMJD8 is a novel endoplasmic reticulum protein with a JmjC domain. *Scientific Reports*, 7(15407), 2017.

D. Yin, Q. Wang, S. Wang, G. Zhu, Q. Tang, and J. Liu. OGFOD1 negatively regulated by miR-1224-5p promotes proliferation in human papillomavirus-infected laryngeal papillomas. *Molecular Genetics and Genomics*, 295(3):675–684, 2020.

N. Yosef, A. K. Shalek, J. T. Gaublomme, H. Jin, Y. Lee, A. Awasthi, C. Wu, K. Karwacz, S. Xiao, M. Jorgolli, D. Gennert, R. Satija, A. Shakya, D. Y. Lu, J. J. Trombetta, M. R. Pillai, P. J. Ratcliffe, M. L. Coleman, M. Bix, D. Tantin, H. Park, V. K. Kuchroo, and A. Regev. Dynamic regulatory network controlling Th17 cell differentiation. *Nature*, 496(7446):461–468, 2013.

Y. You, J. Zhang, Y. Li, Y. Li, G. Shi, L. Ma, and H. Wei. CADM1/TSLC1 inhibits melanoma cell line A375 invasion through the suppression of matrix metalloproteinases. *Molecular Medicine Reports*, 10(5):2621–2626, 2014.

M. Y. Youn, A. Yokoyama, S. Fujiyama-Nakamura, F. Ohtake, K. Minehata, H. Yasuda, T. Suzuki, S. Kato, and Y. Imai. JMJD5, a Jumonji C (JmjC) domain-containing protein, negatively regulates osteoclastogenesis by facilitating NFATc1 protein degradation. *Journal of Biological Chemistry*, 2012.

M. Yu, J. Sun, C. Thakur, B. Chen, Y. Lu, H. Zhao, and F. Chen. Paradoxical roles of mineral dust induced gene on cell proliferation and migration/invasion. *PLoS ONE*, 9(2), 2014.

Y. Yu, H. Ji, J. A. Doudna, and J. A. Leary. Mass spectrometric analysis of the human 40S ribosomal subunit: Native and HCV IRES-bound complexes. *Protein Science*, 14(6):1438–1446, 2005.

D. Zeng, X. Wu, J. Zheng, Y. Zhuang, J. Chen, C. Hong, F. Zhang, M. Wu, and D. Lin. Loss of CADM1/TSLC1 expression is associated with poor clinical outcome in patients with esophageal squamous cell carcinoma. *Gastroenterology Research and Practice*, 2016:6947623, 2016.

J. Zhang, S. S. Ni, W. L. Zhao, X. C. Dong, and J. L. Wang. High expression of JMJD6 predicts unfavorable survival in lung adenocarcinoma. *Tumour Biology*, 34 (4):2397–2401, 2013.

Q. Zhang, C. Thakur, Y. Fu, Z. Bi, P. Wadgaonkar, L. Xu, Z. Liu, W. Liu, J. Wang, B. L. Kidder, and F. Chen. Mdig promotes oncogenic gene expression through antagonizing repressive histone methylation markers. *Theranostics*, 10(2):602–614, 2020.

R. Zhang, Q. Huang, Y. Li, Y. Song, and Y. Li. JMJD5 is a potential oncogene for colon carcinogenesis. *International Journal of Clinical and Experimental Pathology*, 8(6):6482–6489, 2015.

W. Zhang, H. Y. Xie, S. M. Ding, C. Y. Xing, A. Chen, M. C. Lai, L. Zhou, and S. S. Zheng. CADM1 regulates the G1/S transition and represses tumorigenicity through the Rb-E2F pathway in hepatocellular carcinoma. *Hepatobiliary and Pancreatic Diseases International*, 15(3):289–296, 2016.

Y. Zhang, Y. Lu, B. Z. Yuan, V. Castranova, X. Shi, J. L. Stauffer, L. M. Demers, and F. Chen. The human mineral dust-induced gene, mdig, is a cell growth regulating gene associated with lung cancer. *Oncogene*, 24(31):4873–4882, 2005.

Z. Zhao, C. Sun, F. Li, J. Han, X. Li, and Z. Song. Overexpression of histone demethylase JMJD5 promotes metastasis and indicates a poor prognosis in breast cancer. *International Journal of Clinical and Experimental Pathology*, 8(9):10325–10334, 2015.

G. Zheng, J. A. Dahl, Y. Niu, P. Fedorcsak, C. M. Huang, C. J. Li, C. B. Vågbø, Y. Shi, W. L. Wang, S. H. Song, Z. Lu, R. P. Bosmans, Q. Dai, Y. J. Hao, X. Yang, W. M. Zhao, W. M. Tong, X. J. Wang, F. Bogdan, K. Furu, Y. Fu, G. Jia, X. Zhao, J. Liu, H. E. Krokan, A. Klungland, Y. G. Yang, and C. He. ALKBH5 is a mammalian RNA demethylase that impacts RNA metabolism and mouse fertility. *Molecular Cell*, 49 (1):18–29, 2013.

H. Zhu, S. Hu, and J. Baker. JMJD5 regulates cell cycle and pluripotency in human embryonic stem cells. *Stem Cells*, 32(8):2098–110, 2014.

Q. Zhuang, T. Feng, and M. L. Coleman. Modifying the maker: Oxygenases target ribosome biology. *Translation*, 3(1), 2015.

C. Zihni, C. Mills, K. Matter, and M. S. Balda. Tight junctions: form simple barriers to multifunctional molecular gates. *Nature Reviews Molecular Cell Biology*, 17(9): 564–580, 2016.